Investigations on the Reaction Mechanism of Xenobiotic Reductase A

Dissertation

zur Erlangung des Doktorgrades
der Fakultät für Biologie, Chemie und Geowissenschaften
an der Universität Bayreuth

Vorgelegt von
Diplom-Naturwissenschaftlerin
Olivia Spiegelhauer

Bayreuth, 2010

Die vorliegende Arbeit wurde von Januar 2006 bis April 2010 in der Arbeitsgruppe Bioanorganische Chemie unter der Leitung von Prof. Dr. Holger Dobbek angefertigt.

Vollständiger Abdruck der von der Fakultät für Biologie, Chemie und Geowissenschaften der Universität Bayreuth genehmigten Dissertation zur Erlangung des akademischen Grades eines Doktors der Naturwissenschaften (Dr. rer. nat.)

Promotionsgesuch eingereicht am: 21.04.2010
Tag des wissenschaftlichen Kolloquiums: 21.07.2010

Prüfungsausschuss:

Prof. Dr. Holger Dobbek	(Erster Gutachter)
Prof. Dr. Birgitta Wöhrl	(Zweite Gutachterin)
Prof. Dr. Matthias Ullmann	(Vorsitzender)
Prof. Dr. Hans-Werner Schmidt	

„Inmitten der Schwierigkeit liegt die Möglichkeit."

A. Einstein

"I love deadlines. I like the whooshing sound they make as they fly by."

D. Adams

Table of contents

Zusammenfassung

Die Xenobiotika-Reduktase A (XenA) aus *Pseudomonas putida* 86 gehört zur Familie der FMN enthaltenden *Old Yellow Enzyme* Familie. In einem zweistufigen Mechanismus, der sich in eine reduktive und eine oxidative Halbreaktion gliedert, reduziert es in Abhängigkeit von NADH bzw. NADPH verschiedene Substrate wie beispielweise 2-Cyclohexenon, Cumarin, 7- und 8-Hydroxycumarin. Obwohl innerhalb der Familie die Proteinstrukturen sehr ähnlich sind, finden sich deutliche Unterschiede im aktiven Zentrum. Auffällig bei XenA ist, dass ein weitgehend konserviertes Threonin durch ein Cystein ersetzt ist (Cys25). Darüber hinaus befinden sich im aktiven Zentrum von XenA zwei Tyrosine (Tyr27 und Tyr183) und zwei Tryptophane (Trp302 und Trp358).

Um ein besseres Verständnis des Reaktionsmechanismus zu erhalten, wurde XenA in dieser Arbeit durch eine Kombination aus transienten und *steady-state* kinetischen Methoden, sowie Redoxpotentiometrie und Kristallstrukturanalyse untersucht. Durch thermodynamische und kinetische Messungen zeigte sich dabei, dass XenA NADPH gegenüber NADH als Substrat bevorzugt. Zudem folgt die durch XenA katalysierte Reaktion einem Ping-Pong Mechanismus. Bei diesem binden beide Substrate an der selben Stelle im aktiven Zentrum, aber interagieren dort mit verschiedenen Aminosäuren. Des Weiteren wurden die Kristallstrukturen von XenA mit und ohne Cumarin im aktiven Zentrum bei atomarer Auflösung bestimmt. Im oxidierten Zustand des Komplexes befindet sich der Isoalloxazinring des FMN zwischen Cumarin und Proteinrückgrat, wodurch das aktive Zentrum gestaucht wird. In der Kristallstruktur von reduzierter XenA läßt sich eine Verzerrung des Isoalloxazinringes und eine Bewegung von Trp302 ins aktive Zentrum hinein beobachten.

Mit Hilfe von ortsgerichteter Mutagenese wurden zudem die fünf Reste des aktiven Zentrums untersucht. Der Austausch von Cys25 gegen Serin verschob das Redoxpotential zwischen FMN und FMNH$^-$ um +82 mV, erhöhte die maximale Geschwindigkeitskonstante der reduktiven und erniedrigte die maximale Geschwindigkeitskonstante der oxidativen Halbreaktion. Dies bedeutet, dass Cys25 die Bindung und das Redoxpotential von FMN moduliert.

Außerdem konnten wir Tyr27 als Stabilisator des Übergangszustandes während der reduktiven Halbreaktion identifizieren, in welchem die Hydroxylgruppe des Tyrosins mit dem übergehenden Hydridion interagieren kann. Ein Austausch des Tyr183 hingegen hatte eine erniedrigte Affinität von XenA gegenüber NADPH und eine deutlich verringerte Rate der oxidativen Halbreaktion zur Folge. Daraus läßt sich folgern, dass es sich bei Tyr183 um den essentiellen Protonendonor innerhalb der oxidativen Halbreaktion handelt.

Nach der Auswechslung von Trp302 wiesen die Kinetiken beider Halbreaktionen multiple Phasen auf und die Affinität von XenA gegenüber NADPH sank. Da dieser Rest zudem unterschiedliche Positionen im reduzierten und oxidierten Zustand von XenA einnimmt, folgern wir, dass Trp302 in Abhängigkeit des Redoxzustandes die Form und Zugänglichkeit des aktiven Zentrums variiert. Dadurch können die Substrate für die jeweilige Halbreaktion richtig positioniert werden. Dies ist von außerordentlicher Bedeutung für den Reaktionsmechanismus. Ferner konnte gezeigt werden, dass Trp358 eine Rolle bei der korrekten Orientierung des Nicotinamidrings von NAD(P)H spielt.

Üblicherweise werden Kristallstrukturen von Enzym-Substrat-Komplexen in unreaktiven Zuständen gemessen. Da bei der Y183F Variante der Protonendonor der oxidativen Halbreaktion entfernt wurde, konnten die Strukturen der Michaelis Komplexe von reduzierter XenA mit vier verschiedenen Substraten bestimmt werden. Dabei gelang es zum ersten Mal 2-Cyclohexenon im aktiven Zentrum eines Proteins zu beobachten. Schließlich beweisen wir durch diese Strukturen die redoxabhängige Substratbindung von XenA.

Zusammenfassend ermöglichen unsere Ergebnisse detaillierte Einblicke in den Reaktionsmechanismus von XenA und erweitern unser Wissen über die Interaktion von Flavoenzymen mit ihren Substraten.

Summary

Xenobiotic reductase A (XenA) from *Pseudomonas putida* 86 is a member of the Old Yellow Enzyme family of FMN containing enzymes. It catalyzes the NADH/NADPH dependent reduction of various substrates, including 2-cyclohexenone, coumarin, 7- and 8-hydroxycoumarin in a two-step mechanism consisting of a reductive and an oxidative half-reaction. The overall structure of the family members is similar but the active site residues show considerable variations. One distinct difference of XenA compared to other members is the presence of a cysteine residue (Cys25) in the active site, where most other members have a threonine. Further, the active site of XenA is lined up by two tyrosine (Tyr27 and Tyr183) and two tryptophan (Trp302 and Trp358) residues.

To get a better understanding of the reaction mechanism of XenA we analyzed the enzyme using a combination of transient and steady-state kinetics, redox potentiometry and crystal structure analysis. Thermodynamic and kinetic investigations revealed a preference of XenA for NADPH over NADH. Furthermore, the reaction catalyzed by XenA follows a ping-pong mechanism in which both substrates are bound to the same position in the active site but interact with different amino acids. The crystal structures of XenA without and with coumarin bound to the active site were solved at true atomic resolution. The oxidized complex with coumarin showed a compressed active site geometry in which the isoalloxazine ring of FMN is sandwiched between coumarin and the protein backbone. The crystal structure of reduced XenA showed a distortion of the isoalloxazine ring and the movement of Trp302 into the active site.

Furthermore, we analyzed the individual contributions of the five active site residues using site-directed mutagenesis. An exchange of Cys25 against serine shifted the reduction potential of the FMN/FMNH⁻ couple by +82 mV, increased the limiting rate constant of the reductive and decreased the limiting rate constant of the oxidative half-reaction. Therefore we conclude that Cys25 modulates substrate binding and the reduction potential of FMN.

Moreover, we revealed that Tyr27 contributes to the stabilization of the transition state during the reductive half-reaction by an interaction of its hydroxyl group with the transferred hydride ion. The exchange of Tyr183 resulted in a decreased affinity of XenA for NADPH and a considerable decrease of the rate of the oxidative half-reaction. These results are in agreement with its function as indispensable proton donor in the oxidative half-reaction.

Exchanging Trp302 resulted in multiphasic kinetics for both half-reactions and a decreased affinity of XenA for NADPH. In combination with its movement between the reduced and oxidized state of XenA, we propose a redox dependent shaping of the active site by Trp302.

Hence, this residue is responsible for the correct positioning of the substrates in both half-reactions, which is an essential part in the reaction mechanism. The results from the exchange of Trp358 indicated that this residue is involved in the orientation of the nicotinamide ring of NAD(P)H by spatial exclusion.

Crystal structures of enzyme substrate complexes are usually determined from non-reactive states. The Y183F variant of XenA, lacking the proton donor of the oxidative half-reaction, allowed us to freeze-trap the true Michaelis complexes of reduced XenA in complex with four different substrates. For the first time we were able to observe 2-cyclohexenone in an active site. Finally, we prove that mode of substrate binding of XenA is redox dependent.

In summary our results provide a more detailed description of the reaction mechanism of XenA and offer new insights on how substrates interact with flavoenzymes.

1 Introduction

1.1 The Old Yellow Enzyme family of flavoproteins

1.1.1 Old Yellow Enzyme

In 1932 Warburg and Christian isolated a yellow colored protein from brewer's bottom yeast (*Saccharomyces carlsbergensis*) during attempts to investigate the nature of biological oxidations (Warburg & Christian, 1932). They named it 'das gelbe Ferment' or 'Yellow Enzyme'. Upon the discovery of a second 'new' yellow enzyme from yeast in 1938, the earlier found enzyme was termed 'Old Yellow Enzyme' (OYE), which remained its name until today (Haas, 1938). In 1935 Theorell purified the Old Yellow Enzyme and showed that it was composed of a colorless apoprotein and a yellow dye, both later shown to be essential for enzyme activity (Theorell, 1935). The yellow dye had similar characteristics like vitamin B_2 (riboflavin), which was isolated from whey in 1879 (Blyth, 1879). In the following Theorell could clarify the identity of the riboflavin analogue to be riboflavin-5'-phosphate, now termed flavin mononucleotide (FMN) (Theorell, 1955). These initial studies provided the starting point of flavoprotein research. Since then, OYE has been characterized in detail and considerable knowledge about the mechanism of the enzyme has been gained. The physiological reductant of OYE is assumed to be nicotinamide adenine dinucleotide phosphate (NADPH), while the physiological oxidative substrate is still unknown. There are a large number of substrates capable of reoxidizing OYE. Methylene blue, ferricyanide and molecular oxygen are assumed to be alternative electron acceptors due to their slow reactivity compared to others like quinones and the olefinic bonds of α,β-unsaturated compounds (Massey *et al.*, 1969; Vaz *et al.*, 1995).

1.1.2 Members of the Old Yellow Enzyme family

Since the first investigation of OYE many homologous enzymes, which share similar amino acid sequences, have been discovered in yeasts, Gram-positive and Gram-negative bacteria, plants and protozoa - mostly through genome sequencing projects in the late 20th century. For example in the genomes of *Saccharomyces carlsbergensis* (Saito *et al.*, 1991) and *Saccharomyces cerevisiae* (Niino *et al.*, 1995) the presence of at least two closely related OYE genes was discovered. In bacteria investigations in the degradation of nitrate esters, morphine alkaloids, *N*-ethylmaleimide and other xenobiotic compounds revealed several homologous proteins. OYE homologues in plants were first identified in studies of gene induction under different growth conditions. A short summary of well-known OYE

homologues is given in Table 1.1.

Table 1.1: Summary of well-known OYE homologues
Old organism names are given in brackets. From the blue highlighted enzymes structures have been published.

Enzyme name	Organism of Origin	Reference
Bacteria		
morphinone reductase	*Pseudomonas putida* M10	(French & Bruce, 1994)
PETN reductase	*Enterobacter cloacae* PB2	(French *et al.*, 1996)
GTN reductase (NerA)	*Agrobacterium radiobacter*	(Snape *et al.*, 1997)
NemA	*Escherichia coli* W2252	(Miura *et al.*, 1997)
2-cyclohexen-1-one reductase	*Pseudomonas syringae*	(Rohde *et al.*, 1999)
XenA	*Pseudomonas putida* II-B	(Blehert *et al.*, 1999)
XenB	*Pseudomonas fluorescens* I-C	(Blehert *et al.*, 1999)
XenA-XenF	*Pseudomonas putida* KT2440	(van Dillewijn *et al.*, 2008)
YqjM	*Bacillus subtilis*	(Fitzpatrick *et al.*, 2003)
SYE1-4	*Shewanella odeidensis*	(Brige *et al.*, 2006)
TOYE	*Thermoanaerobacter pseudethanolicus* E39	(Adalbjörnsson *et al.*, 2010)
Yeasts		
OYE1	*Saccharomyces pastorianus* (*Saccharomyces carlsbergensis*)	(Saito *et al.*, 1991)
OYE2-3	*Saccharomyces cerevisiae*	(Stott *et al.*, 1993) (Niino *et al.*, 1995)
KYE	*Kluyveromyces lactis*	(Miranda *et al.*, 1995)
HYE1-3	*Pichia angusta* (*Hansenula polymorpha*)	(Komduur *et al.*, 2002)
OYE	*Kluyveromyces marxianus* (*Candida macedoniensis*)	(Kataoka *et al.*, 2004)
Protozoa		
TcOYE	*Trypanosoma cruzi*	(Kubata *et al.*, 2002)
Plants		
*Le*OPR1-2	*Lycopersicon esculentum*	(Strassner *et al.*, 1999)
*At*OPR1-3	*Arabidopsis thaliana*	(Schaller & Weiler, 1997) (Biesgen & Weiler, 1999) (Schaller *et al.*, 2000)
*Os*OPR1	*Oryza sativa*	(Sobajima *et al.*, 2003)

Albeit the investigations on OYE members started nearly 80 years ago, no single physiological role has emerged to explain the relatively high degree of amino acid sequence similarity between the enzymes. Additionally, more distantly related proteins can be found in

bacteria, nematodes and humans. Examples in bacteria are the trimethylamine dehydrogenase from the methylotrophic bacterium W_3A_1 (Lim *et al.*, 1986), the enoate reductases of *Clostridia* (Rohdich *et al.*, 2001) or the 2,4-dienoyl coenzyme A reductase from *Escherichia coli* K-12 (He *et al.*, 1997). In humans and nematodes, the homologous enzymes *Nr1* (Paine *et al.*, 2000) and DCS-1 (Kwasnicka *et al.*, 2003) can be found respectively. In these multidomain proteins an OYE-related domain forms part of the enzyme. These enzymes show strong sequence conservation in the core region, whereas the putative active site residues differ from closely related OYE homologues. In contrast to OYE1, which has a common binding site for reductive and oxidative substrate, these multidomain enzymes have separate sites presumably to optimize catalysis of both reactions.

1.1.3 The structure of OYE family members

The first crystallization experiments with OYE were carried out by Theorell in 1955. But it took about 40 years to get X-ray quality crystals of recombinant OYE1 from *Saccharomyces carlsbergensis*, from which the protein structure could be determined (Fox & Karplus, 1994). The structure revealed that OYE1 belongs to the family of the Class I, eight stranded α,β-barrel flavoproteins (Phillips *et al.*, 1978). The (α,β)$_8$-barrel consist of eight parallel β-strands surrounded by eight α-helices, where each β-strand is connected by a loop to an outer α-helix (see Figure 1.1).
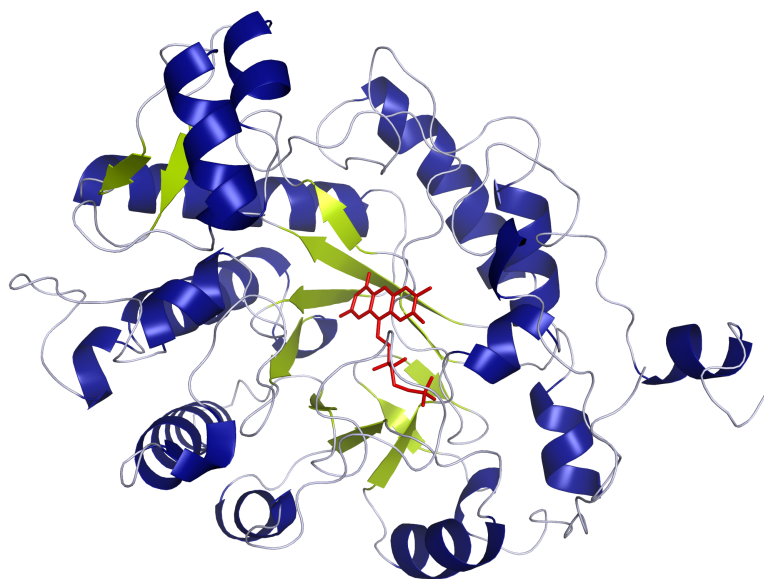
**Figure 1.1:** **Top view on the (α,β)$_8$-barrel of OYE1 from *Saccharomyces pastorianus*.** In the ribbon presentation α-helices are displayed in blue and β-sheets are displayed in green. The FMN cofactor is depicted as a stick model in red (picture generated from PDB 1OYA (Fox & Karplus, 1994) with MacPyMOL).

Amino acids of the loop regions between β-strands and α-helices show the largest sequence variability. Typical for OYE α,β-barrels is that the N-terminus is folded in a hairpin, which closes the bottom of the barrel. This region shows conservation of amino acid residues, presumed to be critical in determining the overall fold of the protein.

Nine structures of OYE homologues have been published to date (highlighted in blue in Table 1.1). The quaternary structures of these homologues differ from each other. While OYE1 (French & Bruce, 1994) and morphinone reductase (Barna *et al.*, 2002) are present as homo/heterodimers, PETN reductase (Barna *et al.*, 2001), *Le*OPR1 (Breithaupt *et al.*, 2001), *Le*OPR3 (Breithaupt *et al.*, 2006), *At*OPR1 (Fox *et al.*, 2005), *At*OPR3 (Malone *et al.*, 2005) as well as many other members are present as monomers. However, the monomeric structure of the OPR enzymes from *Arabidopsis thaliana* may be artificially enforced by the N-terminal His-tag used for purification. Furthermore, YqjM (Kitzing *et al.*, 2005) is present as tetramer and TOYE (Adalbjörnsson *et al.*, 2010) was found to exist in multiple oligomeric states. Whereas in OYE1 the residues 206-216 are part of the dimer interface, in other enzymes the corresponding region is supposed to be a binding site for unknown proteins even though this area is conserved throughout the OYE family (Williams & Bruce, 2002). The average size of the monomers of the OYE family members is around 40 kDa.

The FMN cofactor is always non-covalently bound at the C-terminal top of the barrel and is anchored by an extensive hydrogen-bonding network between the protein matrix and the ribityl phosphate side chain. The *si*-face of the flavin is accessible to the solvent and forms the bottom of the active site. For many of the published structures it was shown that an anion is bound to the *si*-face of the FMN. The isoalloxazine ring is in hydrogen-bonding distance to the backbone and side chain of surrounding residues. Amino acids that contact the FMN with their side chains are more strongly conserved, than amino acids that interact via their backbones. Side chain residues, which lie directly above the plane of the isoalloxazine ring, are either involved in catalysis or form the hydrophobic substrate-binding pocket.

OYE homologues in their oxidized state are able to bind various ligands. For OYE1 (Fox & Karplus, 1994), PETN reductase (Barna *et al.*, 2001), *Le*OPR1 and *Le*OPR3 (Breithaupt *et al.*, 2009) crystal structures in complex with several ligands have been published. Although a ligand bound to the oxidized form of the protein does not represent the physiological binding situation, the crystal structures in combination with site-directed mutagenesis studies can provide insights in the catalytic mechanism and substrate specificities across the OYE family.

In general the aromatic substrates are positioned more or less coplanar to FMN and form π-π interactions with the isoalloxazine ring. In OYE1 His191 and Asn194 are important in binding carbonyl oxygen atoms of α/β-unsaturated substrate molecules and position the β-carbon above the N(5) atom of the FMN. Tyr196 was shown to transfer a proton to the α-carbon of the substrate. While His191 is conserved throughout the OYE family, in half of the homologues mentioned in Table 1.1 Asn194 is replaced by a histidine residue. However, these residues are assumed to have the same function. Tyr196 can be found in all OYE members from Table 1.1 except morphinone reductase, where a cysteine occupies this position. Kinetic investigations of the corresponding residues in morphinone reductase (Barna *et al.*, 2002), PETN reductase (Khan *et al.*, 2005) and NerA (Marshall *et al.*, 2004) revealed high activity in the oxidative half-reaction after exchanging them to alanine (morphinone reductase) and phenylalanine (PETN reductase, NerA). The oxidative half-reaction of Y196F-OYE1 was performed with various substrates and revealed a substrate-dependent decrease of the limiting rate constants. Kohli and Massey proposed that this effect is either due to a concerted transfer of hydride and proton or the stabilization of the transition state for the hydride transfer (Kohli & Massey, 1998). As for morphinone reductase, PETN reductase and NerA different oxidative substrates were used, it is difficult to compare the results to OYE1, but it seems that in these enzymes the corresponding residues are not function as proton donors.

Differences in the active site residues between the OYE homologues do not alter the position of the substrates significantly. For the binding of large ligands like steroids, the loop regions at the top of the α,β-barrel are more important and consequently it is in these loops where the structures of OYE family members differ most, as seen in Figure 1.2.

Structural studies on NAD(P)H binding were performed with OYE1 (Fox & Karplus, 1994), morphinone reductase (Pudney *et al.*, 2007) and TOYE (Adalbjörnsson *et al.*, 2010). In OYE1 the crystals were soaked with the substrate analogue α-O^2-6B-cyclo-1,4,5,6-tetrahydro-nicotinamide adenine dinucleotide phosphate (c-THN)TPN whereas in morphinone reductase and TOYE the crystals were soaked with the substrate analogue 1,4,5,6-tetrahydro-nicotinamide adenine dinucleotide (NADH$_4$). The structures revealed that the nicotinamide moiety binds similarly to phenolic substrates through different hydrogen bonding interactions with the protein environment and stacking interactions with the FMN. In this position the C(4) atom of the reductive substrate (hydride donor) is positioned above the N(5) atom (hydride acceptor) of the flavin (for detailed FMN structure see chapter 1.1.4).
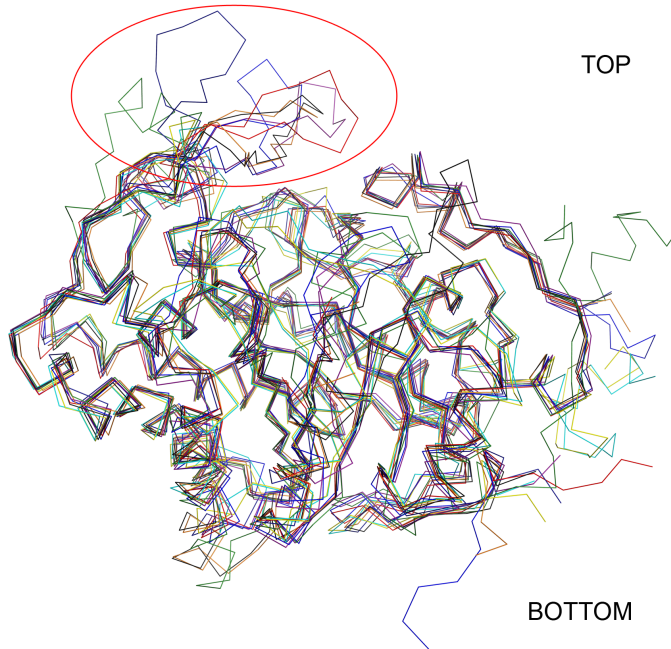
Figure 1.2: **Superposition of Cα backbones of OYE family members.** The protein structures used for the superposition are: OYE1 (1OYA) in green, morphinone reductase (1GWJ) in blue, PETN reductase (1H50) in purple, YqjM (1Z41) in yellow, *Le*OPR1 (1ICS) in red, *Le*OPR3 (2HSA) in grey, *At*OPR1 (1VJI) in deep blue, *At*OPR3 (1G45) in orange and TOYE (3KRU) in cyan. The red circle highlights the major structural differences between the OYE family members at the top of the α,β-barrel. The superposition was performed with COOT (Emsley & Cowtan, 2004) and the picture was generated from PDB codes given in brackets with MacPyMOL.

Structures of two-electron reduced OYE homologues were published for OYE1 (Fox & Karplus, 1994), PETN reductase (Barna *et al.*, 2001) and YqjM (Kitzing *et al.*, 2005). For reduction the protein crystals were soaked with sodium dithionite, sodium borohydride and NADPH respectively. The overall structure of these enzymes remained the same. The anion, bound to the *si*-face of the FMN, was replaced by two water molecules; this reflects the changed electron state of the cofactor. For OYE1 and PETN reductase the isoalloxazine ring shows a butterfly bend along the N(5)-N(10) axis upon reduction. However, in YqjM this bending was already present in the oxidized state and no further movement was observed.

In summary, the monomeric structure of the OYE family members shows the (α,β)$_8$-barrel-fold, while the quaternary structure for the family members differs. The FMN cofactor is bound in the same manner to the (α,β)$_8$-barrel in all homologues and some variation in the amino acids in the active site have been observed. The OYE homologues are able to bind ligands in the oxidized state. The binding behavior was shown to be similar for different enzymes, but these are non-productive complexes and do not necessarily correspond in structure to the Michaelis-complex.

1.1.4 Flavin chemistry

Several hundreds of flavoenzymes have been identified and characterized. It is estimated that 1-3% of the genes in bacterial and eukaryotic genomes encode flavin binding proteins (Nishino *et al.*, 2005). These enzymes contain FMN or flavin adenine dinucleotide (FAD) as cofactor, which are either covalently or non-covalently bound to the protein. The cofactors are generated from riboflavin as precursor (see Figure 1.3). Riboflavin can be synthesized by plants, many bacteria and fungi, but not by animals, which have to take it up by ingestion as vitamin B_2 (De Colibus & Mattevi, 2006).

The isoalloxazine moiety of the flavin cofactor is relatively electron deficient and is the part of the molecule, which is involved in catalysis. It offers several possibilities for interactions with the protein environment. The dimethylbenzene moiety is hydrophobic and therefore can interact with hydrophobic protein areas whereas the pyrimidine ring is hydrophilic and is able to form hydrogen bonds with the protein.
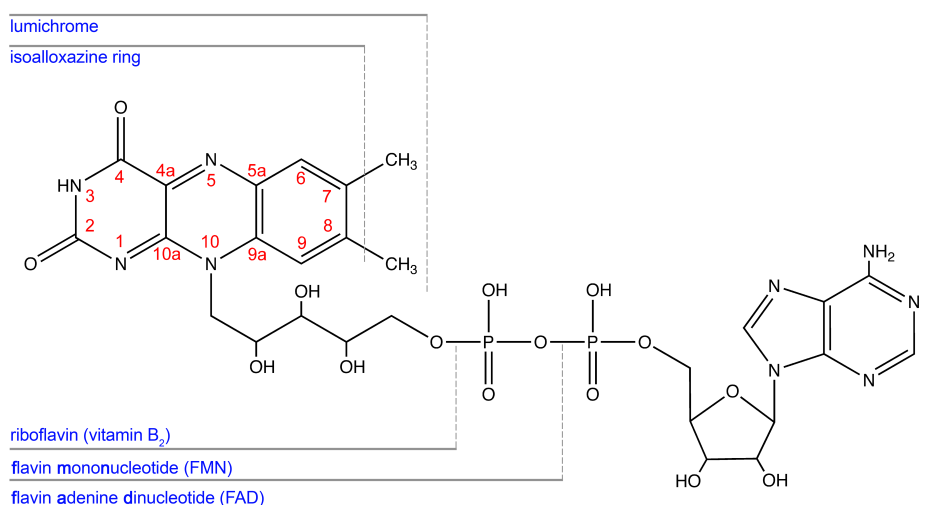
Figure 1.3: **Structure formula of flavin in the oxidized state.**

The flavin can undergo one- and two-electron reactions with the formation of three redox states: quinone (oxidized), semiquinone (radical one electron reduced) and hydroquinone (two electron reduced). Figure 1.4 displays the redox and ionization states of the isoalloxazine ring that play a role in reactions catalyzed by flavoproteins. Due to the distinct protonation patterns in the three redox-states of FMN, different modes of hydrogen bonding interactions can occur with the protein. Each of these redox-levels has very different chemical properties and shows large spectral differences, which provide the possibility to identify them and to monitor events occurring in catalysis. Depending on the protein environment in some

enzymes almost 100 % stabilization of either neutral or anionic semiquinone can be observed, while others do not show semiquinone stabilization at all (Massey, 2000). In the OYE family no detectable amounts of semiquinone species under equilibrium conditions could be observed for PETN reductase (Khan *et al.*, 2002), morphinone reductase (Craig *et al.*, 1998) and YqjM (Fitzpatrick *et al.*, 2003) whereas in OYE1 15-20% of anionic semiquinone was detected (Stewart & Massey, 1985).
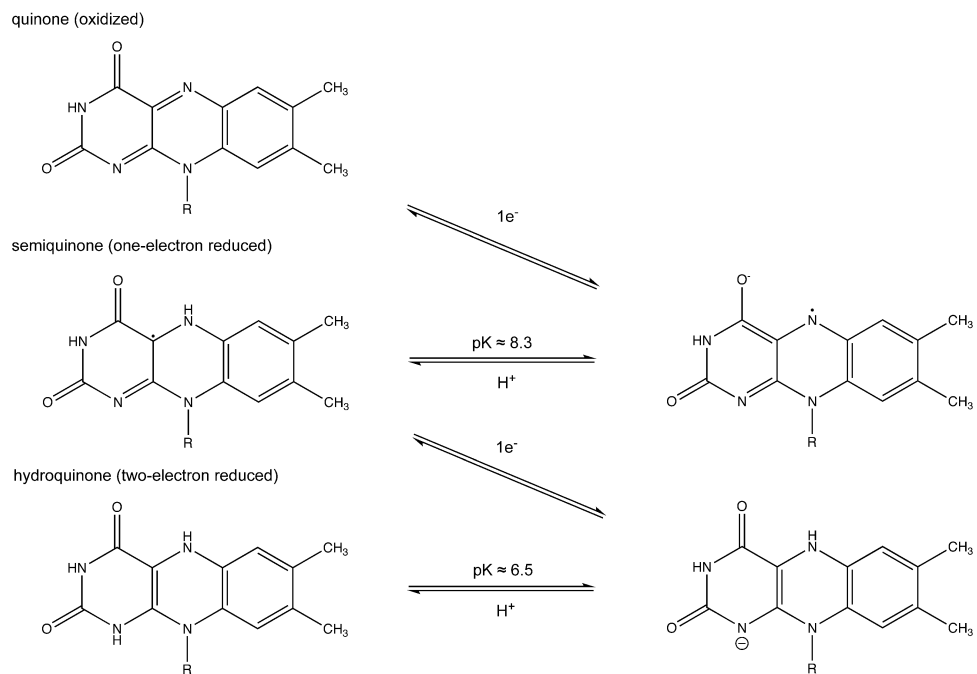
Figure 1.4: **Different redox and ionization states of flavin under physiological conditions.** Given pK_a values are from free flavin in solution. (modified from (Kao *et al.*, 2008))

During reduction the isoalloxazine ring becomes electron rich. Investigations of the electrostatic surface potential of the flavin nucleus by Breinlinger *et al.*, illustrate the areas of changed charge densities (see Figure 1.5). Mostly the positions C(4a) to N(5) are involved in the electron uptake and donation.

The reduction potential of free flavins at neutral pH is about -200 mV, whereas the reduction potentials of the protein-bound cofactors range from -500 mV to +80 mV (Müller, 1983). This corresponds to a free energy difference ($\Delta\Delta G$) of more than 10 kcal/mol, which is an extensive energy range for a single covalent structure. The redox properties of the flavin nucleus are controlled by apoprotein-flavin interactions. These interactions include hydrogen bonding, aromatic stacking and less apparent dipolar/multipolar and steric effects (Cuello *et al.*, 2000).
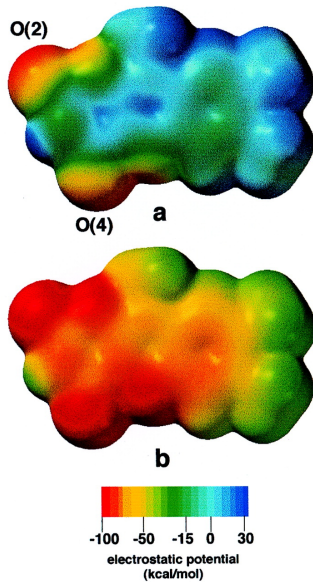
Figure 1.5: **Electrostatic potential maps of (a) the oxidized flavin (Fl_{ox}) and (b) the flavin radical anion (Fl_{red}^-)** (taken from (Breinlinger *et al.*, 1998)).

The effect of the protein environment on the reduction potential has been demonstrated for different OYE family members. In morphinone reductase (Messiha *et al.*, 2005; Messiha *et al.*, 2005), PETN reductase (Khan *et al.*, 2005; Khan *et al.*, 2004) and OYE1 (Xu *et al.*, 1999) substitutions of single amino acids in the FMN binding site altered the reduction potential of the two-electron reduction in the wild type enzymes from -20 to 50 mV.

Due to their chemical versatility, flavoproteins participate in a broad range of biological activities. They have a central role in redox reactions and are involved in nonredox processes, such as blue light perception in plants (Briggs & Huala, 1999), regulation of biological clocks (Cashmore *et al.*, 1999) or DNA repair (Sancar, 1994).

1.1.5 The catalytic mechanism

OYE homologues were found to catalyze quite different reactions: reductive denitrification of nitro-esters and nitro-aromatics, reduction of the aromatic ring of nitro-aromatics and the reduction of unsaturated α/β-bond in aldehydes and ketones. Some examples are shown in Figure 1.6. In many cases the physiological substrate is still unknown and not all enzymes are capable of catalyzing all reactions, but 2-cyclohexenone is observed to be a substrate in most OYE homologues. Although the substrates are very different, the overall reaction mechanism of OYE family members is similar. With only one binding site containing the non-covalently bound FMN, the enzymes act through a ping-pong Bi-Bi mechanism in which the cofactor NAD(P)H and the substrate use the same binding site. So the overall reaction proceeds via two steps - a reductive and an oxidative half-reaction, which can be individually analyzed by

rapid reaction techniques. All OYE homologues have characteristic UV-Vis spectra due to the conjugated double bonds of the isoalloxazine ring system of the cofactor. The spectra show peak maxima around 360 and 450 nm, depending on the protein environment of the FMN. During reduction these maxima vanish and the protein becomes colorless. These spectral changes form the basis for rapid reaction measurements, such as stopped-flow spectrophotometry.
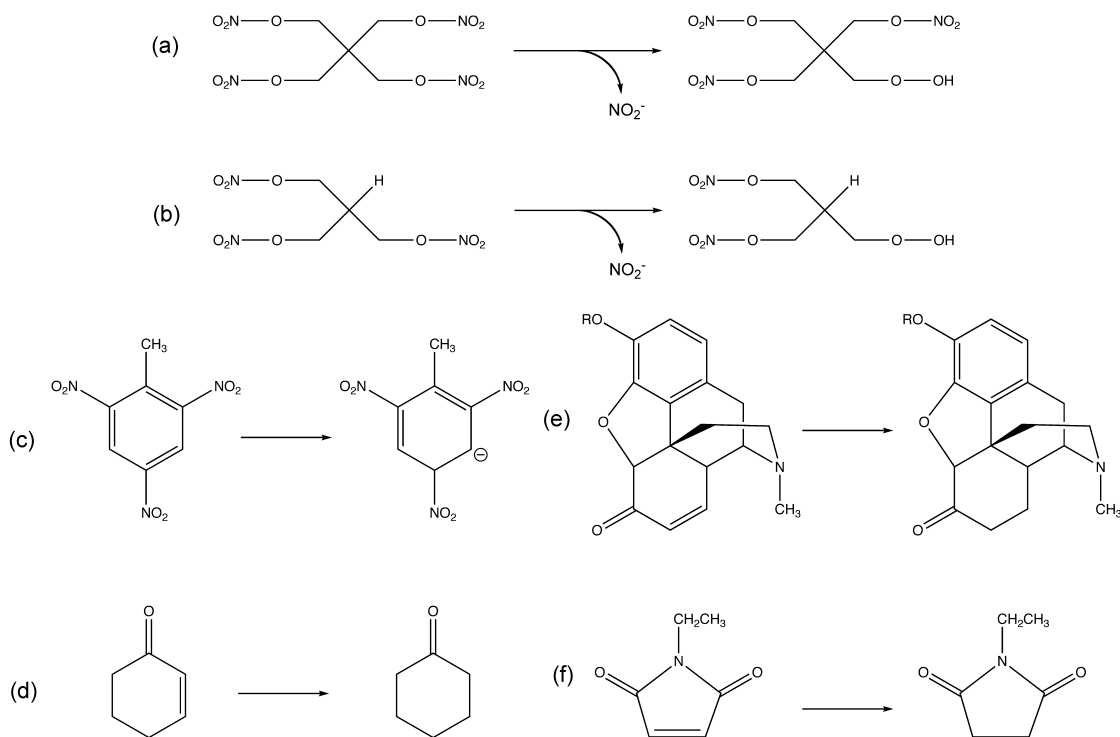
Figure 1.6: **Different reactions catalyzed by OYE family members.** (a) and (b): reductive denitrification of pentaerythritol tetranitrate (PETN) and glycerol trinitrate (nitroglycerine, GTN); (c): reduction of the aromatic ring of trinitrotoluene (TNT); (d): reduction of 2-cyclohexenone; (e): reduction of morphinone (R = H) and codeinone (R = CH$_3$); (f): reduction of N-ethylmaleimid (adapted from (Williams et $al.$, 2004)).

Reductive and oxidative half-reactions have been extensively investigated for OYE1 (Massey & Schopfer, 1986), morphinone reductase (Craig et $al.$, 1998), PETN reductase (Khan et $al.$, 2002) and YqjM (Fitzpatrick et $al.$, 2004). In the first step - the reductive half-reaction - the enzyme is reduced by either NADH or NADPH. The physiological reductant of many OYE family members is assumed to be NADPH, whereas NemA and morphinone reductase prefer NADH. The mechanism by which the enzymes discern between the two nicotinamides is yet unknown (Brige et $al.$, 2006). With stopped-flow measurements it is possible to distinguish between kinetically individual steps during reduction (see Figure 1.7a). For OYE1 two

oxidized enzyme intermediates were observed before the reduction of enzyme-bound flavin takes place. The first step is the binding of NAD(P)H and the formation of a Michaelis-complex. This initial binding step is followed by a charge-transfer complex between the FMN (charge-transfer acceptor) and NAD(P)H (charge-transfer donor). Finally, the reduced enzyme is formed by the reduction of the flavin and the release of $NAD(P)^+$. In the case of PETN reductase, morphinone reductase and YqjM the discrete binding step prior to the charge-transfer complex formation was not observed.

(a) $E_{ox} + NAD(P)H \rightleftharpoons E_{ox}NAD(P)H \rightleftharpoons E_{ox}NAD(P)H^{CT} \rightleftharpoons E_{red}NAD(P)^+ \rightleftharpoons E_{red} + NAD(P)^+$

(b) $E_{red} + Substrate_{ox} \rightleftharpoons E_{red}Substrate_{ox}{}^{CT} \rightleftharpoons E_{ox}Substrate_{red} \rightleftharpoons E_{ox} + Substrate_{red}$
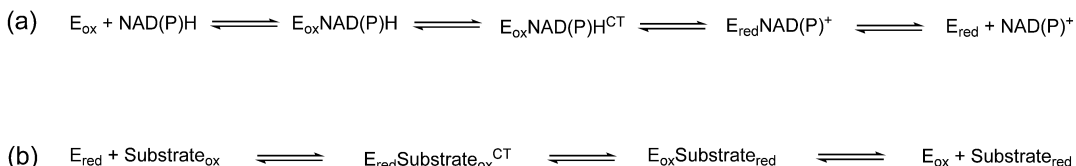
Figure 1.7: **General kinetic scheme for (a) reductive and (b) oxidative half-reactions of OYE family members.** The initial formation of a Michaelis-complex was only observed for OYE1 but not for PETN reductase, morphinone reductase and YqjM.

The oxidative half-reactions of OYE homologues comprise the reduction of different types of substrates. Each enzyme is capable of reducing many different substrates more or less efficiently. 2-cyclohexenone was used as model substrate for the investigation of the oxidative half-reaction of OYE1 (Kohli & Massey, 1998), PETN reductase (Khan *et al.*, 2002) and YqjM (Fitzpatrick *et al.*, 2004). For morphinone reductase the reaction was first performed with the physiological substrate codeinone (Craig *et al.*, 1998) and later with 2-cyclohexenone (Messiha *et al.*, 2005). As in the reductive half-reaction, several individual steps could be discerned for the homologues in the oxidative half-reaction (see Figure 1.7b). In morphinone reductase three resolvable steps were observed during reduction of codeinone. The first was the formation of a charge-transfer complex between reduced FMN and substrate, followed by flavin reoxidation and finally the release of hydrocodone from the oxidized enzyme. However, for the reaction of 2-cyclohexenone with reduced PETN and YqjM no initial charge-transfer formation or product release were observed. Thus, a one step reaction mechanism was assumed to evaluate the kinetic data.

The reaction mechanisms of oxidative half-reactions of OYE homologues have been studied in detail for different substrates. In Figure 1.8 a general scheme for the reaction mechanism of the oxidative half-reaction with 2-cyclohexenone is shown.

For example the reduction of different α/β-unsaturated carbonyls by OYE1 was first investigated by Vaz and co-workers in 1995 (Vaz *et al.*, 1995). Different aldehydes, ketones,

esters, amides, nitriles and acids were tested for their ability to oxidize the reduced enzyme. However, only aldehydes and ketones acted as oxidative substrates. The carbonyl groups of these compounds are more basic than those of esters and amides and than cyano groups. Therefore, hydrogen-bonding interactions between the carbonyl oxygen and an active site residue, like His191 in OYE1, increase the electrophilicity of the β-carbon towards the flavin hydride. To prove the hydride transfer from the N(5) of FMN, Vaz and co-workers tested different alkyl substituents at the α- and β-carbon of the substrates. They found that only substituents in β-position decrease the rate for hydride transfer to the olefinic bond, because of the steric hindrance. Hence the hydride transfer occurs from the reduced FMN to the β-carbon of the substrate (Vaz *et al.*, 1995).

The putative proton donor to the α-carbon in OYE1 could be identified using site directed mutagenesis of active site residues as Tyr196 (Kohli & Massey, 1998). In morphinone reductase, the identification of the possible proton donor failed and Messiha and co-workers infer the solvent as proton source (Messiha *et al.*, 2005). The same assumption was drawn for PETN reductase, where the corresponding residue Tyr186 was also shown not to be involved in a rate-limiting step (Khan *et al.*, 2005).
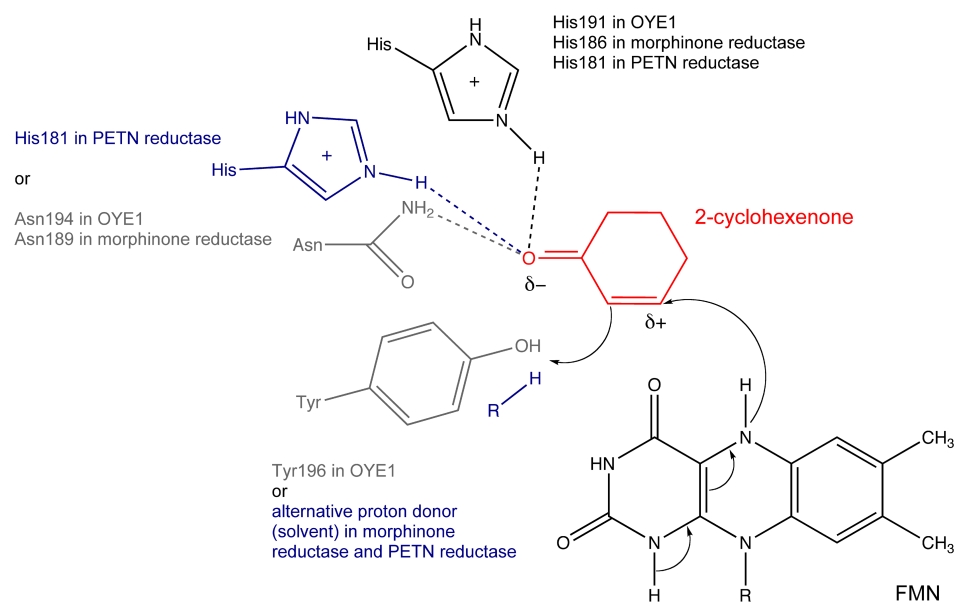
Figure 1.8: **Proposed reaction scheme of the oxidative half-reaction of OYE family members.** In the first step the α/β-unsaturated double bond is polarized by binding to active site residues. This enables the hydride transfer from flavin, followed by the proton addition from an active site residue or the solvent. (adapted from (Messiha *et al.*, 2005))

1.1.6 Quantum tunneling

Over the last 60 years transition state theory (TST) has been used to explain enzyme-catalyzed reactions (Kraut, 1988). TST describes the catalysis of enzymes by lowering the energy required to surmount the 'static' potential energy barrier between reactants and products. In the late 1980s and 1990s the first indications appeared, that the TST could not be used in all cases. A modified form of the TST, which incorporates a quantum tunneling correction (Bell, 1980), could model these observed abnormalities. This correction permits the tunneling of light particles below the saddle point of the potential energy surface. In 1996 Jonsson and co-workers observed large deviations from classical TST, which could not be explained by quantum tunneling correction alone (Jonsson *et al.*, 1996). In reactions, which proceed mostly by quantum tunneling, the kinetic isotope effects (KIE) are greater than expected values for the reaction because of the higher probability of hydrogen over deuterium tunneling. A deuterium atom is much heavier than a hydrogen atom and therefore the probability of tunneling is reduced. In these reactions the KIE is independent of temperature. Studies on the methylamine dehydrogenase revealed that the KIE was temperature independent but the reaction rate was strongly dependent on the temperature. Thus, it was proposed that temperature dependent fluctuations of the enzyme-substrate complex are required to distort the active site geometry to increase the tunneling probability. These fluctuations give rise to the strong temperature dependence of the reaction (Basran *et al.*, 1999).

Proton tunneling has also been shown to play a role in reductive and oxidative half-reactions of PETN reductase and morphinone reductase. The mechanisms of flavin reduction and oxidation in both enzymes were studied by stopped-flow analysis with NAD^2H and $NADP^2H$. In morphinone reductase KIE and reduction rates are temperature dependent. In this case the hydride transfer has a major tunneling component, which is driven by thermally induced vibrations of the protein and is called active or vibrationally gated hydride transfer. In PETN reductase the KIE is independent of the temperature in contrast to the strongly temperature-dependent reaction rate. Here the active site might be more optimally configured for hydride transfer and thus requires little or no vibrational assistance and is called passive hydride transfer. These studies indicated additionally that the hydride transfer from the reduced flavin in morphinone reductase to the substrate 2-cyclohexenone occurs also by tunneling but without temperature dependence of the KIE and is therefore of passive nature. This was the first time that both active and passive tunneling could be observed in the same enzyme (Basran *et al.*, 2003).

1.1.7 Physiological roles

The search for the physiological function of OYE homologues is difficult because of the broad substrate range. The high degree of conservation in regions of the primary and tertiary structures throughout the family would suggest that the enzymes are orthologous. If this is true, the 'single' physiological substrate has yet to be found. The reduction of nitro-esters or other xenobiotic compounds and therefore a general role in detoxification would be attractive. However, the question remained, why such a 'general purpose' enzyme did not undergo evolutionary changes (Williams & Bruce, 2002). Nevertheless, for some homologues tentative and real physiological functions are known.

First knockout mutagenesis studies on *OYE2* and *OYE3* genes from *Saccharomyces cerevisiae* gave no phenotypic difference from wild-type *Saccharomyces cerevisiae*. Later it was shown that the proteins OYE2 (Gasch *et al.*, 2000) and OYE3 (Lee *et al.*, 1999) are strongly induced by H_2O_2 with other oxidative stress response genes. The reactive oxygen species (ROS) produced by hydrogen peroxide react with the sulfhydryls of cysteines to initiate disulfide bond formation. In 2004 Haarer and Amberg could demonstrate that OYE2 reduces the disulfide bridge between Cys284 and Cys374 of actin filaments. Thereby, OYE2 controls the plasticity of the cytoskeleton and protects it from oxidative damage (Haarer & Amberg, 2004). In 2005 Reekmans and co-workers showed that OYE3 interferes with Bax- and H_2O_2-induced cell death. Bax is an important protein in the regulation of apoptosis (Reekmans *et al.*, 2005).

In 2003 Fitzpatrick and co-workers found that the bacteria homologue YqjM from *Bacillus subtilis* was strongly induced by the addition of xenobiotic nitro compounds like GTN and TNT to the medium, which lead to the suggestion that YqjM plays a role in detoxification. However TNT is also known to cause the production of hydrogen peroxide, which causes oxidative stress. Tests with the oxygen stressor H_2O_2 revealed also an increased level of YqjM in the cells indicating its involvement in oxidative stress response, too. Therefore the exact role of the enzymes still remains unclear (Fitzpatrick *et al.*, 2003).

Plant homologues are involved in the metabolism of larger lipid molecules with α/β-unsaturated carbonyl functions (Schaller & Weiler, 1997; Strassner *et al.*, 1999). *At*OPR1 (Schaller & Weiler, 1997) and *At*OPR3 (Schaller *et al.*, 2000) are shown to be a part of the Jasmonate signal pathway (Turner *et al.*, 2002). Jasmonates are signaling molecules produced in plants in response to wounding and other stresses.

*Tc*OYE from *Trypanosoma cruzi* (protozoa) was found to be involved in the prostaglandin pathway. This pathway is similar to the jasmonate signaling pathway and exists in mammals,

worms and protozoa. The prostaglandins mediate inflammatory responses, blood pressure, etc (Kubata *et al.*, 2002). However, the OYE homologue of *Trypanosoma cruzi* additionally participates in stress response.

1.1.8 Biotechnological applications

The enzymes of the OYE family are capable of catalyzing a wide range of chemical reactions, which can be important for industrial use.

One example is the reduction of alkaloids like morphinone and codeinone by morphinone reductase. Morphine and its derivatives are analgesics, which are of important use in clinical medicine today. The naturally occurring alkaloids morphine, codeine and thebaine can be isolated from opium poppy. The pharmaceutical properties of these drugs can be altered by small changes in their chemical structure. Hydromorphone for example is five to seven times more potent than morphine, whereas hydrocodone is a mild analgesic and antitussive. The chemical synthesis of these semi-synthetic opiates is difficult, because of the complexity of the molecules and their lack of functional groups (Hailes & Bruce, 1993). *Pseudomonas putida* M10 is able to use morphine and codeine as sole source of carbon. In the first two steps of this alkaloid degradation pathway morphine and codeine are converted into morphinone and codeinone and hydromorphone and hydrocodone. These steps are performed by morphine dehydrogenase and morphinone reductase, respectively (Hailes & Bruce, 1993). The coexpression of both genes in *Escherichia coli* resulted in an efficient production of the alkaloid derivatives in high yields (Boonstra *et al.*, 2001).

A second example is the reduction of nitro-esters, like GTN or PETN and nitro-aromatics, like TNT by many OYE homologues. These compounds are produced for use as vasodilators and explosives and are intermediates in the production of fertilizers, foams, dyes and other explosives. Most nitro-substituted compounds are toxic for all classes of organisms and therefore the decontamination of soils and groundwater is of great interest. Besides huge contamination of production sites, pollution can also be found around ammunition manufacturing facilities and munitions testing sites. An attractive strategy to get rid of these contaminations is phytoremediation by transgenic plants (Van Aken, 2009; Williams & Bruce, 2002). Advantages of plants over microorganisms are the high biomass, the deep root system and the transpiring of large volumes of groundwater. In 1999 French and co-workers designed the first transgenic plants. The bacterial gene of PETN reductase was introduced into tobacco plants (*Nicotania tabacum*). PETN reductase was derived from *Enterobacter cloacae* PB2, which was isolated from an explosive-contaminated soil (Binks *et al.*, 1996; French *et*

al., 1996). This OYE homologue is able to degrade TNT by either reduction of the nitro groups or the aromatic ring (see Figure 1.6) (French *et al.*, 1998). As result the transgenic tobacco plants showed higher tolerance to GTN and TNT than the wild type (French *et al.*, 1999). Phytoremediation through genetic transformation of plants is a current issue in environmental research and may help to overcome problems in detoxifying of contaminated soils.

1.2   Xenobiotic Reductase A from *Pseudomonas putida* 86

1.2.1   *Pseudomonas putida* 86

Pseudomonas putida 86 is a soil bacterium, which was isolated in 1988 from an area near a coal tar factory (Rütgerswerke) in Castrop-Rauxel in Germany (Schwarz *et al.*, 1988). *Pseudomonas putida* is a species of the family of *Pseudomonadaceae* and belongs to the genus *Pseudomonas* and within this genus to the fluorescent subgroup. These bacteria are chemoautotroph, gram negative and even or light bended rods with polar flagella. They are environmentally important microorganisms in soil and water due to their ability to use diverse organic compounds as a carbon source. Some of the species are known to use over 100 different compounds and only a few of them use less than 20. In contrast to other members of the genus, *Pseudomonas putida* 86 is not a pathogen (Madigan *et al.*, 2003).

1.2.2   Degradation of quinoline in *Pseudomonas putida* 86

Pseudomonas putida 86 was one of 16 bacterial strains, which were isolated during the search for quinoline degrading bacteria. Therefore it was shown that this organism is able to use quinoline as sole nitrogen-, carbon- and energy source (Schwarz *et al.*, 1988).

Quinoline (see Figure 1.9) and its derivatives are ubiquitous contaminants in nature. They are mainly released during combustion of fossil fuels and their environmental distribution is promoted by good water solubility and poor biodegradability. N-heterocyclic compounds are of special interest because they are more biologically active than homocyclic compounds. Many quinoline derivatives have been shown to be indirectly mutagenic. They can cause cancer and their wide distribution leads to an increasing number of persons that exhibit allergic reactions. Quinoline derivatives can also be found in drugs for the treatment of malaria, infections of skin and testis, leprosy or typhoid. Furthermore, they are used during the production of agrochemicals, dyes and paint. Naturally they are produced by higher plants, especially subtropical trees but can also be found in mammals, insects and some bacteria (Fetzner *et al.*, 1998).

Currently four quinoline degradation pathways in bacteria are known: the anthranilate pathway, the 5,6-dihydroxy-1*H*-2-oxoquinoline pathway, the 7,8-dihydroxy-1*H*-2-oxoquinoline pathway and the 8-hydroxycoumarin pathway (Fetzner *et al.*, 1998). The degradation of quinoline in *Pseudomonas putida* 86 was identified to occur via the 8-hydroxycoumarin pathway (Schwarz *et al.*, 1989). This pathway was first described by Shukla *et al.* on the basis of the identification of four intermediates (highlighted in blue in

Figure 1.9) (Shukla, 1986). Within this pathway the N-heterocyclic ring is cleaved to form 8-hydroxycoumarin. 8-hydroxycoumarin is further transformed into 2,3-dihydroxyphenylpropionate, which is then degraded via the citric acid cycle.
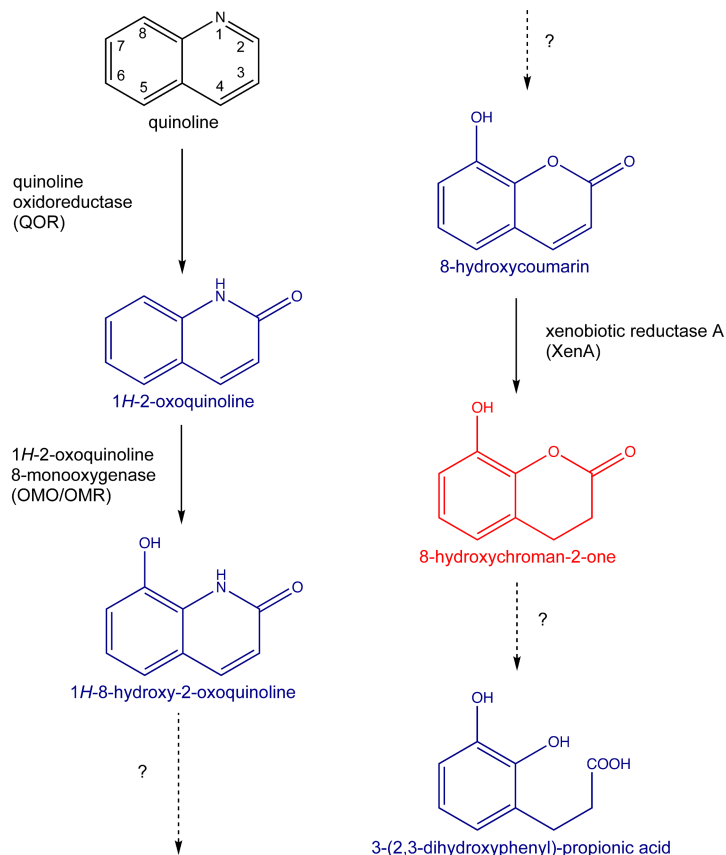

Figure 1.9: **Degradation of quinoline by *Pseudomonas putida* 86 *via* the 8-hydroxycoumarin pathway.** The first step is the hydroxylation at position C(2) catalyzed by quinoline oxidoreductase (QOR). The second hydroxylation at position C(8) is catalyzed by 1*H*-2-oxoquinoline 8-monooxygenase. The conversion to 8-hydroxycoumarin is still unknown. The reduction of the α,β-unsaturated double bond of 8-hydroxycoumarin is performed by xenobiotic reductase A, whereas the enzyme hydrolyzing 8-hydroxychromane-2-one to 2,3-(dihydroxyphenyl)-propionic acid is not known. The intermediates, which are highlighted in blue, were first identified by Shukla *et al* (Shukla, 1986). The intermediate, which is highlighted in red, was identified in our group (Griese *et al.*, 2006).

In 1995 and 1996 two enzymes have been investigated, that perform the initial steps in quinoline degradation. In the first step the hydroxylation of the C(2) of quinoline to form 1*H*-2-oxoquinoline is performed by the molybdo-iron-sulfur flavoprotein quinoline oxidoreductase (QOR) (Blase *et al.*, 1996). In the second step the hydroxylation of the C(8) position to form 1*H*-8-hydroxy-2-oxoquinoline is performed by the multicomponent enzyme 1*H*-2-oxoquinoline 8-monooxygenase (Rosche *et al.*, 1995). How the transformation from

1*H*-8-hydroxy-2-oxoquinoline to 8-hydroxycoumarin proceeds, is still unknown. In 2006 XenA was investigated in our group and was shown to catalyze the reduction of the unsaturated double bond of the heterocyclic ring to form 8-hydroxychroman-2-one (Griese *et al.*, 2006). To determine the products of this reaction real-time NMR spectra were recorded. 8-hydroxychroman-2-one was identified as the single product (highlighted in red in Figure 1.9). As a result it was postulated that this is the last step of the reaction before the heterocyclic ring is hydrolyzed to yield 2,3-(dihydroxyphenyl)-propionic acid. The mechanism of the ring-opening reaction has not been investigated yet.

1.2.3 Characteristics of XenA

XenA was identified as a NAD(P)H-dependent, intracellular, FMN-containing oxidoreductase that belongs to the OYE family. Based on gel filtration chromatography it was found, that XenA is a homodimeric enzyme with 361 amino acids and a size of 39.8 kDa per monomer. The crystal structure of the enzyme was refined to 1.5 Å resolution. A single residue (Trp302) was found to deviate from the Ramachandran statistics. This deviation might have functional relevance, as Trp302 is part of the FMN-binding site. The XenA monomer showed the typical $(\alpha,\beta)_8$-barrel fold (see chapter 1.1.3). One monomer is in the asymmetric unit and related to the second monomer by a crystallographic 2-fold axis, so that the barrel openings are facing in approximately opposite directions (see Figure 1.10a). The dimer interface is built by the two $\alpha 1$ helices of the monomers and the two C-termini from helix αF to αH. The Trp358 residue from helix αH of one monomer is part of the active site of the neighboring monomer and *vice versa* (see Figure 1.10b). In comparison to OYE1 the dimer interface is at the opposite side of the barrel.

The FMN cofactor is bound in a similar way as shown for other OYE members. It is placed at the C-terminal end of the β-barrel with its *si*-face exposed to the solvent. In Figure 1.11a the interactions between the protein and the cofactor are displayed. His178, His181, Arg231 and Gln99 are in hydrogen bonding distance to N(1), O(2) and N(3) of the isoalloxazine ring. The amide protons of Ala57 and Cys25 as well as the γ-sulfhydryl group stabilize O(4) and N(5) of the isoalloxazine ring. Amino acid sequence alignments revealed that XenA shows highest sequence identities to XenA (99.7%), XenD (68.6%) and XenE (44.0%) from *Pseudomonas putida* KT2440, XenA (97.2%) from *Pseudomonas putida* IIB, YqjM (39.9%) from *Bacillus subtilis*, TOYE (38.6%) from *Thermoanaerobacter pseudethanolicus* and NerA (31.3%) from *Agrobacterium radiobacter*. These 6 enzymes have a cysteine in hydrogen bonding distance to O(4), whereas all other OYE homologues mentioned in Table 1.1 have a conserved

threonine. Therefore one can assume, that these members form a subgroup of the OYE family. The dimethylbenzene part is stabilized by Met24 on its *re*-side through hydrophobic interactions and by Trp358 through face-on-edge π-π interactions.

(a)

(b)
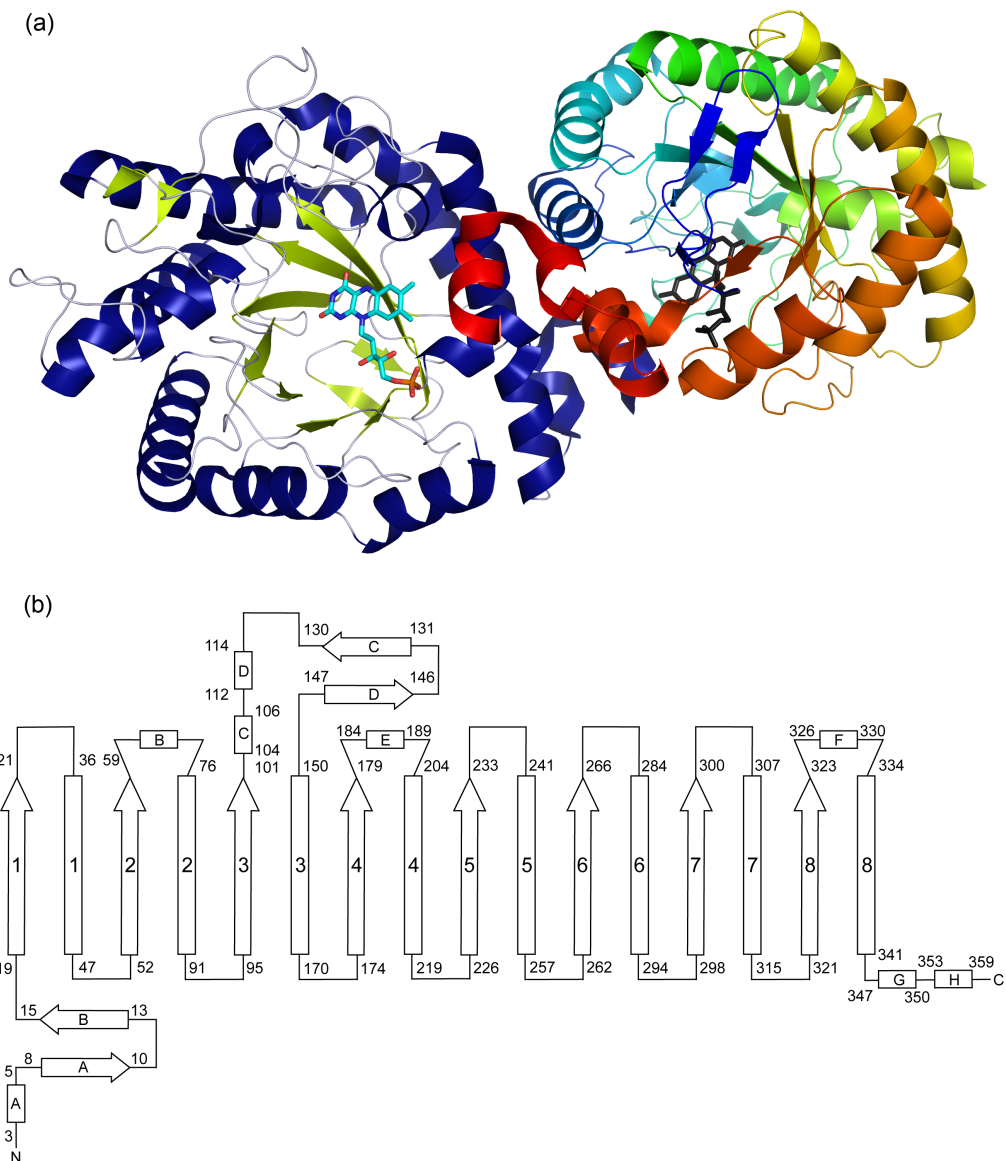
Figure 1.10: **Overall structure of XenA.** (a) The XenA dimer is displayed as ribbon diagram. In the first monomer the α-helices are displayed in blue and β-sheets are displayed in green. In the bound FMN molecule carbon atoms are light blue, oxygen atoms are red, nitrogen atoms are blue and the phosphorus atom is orange. The second monomer is colored in rainbow with N-terminus in blue and C-terminus in red. The bound FMN is displayed in grey. The figure was generated from the PDB code given in brackets using MacPyMOL. (b) Topology map of XenA: α-helices are displayed as rectangles and β-strands are displayed as arrows. Helices and β-strands are numbered according to their order in the barrel. Letters designate secondary structure elements outside the barrel. The numbers at the beginning and the end of each secondary structure element, match the amino acid sequence. (PDB code: 2H8X, (Griese *et al.*, 2006))

2-cyclohexenone, coumarin and 8-hydroxycoumarin were identified as oxidative substrates, whereas 7-hydroxycoumarin was assumed to be an inhibitor. XenA reduces 2-cyclohexenone ten-fold faster than coumarin and 8-hydroxycoumarin and shows a preference for NADPH over NADH.

Structural studies on ligand binding of the oxidized enzyme were performed with coumarin and 8-hydroxycoumarin (see Figure 1.11b and c).
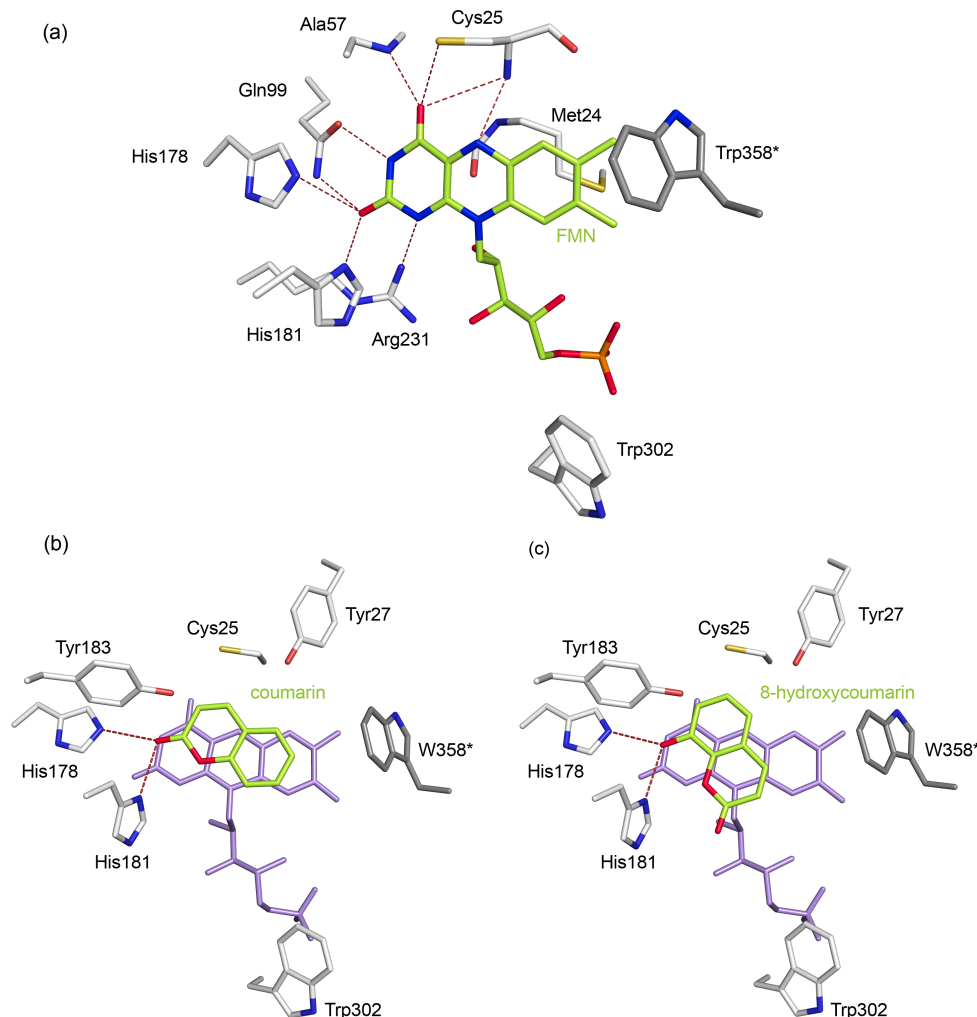

Figure 1.11: **Active site of oxidized XenA.** All residues are displayed as sticks. The carbon atoms of side chain and backbone amino acids are in grey, nitrogen atoms in blue, oxygen atoms in red, sulfur atoms in yellow and phosphorus atoms in orange. Hydrogen bonding interactions are displayed as dashed lines in red. The asterisk denotes the tryptophan residue from the adjacent monomer. (a) Active site of oxidized XenA without substrate. The carbon atoms of the FMN are displayed in green. (b) Active site of oxidized XenA in complex with coumarin. The carbon atoms of coumarin are displayed in green and the FMN cofactor is violet. (c) Active site of oxidized XenA in complex with 8-hydroxycoumarin. The carbon atoms of 8-hydroxycoumarin are displayed in green and the FMN cofactor is violet. The figures were generated from PDB codes given in bracket using MacPyMOL. (PDB codes: 2H8X, 2H9O, 2H8Z (Griese *et al.*, 2006))

21

Coumarin binds nearly coplanar to the isoalloxazine ring and is stabilized by π-π interactions, as it was shown for other OYE family members. The carbonyl oxygen is stabilized by hydrogen bonding interactions with His178 and His181. The α,β-unsaturated double bond is positioned optimally for proton and hydride transfer. The C(4) (β-carbon) of coumarin is positioned directly over N(5) of the FMN whereas the C(3) (α-carbon) is close to Tyr183, which was proposed as a proton donor (see chapter 1.1.5). 8-hydroxycoumarin in contrast is flipped by 180° around the central C(1a)-C(4a) axis in comparison to coumarin. Therefore, the phenolic group is not within hydrogen bonding distance to the histidine pair and the olefinic bond does not lie above the flavin N(5). His181 coordinates the O(1) of the substrate. This binding situation does not allow hydride transfer from the cofactor to the substrate, as the donor and acceptor atoms are too far apart. It is assumed that 8-hydroxycoumarin is bound as the phenolate ion to the oxidized flavin, because the oxidized flavin can stabilize the phenolate ion much better, than the reduced $FMNH_2$. As the orientation of ligands in the active site is mainly enforced by hydrogen bonding interactions to the histidine pair, the deprotonated substrate may preferentially bind with the phenolate oxygen, while the protonated 8-hydroxycoumarin would bind with the carbonyl oxygen. For this reason a productive binding mode is assumed in the reduced state of the enzyme.

2   Objectives

Xenobiotic Reductase A from *Pseudomonas putida* 86 is a member of the OYE family of flavoproteins. This class of enzymes shows a broad substrate range and the physiological roles of most of the members are still unclear. The active site residues of the family members reveal considerable variations, which might be responsible for different redox properties and further functional differences. Mechanistic studies of OYE family members can help to better understand catalysis by flavoenzymes and may provide insights helping to develop novel biocatalysts for fine chemicals, pharmaceuticals and environmental biotechnology. The presented work focuses on the reaction mechanism of XenA and its structural basis in comparison to other well-known OYE family members.

The first aim of this work is to characterize the reactivity of XenA-wt by measuring steady-state and single turnover kinetics as well as by determining the reduction potential of XenA-bound FMN. To get a more detailed model for the active site, the crystal structure of oxidized XenA should be improved to achieve true atomic resolution and the structure of reduced XenA should be determined to reveal redox-dependent conformational changes during the catalytic cycle.

The reaction catalyzed by XenA follows a ping-pong mechanism. This implies that the substrates for the reductive and oxidative half-reactions are bound to the same active site and enable a formal hydride transfer between the various compounds and the FMN cofactor. Both substrates are bound in the same position but interact with different active site amino acids. The main goal of this work is to analyze individual contributions of five different active site residues (Cys25, Tyr27, Tyr183, Trp302 and Trp358) using site-directed mutagenesis, transient kinetics, redox potentiometry and crystal structure analysis.

So far, the structures of substrate complexes of OYE family members are derived from the non-reactive oxidation state of the enzyme. Another aim of this work is to determine the influence of the oxidation state of the FMN on substrate binding and to further elucidate the reaction mechanism, by stabilizing the true Michaelis complexes using site-directed mutagenesis and crystal structure analysis.

3 Synopsis

3.1 Xenobiotic Reductase A from *Pseudomonas putida* 86

XenA was isolated from *Pseudomonas putida* 86 and was shown to be involved in the degradation of quinoline along the 8-hydroxycoumarin pathway. It belongs to the OYE family of flavoproteins and is structurally and functionally similar to other family members from bacteria and yeasts (Griese *et al.*, 2006). Most extensively studied members are OYE1 from *Saccharomyces pastorianus* (Saito *et al.*, 1991), PETN reductase from *Enterobacter cloacae* PB2 (French *et al.*, 1996), morphinone reductase from *Pseudomonas putida* M10 (French & Bruce, 1994), YqjM from *Bacillus subtilis* (Fitzpatrick *et al.*, 2003) and TOYE from *Thermoanaerobacter pseudethanolicus* E39 (Adalbjörnsson *et al.*, 2010). OYE homologues catalyze different reactions, such as the reductive denitrification of nitro-esters and nitro-aromatics, the reduction of the aromatic ring of nitro-aromatics and the reduction of α/β-unsaturated bonds in aldehydes and ketones. Therefore, the biocatalytic potential of the OYE family is useful in a variety of biotechnological and pharmaceutical applications.

3.1.1 Kinetic characterization of XenA

XenA catalyzes the NAD(P)H-dependent reduction of the olefinic bond of different α/β-unsaturated carbonyl compounds, including 2-cyclohexenone, coumarin and 8-hydroxycoumarin. Additionally molecular oxygen was identified as alternative electron acceptor. The reaction can be divided in a reductive and an oxidative half-reaction. XenA reduces 2-cyclohexenone ten-fold faster than coumarin and 8-hydroxycoumarin and shows a preference for NADPH over NADH (Griese *et al.*, 2006).

In publication A we present a kinetic and thermodynamic analysis of XenA and a comparison to other well known OYE homologues. Steady-state kinetic analysis with various concentrations of NADPH and 2-cyclohexenone under anoxic conditions were performed to determine K_{mA} (K_m for 2-cyclohexenone: 37.2 ± 2.4 µM) and K_{mB} (K_m for NADPH: 200 ± 13 µM) as well as V_{max} ($k_{cat} = 7.2 \pm 0.3$ s^{-1}) for the catalyzed reaction (see publication A, Figure 3). The double reciprocal plot revealed parallel lines, which are consistent with a ping-pong Bi-Bi mechanism (Segel, 1993), which was proposed for XenA.

The rate constants of both half-reactions are critically dependent on the reduction potential of the FMN-FMNH$^-$ couple. We performed the reduction potential measurement with a method described by Sucharitakul and co-workers (Sucharitakul *et al.*, 2005), where phenosafranine (with a known reduction potential of -252 mV) served as reference dye and the reduction

potential of XenA (E^0_m = -263 mV (Loach, 1973)) could be calculated (see Figure 3.1).
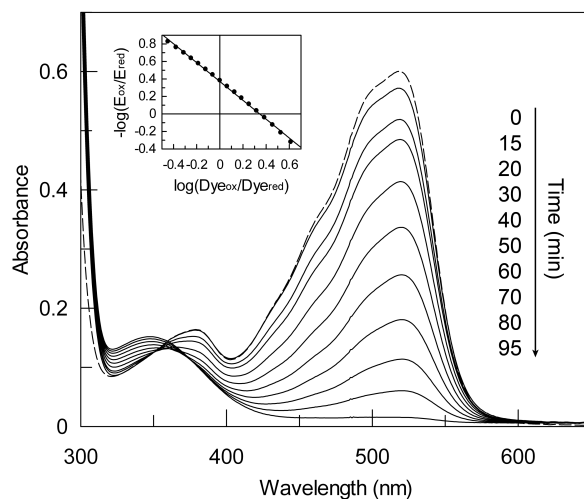
Figure 3.1: **Redox potential determination for the FMN-FMNH⁻ couple of XenA.** Conditions: 15 µM XenA, 15 µM phenosafranine, 2µM methylviologen, 0.05 unit of xanthine oxidase and 50 mM Tris buffer (pH 8.0). The dotted line shows the spectrum of the reaction mixture before the addition of xanthine. The reaction was followed over 1.5 h (—). Absorbance values at 464 and 521 nm were used to calculate the concentrations of oxidized XenA and dye. The inset shows the plot of $\log(E_{ox}/E_{red})$ vs $\log(D_{ox}/D_{red})$. The solid line displays the linear fit with a slope of -1. The reduction potential of XenA was calculated to be -263 mV (publication A, Figure 2).

This reduction potential is lower than the ones found for PETN reductase (-193 mV) (Khan *et al.*, 2002), OYE1 (-230 mV) (Stewart & Massey, 1985) and morphinone reductase (-242 mV) (Messiha *et al.*, 2005), which could be effected by several structural variations between the enzymes. One difference between XenA and other OYE members is the active site Cys25 in the place of a conserved threonine (see publication A, Figure 6). In the homologues enzymes this residue forms a strong hydrogen bond with the O(4) atom of the isoalloxazine ring of the FMN and its exchange against alanine in OYE1 and PETN reductase lower the reduction potential to -263 mV and -290 mV, respectively.

To get a more detailed view of the reaction mechanism of XenA we investigated the reductive and oxidative half-reactions using stopped-flow spectrophotometry, with various concentrations of NADH and NADPH as reductive and 2-cyclohexenone and coumarin as oxidative substrates reacting with XenA. A scheme for the reaction cycle based on these measurements is shown in Figure 3.2 and a summary of the kinetic data can be found in Table 4.1 (Supplementary).
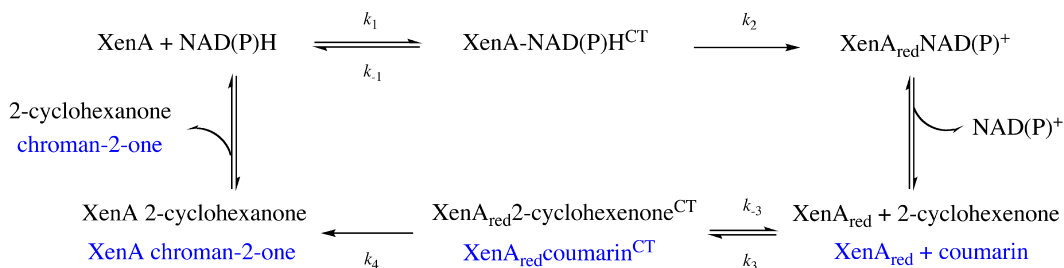
Figure 3.2: **Scheme for the reaction cycle catalyzed by XenA.** The reductive half-reaction is shown in the upper part and the oxidative half-reaction is shown in the lower part (publication A, Figure 7).

In the first step of the reductive half-reaction complexes of oxidized XenA with NADH or NADPH form charge transfer (CT) intermediates, which can be observed by spectral changes at 540 nm and were fitted to double exponential functions to determine individual rate constants (see Figure 3.3b and Figure 3.3c). These formations occur with second order rate constants (k_1) of 9.4×10^5 M^{-1} s^{-1} for NADH and 6.4×10^5 M^{-1} s^{-1} for NADPH. The disappearance of the CT complexes is controlled by the rate constant (k_{-1}) of 210-250 s^{-1} with both substrates. The next step is the hydride transfer of the reduced nicotinamide to the N(5) atom of the FMN. The observed kinetic transients at 464 nm were fit to single exponentials (see Figure 3.3b). Hyperbolic plots of the observed rate constants against substrate concentrations were fitted as described in publication A to yield the limiting rate constants (k_2) and the dissociation constants (K_d) of the enzyme substrate complexes. The limiting rate (k_2) for this step is 24 times more rapid for NADPH than for NADH. This value compensates the lower affinity of XenA for NADPH over NADH as represented by a slightly higher dissociation constant (K_d value) (see Figure 3.3d and Figure 3.3e). The last step in the reductive half-reaction is the NAD(P)$^+$ release.

Docking studies of the interaction of XenA with NADH and NADPH combined with electrostatic energy calculations were performed to get further insights into the binding of the reductive substrate. The additional negative charge of the 2'-phosphate group of NADPH, which is situated above the 1,4-dihydropyridine ring (see publication A, Figure 6) stabilizes NADP$^+$ and is therefore in good agreement with the higher rate constant of the reaction with NADPH.
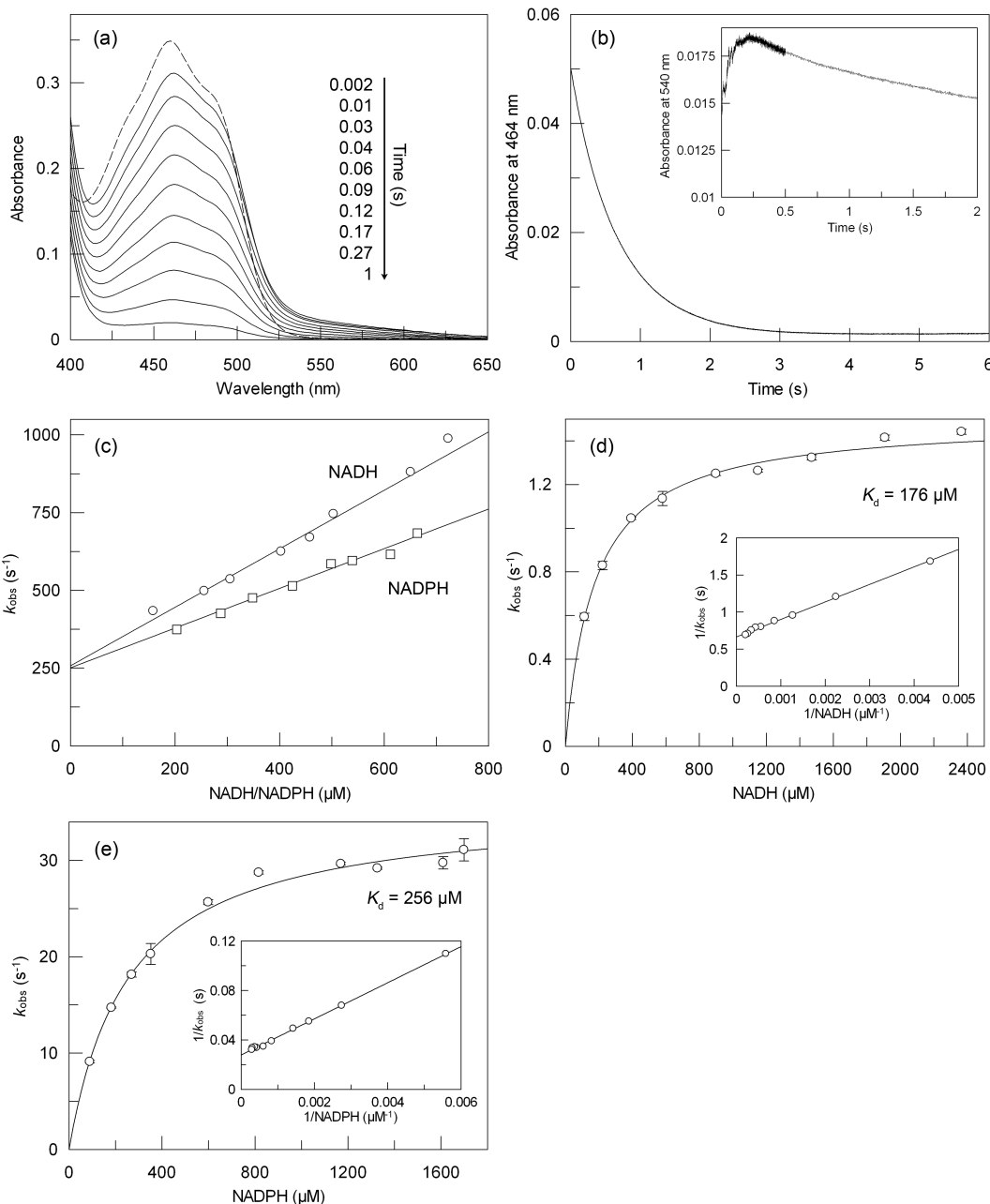
Figure 3.3: **Reductive half-reactions of XenA with NADH and NADPH.** (a) Time-dependent spectral changes of 35 µM $XenA_{ox}$ reacting with 800 µM NADH. The dashed line represents the spectrum of $XenA_{ox}$. (b) Time-dependent absorbance change at 464 nm for the reaction of 5 µM XenA with 2500 µM NADH. The inset displays the absorbance changes at 540 nm, which we attribute to the formation of the CT complex. (c) Dependencies of the observed rates at 540 nm on NADH concentration (O) and NADPH concentration (□) for reactions with 35 µM XenA. (d and e) Concentration dependence of the observed rates at 464 nm (5 µM XenA) for NADH (d) and NADPH (e), with the reciprocal plots in the insets. The curves display the best fits to the data using equation 7 (see publication A). All experiments were conducted under anoxic conditions in 50 mM Tris buffer (pH 8.0) at 20°C (publication A, Figure 4).

We further investigated the oxidative half-reactions, which start with the formation of a CT complex between XenA and the oxidative substrate, followed by the reduction of the

substrates and the product release steps (see Figure 3.2). The limiting rate constant of the reaction of NADH-reduced XenA with 2-cyclohexenone is 50-fold larger than that for the reaction with coumarin, while coumarin binds with a 4-fold higher affinity, which probably reflects the weaker electrophilicity of the β-carbon of coumarin, in contrast to 2-cyclohexenone (see Figure 3.4).

The measured catalytic constants of the steady-state assay ($k_{cat} = 7.2$ s^{-1}) are in good agreement with the transient kinetic data ($k_{cat} = 5.3$ s^{-1}), indicating that the two product release steps occur rapidly and are not rate limiting for the reaction.
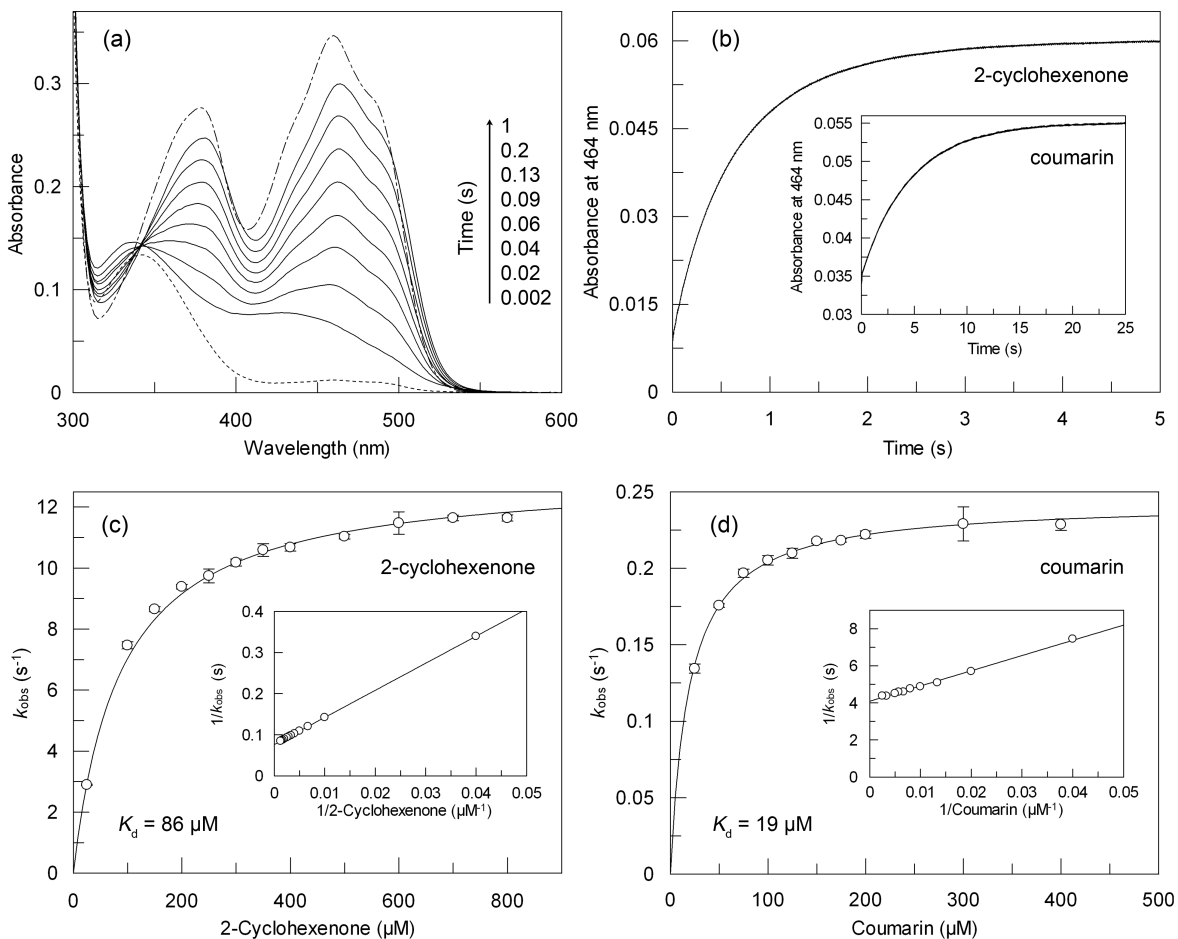

Figure 3.4: **Oxidative half-reaction of reduced XenA with 2-cyclohexenone and coumarin.** (a) Time-dependent spectral changes of 35 μM XenA (NADPH-reduced) reacting with 800 μM 2-cyclohexenone. The dashed line represents the spectrum of reduced XenA. (b) Time-dependent spectral changes at 464 nm for the reaction of 5 μM XenA with 25 μM 2-cyclohexenone. A reaction trace with 25 μM coumarin is shown in the inset of the panel (b). (c and d) Concentration dependence of the observed rate constants at 464 nm for the reaction of 5 μM XenA with 2-cyclohexenone (c) and for coumarin (d). The curves display the best fit to the data using equation 7 (publication A). The reciprocal plots are shown in the insets. All experiments were conducted in 50 mM Tris buffer (pH 8.0) at 20°C under anoxic conditions (see publication A, Figure 5).

3.1.2 Structural analysis of oxidized XenA

The structure of XenA was solved at a resolution of 1.5 Å and at a resolution of 1.42 Å with coumarin bound to the active site. The structure revealed a homodimeric arrangement. One monomer consists of the typical $(\alpha,\beta)_8$-barrel fold (TIM barrel), with one FMN molecule bound on the solvent exposed C-terminal side of the barrel (Griese *et al.*, 2006). The subunit structure is similar to that reported for OYE1 (Fox & Karplus, 1994), PETN reductase (Barna *et al.*, 2001; Khan *et al.*, 2004), morphinone reductase (Barna *et al.*, 2002), YqjM (Kitzing *et al.*, 2005) or TOYE (Adalbjörnsson *et al.*, 2010) (see Figure 1.1 and Figure 1.10). This first characterization indicated a deviation of the isoalloxazine ring from planarity, but the interatomic distances in the active site, which contribute to this distorted conformation, could not be determined reliably.

In publication B we present the structure of XenA refined at a resolution of 1.03 Å without and at a resolution of 1.1 Å with coumarin bound to the active site (see Figure 3.5).
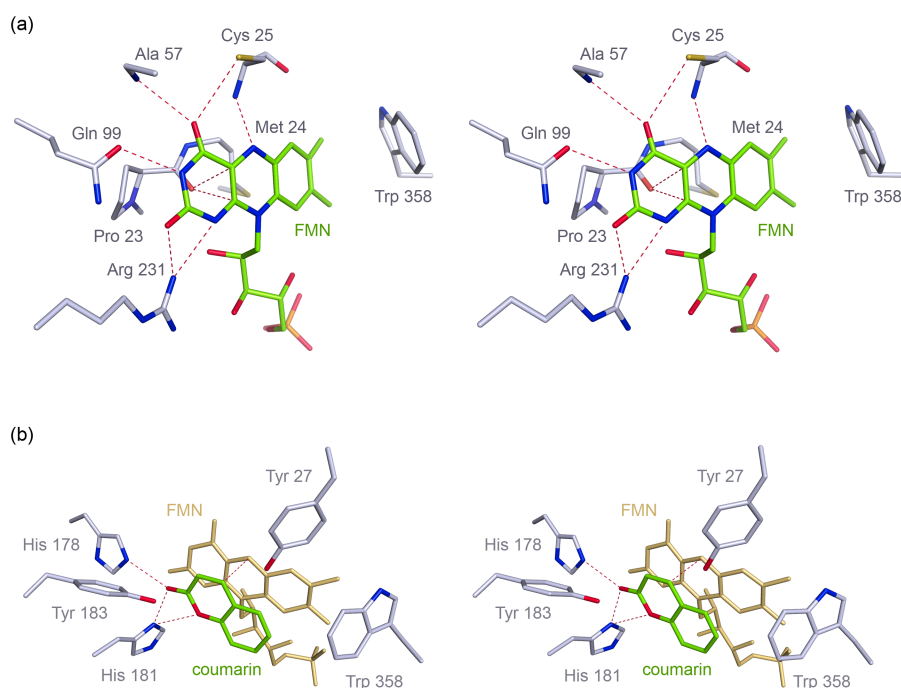

Figure 3.5: **Active site view of XenA.** All residues are displayed in stick representation. (a) Stereoscopic view of the hydrogen-bonding network around FMN. Carbon atoms of the amino acid side chains are gray, carbon atoms of FMN are green, oxygen atoms are red, nitrogen atoms are blue, sulfur atoms are yellow and phosphorous atoms are orange. The broken red lines represent possible interactions between the cofactor and the adjacent amino acids. (b) Stereoscopic view of the hydrogen-bonding network around coumarin bound to the active site. FMN is yellow, carbon atoms of coumarin are green, carbon atoms of amino acid side chains are gray, oxygen atoms are red and nitrogen atoms are blue. The broken lines represent possible interactions between coumarin and XenA (publication B, Figure 6).

The improvement in resolution of XenA gives a better description of the protein-cofactor and protein-substrate interactions. Synchrotron radiation can cause photoreduction of the FMN cofactor. To evaluate the amount of photoreduction we compared the redox-sensitive bond lengths of the FMN cofactor (see publication B) with that expected for oxidized and reduced small molecule flavins (Berkholz *et al.*, 2008). These values are intermediates between the distances expected for both oxidation states. Together with the fact, that also crystals exposed to a lose dose of radiation show a non-planarity of the isoalloxazine ring, we assume that both effects - the partial reduction of the cofactor and the influence of the protein environment - lead to the distorted geometry of the FMN. Additionally, the improvement in resolution provides a better insight in the charge distribution throughout the isoalloxazine ring (see publication B, Figure 5), which is lower in the dimethylbenzene ring and higher in the heteroaromatic ring. Hydrogen bonding interactions between residues Cys25, Ala57, Gln99, Pro23 and Arg231 and the FMN are located exclusively in the area of higher charge densities, whereas the dimethylbenzene ring is stabilized by a face-on-edge π-π interaction with Trp358 and hydrophobic interactions with Met24 on the *re* side (see Figure 3.5).

The structures of true Michaelis complexes (reduced XenA with oxidative substrate) are difficult to achieve because of the high reactivity of the complex. Therefore we reported the structure of oxidized XenA with coumarin bound to the active site at a higher resolution to estimate the relative orientation of substrate and cofactor (see Figure 3.6).
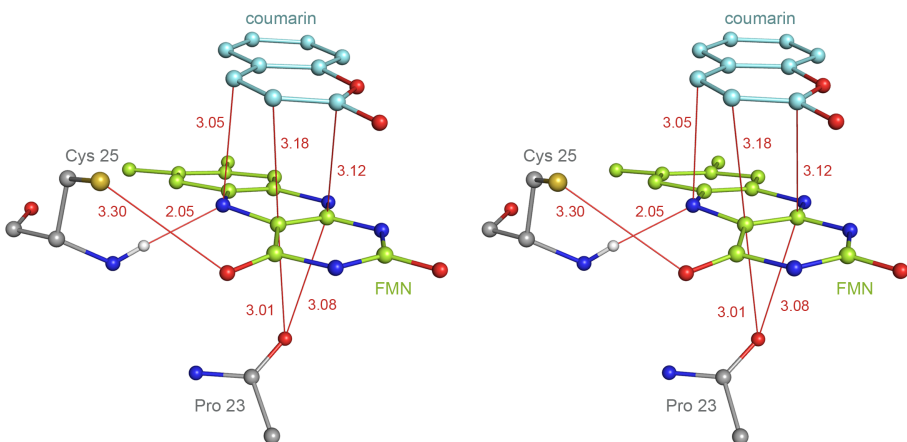

Figure 3.6: **Compression of the flavin in the coumarin complex.** Stereoscopic view of the active site of XenA in complex with coumarin. All residues are shown in stick and ball representation. Carbon atoms of the amino acid side chains are gray, carbon atoms of FMN are green, carbon atoms of coumarin are light blue, oxygen atoms are red, nitrogen atoms are blue, sulfur atoms are yellow and hydrogen atoms are white. Distances between atoms are given in angstrom units and are displayed as red lines (publication B, Figure 7).

We observed no structural changes in coumarin bound XenA compared to the substrate free form. Both structures can be superimposed with a root mean square (rms) deviation of 0.09 Å. Coumarin binds nearly coplanar to the isoalloxazine ring, consistent with π-π interactions between both molecules and the overall arrangement is similar to the average geometry found in other flavoenzymes (Fraaije & Mattevi, 2000). The closest contact, between the β carbon of coumarin and the N(5) of FMN (3.05 Å) is shorter than expected from van der Waals radii (3.2 Å). This indicates that the enamine moiety of the FMN is sterically compressed from the *re* and *si* side. This compression could facilitate the electron/hydride transfer between substrate and cofactor, like described before (Bruice & Benkovic, 2000; Bruice & Pandit, 1960; Jencks, 1963).

3.1.3 Structural analysis of reduced XenA

To investigate conformational changes during reduction/oxidation of XenA, we crystallized the enzyme under anoxic conditions and reported the structure of the reduced XenA at a resolution of 1.75 Å in publication C. In the isoalloxazine ring system the N(5) atom shows a tetrahedral geometry and is positioned above the ring plane pointing towards the substrate binding site, as it was observed for other flavoenzymes (Fraaije & Mattevi, 2000) (see Figure 3.7).
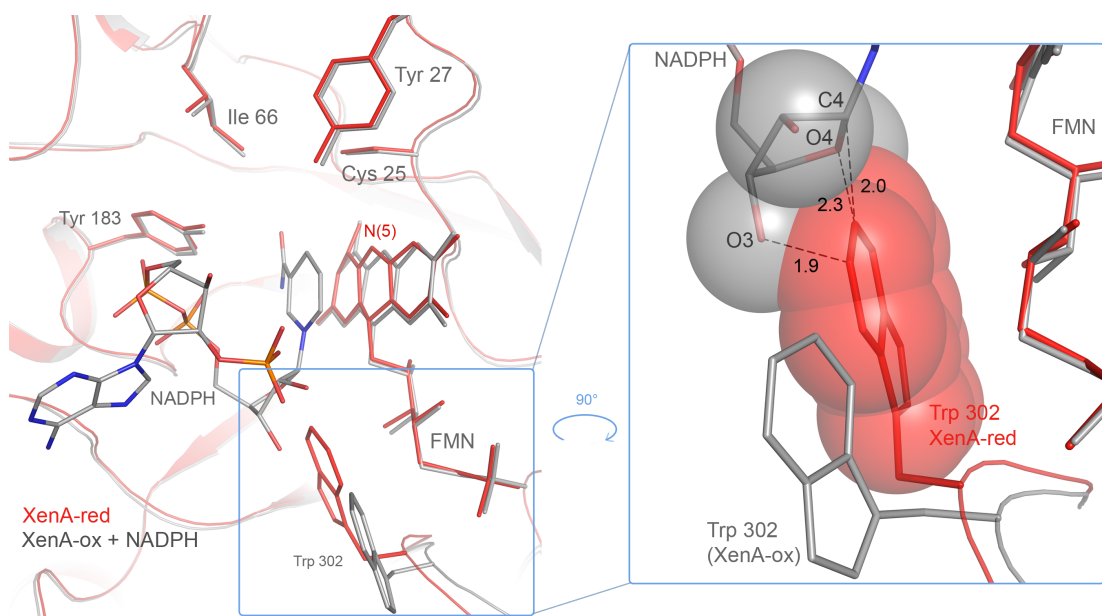

Figure 3.7:   **Superimposition of the XenA$_{ox}$-NADPH complex with XenA$_{red}$.** The active site structure of oxidized XenA in complex with NADPH is shown in gray and reduced XenA in red. All residues are displayed in stick mode. Oxygen atoms are shown in red, nitrogen atoms in blue and phosphorous atoms in orange. Distances between NADPH and Trp302 of the reduced XenA are given in Ångströms and are shown as broken lines in black. Van der Waals surfaces are shown in corresponding colors (publication C, Figure 5).

The main difference between oxidized and reduced XenA is a large conformational change of the residues 302-306. In the oxidized state Trp302 deviates from the Ramachandran statistics ("out"-conformation). In the reduced structure the main chain torsion angles of Trp302 changes (ϕ = 77° and ψ = 39°) and is now in the Ramachandran allowed region ("in"-conformation). The conformational changes also alter the hydrogen-bond network around the main chain atoms of Trp302 and Gly303 (see publication C, Figure 4). We assume that this change is triggered by the oxidation state of the FMN. The small structural changes of the isoalloxazine ring in the reduced state are transferred through the ribityl group to the terminal phosphate, which could be responsible for the rearrangement of the hydrogen bonds. The movement of Trp302 from the "out"- to the "in"-position causes a narrowing of the substrate-binding pocket. A superposition of NADPH-XenA complex with the reduced XenA shows that the van der Waals radii of Trp302 in the "in"-position and the NADPH would overlap and this clash could not be avoided by different conformations of the NADPH (see Figure 3.7). Therefore, the functional consequence of this movement in the reduced state is a disfavored binding of NAD(P)H/NAD(P)$^+$, to allow the binding of substrates with mono- and bicyclic rings like 2-cyclohexenone and coumarin. This shaping of the substrate-binding site in different oxidation states may help to overcome the problem of having one active site to bind and convert the various substrates of a ping-pong reaction.

3.2 Cysteine 25 – A modulator residue

In publication A we reported a lower reduction potential of the FMN/FMNH$^-$ couple (-263 mV) than found for other OYE family members (Khan *et al.*, 2002; Messiha *et al.*, 2005; Stewart & Massey, 1985). We suggested that the Cys25, which replaces a highly conserved threonine residue in the OYE family, is responsible for this effect. Mutagenesis studies of this threonine in OYE1 (Xu *et al.*, 1999) and morphinone reductase (Messiha *et al.*, 2005) suggest, that this residue modulates the reduction potential of the FMN and Cys26 in YqjM (Kitzing *et al.*, 2005) is assumed to act as redox sensor by adopting several conformations. To identify the function of Cys25 we exchanged the residue to alanine and serine and investigated the crystal structures and the effect of the mutations on the kinetics of XenA (see publication B). We decided against preparing a XenA-C25T variation because the threonine would clash with the neighboring tyrosine (Tyr26) and probably lead to bigger structural changes.

3.2.1 Kinetic characterization of XenA-C25A and XenA-C25S

The specific activities for XenA-wt and the variants are given in Table 4.1 (Supplementary). XenA-C25A shows a sixfold decrease, whereas XenA-C25S shows a twofold decrease compared to the wildtype. It should be noted that the XenA-C25A variant tended to precipitate, so the low specific acitivity might be due to a lower effective enzyme concentration in the assay.

We determined the reduction potential of both variants to investigate the influence of Cys25 on the relative stability of the oxidized and reduced state of XenA (see Table 4.1, Supplementary and publication B, Figure 2b). The replacement of cysteine by alanine does not change the reduction potential but the exchange to serine increased the reduction potential by 82 mV. This implies that either oxidized and reduced states are equally stable in XenA-wt and XenA-C25A or the reduced and oxidized state of the FMN are both stabilized or destabilized by the same amount upon loss of the SH group of Cys25. The difference of the reduction potential in XenA-C25S compared to XenA-wt (ΔE^0_m = 82 mV), is larger than the one observed for the exchange of the corresponding threonine against alanine in OYE1 (ΔE^0_m = 33 mV) and morphinone reductase (ΔE^0_m = 48 mV). This increase is stronger than expected from the exchange of a weak S-H…O(4) to a strong O-H…O(4) hydrogen bond. These data indicate that the cysteine does not form a hydrogen bond to O(4).

We also investigated the reductive and oxidative half-reaction of both Cys25 variants with NADH/NADPH as reductive substrates and 2-cyclohexenone and coumarin as oxidative substrates and determined the individual limiting rate constants (k_x) and the dissociation constants (K_d) for the enzyme substrate complexes (see publication B, Figure 3 and Figure 4). The summarized data are depicted in Table 4.1 (Supplementary). The rate constants of both half-reactions for XenA-C25A and XenA-C25S changed slightly by the same factor compared to XenA-wt. We observed a decrease in the reductive and an increase in the oxidative half-reaction for the alanine variant and opposite changes for the serine variant. Both exchanges of the cysteine decrease the binding affinity of XenA for its substrates. The decrease is smaller than expected for the loss of a direct interaction between enzyme and substrate, which indicates an indirect role in substrate binding, through modulation of the electronic structure of the isoalloxazine ring.

From all these data we concluded, that Cys25 is not essential for catalysis but modulates substrate binding and the reduction potential of the FMN. Several copies of xenobiotic reductases can be assigned in the genome of *Pseudomonas putida* (van Dillewijn *et al.*, 2008) with different residues in the position of Cys25 and either cysteine, threonine or alanine are

found. It might be that the different residues in this position adapt the enzymes for different classes of substrates so that these homologues can participate in different pathways of aromatic/heteroaromatic substrates. This could be an explanation for the wide substrate range covered by a single microorganism (Jimenez *et al.*, 2002).

3.2.2 Structural analysis of XenA-C25A and XenA-C25S

The structures of XenA-C25A and XenA-C25S were solved at resolutions of 1.20 Å and 1.80 Å without and at resolutions of 1.28 Å and 1.75 Å with coumarin bound to the active site, respectively (see publication B). The overall structures of both enzyme variants reveal no significant changes of the protein conformation compared to the wildtype (see Figure 3.8).
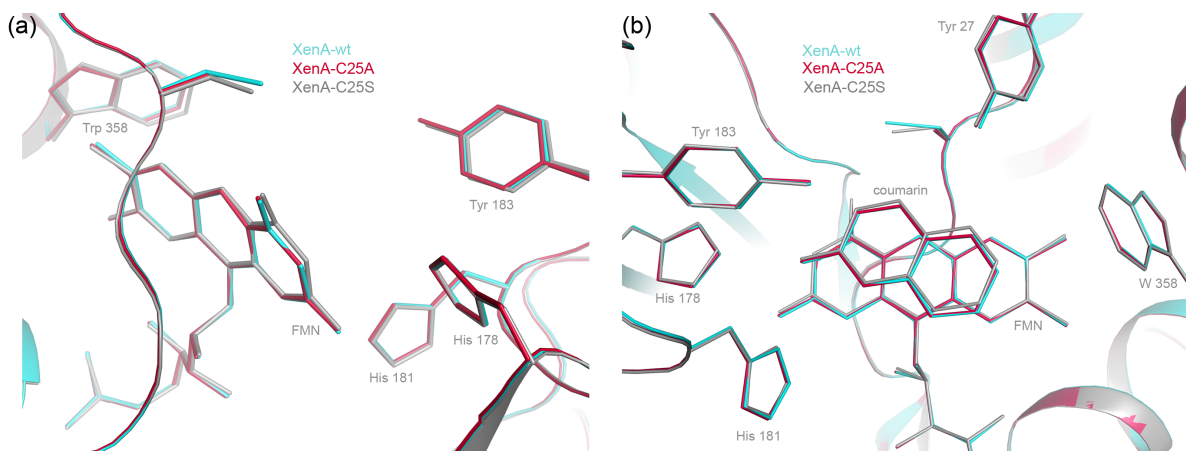

Figure 3.8:   **Comparison of XenA-wt, XenA-C25A and XenA-C25S.** (a) View of the active site of the superimposition of: XenA-wt (blue), XenA-C25A (red) and XenA-C25S (gray). (b) View of coumarin bound to the active site of the superimposition of: XenA-wt (blue), XenA-C25A (red) and XenA-C25S (gray) (publication B, Figure 9).

Therefore, we can assume that the effects of the cysteine exchanges are only local. The isoalloxazine rings in XenA-wt and XenA-C25A are more distorted than in XenA-C25S. In the serine variant the isoalloxazine as well as the pyrimidine ring are more planar, so that the OH…O(4) hydrogen bond is within the typical distance of 2.8 Å. Due to the lower resolution of the structure, the interpretation of the data are less reliable. The position of the coumarin as well as the interactions between protein and substrate are nearly identical (see Figure 3.8), which agrees with the kinetic measurements, in showing that Cys25 is not directly involved in the substrate binding (see Figure 4.1, Supplementary).

3.3 Tyrosine 27 – Stabilizing the transition state in the reductive half-reaction

The active site of XenA is lined by two tyrosine residues (Tyr27 and Tyr183), which could act as possible proton donors in the oxidative half-reaction. The phenolic group of Tyr27 is oriented towards the substrate-binding site and is approximately 5 Å above the N(5) atom of the FMN. In the model complex of XenA with NADPH (see Figure 3.9) the hydroxyl group of Tyr27 is about 3.6 Å away from the hydride donating C(4) of NADPH.
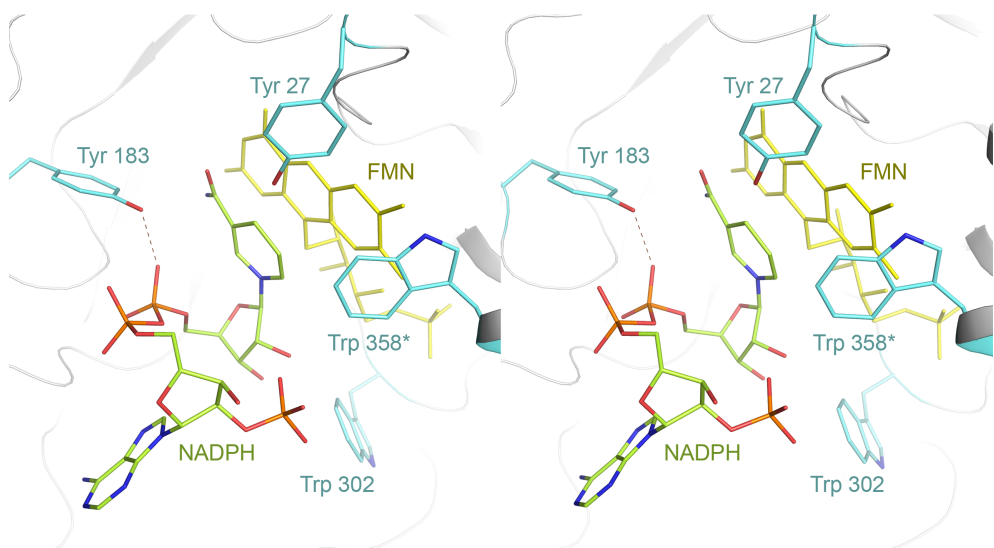

Figure 3.9: **XenA in complex with NADPH.** Stereoscopic view of the active site of XenA in complex with NADPH. The structure was derived by docking calculations (publication A). All residues are displayed in stick representation. The FMN cofactor is shown in yellow. The carbon atoms of amino acid side chains are shown in light blue, carbon atoms of NADPH are shown in green, oxygen atoms in red, nitrogen atoms in blue and phosphorous atoms in orange. The broken lines (red) represent possible interactions between XenA and NADPH (publication C, Figure 1).

To determine the role of Tyr27 during the reductive and oxidative half-reaction of XenA, we exchanged the tyrosine against phenylalanine and investigated the effects of the exchange on the kinetics (see publication C). The specific activity of XenA-Y27F is tenfold lower, than for XenA-wt, whereas the reduction potential does not change. To figure out which half-reaction is most affected by the exchange we performed single-turnover kinetics with NADPH as reductive and 2-cyclohexenone as oxidative substrate. All data are summarized in Table 4.1 (Supplementary). The limiting rate constant of the reductive half-reaction is tenfold decreased, while the oxidative half-reaction is only slightly affected. Also the K_d values for the enzyme substrate complexes show only a small increase (see publication C, Figure S3a and S4a). With temperature dependent measurements of the reductive half-reaction we could determine an increase of the free activation enthalpy of 4 kJ mol^{-1}, which principally agrees

with the tenfold decrease of the limiting rate constant (see publication C, Figure S6). Therefore we assume that Tyr27 is not the proton donor in the oxidative half-reaction, but contributes weakly to a stabilization of the transition state by an interaction of its hydroxyl group with the transferred hydride ion (see Figure 4.1).

3.4   Tyrosine 183 – NAD(P)H binding and Proton donor

Tyr183 has like Tyr27 a central position in the active site and points with its hydroxyl group into the substrate-binding pocket (see Figure 3.5b). In the coumarin bound structure of XenA-wt the hydroxyl group is approximately 3.3 Å away from the α-carbon atom of the double bond to be reduced, so that this residue is also in the distance of a possible proton donor. In publication C we present the exchange of the tyrosine against phenylalanine. We investigated the role of this residue during catalysis using transient kinetics, redox potentiometry and crystal structure analysis. In publication C we report the structure of XenA-Y183F at a resolution of 1.45 Å. The superposition with XenA-wt shows no structural changes, except for the missing hydroxyl-group in the active site (see Figure 3.10). Therefore the differences in the kinetic parameters are most likely directly connected to the amino acid exchange and not to an induced structural change.
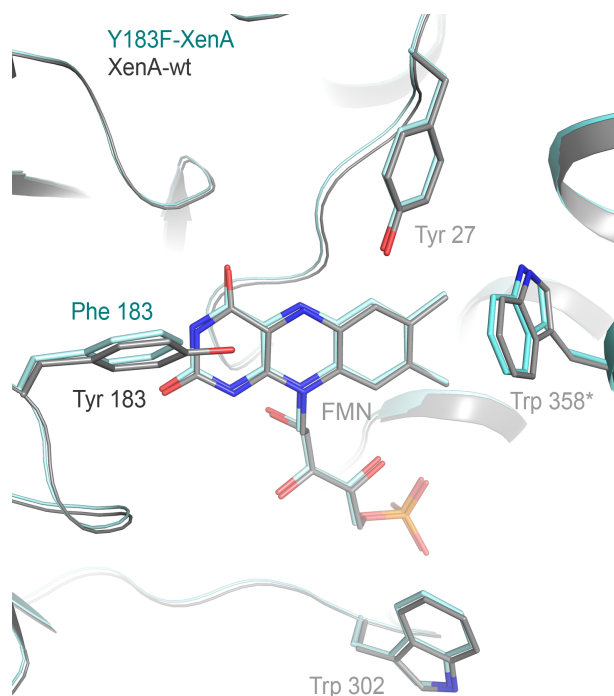

Figure 3.10:   **Comparison of XenA-wt and XenA-Y183F.** View on the superimposed active sites of XenA-wt (gray) and Y183F-XenA (light blue). All residues are shown in stick mode. Oxygen atoms are displayed in red, nitrogen atoms in blue and phosphorous atoms in orange (publication C, Figure 2).

In contrast to XenA-wt we observed a drastic decrease of the specific activity of XenA-Y183F of 100-fold, whereas the reduction potential was unaffected. All kinetic data are summarized in Table 4.1 (Supplementary). For the reductive half-reaction NADPH was used as substrate and the limiting rate constant only slightly increased, whereas the dissociation constant for the XenA-Y183F-NADPH complex is 11-fold larger compared to XenA-wt (see publication C, Figure S3b). In the model structure of XenA-wt with bound NADPH (see Figure 3.9) Tyr183 forms a hydrogen bond with an oxygen atom of the β-phosphate of the ADP moiety of NADPH. So the 11-fold increase of the K_d value is in good agreement with the loss of a hydrogen bond in the enzyme substrate complex.

In the oxidative half-reaction 2-cyclohexenone was used as substrate and the limiting rate constant decreases 260-fold, while the K_d value is not affected (see publication C, Figure S4b). The oxidative half-reaction combines a formal hydride transfer from the N(5) atom of the FMN to the β-carbon of the substrate and a proton uptake by the α-carbon. For OYE1 it was shown that both processes could be coupled at varying degrees (Kohli & Massey, 1998). The results of the transient kinetics measured for XenA are in good agreement with the assumption that the α-carbon of the oxidative substrate takes up the proton from Tyr183. It further indicates that either hydride and proton transfer in the reaction of reduced XenA with 2-cyclohexenone are coupled or that Tyr183 is necessary to stabilize the transition state during the hydride transfer, as it is the reoxidation of FMNH⁻ which proceeds very slowly.

The effect of an exchange of corresponding residues in homologue enzymes to phenylalanine has been published for OYE1 (Tyr196) (Kohli & Massey, 1998) and PETN reductase (Tyr186) (Khan *et al.*, 2005; Khan *et al.*, 2002). In OYE1 the corresponding residue also acts as proton donor in the oxidative half-reaction but is not involved in NAD(P)H binding. In PETN reductase neither the binding of NAD(P)H nor the oxidative half-reaction are affected by the mutation. The different results demonstrate that sequence and structural conservation are not necessarily leading to functional conservation (see Figure 4.1, Supplementary).

3.5   Tryptophan 302 – Redox dependent active site protection

Trp302 was observed to change its conformation from the "out"- to the "in"-position upon reduction of the FMN (see 3.1.3). To confirm the influence of this movement on the half-reactions of XenA, we exchanged the residue to an alanine and characterized the enzyme with transient kinetics, redox potentiometry and crystal structure analysis (see publication C). The amino acid exchange resulted in a fourfold lower specific activity and a change in the reduction potential of + 21 mV compared to XenA-wt (see Table 4.1, Supplementary). In

contrast to all the other mutant variants of XenA, where single turnover kinetics could be fitted to single exponential functions, the reactions of XenA-W302A revealed multiple phases. To describe the reductive half-reaction with NADPH two terms are necessary and to describe the oxidative half-reaction with 2-cyclohexenone three terms are necessary (see publication C, Figure S5). This indicates either a heterogenic protein sample or multiple reactive configurations. The fastest rates of both half-reactions showed clear substrate dependence and were used to calculate limiting rate constants and dissociation constants for the enzyme substrate complexes (see Table 4.1, Supplementary; publication C, Figure S3c and Figure S4c). The values determined for the oxidative half-reaction show no significant changes compared to XenA-wt. In contrast, the limiting rate constant of the reductive half-reaction is decreased ninefold and the dissociation constant for the XenA-W302A-NADPH complex is decreased fivefold. These results are in agreement with Trp302 contributing to the correct positioning of NADPH by partial steric hindrance. Changing the size of the substrate-binding pocket is therefore an essential part in the reaction mechanism, by contributing to a correct positioning of the substrates in both half-reactions (see Figure 4.1, Supplementary).

3.6 Tryptophan 358 – Decreasing the activation energy in the reductive half-reaction

Trp358 is part of the C-terminal α-helix of XenA and restricts the substrate-binding pocket of the neighboring monomer close to the dimethylbenzene ring of the FMN (see Figure 3.5). To examine the role of Trp358 during catalysis and dimerization we exchanged the residue against alanine and characterized the mutant enzyme with transient kinetics, redox potentiometry and crystal structure analysis (see publication C).

The exchange of the amino acid leads to a small perturbation of the C-terminal α-helix (see Figure 3.11). The side chain of the adjacent amino acid His357 rotates approximately 80° and fills now partly the space which was occupied by the indole ring of Trp358. However, no further differences compared to XenA-wt were observed. The specific activity of XenA-W358A is only 4% of XenA-wt, whereas the reduction potential shows no changes (see Table 4.1, Supplementary).
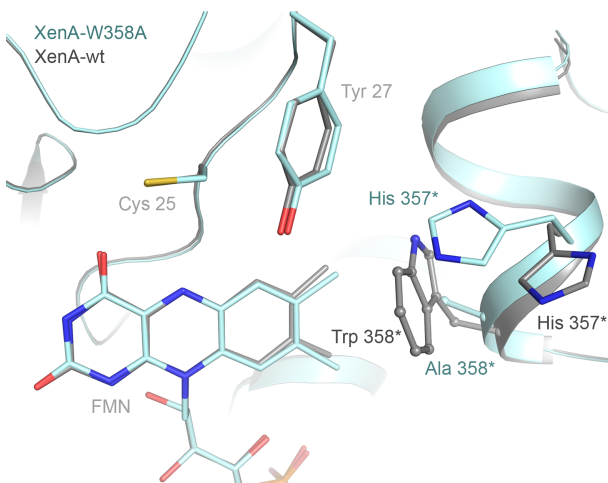
Figure 3.11: **Comparison of XenA-wt and XenA-W358A.** View on the superimposed active sites of wt-XenA-wt (gray) and XenA-W358A (light blue). All residues are shown in stick mode. Oxygen atoms are displayed in red, nitrogen atoms in blue, phosphorous atoms in orange and sulfur atoms in yellow (publication C, Figure 3).

Reductive (see publication C, Figure S3d) and oxidative (publication C, Figure S4d) half-reactions were performed with NADPH and 2-cyclohexenone, respectively, and the data are summarized in Table 4.1 (Supplementary). The dissociation constants for enzyme-substrate complexes in both half-reactions show only a slight increase, but in contrast to the oxidative half-reaction where the limiting rate constant is only slightly increased, k_{red} decreases 112-fold. Thus the reductive half-reaction becomes the rate limiting step in the overall reaction. The absence of Trp358 could allow a non-reactive placement of the nicotinamide ring of NADPH above the dimethylbenzene ring of FMN and additional interactions may be possible with the re-oriented His357. In the oxidative half-reaction substrates like 2-cyclohexenone and coumarin are mostly stabilized by two hydrogen bonds with His178 and His181, which automatically restraints horizontal movements of the substrate. The determination of activation parameters (change in activation enthalpy and entropy compared to XenA-wt) is in agreement with the different relative orientations of the isoalloxazine ring and the nicotinamide ring in XenA-W358A and XenA-wt (see Figure 4.1). But we note that the function of Trp358 during catalysis can be masked by other interactions caused by its exchange (Admiraal *et al.*, 2001; Kraut *et al.*, 2003). Thus, more detailed studies would be necessary to elucidate the role of this residue in the reductive-half-reaction.

3.7 True Michaelis complexes

For OYE family members crystal structures of enzymes in complex with substrates have only been published for non-reactive states. Complexes with substrates of the oxidative half-reaction are produced when the FMN cofactor is oxidized and therefore does not carry the electrons necessary for reduction. So far it was not possible to soak crystals of reduced enzyme with substrates, as the diffusion time of the substrates into the crystal is longer than the time needed for turnover.

In publication C we presented the identification of Tyr183 as the proton donor of the oxidative half-reaction (see 3.4, Synopsis). The enzyme variant XenA-Y183F, which was generated to determine the role of this tyrosine residue, provided the basis for the structure analysis of "true" Michaelis complexes. The limiting rate constant for the oxidative half-reaction of XenA-Y183F with 2-cyclohexenone decreased 260-fold, whereas the dissociation constant of the enzyme-substrate complex was unaffected. Further we know that the reactions with other substrates are slower (publication A, B). Therefore the time of substrate turnover is much smaller than the time needed for diffusion of different substrates into the crystals. As reduced XenA-Y183F crystallized under the same conditions as reduced XenA-wt we were able to soak these crystals with 2-cyclohexenone, coumarin, 8-hydroxycoumarin and 7-hydroxycoumarin. In publication D we present for the first time the structures of Michaelis complexes of an OYE family member and evidence for redox-dependent substrate binding in XenA.

The structures of reduced XenA-Y183F in complex with 2-cyclohexenone, coumarin, 7-hydroxycoumarin and 8-hydroxycoumarin could be solved at resolutions of 2.1 Å, 2.0 Å, 2.3 Å and 2.3 Å respectively (see Figure 3.12; see publication D, Table 1). All structures show the characteristic changes due to the reduction of the flavin; the isoalloxazine ring is distorted like in the reduced XenA-wt and the Trp302 residue is flipped from the "out"- to the "in"-position.

In a previous study the structures of oxidized XenA with 8-hydroxycoumarin and coumarin were published (Griese *et al.*, 2006). His178 and His181 appeared to be exclusively responsible for substrate specificity and orientation by hydrogen-bonding interactions in the active site. The structure of oxidized XenA in complex with 8-hydroxycoumarin revealed a non-productive binding mode of the substrate, in which the phenolic hydroxyl group forms the hydrogen bonds with His178 and His181 (see Figure 1.11c). With a resulting distance of 4.7 Å between C(4) of the 8-hydroxycoumarin and N(5) of the FMN, the hydride transfer would not be allowed. In the reduced XenA-Y183F structure in complex with 8-

hydroxycoumarin, the carbonyl oxygen of the substrate is in hydrogen-bonding distance to the histidine pair (see Figure 3.12a; see publication D, Table 1).
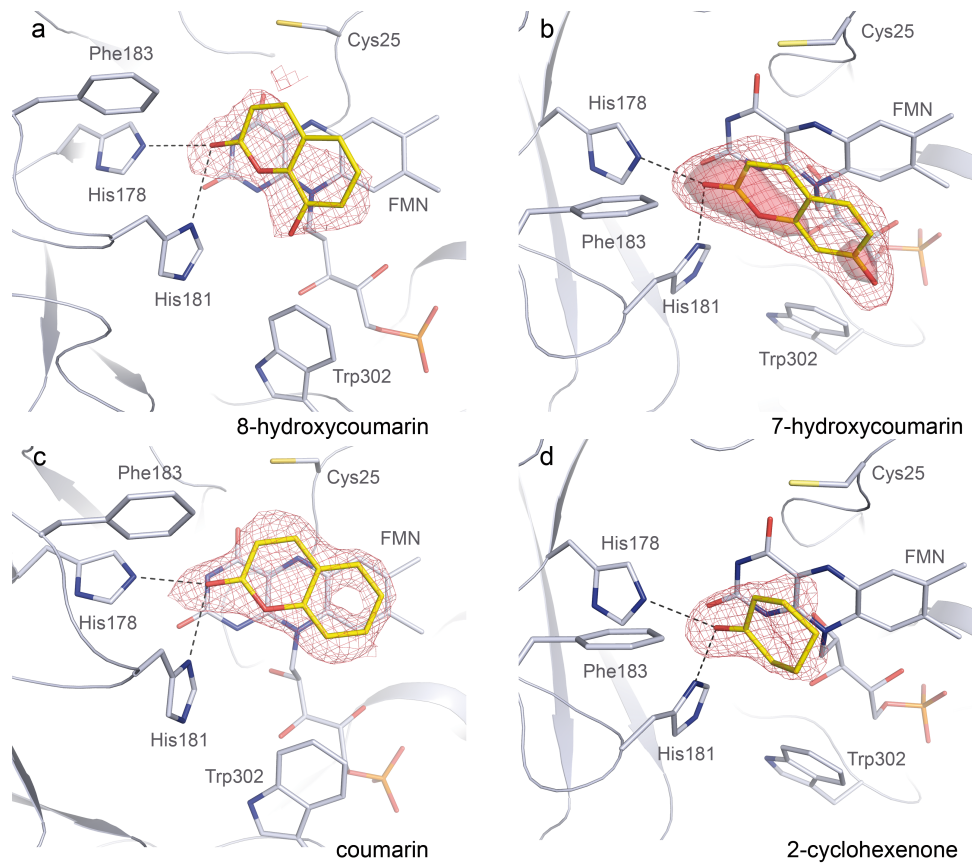

Figure 3.12: **Structures of Michaelis complexes of reduced XenA-Y183F and different substrates.** (a) View of the active site of reduced XenA-Y183F in complex with 8-hydroxycoumarin (yellow). The F_o-F_c map of 8-hydroxycoumarin is contoured at 2.5σ and is shown in red mesh representation. (b) View of the active site of reduced XenA-Y183F in complex with 7-hydroxycoumarin (yellow). The F_o-F_c map of 7-hydroxycoumarin is contoured at 3.0σ (red mesh representation) and at 6.0σ (red surface representation). (c) View of the active site of reduced XenA-Y183F in complex with coumarin (yellow). The F_o-F_c map of coumarin is contoured at 2.5σ and is shown in red mesh representation. (d) View of the active site of reduced XenA-Y183F in complex with 2-cyclohexenone (yellow). The F_o-F_c map of 2-cyclohexenone is contoured at 3.0σ and is shown in red mesh representation. The FMN and the amino acid side chain residues are displayed in stick mode. Carbon atoms shown in grey, nitrogen atoms are shown in blue, sulfur atoms are shown in light yellow and phosphorous atoms are shown in orange. Hydrogen bonding interactions between the enzyme and the substrates are displayed in dashed lines in grey (publication D, Figure 1).

This is equivalent to a 180° flip and a rotation of about 30° of the substrate compared to the binding to oxidized XenA (see publication A, Figure 2a). Now C(4) of the substrate and N(5) of the FMN are closer at a distance of 3.7 Å, which is a typical distance for a hydride transfer in flavoproteins and thus in agreement with the formation of a productive enzyme-substrate

complex (Fraaije & Mattevi, 2000). 7-hydroxycoumarin has also been investigated as a substrate (see Figure 5, publication D) in complex with oxidized and reduced XenA. Also for 7-hydroxycoumarin a non-productive binding-mode was observed in complex with the oxidized enzyme (see publication D, Figure 3). Like 8-hydroxycoumarin the phenolic group is coordinated to the histidine pair and the distance between C(4) of the substrate and N(5) of FMN is 4.0 Å. Interestingly in this case the substrate binding leads to the same flip of Trp302, termed "in" conformation, as observed only in the reduced XenA structures. This might be due to a favorable interaction of the benzene ring of Trp302 with the carbonyl and lactone ring oxygens, which are in an eligible distance to form an O…H-C hydrogen bond frequently found for tryptophan side chains (Petrella & Karplus, 2004) and not because of the reduction of the flavin. In the reduced state the electron density for 7-hydroxycoumarin provide evidence for a flipped binding, in which the lactone group is within hydrogen-bonding distance to the histidine pair (see Figure 3.12b; publication D, Figure 2b). Thus, the mode of binding is similar to 8-hydroxycoumarin.

The coumarin complexes with oxidized and reduced XenA are nearly identical (see Figure 3.12c; publication D, Figure 2c). In both complexes the carbonyl oxygen is in hydrogen bonding distance to the histidine pair and the distances between C(4) of the substrate and N(5) of FMN are with 2.9 Å (reduced XenA-Y183F) and 3.0 Å (oxidized XenA) close together.

Phenolic compounds were proposed to bind as the phenolate anion to oxidized OYE1 to form the typical long wavelength charge-transfer complexes (Abramovitz & Massey, 1976). This was explained by a lowering of the pK_a of the bound phenols by about three units. Very similar long-wavelength CT complexes are observed upon addition of 8-hydroxycoumarin to oxidized XenA, which are not observable with the related coumarin and are most likely characteristic for the interaction of the phenolate anion with the oxidized flavin (Griese *et al.*, 2006). In the oxidized state the isoalloxazine ring of the FMN is electron deficient, has a positive electrostatic potential and can therefore potentially stabilize these anions by donor atom – π bonding to the electron-poor flavin (see Figure 1.5, Introduction) (Breinlinger *et al.*, 1998). As the orientation of the substrate is dominated by the strength of the hydrogen bonding interactions to the histidine pair, 8-hydroxycoumarin and 7-hydroxycoumarin bind preferably with the phenolate oxygen instead of the carbonyl oxygen of the lactone group. In the reduced form of the isoalloxazine ring there is a change in the electronic state as well as in the electrostatic potential. Now the electrons are delocalized over the two outer rings. The middle ring is not aromatic anymore (8π electrons) and is a labile electron-excess system and therefore a good charge transfer donor. In this state the FMN is not electron deficient enough

to lower the pK_a of phenol to produce the phenolate. Therefore the more favorable hydrogen-bonding interaction is to the carbonyl oxygen of the lactone group of the oxidative substrates. 2-cyclohexenone is a substrate of most OYE family members, but up to now no structure of an OYE family member in complex with 2-cyclohexenone has been described. This is due to the low affinity of the substrates to the oxidized enzymes. In contrast we determined the K_d values of 86 µM and 83 µM for the complex of 2-cyclohexenone with XenA-wt and XenA-Y183F, respectively (see Table 4.1, Supplementary; see publication A and C), indicating a higher affinity for the substrate in the reduced state. Therefore we were able to soak the reduced XenA-Y186F crystals with the substrate and solve the structure of the complex. The electron density clearly shows, that the substrate is bound in the *endo*-form above the isoalloxazine ring (see Figure 3.12d and Figure 3.13).
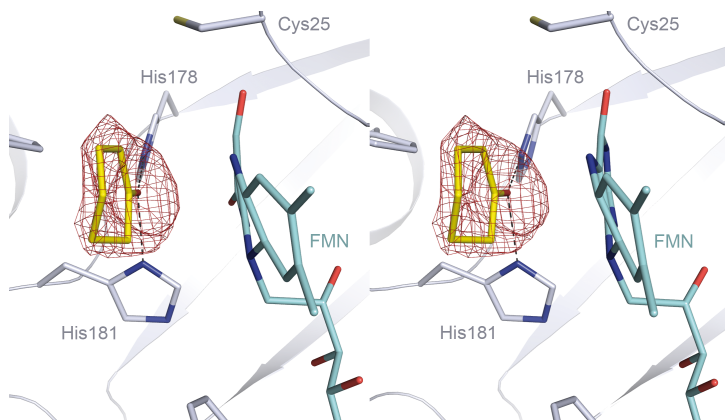

Figure 3.13: **View on the active site of reduced XenA-Y183F in complex with 2-cyclohexenone.** Stereoscopic view on the active site of reduced XenA-Y183F in complex with 2-cyclohexenone. Amino acid side chain residues and the FMN are displayed in stick mode. Carbon atoms of the FMN are shown in light blue, carbon atoms of the side chains are shown in grey, nitrogen atoms are shown in blue and sulfur atoms are shown in light yellow. The F_o-F_c map of 2-cyclohexenone is contoured at 3.0σ and is shown in red mesh representation (publication D, Figure 4).

The distance from the β-carbon (C(3)) to the N(5) is 3.6 Å and is within in the range of distance typically found for hydride transfers. The substrate is bound through hydrogen bonding interactions between its carbonyl oxygen and the histidine pair. Donor atom π-bonding to the electron poor flavin allows the binding of different anions above the FMN, like observed in different structures of OYE family members. These anions may act as competitive ligands against 2-cyclohexenone in the oxidized state but not in the reduced state of the enzyme.

Hence, substrate recognition and productive orientation are directly linked to the redox chemistry of the flavin and may also facilitate product egress.

4 Supplementary

Table 4.1: Specific activities, reduction potentials and transient kinetic data of XenA variants

Enzyme	Specific activity	E^0_m	Reductive half-reaction (NADPH)		Oxidative half-reaction (2-cyclohexenone)	
	(U mg^{-1})	(mV)	K_d (µM)	k_{red} (s^{-1})	K_d (µM)	k_{ox} (s^{-1})
wt-XenA [a]	6.7	-263	256 ± 12	35.7 ± 0.6	86 ± 2	13.1 ± 0.1
C25A [b]	1.11	-266	736 ± 47	19.0 ± 0.4	346 ± 3	26.3 ± 0.1
C25S [b]	3.34	-181	656 ± 86	171 ± 11	187 ± 7	5.12 ± 0.08
Y27F [c]	0.54	-264	463 ± 54	3.6 ± 0.2	151 ± 11	23.0 ± 0.3
Y183F [c]	0.06	-261	2770 ± 450	60 ± 7	83 ± 9	0.051 ± 0.001
W302A [c]	1.27	-242	35 ± 6	4.29 ± 0.09	674 ± 200	24 ± 5
W358A [c]	0.25	-265	509 ± 31	0.32 ± 0.01	192 ± 10	20.4 ± 0.3
			(NADH)		(coumarin)	
wt-XenA [a]			176 ± 14	1.50 ± 0.02	19.3 ± 0.6	0.243 ± 0.001
C25A [b]			1216 ± 81	0.76 ± 0.03	109 ± 10	0.43 ± 0.01
C25S [b]			800 ± 37	6.1 ± 0.2	53 ± 4	0.060 ± 0.001

[a] Data from publication A
[b] Data from publication B
[c] Data from publication C
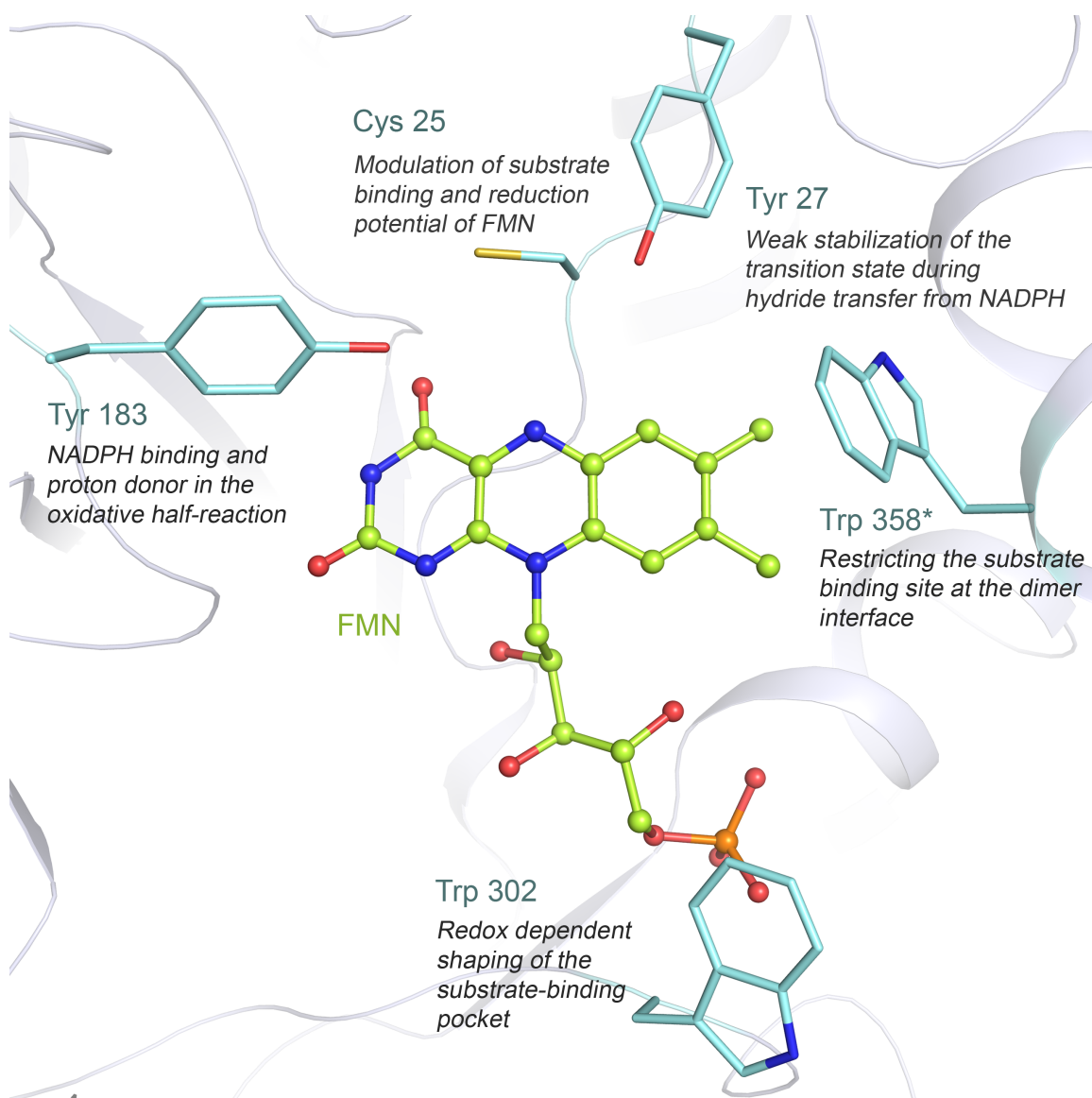
Figure 4.1   **Overall view of the active site of XenA.** Active site view of wt-XenA. All active site amino acid residues are displayed in stick mode. The FMN is shown in ball-and-stick representation. The carbon atoms of the amino acids are shown in light blue, the carbon atoms of FMN are shown in green. Oxygen atoms are shown in red, nitrogen atoms in blue, sulfur atoms in yellow and phosphorous atoms in orange (publication C, Figure 6).

5 List of abbreviations

CT	charge transfer
E_{ox}	oxidized enzyme
E_{red}	reduced enzyme
FAD	flavin adenine dinucleotide
Fl_{ox}	oxidized flavin
Fl_{red}	reduced flavin
FMN	flavin mononucleotide (oxidized form)
$FMNH_2$	flavin mononucleotide (reduced form)
GTN	glyceril trinitrate
HYE	Hansenula Yellow Enzyme
KIE	kinetic isotope effect
KYE	Kluyveromyces Yellow Enzyme
NADH	nicotinamide adenine dinucleotide (reduced form)
$NADH_4$	1,4,5,6-tetrahydro-nicotinamide adenine dinucleotide
NAD^+	nicotinamide adenine dinucleotide (oxidized form)
NADPH	nicotinamide adenine dinucleotide phosphate (reduced form)
$NADP^+$	nicotinamide adenine dinucleotide phosphate (oxidized form)
NemA	*N*-ethylmaleimide reductase
NerA	glycerol trinitrate reductase
NMR	nuclear magnetic resonance
OMO	1*H*-2-oxoquinoline 8-monooxygenase
OMR	1*H*-2-oxoquinoline 8-monooxygenase reductase
*At*OPR1-3	12-oxophytodienoate reductase 1 - 3 from *Arabidopsis thaliana*
*Le*OPR1-2	12-oxophytodienoate reductase 1 - 2 from *Lycopersicon esculentum*
*Os*OPR1	12-oxophytodienoate reductase 1 from *Oryza sativa*
OYE	Old Yellow Enzyme
TcOYE	Old Yellow Enzyme from *Trypanosoma cruzi*
QOR	quinoline oxidoreductase
PETN	pentaerythritol tetranitrate
rms	root mean square
ROS	reactive oxygen species
SYE1-4	Shewanella Yellow Enzyme 1 - 4
TNT	trinitrotoluene

(c-THN)TPN	$\alpha\text{-}O^2$-6B-cyclo-1,4,5,6-tetrahydro-nicotinamide adenine dinucleotide phosphate
TOYE	"ene" reductase from *Thermoanaerobacter pseudethanolicus* E39
TST	transition state theory
UV-Vis	ultraviolet-visible
XenA-F	xenobiotic reductase A - F
YqjM	OYE homologue from *Bacillus subtilis*

6   References

Abramovitz, A. S., and Massey, V. (1976) Interaction of phenols with old yellow enzyme. Physical evidence for charge-transfer complexes. *J Biol Chem* **251:** 5327-5336.

Adalbjörnsson, B. V., Toogood, H. S., Fryszkowska, A., Pudney, C. R., Jowitt, T. A., Leys, D., and Scrutton, N. S. (2010) Biocatalysis with thermostable enzymes: structure and properties of a thermophilic 'ene'-reductase related to old yellow enzyme. *Chembiochem* **11:** 197-207.

Admiraal, S. J., Meyer, P., Schneider, B., Deville-Bonne, D., Janin, J., and Herschlag, D. (2001) Chemical rescue of phosphoryl transfer in a cavity mutant: a cautionary tale for site-directed mutagenesis. *Biochemistry* **40:** 403-413.

Barna, T., Messiha, H. L., Petosa, C., Bruce, N. C., Scrutton, N. S., and Moody, P. C. (2002) Crystal structure of bacterial morphinone reductase and properties of the C191A mutant enzyme. *J Biol Chem* **277:** 30976-30983.

Barna, T. M., Khan, H., Bruce, N. C., Barsukov, I., Scrutton, N. S., and Moody, P. C. (2001) Crystal structure of pentaerythritol tetranitrate reductase: "flipped" binding geometries for steroid substrates in different redox states of the enzyme. *J Mol Biol* **310:** 433-447.

Basran, J., Harris, R. J., Sutcliffe, M. J., and Scrutton, N. S. (2003) H-tunneling in the multiple H-transfers of the catalytic cycle of morphinone reductase and in the reductive half-reaction of the homologous pentaerythritol tetranitrate reductase. *J Biol Chem* **278:** 43973-43982.

Basran, J., Sutcliffe, M. J., and Scrutton, N. S. (1999) Enzymatic H-transfer requires vibration-driven extreme tunneling. *Biochemistry* **38:** 3218-3222.

Bell, R. P. (1980) *The tunnel effect in chemistry*, Chapman and Hall, London, New York.

Berkholz, D. S., Faber, H. R., Savvides, S. N., and Karplus, P. A. (2008) Catalytic cycle of human glutathione reductase near 1 A resolution. *J Mol Biol* **382:** 371-384.

Biesgen, C., and Weiler, E. W. (1999) Structure and regulation of OPR1 and OPR2, two closely related genes encoding 12-oxophytodienoic acid-10,11-reductases from *Arabidopsis thaliana*. *Planta* **208:** 155-165.

Binks, P. R., French, C. E., Nicklin, S., and Bruce, N. C. (1996) Degradation of pentaerythritol tetranitrate by *Enterobacter cloaca*e PB2. *Appl Environ Microbiol* **62:** 1214-1219.

Blase, M., Bruntner, C., Tshisuaka, B., Fetzner, S., and Lingens, F. (1996) Cloning, expression, and sequence analysis of the three genes encoding quinoline 2-oxidoreductase, a molybdenum-containing hydroxylase from *Pseudomonas putida* 86. *J Biol Chem* **271:** 23068-23079.

Blehert, D. S., Fox, B. G., and Chambliss, G. H. (1999) Cloning and sequence analysis of two Pseudomonas flavoprotein xenobiotic reductases. *J Bacteriol* **181:** 6254-6263.

Blyth, A. W. (1879) LVI.-The composition of cows' milk in health and disease. *J Chem Soc, Trans* **35:** 530-539.

Boonstra, B., Rathbone, D. A., and Bruce, N. C. (2001) Engineering novel biocatalytic routes for production of semisynthetic opiate drugs. *Biomol Eng* **18:** 41-47.

Breinlinger, E. C., Keenan, C. J., and Rotello, V. M. (1998) Modulation of Flavin Recognition and Redox Properties through Donor Atom-π Interactions. *J Am Chem Soc.* **120:** 8606-8609.

Breithaupt, C., Kurzbauer, R., Lilie, H., Schaller, A., Strassner, J., Huber, R., Macheroux, P., and Clausen, T. (2006) Crystal structure of 12-oxophytodienoate reductase 3 from tomato: self-inhibition by dimerization. *Proc Natl Acad Sci U S A* **103:** 14337-14342.

Breithaupt, C., Kurzbauer, R., Schaller, F., Stintzi, A., Schaller, A., Huber, R., Macheroux, P., and Clausen, T. (2009) Structural basis of substrate specificity of plant 12-oxophytodienoate reductases. *J Mol Biol* **392:** 1266-1277.

Breithaupt, C., Strassner, J., Breitinger, U., Huber, R., Macheroux, P., Schaller, A., and Clausen, T. (2001) X-ray structure of 12-oxophytodienoate reductase 1 provides structural insight into substrate binding and specificity within the family of OYE. *Structure* **9:** 419-429.

Brige, A., Van den Hemel, D., Carpentier, W., De Smet, L., and Van Beeumen, J. J. (2006) Comparative characterization and expression analysis of the four Old Yellow Enzyme homologues from *Shewanella oneidensis* indicate differences in physiological function. *Biochem J* **394:** 335-344.

Briggs, W. R., and Huala, E. (1999) Blue-light photoreceptors in higher plants. *Annu Rev Cell Dev Biol* **15:** 33-62.

Bruice, T. C., and Benkovic, S. J. (2000) Chemical basis for enzyme catalysis. *Biochemistry* **39:** 6267-6274.

Bruice, T. C., and Pandit, U. K. (1960) Intramolecular Models Depicting the Kinetic Importance of "Fit" in Enzymatic Catalysis. *Proc Natl Acad Sci U S A* **46:** 402-404.

Cashmore, A. R., Jarillo, J. A., Wu, Y. J., and Liu, D. (1999) Cryptochromes: blue light receptors for plants and animals. *Science* **284:** 760-765.

Craig, D. H., Moody, P. C., Bruce, N. C., and Scrutton, N. S. (1998) Reductive and oxidative half-reactions of morphinone reductase from *Pseudomonas putida* M10: a kinetic and thermodynamic analysis. *Biochemistry* **37:** 7598-7607.

Cuello, A. O., McIntosh, C. M., and Rotello, V. M. (2000) Model Systems for Flavoenzyme Activity. The Role of N(3)-H Hydrogen Bonding in Flavin Redox Processes. *J Am Chem Soc* **122:** 3517-3521.

References

De Colibus, L., and Mattevi, A. (2006) New frontiers in structural flavoenzymology. *Curr Opin Struct Biol* **16:** 722-728.

Emsley, P., and Cowtan, K. (2004) Coot: model-building tools for molecular graphics. *Acta Crystallogr D Biol Crystallogr* **60:** 2126-2132.

Fetzner, S., Tshisuaka, B., Lingens, F., Kappl, R., and Huttermann, J. (1998) Bacterial degradation of quinoline and derivatives - Pathways and their biocatalysts. *Angew Chem Int Edit* **37:** 577-597.

Fitzpatrick, T. B., Amrhein, N., and Macheroux, P. (2003) Characterization of YqjM, an Old Yellow Enzyme homolog from *Bacillus subtilis* involved in the oxidative stress response. *J Biol Chem* **278:** 19891-19897.

Fitzpatrick, T. B., Auweter, S., Kitzing, K., Clausen, T., Amrhein, N., and Macheroux, P. (2004) Structural and functional impairment of an Old Yellow Enzyme homologue upon affinity tag incorporation. *Protein Expr Purif* **36:** 280-291.

Fox, B. G., Malone, T. E., Johnson, K. A., Madson, S. E., Aceti, D., Bingman, C. A., Blommel, P. G., Buchan, B., Burns, B., Cao, J., Cornilescu, C., Doreleijers, J., Ellefson, J., Frederick, R., Geetha, H., Hruby, D., Jeon, W. B., Kimball, T., Kunert, J., Markley, J. L., Newman, C., Olson, A., Peterson, F. C., Phillips, G. N., Jr., Primm, J., Ramirez, B., Rosenberg, N. S., Runnels, M., Seder, K., Shaw, J., Smith, D. W., Sreenath, H., Song, J., Sussman, M. R., Thao, S., Troestler, D., Tyler, E., Tyler, R., Ulrich, E., Vinarov, D., Vojtik, F., Volkman, B. F., Wesenberg, G., Wrobel, R. L., Zhang, J., Zhao, Q., and Zolnai, Z. (2005) X-ray structure of *Arabidopsis* At1g77680, 12-oxophytodienoate reductase isoform 1. *Proteins* **61:** 206-208.

Fox, K. M., and Karplus, P. A. (1994) Old yellow enzyme at 2 A resolution: overall structure, ligand binding, and comparison with related flavoproteins. *Structure* **2:** 1089-1105.

Fraaije, M. W., and Mattevi, A. (2000) Flavoenzymes: diverse catalysts with recurrent features. *Trends Biochem Sci* **25:** 126-132.

French, C. E., and Bruce, N. C. (1994) Purification and characterization of morphinone reductase from *Pseudomonas putida* M10. *Biochem J* **301 (Pt 1):** 97-103.

French, C. E., Nicklin, S., and Bruce, N. C. (1996) Sequence and properties of pentaerythritol tetranitrate reductase from *Enterobacter cloacae* PB2. *J Bacteriol* **178:** 6623-6627.

French, C. E., Nicklin, S., and Bruce, N. C. (1998) Aerobic degradation of 2,4,6-trinitrotoluene by *Enterobacter cloac*ae PB2 and by pentaerythritol tetranitrate reductase. *Appl Environ Microbiol* **64:** 2864-2868.

French, C. E., Rosser, S. J., Davies, G. J., Nicklin, S., and Bruce, N. C. (1999) Biodegradation of explosives by transgenic plants expressing pentaerythritol tetranitrate reductase. *Nat Biotechnol* **17:** 491-494.

Gasch, A. P., Spellman, P. T., Kao, C. M., Carmel-Harel, O., Eisen, M. B., Storz, G., Botstein, D., and Brown, P. O. (2000) Genomic expression programs in the response of yeast cells to environmental changes. *Mol Biol Cell* **11:** 4241-4257.

Griese, J. J., R, P. J., Schwarzinger, S., and Dobbek, H. (2006) Xenobiotic reductase A in the degradation of quinoline by *Pseudomonas putida* 86: physiological function, structure and mechanism of 8-hydroxycoumarin reduction. *J Mol Biol* **361:** 140-152.

Haarer, B. K., and Amberg, D. C. (2004) Old yellow enzyme protects the actin cytoskeleton from oxidative stress. *Mol Biol Cell* **15:** 4522-4531.

Haas, E. (1938) Isolierung eines neuen gelben Ferments. *Biochem Z* **298:** 378-390.

Hailes, A. M., and Bruce, N. C. (1993) Biological synthesis of the analgesic hydromorphone, an intermediate in the metabolism of morphine, by *Pseudomonas putida* M10. *Appl Environ Microbiol* **59:** 2166-2170.

He, X. Y., Yang, S. Y., and Schulz, H. (1997) Cloning and expression of the fadH gene and characterization of the gene product 2,4-dienoyl coenzyme A reductase from *Escherichia coli*. *Eur J Biochem* **248:** 516-520.

Jencks, W. P. (1963) Mechanism of Enzyme Action. *Annu Rev Biochem* **32:** 639-676.

Jimenez, J. I., Minambres, B., Garcia, J. L., and Diaz, E. (2002) Genomic analysis of the aromatic catabolic pathways from *Pseudomonas putida* KT2440. *Environ Microbiol* **4:** 824-841.

Jonsson, T., Glickman, M. H., Sun, S., and Klinman, J. P. (1996) Experimental evidence for extensive tunneling of hydrogen in the lipoxygenase reaction: implications for enzyme catalysis. *J Am Chem Soc* **118:** 10319-10320.

Kao, Y. T., Saxena, C., He, T. F., Guo, L., Wang, L., Sancar, A., and Zhong, D. (2008) Ultrafast dynamics of flavins in five redox states. *J Am Chem Soc* **130:** 13132-13139.

Kataoka, M., Kotaka, A., Thiwthong, R., Wada, M., Nakamori, S., and Shimizu, S. (2004) Cloning and overexpression of the old yellow enzyme gene of *Candida macedoniensis*, and its application to the production of a chiral compound. *J Biotechnol* **114:** 1-9.

Khan, H., Barna, T., Bruce, N. C., Munro, A. W., Leys, D., and Scrutton, N. S. (2005) Proton transfer in the oxidative half-reaction of pentaerythritol tetranitrate reductase. Structure of the reduced enzyme-progesterone complex and the roles of residues Tyr186, His181, His184. *FEBS J* **272:** 4660-4671.

Khan, H., Barna, T., Harris, R. J., Bruce, N. C., Barsukov, I., Munro, A. W., Moody, P. C., and Scrutton, N. S. (2004) Atomic resolution structures and solution behavior of enzyme-substrate complexes of *Enterobacter cloacae* PB2 pentaerythritol tetranitrate reductase. Multiple conformational states and implications for the mechanism of nitroaromatic explosive degradation. *J Biol Chem* **279:** 30563-30572.

Khan, H., Harris, R. J., Barna, T., Craig, D. H., Bruce, N. C., Munro, A. W., Moody, P. C., and Scrutton, N. S. (2002) Kinetic and structural basis of reactivity of pentaerythritol tetranitrate reductase with NADPH, 2-cyclohexenone, nitroesters, and nitroaromatic explosives. *J Biol Chem* **277:** 21906-21912.

Kitzing, K., Fitzpatrick, T. B., Wilken, C., Sawa, J., Bourenkov, G. P., Macheroux, P., and Clausen, T. (2005) The 1.3 A crystal structure of the flavoprotein YqjM reveals a novel class of Old Yellow Enzymes. *J Biol Chem* **280:** 27904-27913.

Kohli, R. M., and Massey, V. (1998) The oxidative half-reaction of Old Yellow Enzyme. The role of tyrosine 196. *J Biol Chem* **273:** 32763-32770.

Komduur, J. A., Leao, A. N., Monastyrska, I., Veenhuis, M., and Kiel, J. A. (2002) Old yellow enzyme confers resistance of *Hansenula polymorpha* towards allyl alcohol. *Curr Genet* **41:** 401-406.

Kraut, D. A., Carroll, K. S., and Herschlag, D. (2003) Challenges in enzyme mechanism and energetics. *Annu Rev Biochem* **72:** 517-571.

Kraut, J. (1988) How do enzymes work? *Science* **242:** 533-540.

Kubata, B. K., Kabututu, Z., Nozaki, T., Munday, C. J., Fukuzumi, S., Ohkubo, K., Lazarus, M., Maruyama, T., Martin, S. K., Duszenko, M., and Urade, Y. (2002) A key role for old yellow enzyme in the metabolism of drugs by *Trypanosoma cruzi*. *J Exp Med* **196:** 1241-1251.

Kwasnicka, D. A., Krakowiak, A., Thacker, C., Brenner, C., and Vincent, S. R. (2003) Coordinate expression of NADPH-dependent flavin reductase, Fre-1, and Hint-related 7meGMP-directed hydrolase, DCS-1. *J Biol Chem* **278:** 39051-39058.

Lee, J., Godon, C., Lagniel, G., Spector, D., Garin, J., Labarre, J., and Toledano, M. B. (1999) Yap1 and Skn7 control two specialized oxidative stress response regulons in yeast. *J Biol Chem* **274:** 16040-16046.

Lim, L. W., Shamala, N., Mathews, F. S., Steenkamp, D. J., Hamlin, R., and Xuong, N. H. (1986) Three-dimensional structure of the iron-sulfur flavoprotein trimethylamine dehydrogenase at 2.4-A resolution. *J Biol Chem* **261:** 15140-15146.

Loach, P. A. (1973) Oxidation-reduction potentials: Absorbance bands and molar absorbance of compounds used in biochemical studies, in *Handbook of Biochemistry Selected Data for Molecular Biology* (Sorber, H. A., Ed.), pp J33-J40, CRC Press, Cleveland, Ohio.

Madigan, M. T., Martinko, J. M., and Parker, J. (2003) *Brock Biology of Microorganisms*, 10 ed., Prentice-Hall, Inc., New Jersey.

Malone, T. E., Madson, S. E., Wrobel, R. L., Jeon, W. B., Rosenberg, N. S., Johnson, K. A., Bingman, C. A., Smith, D. W., Phillips, G. N., Jr., Markley, J. L., and Fox, B. G. (2005) X-ray structure of *Arabidopsis* At2g06050, 12-oxophytodienoate reductase isoform 3. *Proteins* **58:** 243-245.

Marshall, S. J., Krause, D., Blencowe, D. K., and White, G. F. (2004) Characterization of glycerol trinitrate reductase (NerA) and the catalytic role of active-site residues. *J Bacteriol* **186:** 1802-1810.

Massey, V. (2000) The chemical and biological versatility of riboflavin. *Biochem Soc Trans* **28:** 283-296.

Massey, V., and Schopfer, L. M. (1986) Reactivity of old yellow enzyme with alpha-NADPH and other pyridine nucleotide derivatives. *J Biol Chem* **261:** 1215-1222.

Massey, V., Strickland, S., Mayhew, S. G., Howell, L. G., Engel, P. C., Matthews, R. G., Schuman, M., and Sullivan, P. A. (1969) The production of superoxide anion radicals in the reaction of reduced flavins and flavoproteins with molecular oxygen. *Biochem Biophys Res Commun* **36:** 891-897.

Messiha, H. L., Bruce, N. C., Sattelle, B. M., Sutcliffe, M. J., Munro, A. W., and Scrutton, N. S. (2005) Role of active site residues and solvent in proton transfer and the modulation of flavin reduction potential in bacterial morphinone reductase. *J Biol Chem* **280:** 27103-27110.

Messiha, H. L., Munro, A. W., Bruce, N. C., Barsukov, I., and Scrutton, N. S. (2005) Reaction of morphinone reductase with 2-cyclohexen-1-one and 1-nitrocyclohexene: proton donation, ligand binding, and the role of residues Histidine 186 and Asparagine 189. *J Biol Chem* **280:** 10695-10709.

Miranda, M., Ramirez, J., Guevara, S., Ongay-Larios, L., Pena, A., and Coria, R. (1995) Nucleotide sequence and chromosomal localization of the gene encoding the Old Yellow Enzyme from *Kluyveromyces lactis*. *Yeast* **11:** 459-465.

Miura, K., Tomioka, Y., Suzuki, H., Yonezawa, M., Hishinuma, T., and Mizugaki, M. (1997) Molecular cloning of the nemA gene encoding N-ethylmaleimide reductase from *Escherichia coli*. *Biol Pharm Bull* **20:** 110-112.

Müller, F. (1983) The flavin redox-system and its biological function, in *Topics in Current Chemistry*, pp 71-107, Springer Verlag, Berlin Heidelberg New York.

Niino, Y. S., Chakraborty, S., Brown, B. J., and Massey, V. (1995) A new old yellow enzyme of *Saccharomyces cerevisiae*. *J Biol Chem* **270:** 1983-1991.

Nishino, T., Miura, R., Tanokura, M., and Fukui, K. (2005) Flavins and Flavoproteins 2005s, in *Proceedings of the 15th International Symposium on Flavins and Flavoproteins*, Japan: ARchiTect Inc, Japan Tokyo.

Paine, M. J., Garner, A. P., Powell, D., Sibbald, J., Sales, M., Pratt, N., Smith, T., Tew, D. G., and Wolf, C. R. (2000) Cloning and characterization of a novel human dual flavin reductase. *J Biol Chem* **275:** 1471-1478.

Petrella, R. J., and Karplus, M. (2004) The role of carbon-donor hydrogen bonds in stabilizing tryptophan conformations. *Proteins* **54:** 716-726.

References

Phillips, D. C., Sternberg, M. J., Thornton, J. M., and Wilson, I. A. (1978) An analysis of the structure of triose phosphate isomerase and its comparison with lactate dehydrogenase. *J Mol Biol* **119:** 329-351.

Pudney, C. R., Hay, S., Pang, J., Costello, C., Leys, D., Sutcliffe, M. J., and Scrutton, N. S. (2007) Mutagenesis of morphinone reductase induces multiple reactive configurations and identifies potential ambiguity in kinetic analysis of enzyme tunneling mechanisms. *J Am Chem Soc* **129:** 13949-13956.

Reekmans, R., De Smet, K., Chen, C., Van Hummelen, P., and Contreras, R. (2005) Old yellow enzyme interferes with Bax-induced NADPH loss and lipid peroxidation in yeast. *FEMS Yeast Res* **5:** 711-725.

Rohde, B. H., Schmid, R., and Ullrich, M. S. (1999) Thermoregulated expression and characterization of an NAD(P)H-dependent 2-cyclohexen-1-one reductase in the plant pathogenic bacterium *Pseudomonas syringae* pv. glycinea. *J Bacteriol* **181:** 814-822.

Rohdich, F., Wiese, A., Feicht, R., Simon, H., and Bacher, A. (2001) Enoate reductases of Clostridia. Cloning, sequencing, and expression. *J Biol Chem* **276:** 5779-5787.

Rosche, B., Tshisuaka, B., Fetzner, S., and Lingens, F. (1995) 2-Oxo-1,2-dihydroquinoline 8-monooxygenase, a two-component enzyme system from *Pseudomonas putida* 86. *J Biol Chem* **270:** 17836-17842.

Saito, K., Thiele, D. J., Davio, M., Lockridge, O., and Massey, V. (1991) The cloning and expression of a gene encoding Old Yellow Enzyme from *Saccharomyces carlsbergensis*. *J Biol Chem* **266:** 20720-20724.

Sancar, A. (1994) Structure and function of DNA photolyase. *Biochemistry* **33:** 2-9.

Schaller, F., Biesgen, C., Mussig, C., Altmann, T., and Weiler, E. W. (2000) 12-Oxophytodienoate reductase 3 (OPR3) is the isoenzyme involved in jasmonate biosynthesis. *Planta* **210:** 979-984.

Schaller, F., and Weiler, E. W. (1997) Molecular cloning and characterization of 12-oxophytodienoate reductase, an enzyme of the octadecanoid signaling pathway from *Arabidopsis thaliana*. Structural and functional relationship to yeast old yellow enzyme. *J Biol Chem* **272:** 28066-28072.

Schwarz, G., Bauder, R., Speer, M., Rommel, T. O., and Lingens, F. (1989) Microbial metabolism of quinoline and related compounds. II. Degradation of quinoline by *Pseudomonas fluorescens* 3, *Pseudomonas putida* 86 and *Rhodococcus* spec. B1. *Biol Chem Hoppe Seyler* **370:** 1183-1189.

Schwarz, G., Senghas, E., Erben, A., Schafer, B., Lingens, F., and Hoke, H. (1988) Microbial-Metabolism of Quinoline and Related-Compounds .1. Isolation and Characterization of Quinoline-Degrading Bacteria. *Syst Appl Microbiol* **10:** 185-190.

Segel, I. H. (1993) *Enzyme Kinetics*, John Wiley and Sons, New York.

Shukla, O. P. (1986) Microbial transformation of quinoline by a *Pseudomonas* sp. *Appl Environ Microbiol* **51:** 1332-1342.

Snape, J. R., Walkley, N. A., Morby, A. P., Nicklin, S., and White, G. F. (1997) Purification, properties, and sequence of glycerol trinitrate reductase from *Agrobacterium radiobacter*. *J Bacteriol* **179:** 7796-7802.

Sobajima, H., Takeda, M., Sugimori, M., Kobashi, N., Kiribuchi, K., Cho, E. M., Akimoto, C., Yamaguchi, T., Minami, E., Shibuya, N., Schaller, F., Weiler, E. W., Yoshihara, T., Nishida, H., Nojiri, H., Omori, T., Nishiyama, M., and Yamane, H. (2003) Cloning and characterization of a jasmonic acid-responsive gene encoding 12-oxophytodienoic acid reductase in suspension-cultured rice cells. *Planta* **216:** 692-698.

Stewart, R. C., and Massey, V. (1985) Potentiometric studies of native and flavin-substituted Old Yellow Enzyme. *J Biol Chem* **260:** 13639-13647.

Stott, K., Saito, K., Thiele, D. J., and Massey, V. (1993) Old Yellow Enzyme. The discovery of multiple isozymes and a family of related proteins. *J Biol Chem* **268:** 6097-6106.

Strassner, J., Furholz, A., Macheroux, P., Amrhein, N., and Schaller, A. (1999) A homolog of old yellow enzyme in tomato. Spectral properties and substrate specificity of the recombinant protein. *J Biol Chem* **274:** 35067-35073.

Sucharitakul, J., Chaiyen, P., Entsch, B., and Ballou, D. P. (2005) The reductase of p-hydroxyphenylacetate 3-hydroxylase from *Acinetobacter baumannii* requires p-hydroxyphenylacetate for effective catalysis. *Biochemistry* **44:** 10434-10442.

Theorell, H. (1935) Reindarstellung der Wirkungsgruppe des gelben Ferments. *Biochem Z* **275:** 344-346.

Theorell, H. (1955) Nobel Prize Lecture. *http://www.nobel.se/medicine/laureates/1955/theorell-lecture.pdf*.

Turner, J. G., Ellis, C., and Devoto, A. (2002) The jasmonate signal pathway. *Plant Cell* **14 Suppl:** S153-164.

Van Aken, B. (2009) Transgenic plants for enhanced phytoremediation of toxic explosives. *Curr Opin Biotechnol* **20:** 231-236.

van Dillewijn, P., Wittich, R. M., Caballero, A., and Ramos, J. L. (2008) Subfunctionality of hydride transferases of the old yellow enzyme family of flavoproteins of *Pseudomonas putida*. *Appl Environ Microbiol* **74:** 6703-6708.

Vaz, A. D., Chakraborty, S., and Massey, V. (1995) Old Yellow enzyme: aromatization of cyclic enones and the mechanism of a novel dismutation reaction. *Biochemistry* **34:** 4246-4256.

Warburg, O., and Christian, W. (1932) Ein zweites sauerstoffübertragendes Ferment und sein Absorptionsspektrum. *Naturwissenschaften* **20:** 688.

Williams, R. E., and Bruce, N. C. (2002) 'New uses for an Old Enzyme'--the Old Yellow Enzyme family of flavoenzymes. *Microbiology* **148:** 1607-1614.

Williams, R. E., Rathbone, D. A., Scrutton, N. S., and Bruce, N. C. (2004) Biotransformation of explosives by the old yellow enzyme family of flavoproteins. *Appl Environ Microbiol* **70:** 3566-3574.

Xu, D., Kohli, R. M., and Massey, V. (1999) The role of threonine 37 in flavin reactivity of the old yellow enzyme. *Proc Natl Acad Sci U S A* **96:** 3556-3561.

7 List of publications

Publication A

Olivia Spiegelhauer, Frank Dickert, Sophia Mende, Dimitri Niks, Russ Hille, G. Matthias Ullmann and Holger Dobbek (2009): Kinetic characterization of xenobiotic reductase A from *Pseudomonas putida* 86. *Biochemistry* **48**, 11412-11420

I established the protein expression, purification, photoreduction and redox potential measurements of XenA as well as the steady state kinetic experiments. The docking simulations and electrostatic calculations were performed by G. Matthias Ullmann and Frank Dickert. I performed the pre-steady state kinetic experiments with the help of Sophia Mende and Dimitri Niks. The project was planned and supervised by Holger Dobbek and Russ Hille. Holger Dobbek and I wrote the manuscript.

Publication B

Olivia Spiegelhauer, Sophia Mende, Frank Dickert, Stefan H. Knauer, G. Matthias Ullmann and Holger Dobbek (2010): Cysteine as a modulator residue in the active site of xenobiotic reductase A: A structural, thermodynamic and kinetic study. *Journal of Molecular Biology* **398**, 66-82

The protein expression and purification was conducted by Sophia Mende. Sophia Mende and myself performed the mutagenesis, the ligand binding studies, the photoreduction experiments, the redox potential determination and the stopped flow studies. Matthias Ullmann and Frank Dickert calculated the protonation probabilities. Crystallization and data collection were done by Stefan H. Knauer, Sophia Mende and myself. Holger Dobbek performed the structure refinement and planned and supervised the project. Holger Dobbek and I wrote the manuscript.

Publication C

Olivia Spiegelhauer, Sophia Mende, Stefan H. Knauer and Holger Dobbek: Determinants of substrate-binding and-protonation in the flavoenzyme xenobiotic reductase A. *Journal of Molecular Biology, in revision.*

I performed the mutagenesis, protein expression, the photoreduction experiments, the redox potential determination, the stopped-flow studies and crystallization. Sophia Mende and I did the protein purification. Holger Dobbek, Stefan Knauer and myself performed the data collection and structure refinement. Holger Dobbek planned and supervised the project. Holger Dobbek and I wrote the manuscript.

Publication D

Olivia Spiegelhauer and Holger Dobbek: Structures of Michaelis complexes provide evidence for redox dependent substrate binding in the flavoenzyme xenobiotic reductase A. *in preparation*

I performed the mutagenesis, protein expression and purification as well as the stopped flow studies. Crystallization and data collection were done by myself. Holger Dobbek and myself performed the structure refinement. Holger Dobbek planned and supervised the project. Holger Dobbek and I wrote the manuscript.

8 Publication A

Olivia Spiegelhauer, Frank Dickert, Sophia Mende, Dimitri Niks, Russ Hille, G. Matthias Ullmann and Holger Dobbek (2009): Kinetic characterization of xenobiotic reductase A from *Pseudomonas putida* 86. *Biochemistry* **48**, 11412-11420.

Kinetic Characterization of Xenobiotic Reductase A from *Pseudomonas putida* 86[†]

Olivia Spiegelhauer,[‡] Frank Dickert,[§] Sophia Mende,[‡] Dimitri Niks,[||] Russ Hille,[||] Matthias Ullmann,[§] and
Holger Dobbek*,[‡]

[‡]*Bioinorganic Chemistry and* [§]*Structural Biology/Bioinformatics, University of Bayreuth, 95447 Bayreuth, Germany, and* [||]*Department
of Biochemistry, University of California, Riverside, California 92507*

Received August 6, 2009; Revised Manuscript Received September 25, 2009

ABSTRACT: Xenobiotic reductase A (XenA) from *Pseudomonas putida* is a member of the old-yellow-enzyme family of flavin-containing enzymes and catalyzes the NADH/NADPH-dependent reduction of various substrates, including 8-hydroxycoumarin and 2-cyclohexenone. Here we present a kinetic and thermodynamic analysis of XenA. In the reductive half-reaction, complexes of oxidized XenA with NADH or NADPH form charge-transfer (CT) intermediates with increased absorption around 520−560 nm, which occurs with a second-order rate constant of $9.4 \times 10^5 \, M^{-1} \, s^{-1}$ with NADH and $6.4 \times 10^5 \, M^{-1} \, s^{-1}$ with NADPH, while its disappearance is controlled by a rate constant of 210−250 s^{-1} with both substrates. Transfer of hydride from NADPH proceeds 24 times more rapidly than from NADH. This modest kinetic preference of XenA for NADPH is unlike the typical discrimination between NADH and NADPH by binding affinity. Docking studies combined with electrostatic energy calculations indicate that the 2′-phosphate group attached to the adenine moiety of NADPH is responsible for this difference. The reductions of 2-cyclohexenone and coumarin in the oxidative half-reaction are both concentration-dependent under the assay conditions and reveal a more than 50-fold larger limiting rate constant for the reduction of 2-cyclohexenone compared to that of coumarin. Our work corroborates the link between XenA and other members of the old-yellow-enzyme family but demonstrates several differences in the reactivity of these enzymes.

Xenobiotic reductases are bacterial enzymes of the old-yellow-enzyme (OYE)[1] family known to catalyze the reduction of the olefinic bond of α,β-unsaturated carbonyl compounds, including ketones and esters with NADH or NADPH as the electron source (*1−7*). Xenobiotic reductase A (XenA) from *Pseudomonas putida* catalyzes the NAD(P)H-dependent reduction of various biotic and abiotic compounds (*8*). Recently, it was shown that XenA catalyzes the reduction of the C3−C4 double bond of 8-hydroxycoumarin, indicating its involvement in the degradation of quinoline, a ubiquitous N-heterocyclic pollutant with carcinogenic properties (*9*), along the 8-hydroxycoumarin pathway in *P. putida* 86 (*10*).

The crystal structure of XenA has been determined for the enzyme alone and in complex with two different substrates (*10*). The structure reveals a dimeric arrangement with one $(\beta/\alpha)_8$ barrel domain per monomer, which binds a FMN molecule on the solvent-exposed C-terminal side of the barrel. A tryptophan residue from the C-terminal helix of the neighboring monomer protrudes into the active site and forms one wall of the substrate-binding pocket. The active site is further lined by histidine and tyrosine residues, which presumably are needed to bind and orient the substrates, stabilize developing charges during

turnover, and donate protons. A feature distinguishing XenA from most members of the OYE family is the presence of a cysteine residue in the active site near the N5 position of the isoalloxazine ring (*10*). XenA shares its overall arrangement and active site architecture with YqjM, and both have been suggested to form a new subfamily within the OYE family (*11*).

Genome sequencing projects revealed the OYE-like enzymes to be a rapidly growing family, which in some organisms, such as *Saccharomyces cerevisiae* (*12*), *Shewanella oneidensis* (*13*), and *P. putida* KT2440 (*14*), occur in up to six copies. The modest substrate specificity of OYE-like enzymes has attracted the attention of biotechnologists (*15*), further motivating more detailed studies of the physiological function and catalytic mechanisms of different variants. Therefore, several members of this enzyme family have been intensely studied, and the structural, kinetic, and thermodynamic characteristics of their interaction with various substrates have been elucidated, which have revealed that despite their similar structures they differ remarkably in their reactivities (*11, 16−33*). Here, we have investigated the thermodynamic characteristics of XenA and studied its reactivity with various substrates. Our data suggest an electrostatic basis for the kinetic preference of XenA for NADPH over NADH.

EXPERIMENTAL PROCEDURES

Chemicals and Enzymes. Complex microbial media were purchased from Roth and Otto Nordwald and were prepared as described by Sambrook et al. (*35*). All chemicals and enzymes were purchased from Fluka and AppliChem. 5-Deaza-10-methyl-3-sulfopropylisoalloxazine was a gift from P. M. H. Kroneck (University of Konstanz, Konstanz, Germany). The extinction

---

coefficients of XenA (ε_{280} = 71050 M^{-1} cm^{-1}, and ε_{464} = 12200 M^{-1} cm^{-1}), NADH (ε_{340} = 6200 M^{-1} cm^{-1}), and NADPH (ε_{340} = 6220 M^{-1} cm^{-1}) were used to calculate the concentrations of the enzyme, cofactor, and substrates.

Protein Expression, Purification, and Activity Assay. The gene of XenA was isolated from *P. putida* 86 and cloned into a pET11a vector as described previously (*10*). *XenA* was expressed in *Escherichia coli* Rosetta(DE3)pLysS using LB medium supplemented with 100 μg/mL ampicillin and 34 μg/mL chloramphenicol, at 20 °C overnight.

Crude cell extracts were prepared in 50 mM Tris buffer (pH 8.0) for a purification that included three chromatographic steps. The first column was a Q-Sepharose FF column, followed by Source 15-ISO and Sephacryl S-200 columns. Before size-exclusion chromatography was conducted, the protein was reconstituted on ice with 5 mM FMN overnight. Eight liters of cell culture yielded 600 mg of enzyme with a purity exceeding 95% estimated via SDS−PAGE (data not shown). The pure enzyme was stored at a concentration of ~50 mg/mL in 50 mM Tris buffer (pH 8.0) at −80 °C.

The specific activity of XenA was determined from absorbance changes at 340 nm due to the oxidation of NADPH. To prevent the oxidase activity of XenA, all kinetic measurements were performed under anoxic conditions. We made solutions anoxic by bubbling them with dinitrogen gas. The cuvettes were sealed by screw caps with a rubber septum and flushed with dinitrogen gas before use. The typical oxidase activity found under these conditions was 0.14 unit mg^{-1}. Activity tests were performed using an Analytik Jena Specord40 spectrophotometer at 25 °C. The reaction mixture contained 50 mM Tris-HCl (pH 8.0), 300 μM 2-cyclohexenone, and 150 μM NADPH. The reaction was started by addition of enzyme to the reaction mixture and conducted in a volume of 1 mL with a XenA concentration of approximately 1×10^{-2} mg mL^{-1}. One activity unit is defined as the oxidation of 1 μmol of NADPH/min.

We determined the flavin content spectrophotometrically by SDS treatment according to the protocol by Aliverti et al. (*36*).

Photoreduction of XenA. Photoreduction of XenA was essentially conducted as described by Massey et al. (*37*). XenA was photoreduced in a glass tonometer with a cuvette attached to a side arm. As a photoreductant, we used the potassium salt of 5-deaza-10-methyl-3-sulfopropylisoalloxazine, a deazaflavin derivative, in catalytic amounts. The cuvette contained 5-deaza-10-methyl-3-sulfopropylisoalloxazine and EDTA in 100 mM Tris buffer (pH 8.0) in a final volume of 1 mL. The tonometer contained XenA and phenosafranine in 100 mM Tris buffer (pH 8.0) in a final volume of 2 mL. Oxygen was removed by repeated evacuation and flushing with dinitrogen gas. After oxygen removal, the two volumes were mixed, resulting in final concentrations of 15 mM EDTA, 30 μM XenA, and 1 μM phenosafranine. For illumination, a 100 W lamp from a slide projector (Agfa, Opticus 100) was used. The reduction of XenA was followed by recording absorption spectra directly after and 3 min after each illumination.

Determination of Reduction Potentials. Determination of the reduction potential of XenA-bound FMN in the presence and absence of 1 mM NAD^+ was conducted as described previously (*38*). The reaction mixture contained 15 μM XenA, 15 μM phenosafranine [$E°_{m,D}$ = −252 mV (*39*)] as a reference dye, 2 μM methylviologen as an electron mediator, and 0.05 unit of xanthine oxidase. The reaction was conducted under anaerobic conditions in a glass tonometer and started by addition of

xanthine with a final concentration of 300 μM. To calculate the concentrations of oxidized XenA (E_{ox}) and oxidized phenosafranine (D_{ox}), the absorbance values at 464 and 521 nm were used and integrated in eqs 1 and 2.

$$A_{464} = \varepsilon^{E_{ox}}_{464} c^{E_{ox}} + \varepsilon^{D_{ox}}_{464} c^{D_{ox}} + \varepsilon^{E_{red}}_{464}(c^{E_{tot}} - c^{E_{ox}})$$
$$+ \varepsilon^{D_{red}}_{464}(c^{D_{tot}} - c^{D_{ox}}) \tag{1}$$

$$A_{521} = \varepsilon^{E_{ox}}_{521} c^{E_{ox}} + \varepsilon^{D_{ox}}_{521} c^{D_{ox}} + \varepsilon^{E_{red}}_{521}(c^{E_{tot}} - c^{E_{ox}})$$
$$+ \varepsilon^{D_{red}}_{521}(c^{D_{tot}} - c^{D_{ox}}) \tag{2}$$

Following are the values of the molar extinction coefficients: ε(oxidized enzyme at 464 nm) = 12.2×10^3 M^{-1} cm^{-1}, ε(reduced enzyme at 464 nm) = 0.6×10^3 M^{-1} cm^{-1}, ε(oxidized enzyme at 521 nm) = 1.5×10^3 M^{-1} cm^{-1}, ε(reduced enzyme at 521 nm) = 0.6×10^3 M^{-1} cm^{-1}, ε(oxidized dye at 464 nm) = 12.9×10^3 M^{-1} cm^{-1}, ε(reduced dye at 464 nm) = 0.3×10^3 M^{-1} cm^{-1}, ε(oxidized dye at 521 nm) = 44.9×10^3 M^{-1} cm^{-1}, and ε(reduced dye at 521 nm) = 0.3×10^3 M^{-1} cm^{-1}.

The reduction potential of XenA ($E°_{m,E}$) can subsequently be determined from the difference ($\Delta E°$) in the reduction potentials of the enzyme and dye. The latter can be obtained from the plot of $\log(E_{ox}/E_{red})$ versus $\log(D_{ox}/D_{red})$ using eq 3.

$$E°_{m,E} = E°_{m,D} + \Delta E° \tag{3}$$

Steady-State Kinetics Experiments. The steady-state kinetics of XenA reacting with various concentrations of 2-cyclohexenone and NADPH were performed under anaerobic conditions. The concentration of 2-cyclohexenone was varied between 10 and 160 μM, and the concentration of NADPH was varied between 10 and 400 μM. Each single measurement was performed three times. 2-Cyclohexenone and NADPH were both added from a freshly prepared 1 mM stock solution, and the concentration of XenA was approximately 250 nM. The apparent values for K_{mA}, K_{mB}, and V_{max} have been determined by multiple nonlinear regression analysis of the measured rates using eq 4 (*40*):

$$v = \frac{V_{max}[A][B]}{K_{mB}[A] + K_{mA}[B] + [A][B]} \tag{4}$$

where [A] is the concentration of 2-cyclohexenone, [B] is the concentration of NADPH, v is the observed rate, V_{max} is the rate at saturating substrate concentrations, K_{mA} is the K_m for 2-cyclohexenone at saturating NADPH levels, and K_{mB} is the K_m for NADPH at saturating 2-cyclohexenone levels.

Rapid Reaction Techniques. Measurements on the kinetics of the reductive half-reaction were performed under anaerobic conditions using an Applied Photophysics SX-20MV kinetic spectrophotometer with a 1 cm observation path length cuvette coupled either to a diode array detector or to a monochromator and photomultiplier. The reaction temperature was controlled with a Haake F8/C25 thermostat. Standard reaction conditions were 50 mM Tris (pH 8.0) at 20 °C. In a typical experiment, enzyme at a XenA concentration of approximately 10 μM was mixed with an equal volume of substrate solution, the latter at concentrations ranging from 50 to 5000 μM. Each experiment was repeated at least five times for each substrate concentration. The reactions were monitored at 464 and 540 nm over an appropriate time scale. Observed kinetic transients at 464 nm were fit to single exponentials, and transients at 540 nm,
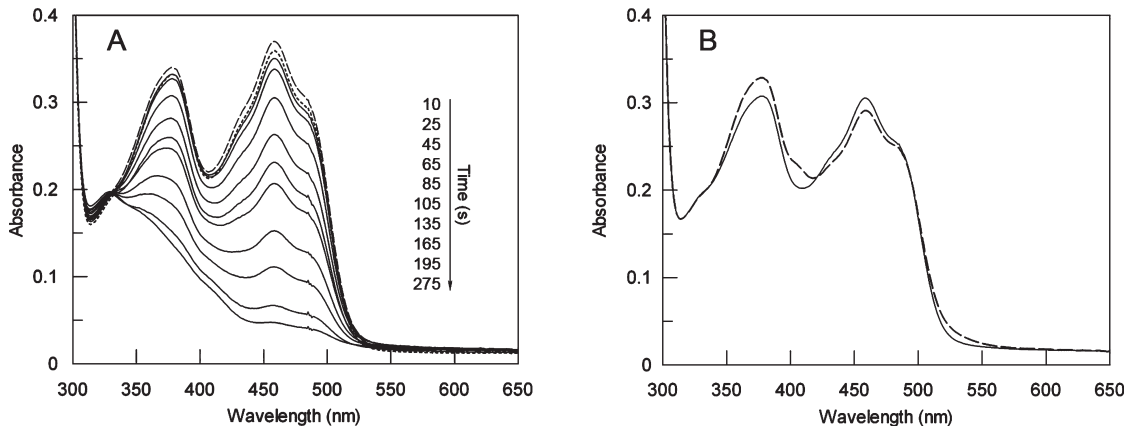
FIGURE 1: Photoreduction of XenA. Conditions: 30 μM XenA, 15 mM EDTA, 1 μM phenosafranine, 100 mM Tris buffer (pH 8.0), and traces of 5-deaza-10-methyl-3-sulfopropylisoalloxazine as catalyst. (A) Time-dependent reduction of XenA after illumination. The figure shows the spectra recorded before (···) and after (—) different periods of illumination. The spectrum of reoxidized XenA is displayed as a dashed line. (B) Spectra recorded directly (- - -) and 3 min (—) after a single irradiation step.

monitoring formation and decay of charge-transfer complexes, were fit with double exponentials using Pro-Data (Applied Photophysics) to yield observed rate constants (k_{obs}).

The reductive half-reaction sequence was modeled as shown in eq 5

$$A + B \underset{k_{-1}}{\overset{k_1}{\rightleftharpoons}} C \overset{k_2}{\rightarrow} D \qquad (5)$$
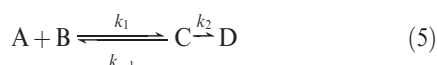
where A is XenA$_{ox}$, B is NAD(P)H, C is the XenA−NAD(P)H charge-transfer complex, and D is XenA containing the two-electron-reduced state of FMN and bound NAD(P)$^+$.

The oxidative half-reaction sequence was modeled as shown in the general eq 6

$$E + F \underset{k_{-3}}{\overset{k_3}{\rightleftharpoons}} G \overset{k_4}{\rightarrow} H \qquad (6)$$
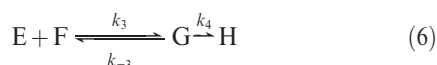
where E is XenA$_{red}$, F is 2-cyclohexenone (coumarin), G is the XenA$_{red}$−2-cyclohexenone (coumarin) charge-transfer complex, and H is XenA$_{ox}$ with bound 2-cyclohexanone (chroman-2-one).

Hyperbolic plots of observed rate constants versus substrate concentration were fitted using eq 7 to yield the limiting rate of reaction at high [S], k_X, and the dissociation constant K_D (*41*).

$$k_{obs} = k_X[S]/(K_D + [S]) \qquad (7)$$

$$k_{obs} = k_1[S] + k_{-1} + k_2 \qquad (8)$$

Rate constants for the formation of the charge-transfer complex between oxidized XenA and NADH/NADPH were approximated by linear regression analysis with eq 8, where k_2 is the limiting rate of reduction of XenA with the respective nicotinamide used.

To relate the individual limiting rate constants of the reductive and oxidative half-reactions to the steady-state catalytic constants, eq 9 has been used:

$$k_{cat} = k_2 k_4/(k_2 + k_4) = k_{red} k_{ox}/(k_{red} + k_{ox}) \qquad (9)$$

Solutions of oxidized XenA were made anoxic in a glass tonometer as described above. Solutions of reduced XenA were made anoxic in a tonometer with a cuvette side arm and titrated with NADH to achieve complete flavin reduction. We made all substrate solutions anoxic by flushing them with dinitrogen gas.

Docking. NADPH was docked to the crystal structure of XenA (PDB entry 2H8X) using DOCK 6 (*42*). The charges were taken from the CHARMM27 force field (*43*). A "divide and conquer" approach was used to reduce the number of rotatable bonds. The nicotinamide was docked close to FMN using chemical docking, which was used to incorporate information about the chemical complementarity of ligand and receptor moieties into the matching process. In a second step, adenosine was independently docked within a radius of 25 Å from FMN. The remaining parts of NAD(P)H (i.e., the ribose and phosphates) were constructed geometrically and subsequently energetically minimized using CHARMM (*44*), while the rest of the protein, the nicotinamide ring and the adenine ring, was kept fixed.

Electrostatic Calculations. To study the effects of the phosphate group of NADPH on the hydride-transfer energies between the nicotinamide ring and the isoalloxazine ring, electrostatics were calculated using the program SOLINPROT of the MEAD package (*45*). We calculated the interaction of the nicotinamide ring and the isoalloxazine ring with the monophosphate group bound to the ribose before and after the electron transfer. The XenA dimer was used to define the dielectric boundaries. For this calculation, only the charges of the nicotinamide ring and the phosphate group of NADPH and the isoalloxazine ring of the FMN were considered. The dielectric constants of protein and of water were set to 4.0 and 80.0, respectively. The ionic strength was set to 0.1 M. The calculation was done in two focusing levels with grids of $181 \times 180 \times 180$ grid points. The grid spacing was set to 1.0 and 0.25 Å for the outer and the inner grid, respectively. The outer grid was centered at the coordinate center of the protein; the inner grid was centered at the N1 atom of FMN.

RESULTS

Photoreduction of XenA. XenA was reduced using the light-mediated generation of electrons by the deazaflavin−EDTA couple in the presence of phenosafranine as the redox mediator (Figure 1A). This method has been applied to ensure single electron transfer to allow for initial semiquinone formation. Photoreduction proceeds in a two-step mechanism. Directly after each illumination period, we observe a signal increase around 350 nm, which we assign to the formation of the red anionic
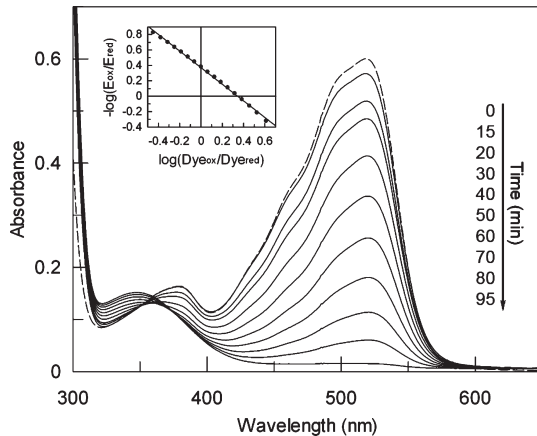
FIGURE 2: Redox potential determination for the FMN−FMNH⁻ couple of XenA. Conditions: 15 μM XenA, 15 μM phenosafranine, 2 μM methylviologen, 0.05 unit of xanthine oxidase, and 50 mM Tris buffer (pH 8.0). The dotted line shows the spectrum of the reaction mixture before the addition of xanthine. The reaction was followed over 1.5 h (—). Absorbance values at 464 and 521 nm were used to calculate the concentrations of oxidized XenA and the dye. The inset shows the plot of $\log(E_{ox}/E_{red})$ vs $\log(D_{ox}/D_{red})$. The solid line displays the linear fit with a slope of −1. The redox potential of XenA was calculated to be −263 mV.

semiquinone. Figure 1B shows the spectrum (dashed line) with a characteristic peak around 400 nm and an increase in signal magnitude between 500 and 550 nm. Three minutes after illumination, the semiquinone signature was not observed any more and the enzyme-bound flavin was converted to the dihydroflavin form as a result of the dismutation of the semiquinone. After complete reduction of the enzyme, the cuvette was exposed to air, allowing XenA to reoxidize, resulting in a spectrum indistinguishable from the starting spectrum.

Determination of Reduction Potential. The generation of electrons by the xanthine oxidase−xanthine couple has been used as an alternative method to reduce XenA. The presence of a reference dye (phenosafranine; $E^{\circ}_{m} = -252$ mV) allowed the determination of the reduction potential of XenA-bound FMN. The small amount of xanthine oxidase ensured equilibrium conditions at all times, whereas both enzyme and dye take up two electrons. Reduction of XenA by xanthine oxidase in the absence of phenosafranine showed the slow conversion of FMN from the quinone to the hydroquinone state without any detectable formation of semiquinone species (data not shown). Spectra recorded during the reaction with phenosafranine show that XenA and phenosafranine are reduced to similar extents (Figure 2). The absorbance values at 464 and 521 nm were used to calculate the amount of oxidized XenA and dye using eqs 1 and 2. Equation 3 gives a reduction potential of −263 mV for XenA. The linear fit of the plot of $\log(E_{ox}/E_{red})$ versus $\log(D_{ox}/D_{red})$ shows a slope of −1, confirming that both XenA and phenosafranine received the same amount of electrons and reacted under equilibrium conditions. There was no difference observed in the presence of 1 mM NAD⁺ and 1 mM NADP⁺.

Steady-State Kinetics. Catalytic turnover of XenA with various concentrations of 2-cyclohexenone and NADPH under anaerobic conditions was analyzed to determine the values of K_{mA}, K_{mB}, and V_{max}. The inset in Figure 3 shows the rate dependencies of 2-cyclohexenone for different NADPH concentrations and the corresponding nonlinear fits using the normal Michaelis−Menten equation. The parallel lines in the double-reciprocal plot
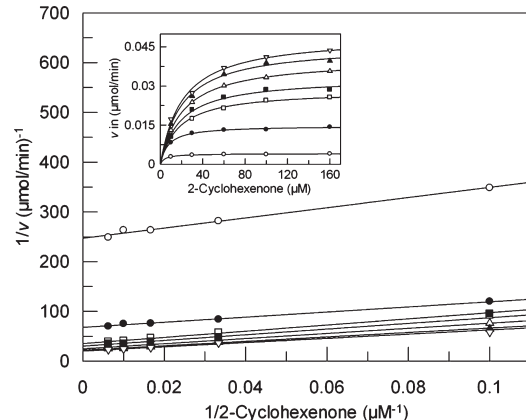

FIGURE 3: Steady-state kinetic data of the XenA-catalyzed reduction of 2-cyclohexenone by NADPH. Lineweaver−Burk plot with linear regression analysis using the simple Michaelis−Menten equation. Each point represents the mean of three independent measurements. The assays were performed in 50 mM Tris buffer (pH 8.0) at 25 °C. The final volume of 1 mL contained 250 nM XenA, varying concentrations of 2-cyclohexenone (10−160 μM), and varying concentrations of NADPH (10−400 μM). Each line displays one distinct NADPH concentration: (○) 10 μM NADPH, (●) 50 μM NADPH, (□) 100 μM NADPH, (■) 150 μM NADPH, (△) 200 μM NADPH, (▲) 300 μM NADPH, and (▽) 400 μM NADPH. The inset displays the direct rate dependencies of 2-cyclohexenone for the different NADPH concentrations (see above) and the nonlinear fits using the simple Michaelis−Menten equation.

(Figure 3) are consistent with a double-displacement (ping-pong) mechanism (*40*). Consequently, the measured rates were analyzed by multiple nonlinear regression analysis using eq 4, resulting in the following values: $k_{cat} = 7.2 \pm 0.3$ s⁻¹, K_{mA} (the K_{m} for 2-cyclohexenone) = 37.2 ± 2.4 μM, and K_{mB} (the K_{m} for NADPH) = 200 ± 13.0 μM.

Reductive Half-Reaction. The reaction of XenA with NADH and NADPH was next examined following the spectral change associated with reduction of the enzyme's flavin (Figure 4A). No spectral changes indicating the formation of a Michaelis complex in the dead time of the stopped-flow experiment were observed (Figure 4A). Formation of a CT complex, on the other hand, can be discerned by an absorption increase at 520−560 nm (Figure 4B, inset), which decays with a rate constant comparable to that of FMN reduction recorded at 464 nm (Figure 4B). The characteristic absorption around 464 nm shows that the weak CT complex is indeed formed between oxidized XenA and the NADH or NADPH and is not a complex of the reduced enzyme (Figure 4A). The observed rate constant for the formation of the CT complex depends linearly on the concentration of NADH or NADPH (Figure 4C). Using eq 8 to fit the observed dependence of observed rate constants on the concentration of NAD(P)H under pseudo-first-order conditions gives a second-order rate constant (k_{1}) of $(9.4 \pm 0.5) \times 10^{5}$ M⁻¹ s⁻¹ with NADH and $(6.4 \pm 0.3) \times 10^{5}$ M⁻¹ s⁻¹ with NADPH for the formation of the CT complex. The rate constants for the dissociation of NAD(P)H from the CT complex (k_{-1}) have been derived from the positive intercept on the ordinate, which is approximated to be $k_{-1} + k_{2}$. The values for k_{-1} are very similar for both nicotinamides with 256 ± 17 s⁻¹ for NADH and 215 ± 11 s⁻¹ for NADPH. The rate constants determined for the decay of the CT complex at long wavelengths (Figure 4B, inset) correspond to the observed rates measured for the reduction of FMN seen at 464 nm and show a hyperbolic dependence on the concentration of reduced nicotinamide (Figure 4D,E). The linear
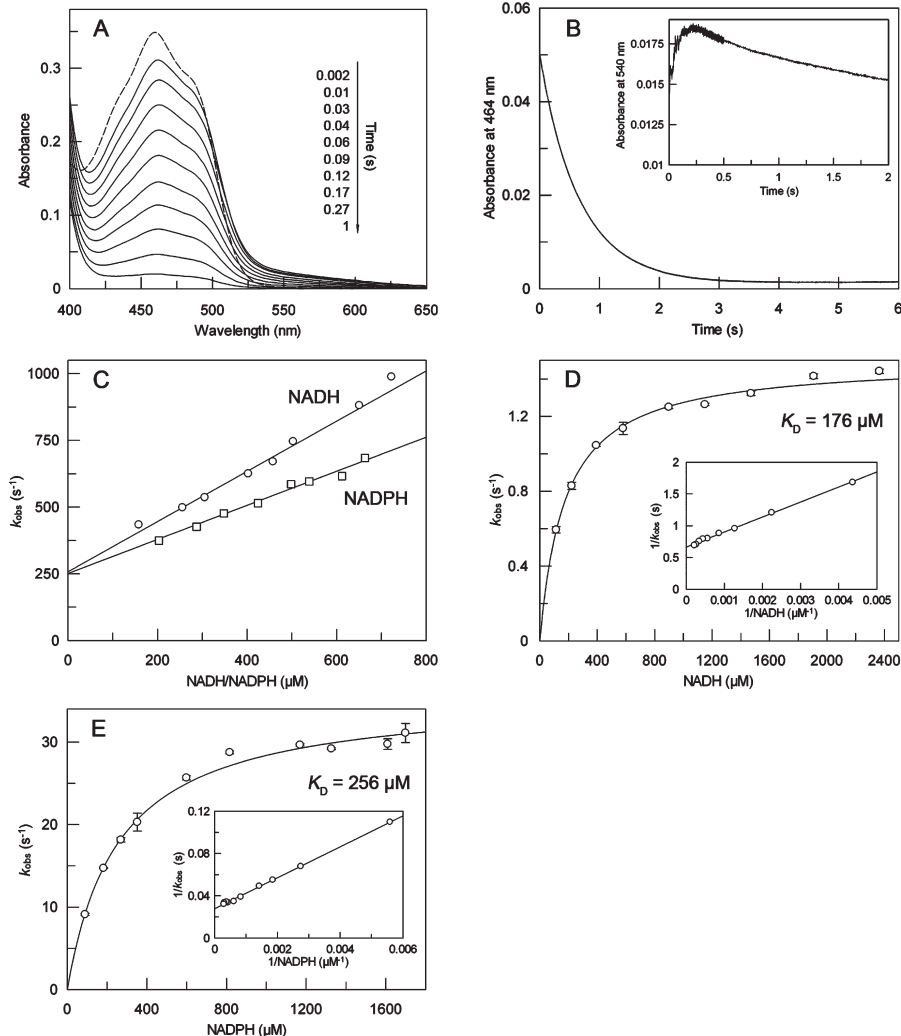
FIGURE 4: Reductive half-reactions of XenA with NADH and NADPH. (A) Time-dependent spectral changes of 35 μM XenA$_{ox}$ reacting with 800 μM NADH (corresponding to 70 μM XenA$_{ox}$ and 1600 μM NADH before mixing). The dashed line represents the spectrum of XenA$_{ox}$. (B) Time-dependent absorbance change at 464 nm for the reaction of 5 μM XenA with 2500 μM NADH. The inset displays the absorbance changes at 540 nm (with 35 μM XenA and 50 μM NADH), which we attribute to the formation of the CT complex. (C) Dependencies of the observed rates at 540 nm (CT formation) on NADH concentration ($\bigcirc$) and NADPH concentration ($\square$) for reactions with 35 μM XenA. (D and E) Concentration dependence of the observed rates at 464 nm (5 μM XenA) for NADH (D) and NADPH (E), with the reciprocal plots in the insets. The curves display the best fits to the data using eq 7. All experiments were conducted under anaerobic conditions in 50 mM Tris buffer (pH 8.0) at 20 °C.

correlation of $1/k_{obs}$ with $1/[NADH]$ or $1/[NADPH]$ (Figure 4D, E, insets) indicates that the equilibrium condition for the XenA–NAD(P)H reaction ($k_{-1} \gg k_2$) holds, as seen experimentally, and that eq 7 can be used to determine the limiting rate constant for the reduction of FMN (k_2) and the dissociation constant (K_D) of the complex (*41*). For the reaction of XenA$_{ox}$ with NADH, a rate constant (k_2) of 1.50 ± 0.02 s^{-1} is obtained, while with NADPH, the rate constant is 24 times higher, 35.7 ± 0.6 s^{-1}. The dissociation constants for the XenA$_{ox}$–NADH complex of 176 ± 14 μM and for the XenA$_{ox}$–NADPH complex of 256 ± 12 μM obtained using the rapid equilibrium model are in good agreement with the ratio between the rate constants for the formation of the CT complexes (XenA$_{ox}$–NADH, $k_{-1}/k_1 = 272$ μM; XenA$_{ox}$–NADPH, $k_{-1}/k_1 = 336$ μM). Appreciable rates for the back reaction would cause the double-reciprocal plot of $1/k_{obs}$ versus $1/[NAD(P)H]$ to curve down for high substrate concentrations (*41*), which is not observed (Figure 4D,E, insets). Furthermore, an adaptation of the model to include the rate constant of the back-reaction (k_{-2}) did not improve the fit to the observed rates, as judged from testing the goodness of fit. We

conclude that k_{-2} is very small and that reduction of XenA by either NADH or NADPH is functionally irreversible.

Oxidative Half-Reaction. To examine the reoxidation of XenA, two different substrates have been studied, 2-cyclohexenone and coumarin. 2-Cyclohexenone has been used as a substrate in most rapid kinetic studies with members of the OYE family, notably with OYE (*19*), morphinone reductase (*24*, *46*), PETN reductase (*29*), and YqjM (*34*), and it is therefore possible to compare the reactivity of XenA with the reactivities of these enzymes. However, since we have recently shown that XenA participates in the degradation of quinoline along the 8-hydroxycoumarin pathway and is able to reduce the C3–C4 double bonds of heteroaromatic compounds such as coumarin (*10*), we have also examined the reaction of XenA with this substrate.

Spectral changes are observed directly after reduced XenA reacts with 50 μM 2-cyclohexenone, as compared to the spectrum of reduced XenA with substrate (Figure 5A). The observed maximum at 424 nm 5 ms after reduced XenA is mixed with 2-cyclohexenone indicates that it is not due to a fast reaction
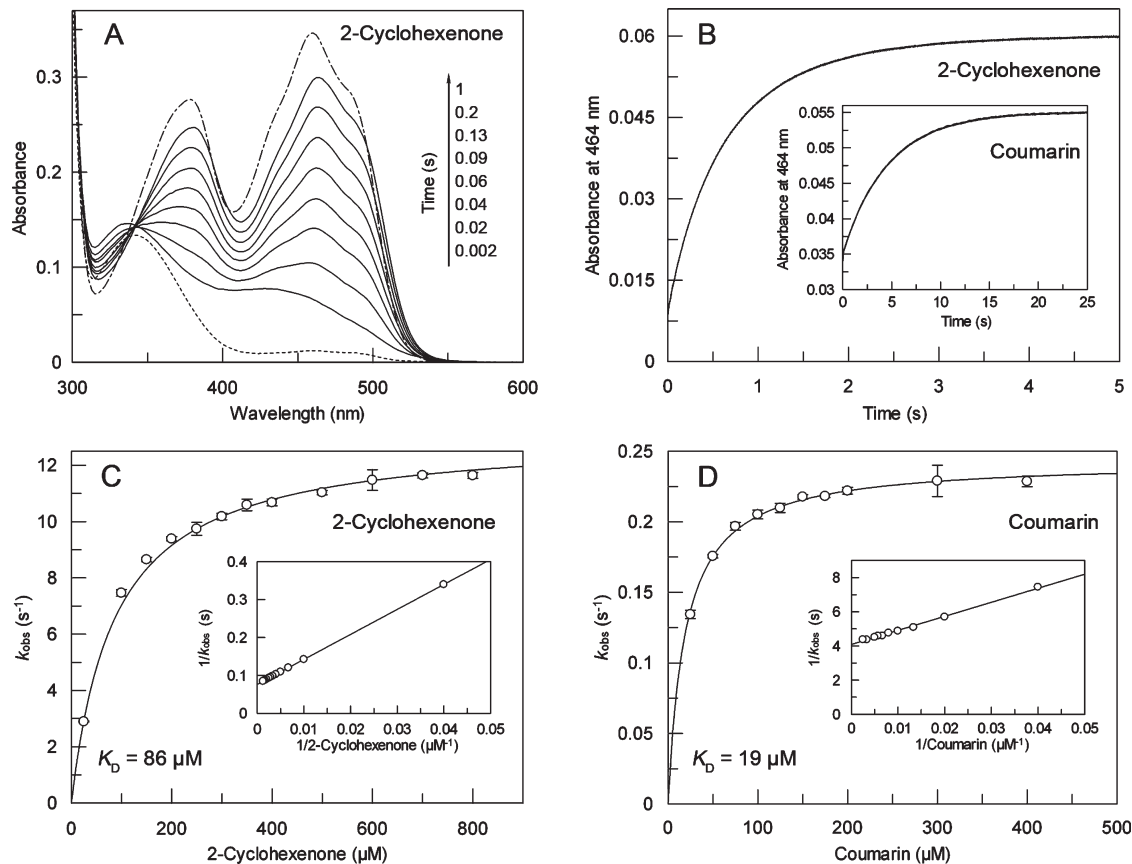
FIGURE 5: Oxidative half-reaction of reduced XenA with 2-cyclohexenone and coumarin. (A) Time-dependent spectral changes of 35 μM XenA (NADH-reduced) reacting with 800 μM 2-cyclohexenone. The dashed line represents the spectrum of reduced XenA. (B) Time-dependent spectral changes at 464 nm for the reaction of 5 μM XenA with 25 μM 2-cyclohexenone. A reaction trace with 25 μM coumarin is shown in the inset of panel B. (C and D) Concentration dependence of the observed rate constants at 464 nm for the reaction of 5 μM XenA with 2-cyclohexenone (C) and for coumarin (D). The curves display the best fits to the data using eq 7. The reciprocal plots are shown in the insets. All experiments were conducted in 50 mM Tris buffer (pH 8.0) at 20 °C under anaerobic conditions.

phase in which FMN is oxidized but rather that another reaction intermediate involving reduced XenA and 2-cyclohexenone is formed rapidly within the dead time of the instrument. Formation of a CT complex is discernible with both substrates by an initial absorption increase around 650 nm (data not shown). The CT complex forms very rapidly and decays with the same rate as XenA becomes oxidized. The low absorbance around 464 nm at very short times indicates that the CT complex involves reduced XenA and substrate. A larger absorption increase is subsequently observed at 464 nm (Figure 5B). The rate constant observed for the majority of the absorbance increase at 464 nm shows a hyperbolic dependence on the concentration of 2-cyclohexenone and coumarin (Figure 5C,D). The linear relation between $1/k_{obs}$ and 1/[2-cyclohexenone] or 1/[coumarin] (Figure 5C,D, insets) indicates that it is justified to include the rapid equilibrium condition in our model (*41*). A rate constant (k_4) of 13.1 $\pm$ 0.1 s^{-1} and a K_D of 86 $\pm$ 2 μM have been determined for 2-cyclohexenone. The reduction of coumarin is slower than the reduction of 2-cyclohexenone by a factor of 50 with a rate constant (k_4) of 0.243 $\pm$ 0.001 s^{-1}, and the complex has a K_D of 19.3 $\pm$ 0.2 μM.

Modeling NADH and NADPH in the Active Site of XenA. We next examined a model for both NADH and NADPH bound to oxidized XenA, generated using the DOCK 6 program. In this model, NADH and NADPH bind both in the same way to XenA. The nicotinamide ring of NAD(P)H docks in a stacked conformation with the isoalloxazine ring of FMN (Figure 6) and is hydrogen-bonded to His178, His181, and

Cys25. The diphosphate forms a salt bridge with Lys106 and a hydrogen bond with Tyr183. The distance between the phosphorus atom of the 2'-phosphate of NADPH and N1 of the nicotinamide is 6.2 Å. The 2'-phosphate of NADPH is oriented toward the solvent and does not interact with the protein matrix but does form a hydrogen bond to the 2'-OH group of the ribose attached to nicotinamide (Figure 6).

From electrostatic calculations using the Poisson−Boltzmann equation, we find that the free energy of the transfer of hydride from the nicotinamide to the isoalloxazine ring of the FMN is shifted by −1.83 kcal/mol due to the presence of the 2'-phosphate on NADPH compared to NADH. Thus, the hydride transfer is more favorable with NADPH than with NADH. Most of this difference in free energy manifests itself in a lower activation energy for NADPH versus NADH as reflected in the relative limiting rates of reduction (36 s^{-1} vs 1.5 s^{-1}, respectively).

DISCUSSION

Recently, we have shown that XenA participates in the degradation of quinoline and reacts with heteroaromatic compounds such as coumarin and 8-hydroxycoumarin using both NADH and NADPH as electron sources (*10*). Here we have examined its reactivity with both reducing and oxidizing substrates, allowing us to compare it to related flavoenzymes.

No stable semiquinone form of XenA was observed in the course of the reductive titrations (using either the xanthine−xanthine oxidase or deazaflavin−light couple as the reductant), indicating
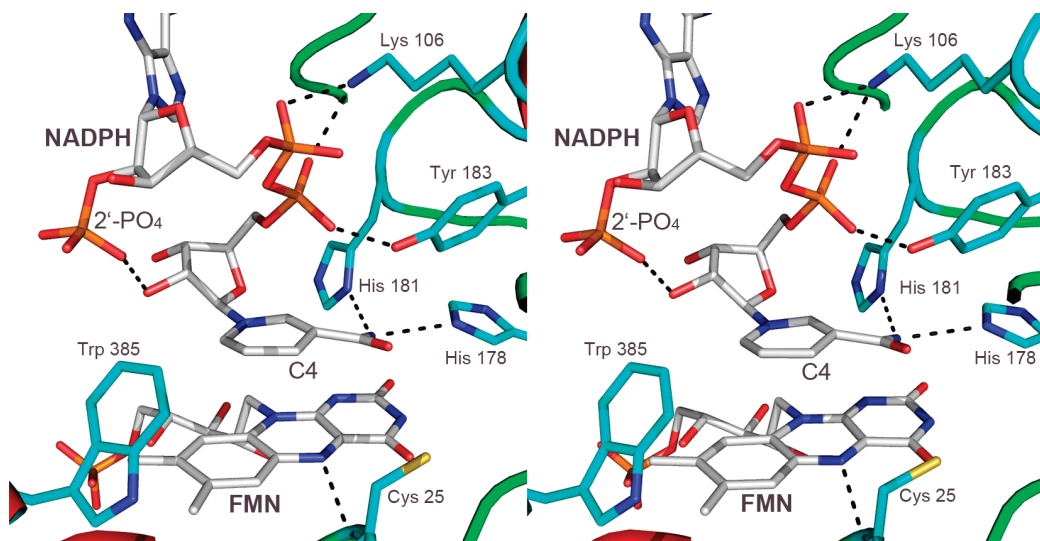
FIGURE 6: Docked complex between XenA and NADPH. The stereoview shows residues of the active site in the vicinity of NADPH depicted as stick models with carbon atoms colored cyan. Interactions mentioned in the text are represented by dashed lines. NADPH and FMN are shown as stick models with carbon atoms colored white. NADH binds to XenA in the same way as NADPH. This figure was generated using PyMol (48).
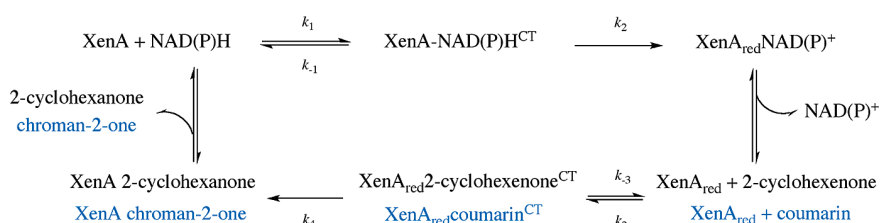

FIGURE 7: Scheme for the reaction cycle catalyzed by XenA.

that transiently formed red, anionic semiquinone rapidly disproportionated. The hydrogen bonding distance between the amide nitrogen of Cys25 and N5 of FMN (Figure 6) indicates that the amide nitrogen acts as hydrogen bond donor and N5 as hydrogen bond acceptor in the oxidized state. This interaction disfavors the formation of the neutral semiquinone as the hydrogen bond would be broken when N5 becomes protonated. The anionic semiquinone is therefore favored; however, as frequently observed, it is thermodynamically unstable. The protein environment thus does not stabilize the semiquinone state to any significant degree. Morphinone reductase (24), PETN reductase (29), and YqjM (2) also fail to form detectable amounts of semiquinone, although OYE forms 15−20% of the anionic semiquinone species under equilibrium conditions (47).

The rate constants for the reaction of reductases with both reducing and oxidizing substrates are critically dependent on the reduction potential of the flavin cofactor, which determines which reactions are thermodynamically feasible. The reduction potential of the FMN−FMNH$^-$ couple in XenA is −263 mV, substantially lower than found for PETN reductase (−193 mV) (29), OYE (−230 mV) (47), and morphinone reductase (−242 mV) (26). XenA has several structural peculiarities that may be responsible for this, including the presence of an active site cysteine residue [Cys25 (Figure 6)] in place of a conserved threonine residue found in other members of the OYE family. The hydroxyl group of the threonine residue of other family members forms a hydrogen bond with the C4 oxygen atom of the isoalloxazine ring, and its replacement with alanine lowered the reduction potential of the FMN−FMNH$^-$ couple from −230 to −263 mV in OYE (21) and from −242

to −290 mV in morphinone reductase (26). It may therefore be that the presence of the cysteine residue in place of the threonine contributes to the low reduction potential of XenA. We have also examined the reductive and oxidative half-reactions to improve our understanding of the reactivity of XenA. The first observed step in the reductive half-reaction with both NADH and NADPH is the formation of a CT complex. The linear relationship between observed rates of CT complex formation and the concentration of reductants is consistent with a simple bimolecular reaction (Figure 7). There is good agreement between the apparent dissociation constants for the complexes between oxidized XenA and NAD(P)H obtained from the hyperbolic plots of k_{red} versus [NAD(P)H] and the ratio between on and off rate constants for the formation of the CT complexes (k_{-1} and k_1, respectively, in Figure 6 and Table 1).

To gain further insight into the interaction of NAD(P)H with XenA, we performed docking simulations. In the docked structure, both NADPH and NADH are kept in position by H-bonds to amino acids like His178 and Tyr183, which are highly conserved within the OYE family. The binding mode of NADPH in complex with XenA, including the short distance between the 2′-phosphate and the nicotinamide ring, has not been observed so far. In most flavoprotein structures, the 2′-phosphate is oriented away from the nicotinamide ring and is stabilized by arginine residues.

The second step in the reaction of XenA$_{ox}$ with NAD(P)H is the transfer of hydride from the reduced nicotinamide to the N5 atom of XenA-bound FMN. The rate constants (k_2) for this step differ by a factor of 24 for NADH and NADPH, with the latter being faster. The main difference in the structure of the docked

Table 1: Stopped-Flow Kinetic Data

	Reductive Half-Reaction			
substrate	K_d (μM)	k_1 (M^{-1} s^{-1})	k_{-1} (s^{-1})	k_2 (s^{-1})
NADH	176 ± 14	$(9.4 \pm 0.5) \times 10^5$	256 ± 17	1.50 ± 0.02
NADPH	256 ± 12	$(6.4 \pm 0.3) \times 10^5$	215 ± 11	35.7 ± 0.6

	Oxidative Half-Reaction	
substrate	K_d (μM)	k_4 (s^{-1})
2-cyclohexenone	86 ± 2	13.1 ± 0.1
coumarin	19.3 ± 0.6	0.243 ± 0.001

complexes of NAD(P)H with oxidized XenA is the presence of the 2′-phosphate group, which is situated above the 1,4-dihydropyridine ring of NADPH near the transferred hydrogen at C4. An additional negative charge above the pyridine ring could further stabilize NADP$^+$ and would therefore be expected to decrease the reduction potential of the NADP$^+$–NADPH couple in the XenA-bound state. The calculated $\Delta\Delta G$ of -1.83 kcal/mol for the hydride-transfer reaction of XenA-bound NADPH to FMN compared to XenA-bound NADH indicates that the higher rate constant in the reaction with NADPH is due to the interaction of the 2′-phosphate group of NADPH with the nicotinamide ring and the FMN. The lower affinity of XenA for NADPH compared to NADH is more than compensated by its higher reactivity. Using k_2/K_d as a criterion for the specificity of XenA with the two nicotinamides, we obtain apparent second-order rate constants of 8.5×10^3 M^{-1} s^{-1} for NADH and 1.39×10^5 M^{-1} s^{-1} for NADPH, indicating that under physiological conditions XenA reacts preferentially with NADPH. We note that this is an exceptionally low level of selectivity for a flavoprotein. The last step of the reductive half-reaction would be the release of NAD$^+$ or NADP$^+$. We do not observe CT complexes after transfer of hydride to the flavin or any appreciable back-reaction of reduced XenA with NAD$^+$ or NADP$^+$ (consistent with the observation that during reductive titrations XenA can be fully reduced with a stoichiometric amount of NADH).

We have also examined the oxidative half-reaction of XenA with 2-cyclohexenone and coumarin. As 2-cyclohexenone is also a substrate of OYE, PETN reductase, and morphinone reductase, we focus our discussion on this substrate. The oxidative half-reaction of the catalytic cycle is initiated by the formation of a CT complex between 2-cyclohexenone and reduced XenA for which the equilibrium dissociation constant could be determined (86 μM). Only one intermediate was included in our kinetic model for the oxidative half-reaction, although our data suggest the existence of two different intermediates. The rapid formation of an intermediate in the reaction of reduced OYE and 2-cyclohexenone within the dead time of the stopped-flow spectrophotometer has also been observed, having an absorbance maximum at 455 nm, and was interpreted as a CT complex (*19*). The observation of two intermediates between reduced XenA and 2-cyclohexenone indicates that their relative orientations are changing from the encounter complex to the reactive complex before the hydride transfer occurs in the fourth step of the reaction. Again we have no indication that an appreciable back-reaction between 2-cyclohexanone and oxidized XenA occurs. The limiting rate constant of the reaction of NADH-reduced XenA with coumarin is 50-fold smaller than that for the reaction

with 2-cyclohexenone, while coumarin binds with a 4-fold higher affinity. The lower reactivity with coumarin probably reflects the weaker electrophilicity of the β-carbon of coumarin compared to 2-cyclohexenone. The good agreement of the catalytic constant derived from eq 4 with NADPH and 2-cyclohexenone as substrates in the steady-state assay ($k_{cat} = 7.2$ s^{-1}) with the catalytic constant following from the limiting rate constants of the reductive and oxidative half-reactions with NADPH and 2-cyclohexenone (eq 9; $k_{cat} = 5.3$ s^{-1}) indicates that the two product release steps, which have not been observed by our transient kinetic analysis, occur rapidly and are not limiting the reaction rate of XenA.

The structures of XenA and other members of the OYE family are very similar, but at the same time, some distinct features in the composition of the active site do exist. This analysis of native XenA revealed further remarkable properties of the enzyme such as its low reduction potential and its only modest specificity for NADPH over NADH.

REFERENCES

1. Binks, P. R., French, C. E., Nicklin, S., and Bruce, N. C. (1996) Degradation of pentaerythritol tetranitrate by *Enterobacter cloacae* PB2. *Appl. Environ. Microbiol. 62*, 1214–1219.
2. Fitzpatrick, T. B., Amrhein, N., and Macheroux, P. (2003) Characterization of YqjM, an Old Yellow Enzyme homolog from *Bacillus subtilis* involved in the oxidative stress response. *J. Biol. Chem. 278*, 19891–19897.
3. Blehert, D. S., Knoke, K. L., Fox, B. G., and Chambliss, G. H. (1997) Regioselectivity of nitroglycerin denitration by flavoprotein nitroester reductases purified from two *Pseudomonas* species. *J. Bacteriol. 179*, 6912–6920.
4. Snape, J. R., Walkley, N. A., Morby, A. P., Nicklin, S., and White, G. F. (1997) Purification, properties, and sequence of glycerol trinitrate reductase from *Agrobacterium radiobacter*. *J. Bacteriol. 179*, 7796–7802.
5. Miura, K., Tomioka, Y., Suzuki, H., Yonezawa, M., Hishinuma, T., and Mizugaki, M. (1997) Molecular cloning of the *nemA* gene encoding N-ethylmaleimide reductase from *Escherichia coli*. *Biol. Pharm. Bull. 20*, 110–112.
6. French, C. E., and Bruce, N. C. (1994) Purification and characterization of morphinone reductase from *Pseudomonas putida* M10. *Biochem. J. 301* (Part 1), 97–103.
7. Rohde, B. H., Schmid, R., and Ullrich, M. S. (1999) Thermoregulated expression and characterization of an NAD(P)H-dependent 2-cyclohexen-1-one reductase in the plant pathogenic bacterium *Pseudomonas syringae* pv. *glycinea*. *J. Bacteriol. 181*, 814–822.
8. Blehert, D. S., Fox, B. G., and Chambliss, G. H. (1999) Cloning and sequence analysis of two *Pseudomonas* flavoprotein xenobiotic reductases. *J. Bacteriol. 181*, 6254–6263.
9. Fetzner, S., Tshisuaka, B., Lingens, F., Kappl, R., and Hüttermann, J. (1998) Bacterial degradation of quinoline and derivatives: Pathways and their biocatalysts. *Angew. Chem., Int. Ed. 37*, 577–597.
10. Griese, J. J., Jakob, R. P., Schwarzinger, S., and Dobbek, H. (2006) Xenobiotic reductase A in the degradation of quinoline by *Pseudomonas putida* 86: Physiological function, structure and mechanism of 8-hydroxycoumarin reduction. *J. Mol. Biol. 361*, 140–152.
11. Kitzing, K., Fitzpatrick, T. B., Wilken, C., Sawa, J., Bourenkov, G. P., Macheroux, P., and Clausen, T. (2005) The 1.3 Å crystal structure of the flavoprotein YqjM reveals a novel class of Old Yellow Enzymes. *J. Biol. Chem. 280*, 27904–27913.
12. Niino, Y. S., Chakraborty, S., Brown, B. J., and Massey, V. (1995) A new old yellow enzyme of *Saccharomyces cerevisiae*. *J. Biol. Chem. 270*, 1983–1991.
13. Brige, A., Van den Hemel, D., Carpentier, W., De Smet, L., and Van Beeumen, J. J. (2006) Comparative characterization and expression analysis of the four Old Yellow Enzyme homologues from *Shewanella*

oneidensis indicate differences in physiological function. *Biochem. J. 394*, 335–344.

14. van Dillewijn, P., Wittich, R. M., Caballero, A., and Ramos, J. L. (2008) Subfunctionality of Hydride Transferases of the Old Yellow Enzyme Family of Flavoproteins of *Pseudomonas putida*. *Appl. Environ. Microbiol. 74*, 6703–6708.

15. Williams, R. E., and Bruce, N. C. (2002) 'New uses for an Old Enzyme': The Old Yellow Enzyme family of flavoenzymes. *Microbiology 148*, 1607–1614.

16. Abramovitz, A. S., and Massey, V. (1976) Interaction of phenols with old yellow enzyme. Physical evidence for charge-transfer complexes. *J. Biol. Chem. 251*, 5327–5336.

17. Fox, K. M., and Karplus, P. A. (1994) Old yellow enzyme at 2 Å resolution: Overall structure, ligand binding, and comparison with related flavoproteins. *Structure 2*, 1089–1105.

18. Karplus, P. A., Fox, K. M., and Massey, V. (1995) Flavoprotein structure and mechanism. 8. Structure-function relations for old yellow enzyme. *FASEB J. 9*, 1518–1526.

19. Kohli, R. M., and Massey, V. (1998) The oxidative half-reaction of Old Yellow Enzyme. The role of tyrosine 196. *J. Biol. Chem. 273*, 32763–32770.

20. Brown, B. J., Deng, Z., Karplus, P. A., and Massey, V. (1998) On the active site of Old Yellow Enzyme. Role of histidine 191 and asparagine 194. *J. Biol. Chem. 273*, 32753–32762.

21. Xu, D., Kohli, R. M., and Massey, V. (1999) The role of threonine 37 in flavin reactivity of the old yellow enzyme. *Proc. Natl. Acad. Sci. U.S.A. 96*, 3556–3561.

22. Fox, K. M., and Karplus, P. A. (1999) The flavin environment in old yellow enzyme. An evaluation of insights from spectroscopic and artificial flavin studies. *J. Biol. Chem. 274*, 9357–9362.

23. Brown, B. J., Hyun, J. W., Duvvuri, S., Karplus, P. A., and Massey, V. (2002) The role of glutamine 114 in old yellow enzyme. *J. Biol. Chem. 277*, 2138–2145.

24. Craig, D. H., Moody, P. C., Bruce, N. C., and Scrutton, N. S. (1998) Reductive and oxidative half-reactions of morphinone reductase from *Pseudomonas putida* M10: A kinetic and thermodynamic analysis. *Biochemistry 37*, 7598–7607.

25. Barna, T., Messiha, H. L., Petosa, C., Bruce, N. C., Scrutton, N. S., and Moody, P. C. (2002) Crystal structure of bacterial morphinone reductase and properties of the C191A mutant enzyme. *J. Biol. Chem. 277*, 30976–30983.

26. Messiha, H. L., Bruce, N. C., Sattelle, B. M., Sutcliffe, M. J., Munro, A. W., and Scrutton, N. S. (2005) Role of active site residues and solvent in proton transfer and the modulation of flavin reduction potential in bacterial morphinone reductase. *J. Biol. Chem. 280*, 27103–27110.

27. Pudney, C. R., Hay, S., Pang, J., Costello, C., Leys, D., Sutcliffe, M. J., and Scrutton, N. S. (2007) Mutagenesis of morphinone reductase induces multiple reactive configurations and identifies potential ambiguity in kinetic analysis of enzyme tunneling mechanisms. *J. Am. Chem. Soc. 129*, 13949–13956.

28. Barna, T. M., Khan, H., Bruce, N. C., Barsukov, I., Scrutton, N. S., and Moody, P. C. (2001) Crystal structure of pentaerythritol tetranitrate reductase: "Flipped" binding geometries for steroid substrates in different redox states of the enzyme. *J. Mol. Biol. 310*, 433–447.

29. Khan, H., Harris, R. J., Barna, T., Craig, D. H., Bruce, N. C., Munro, A. W., Moody, P. C., and Scrutton, N. S. (2002) Kinetic and structural basis of reactivity of pentaerythritol tetranitrate reductase with NADPH, 2-cyclohexenone, nitroesters, and nitroaromatic explosives. *J. Biol. Chem. 277*, 21906–21912.

30. Khan, H., Barna, T., Harris, R. J., Bruce, N. C., Barsukov, I., Munro, A. W., Moody, P. C., and Scrutton, N. S. (2004) Atomic resolution structures and solution behavior of enzyme-substrate complexes of *Enterobacter cloacae* PB2 pentaerythritol tetranitrate reductase. Multiple conformational states and implications for the mechanism of nitroaromatic explosive degradation. *J. Biol. Chem. 279*, 30563–30572.

31. Khan, H., Barna, T., Bruce, N. C., Munro, A. W., Leys, D., and Scrutton, N. S. (2005) Proton transfer in the oxidative half-reaction of pentaerythritol tetranitrate reductase. Structure of the reduced enzyme-progesterone complex and the roles of residues Tyr186, His181, His184. *FEBS J. 272*, 4660–4671.

32. Breithaupt, C., Kurzbauer, R., Lilie, H., Schaller, A., Strassner, J., Huber, R., Macheroux, P., and Clausen, T. (2006) Crystal structure of 12-oxophytodienoate reductase 3 from tomato: Sself-inhibition by dimerization. *Proc. Natl. Acad. Sci. U.S.A. 103*, 14337–14342.

33. Breithaupt, C., Strassner, J., Breitinger, U., Huber, R., Macheroux, P., Schaller, A., and Clausen, T. (2001) X-ray structure of 12-oxophytodienoate reductase 1 provides structural insight into substrate binding and specificity within the family of OYE. *Structure 9*, 419–429.

34. Fitzpatrick, T. B., Auweter, S., Kitzing, K., Clausen, T., Amrhein, N., and Macheroux, P. (2004) Structural and functional impairment of an Old Yellow Enzyme homologue upon affinity tag incorporation. *Protein Expression Purif. 36*, 280–291.

35. Sambrook, J., and Russel, D. (2001) Molecular Cloning: A Laboratory Manual , Vol. 1, Cold Spring Harbor Laboratory Press, Plainview, NY.

36. Aliverti, A., Curti, B., and Vanoni, M. A. (1999) Identifying and quantitating FAD and FMN in simple and in iron-sulfur-containing flavoproteins. *Methods Mol. Biol. 131*, 9–23.

37. Massey, V., Stankovich, M., and Hemmerich, P. (1978) Light-mediated reduction of flavoproteins with flavins as catalysts. *Biochemistry 17*, 1–8.

38. Sucharitakul, J., Chaiyen, P., Entsch, B., and Ballou, D. P. (2005) The reductase of p-hydroxyphenylacetate 3-hydroxylase from *Acinetobacter baumannii* requires p-hydroxyphenylacetate for effective catalysis. *Biochemistry 44*, 10434–10442.

39. Loach, P. A. (1973) Oxidation-reduction potentials: Absorbance bands and molar absorbance of compounds used in biochemical studies. In Handbook of Biochemistry Selected Data for Molecular Biology (Sorber, H. A., Ed.) pp J33−J40, CRC Press, Cleveland, OH.

40. Segel, I. H. (1993) Enzyme Kinetics , John Wiley and Sons, New York.

41. Strickland, S., Palmer, G., and Massey, V. (1975) Determination of dissociation constants and specific rate constants of enzyme-substrate (or protein-ligand) interactions from rapid reaction kinetic data. *J. Biol. Chem. 250*, 4048–4052.

42. Lang, P. T., Brozell, S. R., Mukherjee, S., Pettersen, E. F., Meng, E. C., Thomas, V., Rizzo, R. C., Case, D. A., James, T. L., and Kuntz, I. D. (2009) DOCK 6: Ccombining techniques to model RNA-small molecule complexes. *RNA 15*, 1219–1230.

43. MacKerell, A. D.Jr., Banavali, N., and Foloppe, N. (2000) Development and current status of the CHARMM force field for nucleic acids. *Biopolymers 56*, 257–265.

44. Brooks, B. R., Brooks, C. L.III, Mackerell, A. D.Jr., Nilsson, L., Petrella, R. J., Roux, B., Won, Y., Archontis, G., Bartels, C., Boresch, S., Caflisch, A., Caves, L., Cui, Q., Dinner, A. R., Feig, M., Fischer, S., Gao, J., Hodoscek, M., Im, W., Kuczera, K., Lazaridis, T., Ma, J., Ovchinnikov, V., Paci, E., Pastor, R. W., Post, C. B., Pu, J. Z., Schaefer, M., Tidor, B., Venable, R. M., Woodcock, H. L., Wu, X., Yang, W., York, D. M., and Karplus, M. (2009) CHARMM: The biomolecular simulation program. *J. Comput. Chem. 30*, 1545–1614.

45. Bashford, D., and Karplus, M. (1990) pKa's of ionizable groups in proteins: Atomic detail from a continuum electrostatic model. *Biochemistry 29*, 10219–10225.

46. Messiha, H. L., Munro, A. W., Bruce, N. C., Barsukov, I., and Scrutton, N. S. (2005) Reaction of morphinone reductase with 2-cyclohexen-1-one and 1-nitrocyclohexene: Proton donation, ligand binding, and the role of residues Histidine 186 and Asparagine 189. *J. Biol. Chem. 280*, 10695–10709.

47. Stewart, R. C., and Massey, V. (1985) Potentiometric studies of native and flavin-substituted Old Yellow Enzyme. *J. Biol. Chem. 260*, 13639–13647.

48. DeLano, W. L. (2002) The PyMol Molecular Graphics System , DeLano Scientific, San Carlos, CA.

9 Publication B

Olivia Spiegelhauer, Sophia Mende, Frank Dickert, Stefan H. Knauer, G. Matthias Ullmann and Holger Dobbek (2010): Cysteine as a modulator residue in the active site of xenobiotic reductase A: A structural, thermodynamic and kinetic study. *Journal of Molecular Biology* **398**, 66-82

Available online at www.sciencedirect.com

ScienceDirect

Cysteine as a Modulator Residue in the Active Site of Xenobiotic Reductase A: A Structural, Thermodynamic and Kinetic Study

Olivia Spiegelhauer[1], Sophia Mende[1], Frank Dickert[2], Stefan H. Knauer[1], G. Matthias Ullmann[2] and Holger Dobbek[1]*

[1]*Bioinorganic Chemistry, Universität Bayreuth, Universitätsstrasse 30, 95447 Bayreuth, Germany*

[2]*Structural Biology/ Bioinformatics, Universität Bayreuth, Universitätsstrasse 30, 95447 Bayreuth, Germany*

Xenobiotic reductase A (XenA) from *Pseudomonas putida* 86 catalyzes the NADH/NADPH-dependent reduction of various substrates, including 2-cyclohexenone and 8-hydroxycoumarin. XenA is a member of the old yellow enzyme (OYE) family of flavoproteins and is structurally and functionally similar to other bacterial members of this enzyme class. A characteristic feature of XenA is the presence of a cysteine residue (Cys25) in the active site, where in most members of the OYE family a threonine residue is found that modulates the reduction potential of the FMN/FMNH⁻ couple. We investigated the role of Cys25 by studying two variants in which the residue has been exchanged for a serine and an alanine residue. While the exchange against alanine has a remarkably small effect on the reduction potential, the reactivity and the structure of XenA, the exchange against serine increases the reduction potential by +82 mV, increases the rate constant of the reductive half-reaction and decreases the rate constant in the oxidative half-reaction. We determined six crystal structures at high to true atomic resolution (d_{min} 1.03–1.80 Å) of the three XenA variants with and without the substrate coumarin bound in the active site. The atomic resolution structure of XenA in complex with coumarin reveals a compressed active site geometry in which the isoalloxazine ring is sandwiched between coumarin and the protein backbone. The structures further reveal that the conformation of the active site and substrate interactions are preserved in the two variants, indicating that the observed changes are due to local effects only. We propose that Cys25 and the residues in its place determine which of the two half-reactions is rate limiting, depending on the substrate couple. This might help to explain why the genome of *Pseudomonas putida* encodes multiple xenobiotic reductases containing either cysteine, threonine or alanine in the active site.

© 2010 Elsevier Ltd. All rights reserved.

Edited by R. Huber

Introduction

Xenobiotic reductases catalyze the NAD(P)H-dependent reduction of the olefinic bond of different α,β-unsaturated carbonyl compounds, including ketones and esters, and belong to the old yellow enzyme (OYE) family. Members of this family have been found in bacteria, yeasts, plants and nematodes,[1] and their physiological functions are mostly unknown. The genome of several bacteria contain multiple open-reading-frames encoding OYE homologs,[2,3] and the largest number of different OYE homologs are present in the genome of *Pseudomonas putida* KT2440, which encodes six variants named XenA – XenF.[4] On the basis of amino acid sequence alignments, these variants can be related to different subgroups of the

---

*Corresponding author. Institut für Biologie, Strukturbiologie/Biochemie, Humboldt-Universität zu Berlin, 10115 Berlin, Germany. E-mail address: Holger.Dobbek@uni-bayreuth.de.

Abbreviations used: OYE, old yellow enzyme; RHR, reductive half-reaction; OHR, oxidative half-reaction; MC, Monte Carlo.

OYE family and are likely to have evolved from different ancestors. XenA isolated from *P. putida* 86 was recently shown to be involved in the degradation of quinoline[5] along the 8-hydroxycoumarin pathway due to its ability to reduce the C3=C4 double bond of 8-hydroxycoumarin and its abundance, when *P. putida* 86 is grown in the presence of quinoline.[6] It shares the highest sequence identity with XenA, XenD and XenE from *P. putida* KT2440 and YqjM from *Bacillus subtilis*.[4] The crystal structure of XenA has been solved for the oxidized enzyme alone and with two substrates bound to the active site at a resolution of 1.5 Å.[6] XenA is a homodimer in solution and the crystal, and one FMN molecule is bound to each monomer. The subunit structure is similar to that reported for OYE,[7] morphinone reductase[8], PETN reductase[9,10], *Shewanella* yellow enzyme 1[11] and YqjM.[12] They all consist of the typical $(\beta/\alpha)_8$ barrel and FMN is bound at the C-terminal end. The *re* side of the flavin is facing the protein and the *si* side defines the bottom of a wide active site pocket. The reaction of XenA is consistent with a ping pong mechanism and can be divided into two half-reactions. A kinetic investigation using NADH and NADPH as substrates in the reductive half-reaction and 2-cyclohexenone and coumarin in the oxidative half-reaction revealed that either half-reaction can be rate-limiting, depending on the combination of substrates. In the reductive half-reaction the enzyme is reduced efficiently by NADPH, while the reaction with NADH is about 20-fold slower. The first step in this reaction is the formation of a charge transfer complex between the flavin cofactor and the nicotinamide, which is followed by a hydride transfer from NAD(P)H to FMN. In the oxidative half-reaction the enzyme can reduce different α,β-unsaturated carbonyl compounds. In this case we assume two different intermediates before the equivalents of two electrons and two protons are transferred on the substrate, suggesting that the relative orientations of FMN and the substrate changes from the encounter complex to the reactive complex. The rate constants for reductive and oxidative half-reactions are dependent on the reduction potential of the flavin cofactors.[13] The reduction potential of the FMN/FMNH⁻ couple in XenA was previously determined to be –263 mV,[13] which is considerably lower than the values found for other members of the OYE family.[14–16] XenA shows several structural variations that can be responsible for the difference in the reduction potential. One is a cysteine residue (Cys25) in the active site, which replaces a highly conserved threonine residue. The side chains of cysteine in XenA and the threonine residue are within hydrogen bonding distance to the O(4) carbonyl oxygen atom of the isoalloxazine ring. Mutagenesis studies of this threonine residue (Thr37 in OYE[17] and Thr32 in morphinone reductase[15)] indicated that this residue modulates the flavin reduction potential. Cys26 in YqjM, which is analogous to Cys25 in XenA, was shown to adopt several conformations

interacting either with O(4) or with N(5) and might interact with the delocalized ring electrons of the adjacent Tyr28. It is therefore assumed that Cys26 acts as a redox sensor that is able to control the reduction potential of FMN, depending on the presence of substrates.[12] The exchange of Cys26 (C26D and C26G) altered the reactivity of YqjM and changed its enantioselectivity.[18]

The recent structural[6] and kinetic[13] studies of XenA did not reveal the contributions of individual active site residues. To gain insight into the role of Cys25 we studied its effect on the structure, the stabilization of substrate complexes and the kinetics of the catalytic cycle. We report the crystal structures of XenA and variants in which Cys25 has been replaced by alanine and serine with and without substrate bound in the active site, as well as the effect of the mutations on ligand binding and the kinetics of XenA. Threonine is the most frequently encountered amino acid at the position of Cys25 in related flavoenzymes. An inspection of the crystal structure of XenA reveals that the methyl group of threonine in a C25T variant of XenA would clash with the neighboring tyrosine residue (Tyr27) and we therefore preferred the exchange of cysteine for serine and cysteine for alanine. Our earlier structural characterization of XenA at a resolution of 1.5 Å indicated a deviation of the isoalloxazine ring from planarity; however, the interatomic distances within the active site, which contribute to create this strained conformation, could not be determined reliably.[6] We therefore extended our analysis to true atomic resolution (d_{min} 1.03 Å) to reveal the individual contributions to the deformation of the flavin. Our earlier analysis showed that Cys25 is close to the substrate-binding site but did not reveal any direct interaction between the residue and the substrate.[6] We were specifically interested in whether Cys25 would contribute to the stabilization of an intermediate or transition state of the reaction in comparison to the unreacted substrate to accelerate the overall reaction. The stabilization of a transition state cannot be revealed by a crystal structure, so we analyzed the kinetics of the two half-reactions of the XenA variants and compare it to that of the wild type protein.

Results and Discussion

Mutagenesis

The QuickChange mutagenesis protocol from Stratagene was used to mutate Cys25 in XenA wild type. PCR primers were designed to exchange this cysteine with alanine and with serine, and gene sequencing of the resulting expression plasmids confirmed the correct single site mutations. Both variants could be expressed and purified like the wild type enzyme. Mutagenesis did not result in a loss of FMN and all enzymes have an FMN content of 70 – 80%.

Spectroscopic properties and specific activity

Wild type Xen (XenA-wt), XenA-C25A and XenA-C25S showed only small differences in their absorbance spectra. The maximum peak of FMN was shifted from 464 nm in the wild type protein to 456 nm in XenA-C25A and to 460 nm in XenA-C25S (Supplementary Data Fig. S1). The extinction coefficients for the two peaks ($\varepsilon_{456} = 12.7$ mM^{-1} cm^{-1}; $\varepsilon_{460} = 11.4$ mM^{-1} cm^{-1}) are about the same as those for the wild type protein ($\varepsilon_{464} = 12.20$ mM^{-1} cm^{-1}).[6] Both variants show higher absorption around 550 nm and their spectra are red-shifted compared to XenA-wt. With coumarin (2*H*-chromen-2-one) bound to the oxidized enzyme, the absorbance maxima of XenA-wt is 470 nm. XenA-C25A with a maximum at 468 nm shows a red-shift of 2 nm, whereas the maximum of XenA-C25S is blue-shifted to 476 nm (Supplementary Data Fig. S1). The specific activities for XenA-wt and variants, measured with NADPH and 2-cyclohexenone as substrates are given in Table 1. XenA-C25A shows a sixfold decrease in specific activity, whereas the specific activity of XenA-C25S is half of XenA-wt. However, the XenA-C25A variant tended to precipitate under the assay conditions, making it likely that the low specific activity of XenA-C25A is due, at least in part, to a lower effective enzyme concentration in the assay. Furthermore, the specific activity of XenA-wt and both variants was determined at pH values ranging from 5 to 10.5 (data not shown) to detect possible changes in the pH-activity profile. The specific activities of the three XenA variants have an activity optimum around pH 8, change less than 50 % within the pH range 6 – 10 and show all the same principal pH-activity profile.

Ligand binding

XenA-wt and the two cysteine variants were titrated under identical conditions by stepwise addition of coumarin. Binding of coumarin perturbs the spectrum of XenA and therefore allows to detect complex formation (Fig. 1). Isosbestic points, consistent with a two-state binding process, are observed with all three proteins. Plots of the absorbance change at the maximum against ligand concentration and regression analysis using the Eq. (1) were used to determine the dissociation constants (K_d) for XenA-wt and the variants. K_d for the XenA-wt coumarin complex was 8.4 (± 1.0) µM, which is similar to the value of 5.0 (± 1.0) µM determined earlier.[6] For both variants, the exchange of cysteine resulted in small increases of the dissociation constant; a twofold increase for XenA-C25A and a sevenfold increase for XenA-C25S compared to the wild type protein (Table 1). Binding of coumarin causes no additional charge transfer interaction with strong absorbance in the long wavelength range.[19] The small changes of K_d are in agreement with a weak and likely indirect contribution of Cys25 to the formation of the complex between oxidized XenA and coumarin.

Table 1. Specific activities and K_d values of XenA-wt, XenA-C25A and XenA-C25S

	Specific activity (U mg^{-1})	K_d (µM) for coumarin
XenA	6.7	8.4±1.0
C25A	1.11	20.9±3.2
C25S	3.34	69.2±3.6

Photoreduction and determination of reduction potentials

Both XenA variants were reduced using the light-mediated generation of electrons with the deaza-flavin/EDTA couple in the presence of phenosafranine as redox mediator. This method was used to ensure single electron transfer and allow the formation of semiquinone species. Unlike XenA-wt, which shows the initial formation of an anionic semiquinone,[13] only quinone and hydroquinone species of FMN are observed during photoreduction of XenA-C25S and XenA-C25A (Fig. 2a). We therefore assume that, as in XenA-wt, the reduction potential of the FMN/FMNH$^-$ couple is substantially lower than the FMN/FMNH$^-$ couple and that either the enzyme or the reaction conditions allowed for faster equilibration than observed in the experiment with XenA-wt.[13] The inability to form semiquinone species has been observed also for the related flavoenzymes morphinone reductase,[20] PETN reductase[14] and YqjM.[21]

To investigate the influence of Cys25 on the relative stability of the oxidized and reduced state of XenA, we determined the reduction potentials of the FMN/FMNH$^-$ redox couple of both variants. The reduction potentials of XenA-C25A and XenA-C25S were calculated (using Eq. (4)) to be –266 mV and –181 mV, respectively. Thus, the replacement of cysteine with alanine does not change the reduction potential (XenA-wt: $E^0_m = -263$ mV),[13] whereas the exchange with serine increased the reduction potential by +82 mV. The linear fit of the plot of log(E_{ox}/E_{red}) *versus* log(Dye_{ox}/Dye_{red}) shows a slope of –1 in both cases, confirming that the enzyme and the dye received the same amount of electrons and reacted under equilibrium conditions. The determination of the reduction potential of XenA-C25A with phenosafranine as reference dye is illustrated by Fig. 2b.

The mutations of Cys25 to alanine and serine were expected to alter the reduction potential of the FMN as shown for OYE[17] and morphinone reductase.[15] The corresponding threonine residue in these two enzymes forms an O-H...O hydrogen bond to the C$_{(4)}$ oxygen atom of the isoalloxazine ring and stabilizes the negative charge of the reduced FMN. The hydrogen bond is lost when this residue is replaced by alanine and the reduction potential of the FMN/FMNH$^-$ couple is decreased from –230 mV to –263 mV in OYE[17] and from –242 mV to –290 mV in morphinone reductase.[15] As the γ-sulfhydrylgroup of Cys25 is within hydrogen bonding distance to O$_{(4)}$ of the isoalloxazine ring,
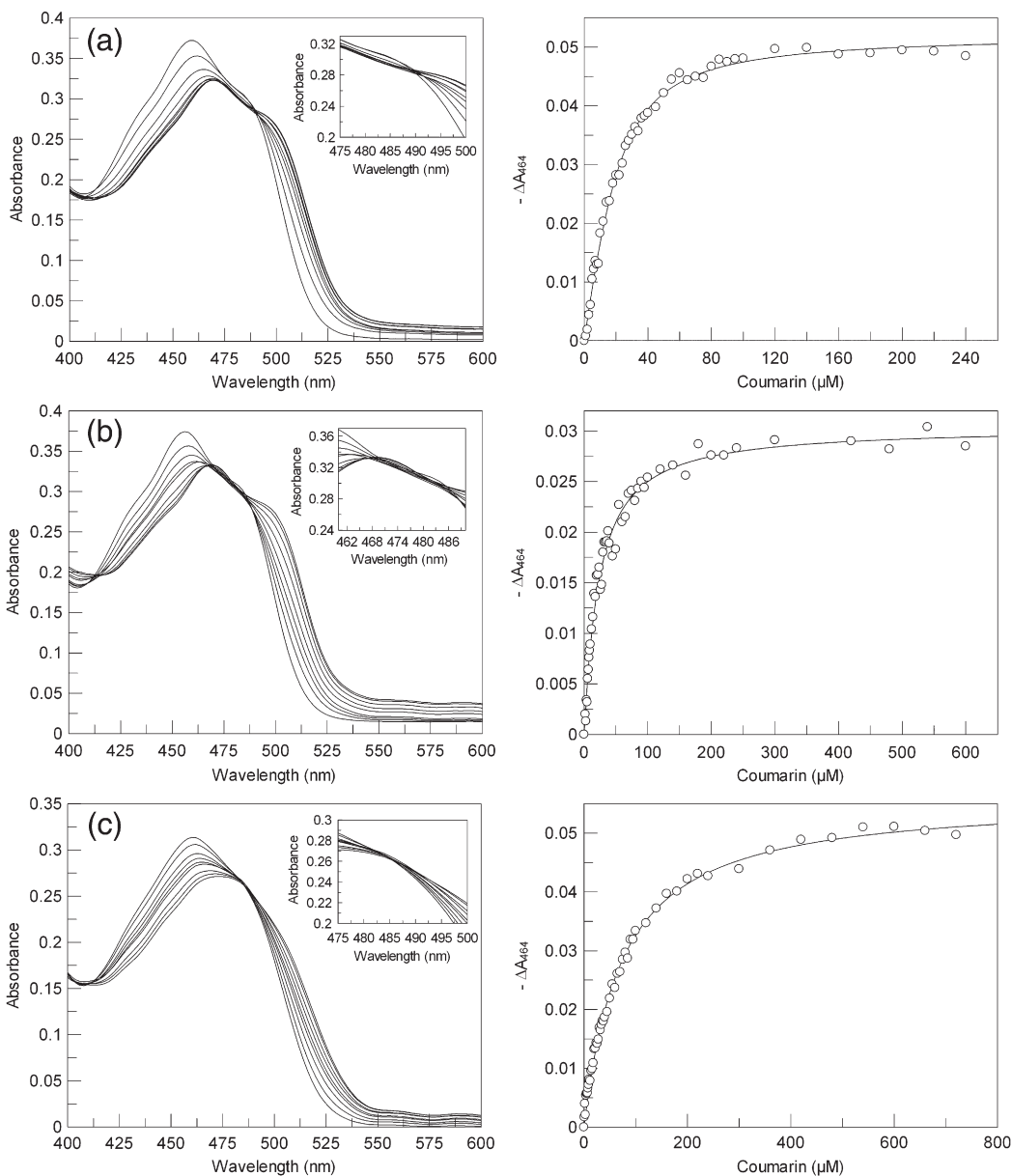
Fig. 1. Titration of XenA-wt, XenA-C25A and XenA-C25S with coumarin. Spectra were recorded in 50 mM Tris buffer, pH 8.0 at 25 °C. (a) Left-hand side: For XenA-wt (30 µM), the spectra are shown in the presence of 0, 8, 22, 38, 55, 75, 95, 160 and 200 µM coumarin. Right-hand side: A plot of absorbance changes as a function of the coumarin concentrations for the data shown on the left-hand side. (b) Left-hand side: For XenA-C25A, the spectra are shown in the presence of 0, 8, 18, 30, 45, 80, 160, 360 and 780 µM coumarin. Right-hand side: A plot of absorbance changes as a function of the coumarin concentrations for the data shown on the left-hand side. (c) Left-hand side; For XenA-C25S, the spectra are shown in the presence of 1, 10, 30, 50, 65, 85, 140, 240 and 360 µM coumarin. Right-hand side: A plot of absorbance changes as a function of the coumarin concentrations for the data shown on the left-hand side. The insets in the left-hand side of (a) – (c) show the region of the isosbestic points in detail.

we expected that the mutation to alanine would lead to a substantial decrease of the reduction potential. However, the reduction potential of XenA-C25A was practically the same as that of the wild type enzyme. This implies that either the oxidized and reduced states are equally stabile in XenA-wt and XenA-C25A or the reduced and oxidized state of the flavine are both stabilized or destabilized by the same amount upon loss of the SH group of Cys25.

The reduction potential of XenA-C25S changes to –181 mV. The difference in reduction potential of

+82 mV compared to the wild type enzyme and +87 mV compared to XenA-C25A is distinctly larger than that observed for the exchange of the corresponding threonine against alanine in OYE ($\Delta E^0{}_m = +33$ mV) and morphinone reductase ($\Delta E^0{}_m = +48$ mV). The more strongly polarized hydroxyl group of Ser25 can form a strong O-H···$O_{(4)}$ hydrogen bond with FMN and is therefore able to stabilize both FMN and FMNH⁻. However, the increase of reduction potentials is stronger than expected from the exchange of a weak S-H...$O_{(4)}$
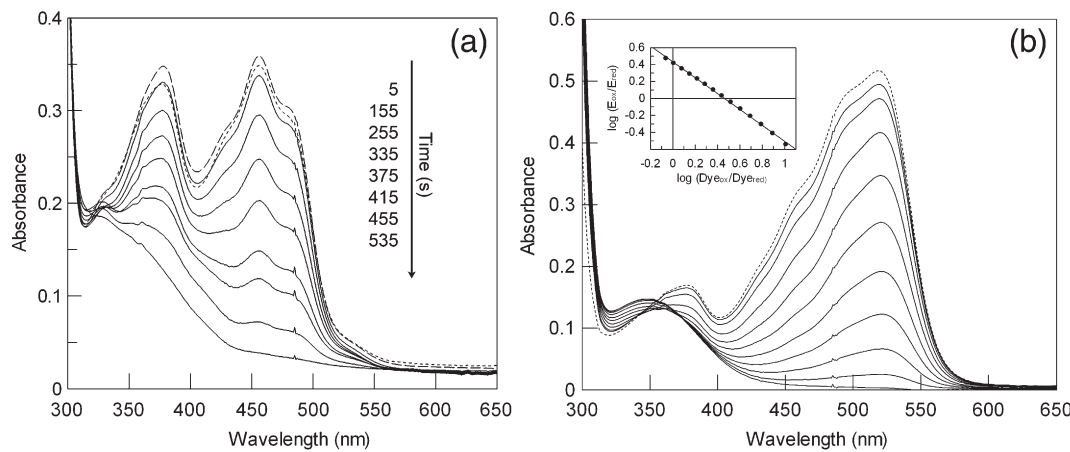
Fig. 2. Photoreduction and determination of the reduction potential of the FMN/FMNH⁻ couple in XenA-C25A. (a) Conditions: 30 μM XenA-C25A, 15 mM EDTA, 1 μM phenosafranine, 100 mM Tris buffer, pH 8.0 and traces of 5-deaza-10-methyl-3-sulfopropyl-isoalloxazine as catalyst. The spectra are shown before (dotted line) and after different illumination steps (continuous lines). The spectrum of reoxidized XenA-C25A is displayed as a broken line. (b) Conditions: 15 μM XenA-C25A, 15 μM phenosafranine, 2 μM methylviologen, 0.05 U xanthine oxidase, 50 mM Tris buffer, pH 8.0. The reduction of XenA-C25A with phenosafranine as reference dye is shown over a time range of 1.5 h (continuous lines). The spectrum recorded before the addition of xanthine is displayed as a dotted line. Absorbance values at 456 nm and 521 nm were used to calculate the concentrations of oxidized C25A and dye. The inset shows the plot of $\log(E_{ox}/E_{red})$ against $\log(Dye_{ox}/Dye_{red})$. The continuous line displays the linear fit with a slope of –1. The reduction potential of XenA-C25A was –266 mV.

hydrogen bond by the stronger O-H...O$_{(4)}$ hydrogen bond. The small change in reduction potential upon loss of the γ-sulfhydryl group and the large change when it was exchanged for a hydroxyl group indicated that it did not form a hydrogen-bond to O$_{(4)}$.

Transient kinetic analyses of the two half-reactions

Stopped flow spectrophotometry on the two half-reactions of XenA-C25A and XenA-C25S with different substrates was used to gain further insights into the role of Cys25 for the reactivity of XenA.

To initiate the reductive half-reactions (RHR) the enzymes were mixed under anoxic conditions in the stopped flow cuvette with different concentrations of NADH and NADPH and the signal change was followed at 464 nm. The kinetics of the oxidative half-reactions (OHR) of both XenA variants were studied with various concentrations of 2-cyclohexenone and coumarin. Before the OHR, the enzymes were reduced with equimolar amounts of NADH, which was sufficient to achieve complete reduction of FMN. Both variants were mixed with 2-cyclohexenone and coumarin under anoxic conditions in the stopped flow cuvette and the signal increase was followed at 464 nm. All of the substrates were used in our earlier study of XenA-wt,[13] which allows us to compare the reactivities of the variants with that of the wild type protein.

All of the observed rate constants showed a hyperbolic dependence on the substrate concentrations used (RHR in Fig. 3a–d; OHR in Fig. 4a–d). The linear correlations between $1/k_{obs}$ and $1/$[NADH or NADPH] (Fig. 3a–d, insets) and $1/k_{obs}$ and $1/$[2-cyclohexenone or coumarin] (Fig. 4a–d, insets) indicate equilibrium conditions for the reaction so that Eq. (7) can be used to determine the individual rate constants (k_x) and the dissociation constant (K_d) for the XenA substrate complexes.

In contrast to what was found for XenA-wt,[13] there was no indication of the formation of a charge transfer complex at 520 – 560 nm with the two variants in the RHR. The limiting rate constants of the reduction (k_{red}) of XenA-C25A were 0.76 (± 0.03) s^{-1} for the reaction with NADH and 19.0 (± 0.4) s^{-1} for the reaction with NADPH. These rate constants are slightly smaller than that found for XenA-wt and, like in the wild type enzyme, the XenA variants reacted 20-fold faster with NADPH than with NADH.[13] The limiting rate constants for the oxidation of XenA-C25A were 26.3 (± 0.1) s^{-1} with 2-cyclohexenone and 0.43 (± 0.01) s^{-1} with coumarin as substrate. The dissociation constants of all XenA-C25A substrates complexes are increased five- to sevenfold by the replacement of cysteine with alanine (RHR: NADH, 1216 (± 81) μM and NADPH, 726 (± 46) μM. OHR: 2-cyclohexenone, 346 (± 3) μM; coumarin, 109 (± 10) μM). As the reduction potentials of the FMN/FMNH⁻ couple of XenA-C25A and XenA-wt are very similar, we expected practically unchanged rate constants for the two half-reactions. However, we observed small but consistent changes and the exchange of cysteine against alanine decreased the rate constant of the RHR by a factor of 2 and increased the rate constant of the OHR by the same factor.

The rate constants for the reduction of the XenA-C25S variant were 6.1 (± 0.2) s^{-1} for NADH and 171
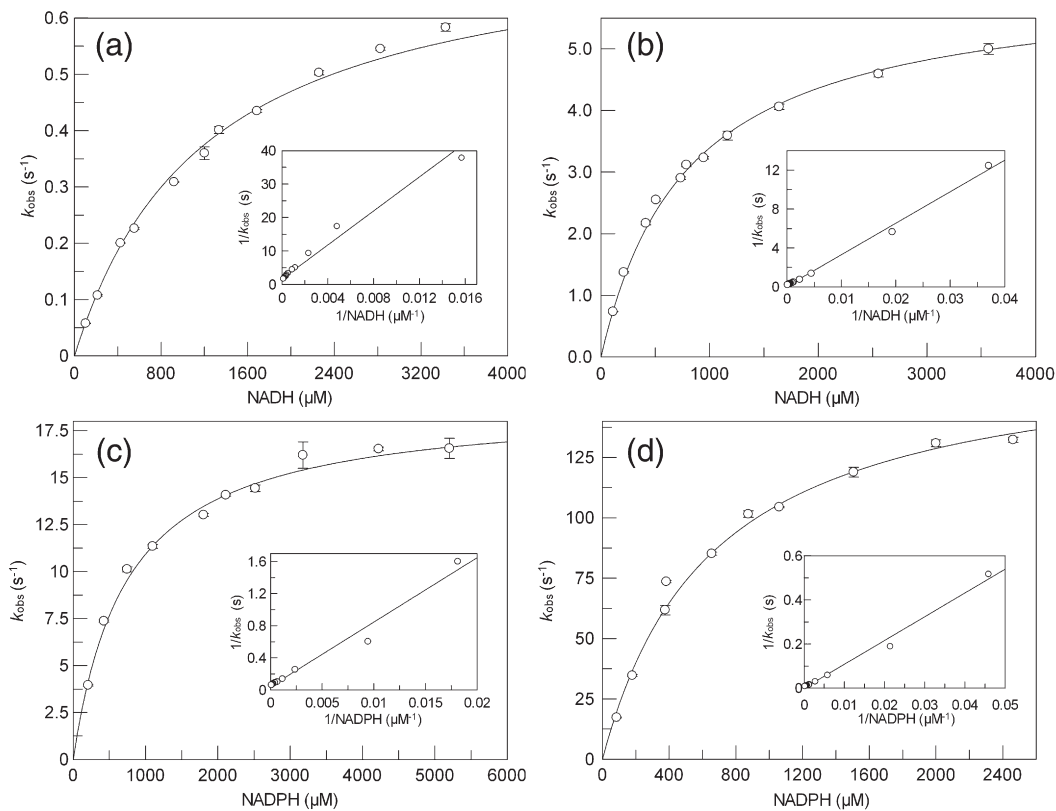
Fig. 3. Reductive half-reactions of XenA-C25A and XenA-C25S with NADH and NADPH. The concentration dependence of the observed rates at 464 nm for the reaction of 5 μM enzyme with the reductive substrates is shown. (a) Reaction of XenA-C25A with different concentrations of NADH. (b) Reaction of XenA-C25S with different concentrations of NADH. (c) Reaction of XenA-C25A with different concentrations of NADPH. (d) Reaction of XenA-C25S with different concentrations of NADPH. The reciprocal plots are shown in the insets.

($\pm$ 10) s^{-1} for NADPH, which is about three- to fourfold higher than that for XenA-wt, while the rate constants of the oxidation of XenA-C25S with 2-cyclohexenone (5.12 ($\pm$ 0.08) s^{-1}) and with coumarin (0.060 ($\pm$ 0.001) s^{-1}) are fourfold smaller than those for XenA-wt. Again, as seen with the replacement of cysteine by alanine, the rate constants of both half-reactions changed by the same factor. However, the replacement of cysteine with serine accelerated the reductive half-reaction and decelerated the oxidative half-reaction. The dissociation constants for all four enzyme–substrate complexes were increased. The dissociation constants of the XenA-C25S-NAD(P)H complex were 800 ($\pm$ 37) μM for NADH and 655 ($\pm$ 85) μM for NADPH, which is within the same range as that of XenA-C25A and are four- to sevenfold greater than that of XenA-wt, while the dissociation constants of the complexes with 2-cyclohexenone (187.1 ($\pm$ 7.1) μM) and coumarin (53.0 ($\pm$ 4.0) μM) were approximately doubled. The reduction potential of the FMN/FMNH$^-$ couple of XenA-C25S is more positive by 82 mV than that for XenA-wt. We assume that the stronger stabilization of the reduced flavin results in product stabilization in the RHR and a destabilization of the educts in the OHR compared to the reaction of XenA-wt. A similar effect was observed for the threonine-alanine exchange in OYE and morphinone reductase.

The rate constants determined for the both half-reactions and the kinetic dissociation constants are summarized in Table 2. From these data we can conclude that Cys25 is not essential for catalysis, but its presence shifts the enzyme reactivity more to the RHR (compared to XenA-C25A) or the OHR (compared to XenA-C25S). Both exchanges of the cysteine residue decrease the affinity of the enzyme for its substrates corresponding to a change in the apparent binding energy ($\Delta G_{app} = RT \ln K_S / K'_S$) of 1.7 – 4.7 kJ/mol. Due to the effect of the mutations on the electronic structure and likely the conformation of the isoalloxazine ring and the $\pi\pi$ interactions of the substrate with the isoalloxazine ring, there are several different contributions to ΔG_{app}, and the local binding energy (ΔG_{bind}) between Sγ-Cys25 with the substrate may be only a small part of this sum. We therefore assume that the loss of a direct Cys25–substrate interaction, e.g. formation of a hydrogen bond in the Michaelis complexes, would have resulted in a greater increase of ΔG_{app} and we conclude that Cys25 does not contribute to the binding of the substrate in either the oxidized or the reduced state.

Active site structure of XenA-wt

The structure of XenA-wt was refined at a resolution of 1.03 Å without and at 1.1 Å with
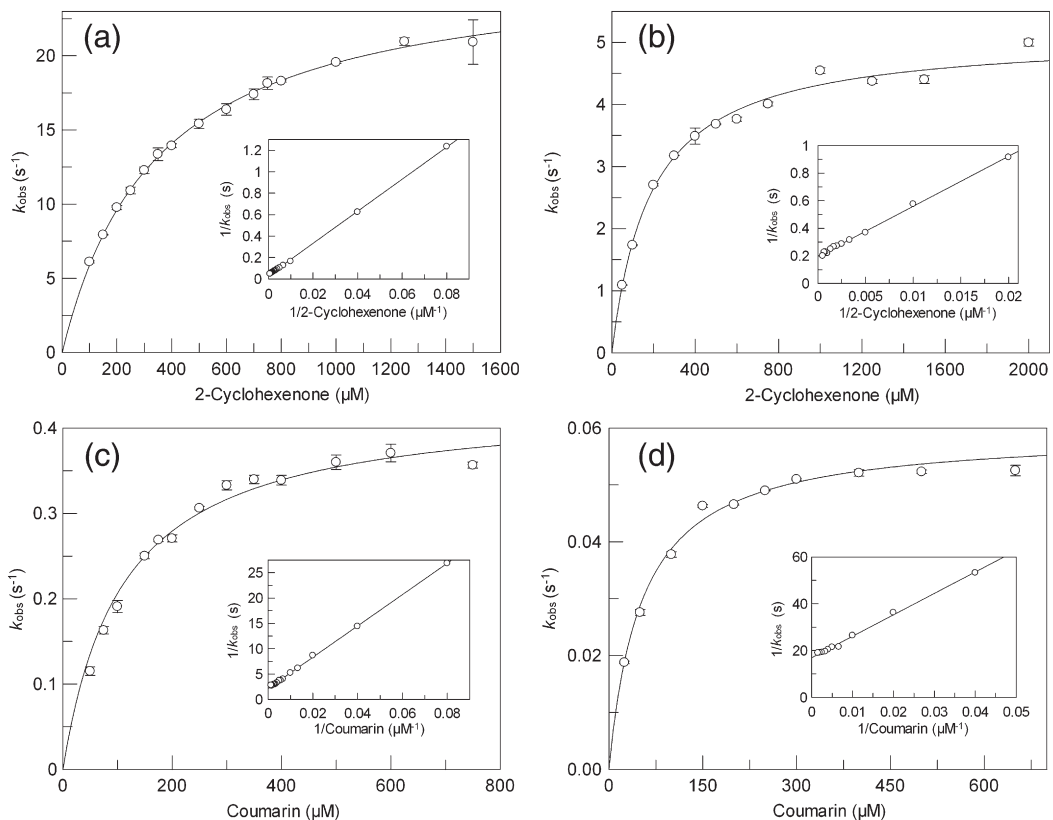
Fig. 4. Oxidative half-reactions of XenA-C25A and XenA-C25S with 2-cyclohexenone and coumarin. All figures show the concentration dependence of the observed rates at 464 nm for the reaction of 5 μM enzyme with the oxidative substrates is shown. (a) Reaction of XenA-C25A with different concentrations of 2-cyclohexenone. (b) Reaction of XenA-C25S with different concentrations of 2-cyclohexenone. (c) Reaction of XenA-C25A with different concentrations of coumarin. (d) Reaction of XenA-C25S with different concentrations of coumarin. The reciprocal plots are shown in the insets.

coumarin bound to the active site (Fig. 5a and b). For the refinement, hydrogen atoms were included and all non-hydrogen atoms were refined with anisotropic *B*-factors. The high resolution revealed multiple conformations for 7.5 % of the side chains. A large number of hydrogen atoms are clearly defined in the electron density, and on leaving out the amide protons of the main chain of XenA 37 % of the corresponding H atoms produce peaks with more than 0.2 e/Å[3], corresponding to a σ-level of 3.0, in the difference density map. The incomplete coverage of the observed amide hydrogens is most likely due to the correlation between the maximum electron

density peak for an atom and the root-mean-square (rms) deviation of the atomic position. To estimate whether our measuring strategy induced photoreduction of the flavin by the X-rays, we compared the bond length within the isoalloxazine ring to the values given for oxidized and reduced small flavin derivatives.[22] The FMN in XenA-wt has the following redox-sensitive bond lengths: $N_{(5)}$–$C_{(4a)}$, 1.37 Å; $C_{(4a)}$–$C_{(4)}$, 1.44 Å; $C_{(4a)}$–$C_{(10a)}$, 1.40 Å; and $C_{(10a)}$–$N_{(1)}$, 1.31 Å. These values are not typical for oxidized or reduced flavins and are intermediate between the distances expected for both oxidation states. These deviations might reflect the influence of the protein

Table 2. Transient kinetic data

	XenA-wt[a]		XenA-C25A		XenA-C25S	
	k_{red} (s^{-1})	K_d (μM^{-1})	k_{red} (s^{-1})	K_d (μM^{-1})	k_{red} (s^{-1})	K_d (μM^{-1})
NADH	1.50±0.02	176±14	0.76±0.03	1216±81	6.1±0.2	800±37
NADPH	35.7±0.6	256±12	19.0±0.4	736±47	171±11	656±86
	k_{ox} (s^{-1})	K_d (μM^{-1})	k_{ox} (s^{-1})	K_d (μM^{-1})	k_{ox} (s^{-1})	K_d (μM^{-1})
2-Cyclohexenone	13.1±0.1	86±2	26.3±0.1	346±3	5.12±0.08	187±7
Coumarin	0.243±0.001	19.3±0.6	0.43±0.01	109±10	0.060±0.001	53±4

[a] Data from the wild type enzyme XenA are from Ref. [12].
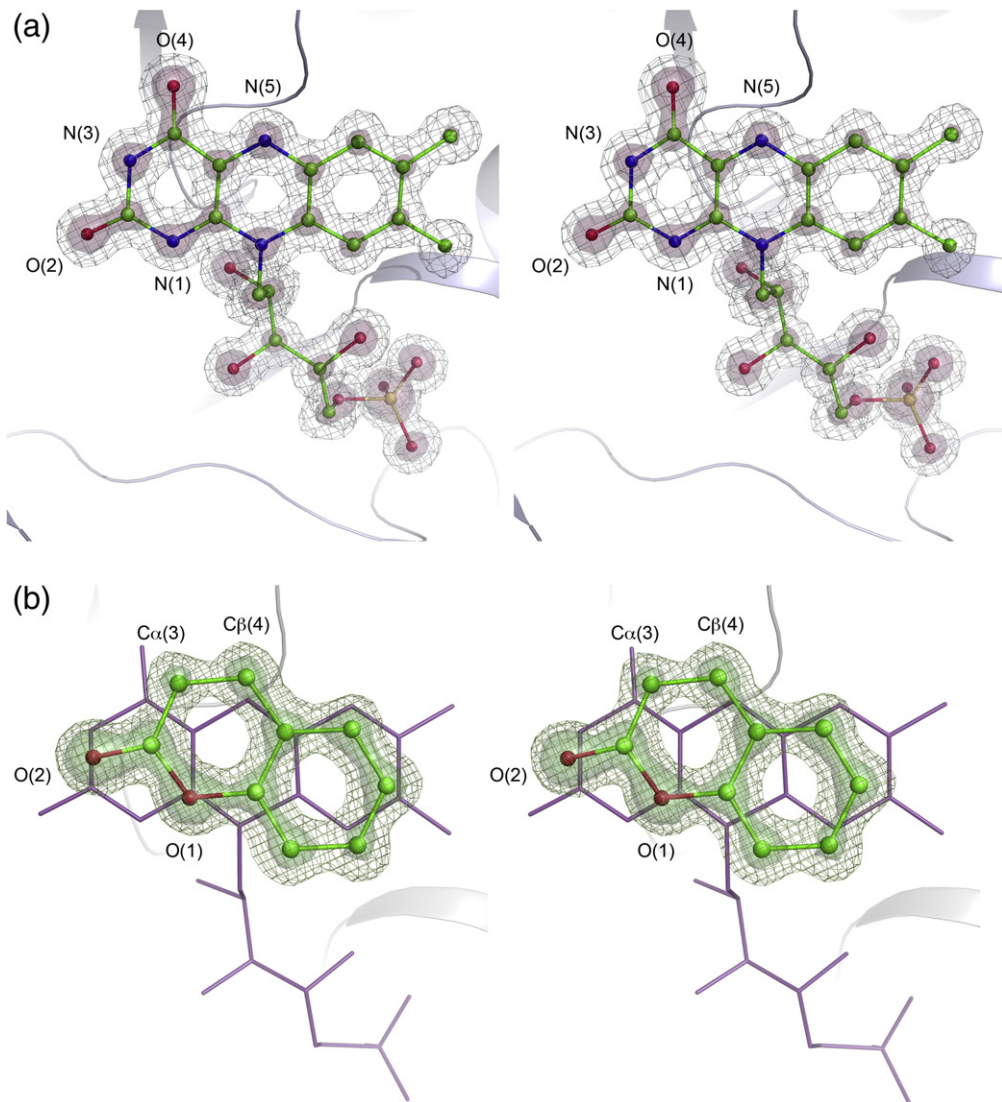
Fig. 5. Atomic resolution structure of XenA-wt. (a) Stereoscopic view of the electron density map of the FMN cofactor. The $2F_o - F_c$ map contoured at 1.0σ is shown in gray mesh representation, the $2F_o - F_c$ map contoured at 5.0σ is shown in brown surface representation. FMN is shown in stick and ball mode. Oxygen atoms, red; nitrogen atoms, blue; carbon atoms, green; and phosphorus, yellow. (b) Stereoscopic view of FMN in complex with coumarin. The $2F_o - F_c$ map contoured at 1.0σ is shown in green mesh representation and the $2F_o - F_c$ map contoured at 5.0σ is shown in green surface representation. FMN (violet) is shown in stick mode. Coumarin is displayed in stick and ball representation with carbon atoms in green and oxygen atoms in red.

environment on the geometry of the cofactor. However, it is likely that the synchrotron radiation, at least in part, reduced the protein during data collection resulting in a mixture of oxidized and reduced molecules. We therefore refrain from an in-depth discussion of the flavin geometry. Nevertheless, the improvement in resolution provides a better description of the active site structure, particularly on the protein–cofactor and protein–substrate interactions. The atomic resolution structure allows us to reassess the geometry of residues with an unusual conformation. In the earlier structure, a single tryptophan residue (Trp358) was found to deviate from the Ramachandran statistics. This deviation is likely of functional relevance, as Trp358 is part of the FMN-binding site and the unusual conformation of

the peptide backbone has been confirmed in the atomic resolution structure.

Furthermore, the electron density can provide direct insight in the charge distribution throughout the isoalloxazine ring, provided the ring atoms have comparable B-factors. The average B-factor of the ring atoms was 6.0 Å^2, and the deviations from this value were within $\pm 15\%$. The electron density distribution was lowest within the dimethylbenzene ring and stronger for the heteroaromatic rings. These areas are expected to interact favorably with donor atoms.[23,24] The FMN cofactor is non-covalently bound to the protein by different interactions between the protein environment and the FMN. Hydrogen bonding interactions are located exclusively in the area of higher charge density (Fig. 6a). $O_{(4)}$ of the isoalloxa-
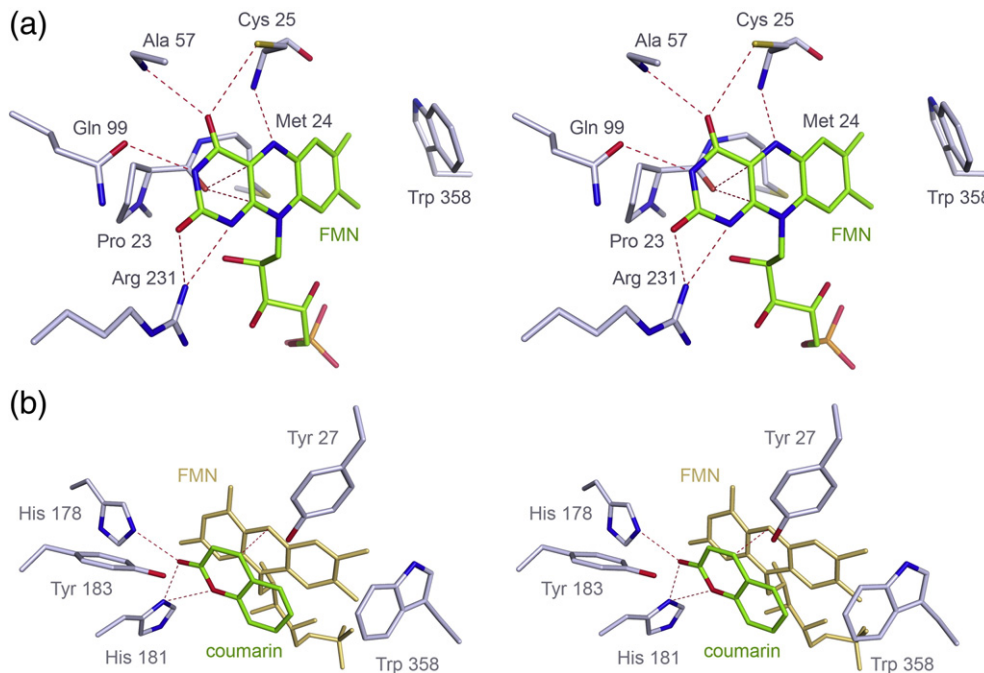
Fig. 6. Active site view. (a) Stereoscopic view of the hydrogen-bonding network around FMN. All residues are displayed in stick representation. Carbon atoms of the amino acid side chains, gray; carbon atoms of FMN, green; oxygen atoms, red; nitrogen atoms, blue, sulfur atoms, yellow; and phosphorus, orange. The broken red lines represent possible interactions between the cofactor and the adjacent amino acids. (b) Stereoscopic view of the hydrogen bonding network around coumarin bound to the active site. All residues are displayed in stick representation. FMN, yellow; carbon atoms of coumarin, green; carbon atoms of the amino acid side chains, gray; oxygen atoms, red; and nitrogen atoms, blue. The broken red lines represent possible interactions between coumarin and XenA-wt.

zine ring is within hydrogen bonding distance to the amide proton of Ala57 and the γ-sulfhydryl group of Cys25. The distance between the γ-sulfhydryl group of Cys25 and $O_{(4)}$ is 3.28 Å, indicating that a weak hydrogen bond might be present. $N_{(5)}$ is within hydrogen bonding distance to the amide proton of Cys25. $N_{(1)}$ as well as $O_{(2)}$ are within hydrogen bonding distance to the guanidinium group of Arg231 with a distance of 2.99 Å and the proton of $N_{(3)}$ interacts with the carbonyl group of Gln99 with a N–O distance of 2.80 Å.

The dimethylbenzene ring is stabilized by a face-on-edge π–π interaction with Trp358 of the second monomer and hydrophobic interactions with Met24 on the *re* side. Further close contacts between protein and cofactor are found for the $C_{(4a)}$ and $C_{(10a)}$ atoms of the isoalloxazine ring, which are only 3.06 Å away from the carbonyl oxygen of Pro23. The oxygen atom is positioned exactly in the middle below the bond between $C_{(4a)}$ and $C_{(10a)}$ on the *re* side and it is substantially closer to the two carbon atoms than the van der Waals radii would suggest. The isoalloxazine ring is distinctly non-planar. This deviation from planarity might be, in part, a consequence of a partial photoreduction of the ring. However, given the short distance between Cys25 Sγ and $O_{(4)}$ and the observed non-planarity of the flavin of crystals exposed to a lose dose of radiation,[6] it appears to be unlikely that the isoalloxazine ring is planar in the oxidized state, as that would lead to a strong overlap of the van der Waals radii of the two atoms if Cys25 is kept fixed.

The observed overlap of the van der Waals radii between the carbonyl oxygen of Pro23 and the $C_{(4a)}$ and $C_{(10a)}$ carbon on the *re* side of the flavin with the short S...$O_{(4)}$ distance in the *si* side indicated that the protein environment exerts a considerable strain on the isoalloxazine ring and that Cys25 is part of a protein clamp for the cofactor. The active site pocket is not empty and a sulfate molecule, a constituent of the crystallization solution, is bound above the *si* side of the isoalloxazine ring.

Active site structure with bound coumarin

The crystal structure of true Michaelis complexes between enzyme and substrates are difficult to achieve due to their inherent reactivity. As a substitute, we determined the structure of oxidized XenA in complex with coumarin to infer the relative orientation of substrate and cofactor. The structure of XenA-wt with coumarin bound was refined at a resolution of 1.10 Å (Fig. 6b). The statistics of the dataset revealed that the overall quality is not as good as that of the other datasets and we believe the lower data quality is the reason why the *R* value for the model is not as low as expected for a structure at this resolution (Table 4). There is no indication of structural change occurring upon coumarin binding, and the Cα atoms of the substrate-bound and substrate-free structures can be superimposed with an rms deviation of 0.09 Å. Coumarin is bound nearly coplanar above the isoalloxazine ring,
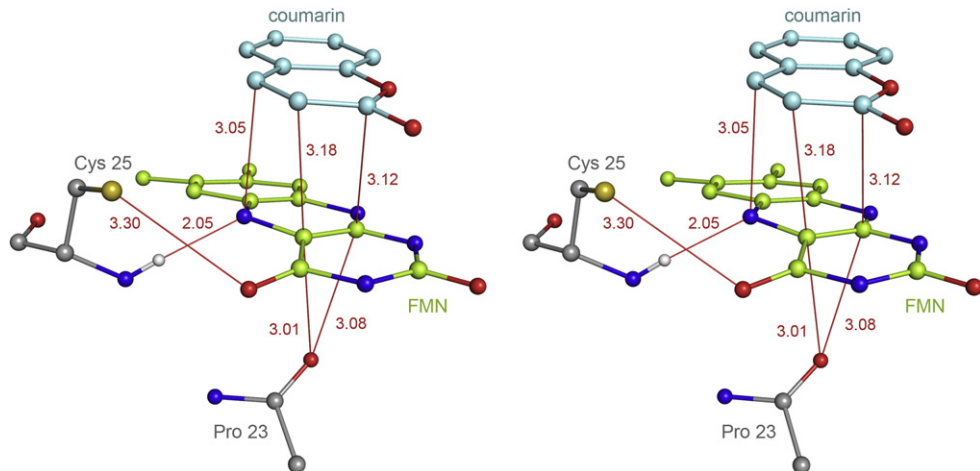
Fig. 7. Compression of the flavin in the coumarin complex. Stereoscopic view of the active site of XenA-wt in complex with coumarin. All residues are shown in stick and ball representation. Carbon atoms of the amino acid side chains, gray; carbon atoms of FMN, green; carbon atoms of coumarin, light blue; oxygen atoms, red; nitrogen atoms, blue; sulfur atoms, yellow; and hydrogen atoms, white. Distances between atoms are given (in ångström units) and are displayed as red lines.

consistent with π–π interactions between both molecules (Fig. 6b). The carbonyl oxygen of coumarin is within hydrogen bonding distance to His178 (2.90 Å) and His181 (2.84 Å). His181 is also in hydrogen bonding distance to $O_{(1)}$ of coumarin. The closest contact between coumarin and the isoalloxazine ring is between the β carbon of coumarin and $N_{(5)}$ of FMN. The distance of 3.05 Å is shorter than expected from the van der Waals radii (van der Waals distance 3.2 Å), indicating that the enamine moiety of FMN is sterically compressed from both sides in the substrate-bound form (Fig. 7). While the carbonyl oxygen of Pro23 is close to $C_{(4a)}$ and $C_{(10a)}$ on the *re* side of the flavin, coumarin presses on the *si* side of the isoalloxazine ring. The short distance between $N_{(5)}$ and the β carbon of coumarin is especially notable, as the observed compression could facilitate the electron/hydride transfer between the atoms. A role of sterical compression to enhance catalysis has been suggested.[25–27] The α carbon of coumarin is 3.28 Å away from the potential catalytic proton donor Tyr183 (Fig. 6b). The shortest distance between the γ-sulfhydryl group of Cys25 and the coumarin ring is 4.0 Å and there is no indication of a direct interaction between coumarin and Cys25, nor does the conformation of Cys25 change upon coumarin binding. The principal arrangement of the enzyme-bound flavin and the substrate is similar to the average geometry found in a number of flavoenzymes,[28] in which the carbon atom of the substrate to be activated by electron/hydride transfer from the $N_{(5)}$ atom is, on average, 3.5 Å away (here 3.05 Å) and makes an angle with the $N_{(5)}$-$N_{(10)}$ atoms of 96–117° (here 98°).

Structures of XenA-C25A and XenA-C25S alone and in complex with coumarin

The structures of XenA-C25A and XenA-C25S were solved at resolutions of 1.20 Å and 1.80 Å,

respectively (Fig. 8a and b). The overall structures of both mutant enzymes reveal no significant changes of the protein conformation and confirm the exchange of Cys25 with Ser and Ala. All other residues in the active site are unaltered and superimpose exactly with the structure of XenA-wt. The replacement of cysteine by serine brings a stronger hydrogen bond donor/acceptor into the active site, while the replacement of cysteine by alanine creates a small void and both can perturb the local water structure. The high resolution of the two variants clearly defines the location of individual ordered water molecules, which are superimposable with XenA-wt in both cases, indicating that the mutations have no effect on the water structure of the active site.

The atomic resolution structures of XenA-wt and XenA-C25A provide a better description of the bending of the isoalloxazine ring (Fig. 9a). In comparison to the subatomic resolution structure of PETN reductase[10] and the 1.3 Å resolution structure of YqjM,[12] the isoalloxazine rings of XenA-wt and XenA-C25A are more domed and point with the ends towards its *re* side. Furthermore, the $C_{(4)}$–$O_{(4)}$ carbonyl group of the pyrimidine rings is moved further out of the ring plane towards the *re* side of the FMN (Fig. 9b). XenA-C25S did not show these distortions. Here, the isoalloxazine as well as the pyrimidine ring are more planar, allowing the hydroxyl group of serine and $O_{(4)}$ of FMN to be within the typical hydrogen bond distance of 2.8 Å. However, the structures of the C25S variant have been determined at lower resolution and the interpretations of the distortion of the isoalloxazine-ring are less reliable. The position of coumarin in the active site pocket (Fig. 8c and d), as well as the interactions between protein and coumarin, are indistinguishable for XenA-wt, XenA-C25A and XenA-C25S (Fig. 9b).

The structures of the two XenA variants show that the effects of the cysteine exchanges are only local
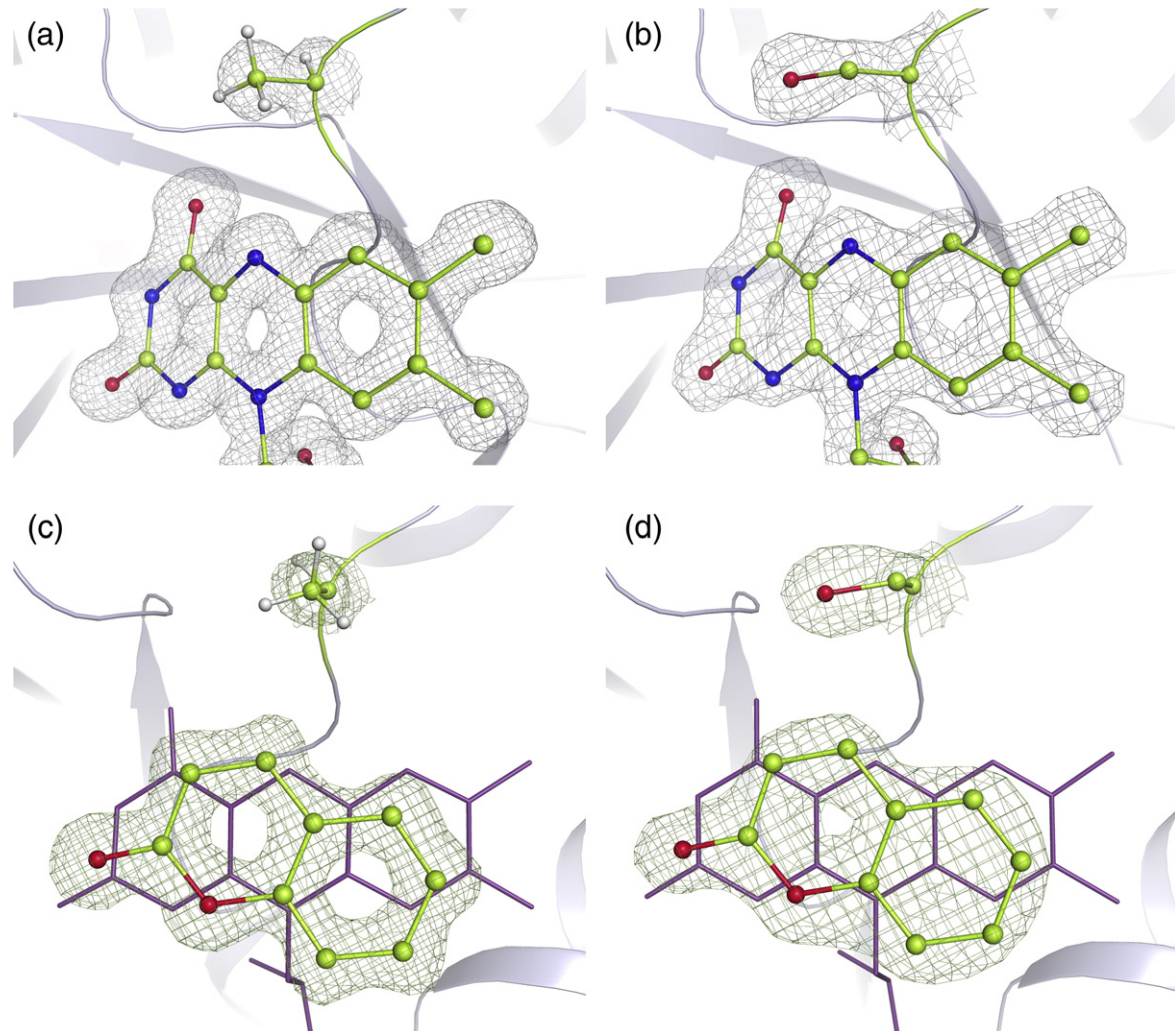
Fig. 8. XenA variants. (a) Active site of XenA-C25A. The $2F_o - F_c$ map contoured at 1.0σ is shown in gray mesh representation. (b) Active site of XenA-C25S. The $2F_o - F_c$ map contoured at 1.5σ is shown in gray mesh representation. All residues are displayed in stick and ball mode. Carbon atoms, green; nitrogen atoms, blue; oxygen atoms, red; and hydrogen atoms, white. (c) Active site of XenA-C25A in complex with coumarin. The $2F_o - F_c$ map of coumarin and Ala25 contoured at 1.5σ is shown in green mesh representation. (d) Active site of XenA-C25S in complex with coumarin. The $2F_o - F_c$ map of coumarin and Ser25 contoured at 1.5σ is shown in green mesh representation. FMN (violet) is displayed in stick mode. Coumarin and residues 25 are displayed in stick and ball mode. Carbon atoms, green; oxygen atoms, red; and hydrogen atoms, white.

and do not result in any further change of the active site. The conserved position of the substrate confirms that Cys25 is not important for the placement of the substrate in the active site, nor does it change the conformation of residues relevant for substrate binding. We can thus be confident that the observed changes of the spectra, reduction potential and reactivity of XenA, originate from the exchange of the γ-sulfhydryl group of Cys25 and not from further structural perturbations, which are frequently caused by mutations.

Conclusions

Its central place within the active site just above the $N_{(5)}$ atom of the isoalloxazine ring (Fig. 6a) suggested that Cys25 could be involved in the

interaction with and conversion of the substrates. To understand how Cys25 contributes to fine-tune the chemistry of the flavin cofactor, we investigated its role in the structure, reduction potential, substrate binding and reactivity of XenA.

The γ-sulfhydryl group of Cys25 is close to the bound substrate in the crystal structure of oxidized XenA (Fig. 6b) and only small rearrangements within the active site would be necessary for a direct interaction. As we have no direct insight into the structure of the true Michaelis complex, we determined the dissociation constants of the substrate – XenA variant complexes and compared it to XenA-wt. Both Cys25 variants of XenA have a slightly decreased affinity for the substrates, which argues that Cys25 contributes to substrate binding. However, changes of two to sevenfold in the dissociation constants are less than expected for the loss of a
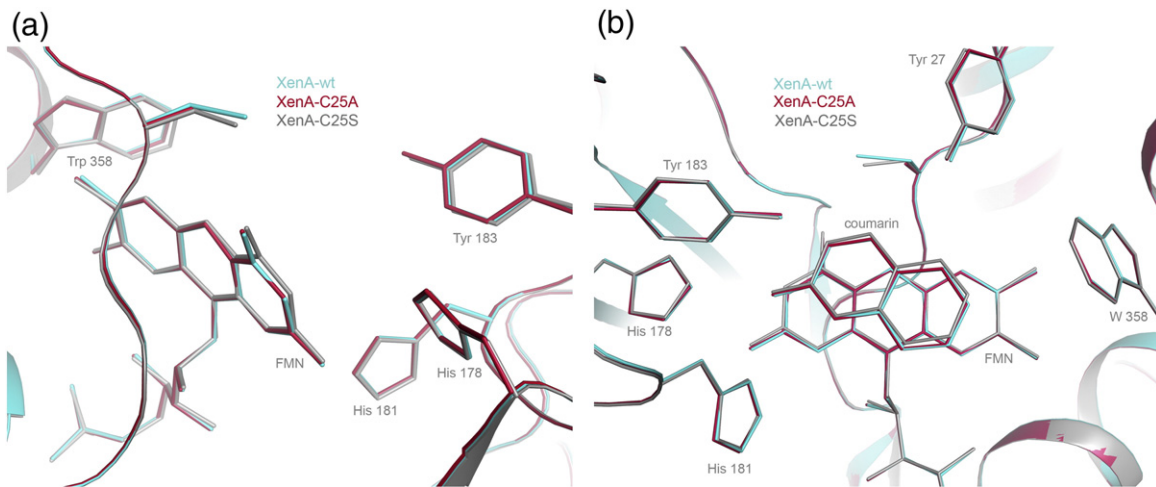
Fig. 9. Comparisons. (a) View of the active site of the superimposition of XenA-wt (blue), XenA-C25A (red) and C25S (grey). (b) View of coumarin bound to the active site of the superimposition of: XenA-wt, blue; XenA-C25A, red; and C25S, gray. All residues are shown in stick mode.

direct interaction between enzyme and substrate and are in agreement with an indirect role of Cys25 in substrate binding. This indirect role could be the modulation of the electronic structure of the isoalloxazine ring by restraining its planarity, which is in agreement with the short distances found in the active site (Fig. 7) and the bent conformation of the isoalloxazine ring.

In the structure of YqjM, Cys26 was shown to have two conformations in the absence of bound ligands: in one conformation the γ-sulfhydryl group is closer to $O_{(4)}$ and in one it is within hydrogen bonding distance to $N_{(5)}$.[12] The conformational change was not dependent on the oxidation state of YqjM and the modeled structures of oxidized and reduced YqjM are virtually identical.[12] To determine whether a conformational change of Cys25 contributes to the reactivity of XenA, we compared the reactivity of XenA-wt with XenA-C25A. The C25A variant is only twofold slower in the RHR and twofold faster in the OHR than XenA-wt, indicating that if there is a conformational change of Cys25 during the reaction, it does not contribute to catalysis and even the loss of the γ-sulfhydryl group does not compromise the reactivity of XenA.

Cysteine residues typically have pK_a values around 8.3[29] and can act as catalytic acids. As the γ-sulfhydryl group of Cys25 is close to the Cβ=Cγ double bond of coumarin to which in the course of the reaction two protons and two electrons are transferred, we speculated that Cys25 might act as proton donor in the reaction. However, our analysis showed that: (I) the activity of XenA varies weakly with pH and the same profile is observed for XenA-wt, XenA-C25A and XenA-C25S; (II.) the loss of activity upon replacing Cys25 with alanine is modest in both half reactions; and (III.) the calculated protonation probability reveals it to be protonated over a wide pH range. We therefore conclude that Cys25 does not act as a proton donor in the reaction and it is most likely protonated during the complete course of the reaction.

On the basis of our experiments, we conclude that Cys25 is not essential for the reactivity, but modulates substrate binding and the reduction potential of XenA. Modulation of the reduction potential is of physiological relevance in this class of enzymes. While it is likely that in the reductive half-reaction reduced nicotinamide is used as a substrate, a wide range of substrates might be converted in the oxidative half-reaction. Depending on the substrates, either the oxidative or the reductive half-reaction can become rate limiting. We used Eq. (8), which is valid for ping pong mechanisms, to calculate the influence of each individual rate constant on the turnover number (k_{cat}) under substrate-saturated conditions. With coumarin as a substrate, the limiting reaction is always the OHR and thus the highest turnover can be achieved by XenA-C25A. With 2-cyclohexenone as substrate, either the OHR or the RHR can be rate limiting, depending on the XenA variant and the substrate in the RHR. While the RHR is rate limiting for XenA-wt and XenA-C25A with NADH as reducing substrate, the rate of both half-reactions are balanced in XenA-C25S and, indeed, XenA-C25S can achieve the highest turnover for this substrate. With NADPH as reducing substrate, both XenA-wt and XenA-C25A have a high turnover under which none of the two half-reactions is limiting, while XenA-C25S is severely limited by a slow OHR and has a lower turnover number than the other variants.

Several copies of sequences homologous to XenA are found in the genome of *P. putida*[4] and three of the copies have a cysteine residue, two have a threonine residue and one has an alanine residue in place of Cys25. A common characteristic for many enzymes of the OYE family is a wide range of possible substrates in the OHR. It is tempting to speculate that the different active site residues at the position of Cys25 in XenA adapt the enzymes for different classes of substrates, such that none of the two half-reactions severely limits

the rate of the overall reaction. This would be a further indication that the different xenobiotic reductases in *P. putida* could participate in the several pathways along which aromatic/heteroaromatic substrates are degraded and helps us to understand how such a wide range of substrates can be converted by a single microorganism.[30]

Materials and Methods

Chemicals and enzymes

All materials were purchased from Fluka, AppliChem, Roth and Otto Nordwald. Microbial media were prepared as described.[31] 5-Deaza-10-methyl-3-sulfopropyl-isoalloxazine was a gift from Peter M.H. Kroneck (University of Konstanz, Germany).

Mutagenesis, protein expression and purification

The mutation of Cys25 was done with the QuickChange mutagenesis protocol from Stratagene. The PCR primers were: for C25A

5′-GCCATTCCGCCGA-TG*G*CCCAATACATGGCC-GAAG-3′
5′-CTTCGGCCATGTATTG*G*GCCATACA-TGGC-CGAAG-3′

and for C25S

5′-GCCATTCCGCCGATG*A*GCCAATACATGGCC-GAA-GAC-3′
5′-GTCTTCGGCCATGTATTG*G*GCTCATCGGCG-GAATGGC-3′

pET_XenA was used as the template as described.[6] The double-stranded wild type DNA was removed by digestion with the restriction enzyme DpnI. The mutated genes *xenA*_C25A and *xenA*_C25S were sequenced by Eurofins MWG Operon. The mutated plasmids were transformed into the expression strain *Escherichia coli* Rosetta(DE3)pLysS and the genes were expressed as the wild type gene *xenA*.[6,13] Both enzyme variants XenA-C25A and XenA-C25S were purified as described for XenA-wt, including a reconstitution with FMN before the final size-exclusion chromatography step.[6,13] The yield from 4 L of cell culture was 190 mg of the XenA-C25A variant and 180 mg of the XenA-C25S variant, both with purity exceeding 95% as estimated by SDS-PAGE (data not shown). Activity assays were done in 50 mM Tris buffer (pH 8.0), 150 µM NADPH, 300 µM 2-cyclohexenone at 25 °C. The reaction mixture was flushed with nitrogen gas in a quartz cuvette sealed by a screw-cap with a rubber septum. The reaction was started by using a Hamilton syringe to add 5 µL of the enzymes (2 mg mL^{-1}) to 995 µL of reaction buffer. The signal was followed for 2 min at a wavelength of 340 nm. One activity unit (U) is defined as the oxidation of 1 µmol of NADPH per minute. Flavin contents were determined by treatment with SDS as described.[32] Extinction coefficients of protein-bound FMN were calculated for both variants, for which the protein was denatured by the addition of 0.05 volume of 10% (w/v) SDS. After incubation for 10 min at room temperature, a spectrum was recorded to follow the release of FMN from the protein. The extinction coefficient of the enzyme-bound flavin was calculated from the known extinction coefficient of free FMN (12.200 M^{-1} cm^{-1}).

Ligand binding studies

Oxidized XenA (XenA-wt, XenA-C25A, XenA-C25S) at a concentration of 30 µM in 50 mM Tris buffer (pH 8.0) in a 1 cm quartz cuvette at 25 °C was titrated by addition of small amounts of a coumarin stock solution. Absorption spectra from 200 nm to 800 nm were recorded using an Agilent 8453 UV-visible spectrophotometer. Changes of absorption at 464 nm were plotted against ligand concentration. Dissociation constants (K_d) for the enzyme–ligand complex were determined by non-linear regression analysis of the data with GraFit-5 (Version 5.0, Erithacus Software Limited, UK) using:

$$\Delta A = \frac{\Delta A_{\max}}{2nE}\left[\left(L + nE + K_d\right) - \left(\left(L + nE + K_d\right)^2 - \left(4LnE\right)\right)^{0.5}\right] \quad (1)$$

where $\Delta A_{\max}$ is the maximum absorbance change at 464 nm, L is the total ligand concentration, E is the total enzyme concentration and n is the number of ligand-binding sites.

Photoreduction and determination of reduction potentials

Photoreduction of XenA variants was done in a glass tonometer with a cuvette side arm as described.[33] We used the potassium salt of 5-deaza-10-methyl-3-sulfopropyl-isoalloxazine as the photoreductant in catalytic amounts. The reaction mixture contained final concentrations of 15 mM EDTA, 30 µM enzyme and 1 µM phenosafranine as electron mediator in 100 mM Tris buffer (pH 8.0) and was made anoxic by repeated evacuation and flushing with nitrogen gas. Solutions of the deazaflavin derivative and EDTA were stored in the side arm cuvette during this process and mixed with the enzyme directly before the light irradiation steps were performed with a 100 W lamp from a slide projector (Agfa, Opticus 100). Each illumination step lasted 10 s and absorption spectra were recorded for 3 min after the illumination. To check for reversibility of the reduction, air was allowed to enter the tonometer and cuvette after the photoreduction of the enzyme was complete and a UV/vis spectrum of the reoxidized sample was recorded. The determination of the reduction potential was done as described.[34] We used phenosafranine ($E^0_{m,D} = -252$ mV[35]) with XenA-C25A and anthraquinone-2,6-disulfonate ($E^0_{m,D} = -184$ mV[36]) with XenA-C25S as reference dyes. The absorbance values and corresponding extinction coefficients used to calculate the concentrations of oxidized enzyme and dye are given in Table 3. Concentrations of oxidized enzyme (E_{ox}) and oxidized dye (Dye_{ox}) were calculated with Eqs (2) and (3).

$$A^{456} = \varepsilon_{456}^{Eox}c^{Eox} + \varepsilon_{456}^{Dox}c^{Dox} + \varepsilon_{456}^{Ered}\left(c^{Etot} - c^{Eox}\right) + \varepsilon_{456}^{Dred}\left(c^{Dtot} - c^{Dox}\right) \quad (2)$$

$$A^{521} = \varepsilon_{521}^{Eox}c^{Eox} + \varepsilon_{521}^{Dox} + c^{Dox} + \varepsilon_{521}^{Ered}\left(c^{Etot} - c^{Eox}\right) + \varepsilon_{521}^{Dred}\left(c^{Dtot} - c^{Dox}\right) \quad (3)$$

Table 3. Absorbance values and molar extinction coefficients

	Absorbance value (nm)	Molar extinction coefficient (M^{-1} cm^{-1}) oxidized form	Molar extinction coefficient (M^{-1} cm^{-1}) reduced form
C25A	456	12.7×10^3	0.6×10^3
	521	2.1×10^3	0.6×10^3
Phenosafranine	456	11.2×10^3	0.3×10^3
	521	44.7×10^3	0.3×10^3
C25S	460	11.4×10^3	0.5×10^3
	328	4.7×10^3	4.7×10^3
Anthraquinone-2, 6-disulfonate	460	0	1.2×10^3
	328	5.7×10^3	0

Equations (2) and (3) are displayed for XenA-C25A and the reference dye phenosafranine. For XenA-C25S and the reference dye anthraquinone-2,6-disulfonate, the listed (Table 3) absorbance values and corresponding molar extinction coefficients were used respectively. The reduction potential of XenA ($E^0_{m,E}$) was determined from the difference (ΔE^0) in the reduction potentials of enzyme and dye (see Eq. (4)).

$$E^0_{m,E} = E^0_{m,D} + \Delta E \qquad (4)$$

Stopped-flow spectrophotometry

Reductive half-reaction

The reductive half reactions of the mutant enzymes with NADH and NADPH were measured in 50 mM Tris buffer (pH 8.0) under anoxic conditions at 20 °C as described.[13] The reactions were monitored at 464 nm with an Applied Photophysics SX-20MV kinetic spectrophotometer with a 1 cm observation pathlength cuvette. Enzyme at a concentration of 10 μM was mixed with NAD(P)H at concentrations of 50 – 11,000 μM. The measurement was done at least five times for each concentration of substrate.

Oxidative half-reaction

2-Cyclohexenone and coumarin were used as oxidative substrates with concentrations of 50 – 5000 μM. To achieve complete reduction the enzymes were reduced by titration with appropriate amounts of NADH in a glass tonometer with a cuvette side arm. The observed kinetic transients at 464 nm for reductive and oxidative half-reactions were fit to single-exponential equations using Pro-Data software (Applied Photophysics, UK). The rate constants (k_{obs}) were plotted against the respective substrate concentrations. The reductive half-reaction was modeled as:

$$A + B \overset{K_d}{\rightleftharpoons} C \overset{K_{red}}{\to} D \qquad (5)$$

where A is the enzyme in the oxidized state, B is the reductive substrate – NAD(P)H, C is the enzyme$_{ox}$ – substrate charge-transfer complex and D is the enzyme containing the two-electron reduced state of FMN and bound NAD(P)$^+$. The oxidative half-reaction was modeled as:

$$E + F \overset{K_d}{\rightleftharpoons} G \overset{K_{ox}}{\to} H \qquad (6)$$

where E is the enzyme in the reduced state, F is the oxidative substrate – 2-cyclohexenone, coumarin, G is the enzyme$_{red}$ – substrate charge-transfer complex and H is the oxidized enzyme with bound product (2-cyclohexanon, chroman-2-one).

The hyperbolic plots were fit to Eq. (7) using the program GraFit-5 (Version 5.0, Erithacus Software Limited, UK) to obtain the limit of the reaction rate $k_{red/ox}$ at high substrate concentrations [S] and the dissociation constant K_d:[37]

$$k_{obs} = k_X[S] / (K_d + [S]) \qquad (7)$$

Equation (8) was used to relate the limiting rate constants to the steady-state catalytic constants:

$$k_{cat} = \frac{k_{red}k_{ox}}{(k_{red} + k_{ox})} \qquad (8)$$

Calculation of protonation probabilities

The protonation of Cys25 and all other titratable residues in the protein were calculated using a continuum electrostatic approach combined with a Monte Carlo (MC) titration.[38,39] The Poisson–Boltzmann equation was solved by a finite-difference method using the MEAD program suite.[40] All aspartate, histidine, glutamate, lysine, arginine, and tyrosine residues were considered as protonatable sites. Atomic partial charges for standard amino acid groups were taken from the CHARMM27 parameter set.[41] The pK_a values of the model compounds were taken from the literature.[39,42] The partial charges of FMN were obtained by fitting the electrostatic potentials derived from density functional calculations using ADF.[43] The dielectric constant of the protein was set to 4, and that of the solvent was set to 80. The ionic strength was set to 0.1 M. The thickness of the ion exclusion layer was set to 2.0 Å. Continuum electrostatics calculations were performed using the focusing technique[44] in two steps using a grid with 151^3 points. The outer grid had a grid spacing of 1.0 Å and was placed at the geometric center of the protein. The inner grid had a grid spacing of 0.25 Å and was centered at the titratable site. A similar procedure was used for the model compound, with all grids centered at the titratable site.

The protonation probabilities were calculated for pH values of 0 to 14 in steps of 0.2 using Metropolis MC. The temperature was set to 300 K. At each pH value, a randomly chosen initial state vector was equilibrated with 200 MC scans, where one MC scan comprises as many MC moves as there are titratable sites in the protein. Subsequently, 10,000 MC scans were performed to determine the protonation probability of each site.

Data collection and structure refinement

Crystals of the XenA mutants were grown as described for the wild type XenA.[6] The crystals were cross-linked for 1 h in a harvesting solution containing 100 mM Hepes (pH 7.5), 2.4 M ammonium sulfate and 0.002% (v/v) glutaraldehyde. To soak crystals with substrate, they were further incubated for 1 h in harvesting buffer containing approximately 5 mM coumarin. Crystals were shock-frozen in harvesting buffer containing 20% (v/v) 2R,3R-butanediol and stored in liquid nitrogen. The crystals belong to the space group I222 and the cell dimensions are given in Table 4. X-ray

Table 4. Crystallographic data and refinement statistics

	XenA-wt		XenA-C25A		XenA-C25S	
	Native	Coumarin	Native	Coumarin	Native	Coumarin
A. *Data collection*						
Spacegroup cell constants *a* (Å)	*I*222	*I*222	*I*222	*I*222	*I*222	*I*222
a (Å)	57.89	57.99	58.06	57.77	57.99	58.33
b (Å)	83.41	83.37	83.27	83.62	83.61	83.56
c (Å)	156.72	156.67	157.63	157.17	157.24	156.72
Wavelength (Å)	0.9184	0.9184	0.9184	0.9184	0.9184	0.9184
Total reflections	750,322	555,063	405,950	338,576	125,475	129,228
Unique reflections	180,933	147,817	110,585	96,594	64,188	36,914
Resolution (Å)	30-1.02	30-1.10	30-1.20	30-1.28	30-1.80	30-1.75
	(1.06–1.03)	(1.13–1.10)	(1.23–1.20)	(1.31–1.28)	(1.85–1.80)	(1.80–1.75)
R_s[a] (%)	5.7 (58.7)	9.3 (43.0)	4.9 (46.7)	6.2 (54.9)	4.7 (31.4)	6.5 (44.8)
Completeness (%)	97.1 (86.8)	96.4 (94.8)	92.8 (86.4)	98.5 (88.2)	93.7 (80.1)	94.5 (83.3)
$I / \sigma I$	13.11 (2.16)	8.82 (2.54)	14.22 (2.76)	12.75 (2.31)	12.54 (2.26)	14.05 (2.64)
B. *Refinement*						
R_{work} / R_{free}(%)[b]	12.9 / 14.8	19.0 / 21.6	12.5 / 14.9	13.4 / 16.4	18.2 / 23.0	18.0 / 21.2
rms deviation from ideality						
Bond length (Å)	0.010	0.012	0.011	0.011	0.006	0.006
Bond angle (°)	1.42	1.47	1.39	1.41	0.96	0.98
No. molecules						
Atoms/ASU[c]	3600	3565	3623	3689	3445	3469
Ligand/ion	10	12	10	11	9	11
Water	587	561	143	622	599	596
Estimated coordinate errors based on						
R	0.021	0.039	0.034	0.044	0.147	0.131
R_{free}	0.023	0.039	0.034	0.042	0.141	0.122

Values in parentheses are for the highest resolution shell.

The Friedel mates of the native data set of XenA-C25S were treated as independent reflections to allow the use of the anomalous scattering to detect the presence/absence of sulfur.

[a] $R_s = \Sigma_h \Sigma_i \mid I_i(h) - <I(h)> \mid / \Sigma_h \Sigma_i I_i(h)$ where *i* are the independent observations of reflection *h*.

[b] R_{free} was calculated from 5% of the data, which were removed at random before the refinement was carried out.

[c] Refined atoms in the asymmetric unit.

diffraction data were collected at the beam line BL14.2 (BESSY, Berlin, Germany). All diffraction data were processed and scaled using the XDS package.[45] The structures were solved using difference Fourier techniques with the isomorphous structure of XenA$_{ox}$ determined at 1.5 Å.[6] Subsequent rounds of model building and refinement were performed using the programs Coot[46] and PHENIX.[47] The structures at true atomic resolution (d_{min} <1.2 Å) were refined as models with riding hydrogen atoms and included anisotropic *B*-factors.

Protein Data Bank accession numbers

The coordinates and structure factor amplitudes have been deposited in the RCSB Protein Data Bank with ID codes *3L5L* (XenA-wt), *3L5M* (XenA-wt with coumarin), *3L67* (XenA-C25S), *3L68* (XenA-C25S with coumarin), *3L65* (XenA-C25A) and *3L66* (XenA-C25A with coumarin).

Supplementary Data

Supplementary data associated with this article can be found, in the online version, at doi:10.1016/j.jmb.2010.02.044

References

1. Williams, R. E. & Bruce, N. C. (2002). 'New uses for an old enzyme'–the old yellow enzyme family of flavoenzymes. *Microbiology*, **148**, 1607–1614.
2. Brige, A., Van den Hemel, D., Carpentier, W., De Smet, L. & Van Beeumen, J. J. (2006). Comparative characterization and expression analysis of the four old yellow enzyme homologues from *Shewanella oneidensis* indicate differences in physiological function. *Biochem. J.* **394**, 335–344.
3. Niino, Y. S., Chakraborty, S., Brown, B. J. & Massey, V. (1995). A new old yellow enzyme of *Saccharomyces cerevisiae*. *J. Biol. Chem.* **270**, 1983–1991.
4. van Dillewijn, P., Wittich, R. M., Caballero, A. &

Ramos, J. L. (2008). Subfunctionality of hydride transferases of the old yellow enzyme family of flavoproteins of *Pseudomonas putida*. *Appl. Environ. Microbiol.* **74**, 6703–6708.

5. Fetzner, S., Tshisuaka, B., Lingens, F., Kappl, R. & Huttermann, J. (1998). Bacterial degradation of quinoline and derivatives – pathways and their biocatalysts. *Angew. Chem. Int. Ed.* **37**, 577–597.

6. Griese, J. J., P Jakob, R., Schwarzinger, S. & Dobbek, H. (2006). Xenobiotic reductase A in the degradation of quinoline by *Pseudomonas putida* 86: physiological function, structure and mechanism of 8-hydroxycoumarin reduction. *J. Mol. Biol.* **361**, 140–152.

7. Fox, K. M. & Karplus, P. A. (1994). Old yellow enzyme at 2 Å resolution: overall structure, ligand binding, and comparison with related flavoproteins. *Structure*, **2**, 1089–1105.

8. Barna, T., Messiha, H. L., Petosa, C., Bruce, N. C., Scrutton, N. S. & Moody, P. C. (2002). Crystal structure of bacterial morphinone reductase and properties of the C191A mutant enzyme. *J. Biol. Chem.* **277**, 30976–30983.

9. Barna, T. M., Khan, H., Bruce, N. C., Barsukov, I., Scrutton, N. S. & Moody, P. C. (2001). Crystal structure of pentaerythritol tetranitrate reductase: "flipped" binding geometries for steroid substrates in different redox states of the enzyme. *J. Mol. Biol.* **310**, 433–447.

10. Khan, H., Barna, T., Harris, R. J., Bruce, N. C., Barsukov, I., Munro, A. W. *et al.* (2004). Atomic resolution structures and solution behavior of enzyme-substrate complexes of *Enterobacter cloacae* PB2 pentaerythritol tetranitrate reductase. Multiple conformational states and implications for the mechanism of nitroaromatic explosive degradation. *J. Biol. Chem.* **279**, 30563–30572.

11. van den Hemel, D., Brige, A., Savvides, S. N. & Van Beeumen, J. (2006). Ligand-induced conformational changes in the capping subdomain of a bacterial old yellow enzyme homologue and conserved sequence fingerprints provide new insights into substrate binding. *J. Biol. Chem.* **281**, 28152–28161.

12. Kitzing, K., Fitzpatrick, T. B., Wilken, C., Sawa, J., Bourenkov, G. P., Macheroux, P. & Clausen, T. (2005). The 1.3 Å crystal structure of the flavoprotein YqjM reveals a novel class of old yellow enzymes. *J. Biol. Chem.* **280**, 27904–27913.

13. Spiegelhauer, O., Dickert, F., Mende, S., Niks, D., Hille, R., Ullmann, M. & Dobbek, H. (2009). Kinetic characterization of xenobiotic reductase A from *Pseudomonas putida* 86. *Biochemistry*, **48**, 11412–11420.

14. Khan, H., Harris, R. J., Barna, T., Craig, D. H., Bruce, N. C., Munro, A. W. *et al.* (2002). Kinetic and structural basis of reactivity of pentaerythritol tetranitrate reductase with NADPH, 2-cyclohexenone, nitroesters, and nitroaromatic explosives. *J. Biol. Chem.* **277**, 21906–21912.

15. Messiha, H. L., Bruce, N. C., Sattelle, B. M., Sutcliffe, M. J., Munro, A. W. & Scrutton, N. S. (2005). Role of active site residues and solvent in proton transfer and the modulation of flavin reduction potential in bacterial morphinone reductase. *J. Biol. Chem.* **280**, 27103–27110.

16. Stewart, R. C. & Massey, V. (1985). Potentiometric studies of native and flavin-substituted old yellow enzyme. *J. Biol. Chem.* **260**, 13639–13647.

17. Xu, D., Kohli, R. M. & Massey, V. (1999). The role of threonine 37 in flavin reactivity of the old yellow enzyme. *Proc. Natl Acad. Sci. USA*, **96**, 3556–3561.

18. Bougioukou, D. J., Kille, S., Taglieber, A. & Reetz, M. T.

(2009). Directed evolution of an enantioselective enoate-reductase: testing the utility of iterative saturation mutagenesis. *Adv. Synth. Catal.* **351**, 3287–3305.

19. Abramovitz, A. S. & Massey, V. (1976). Interaction of phenols with old yellow enzyme. Physical evidence for charge-transfer complexes. *J. Biol. Chem.* **251**, 5327–5336.

20. Craig, D. H., Moody, P. C., Bruce, N. C. & Scrutton, N. S. (1998). Reductive and oxidative half-reactions of morphinone reductase from *Pseudomonas putida* M10: a kinetic and thermodynamic analysis. *Biochemistry*, **37**, 7598–7607.

21. Fitzpatrick, T. B., Amrhein, N. & Macheroux, P. (2003). Characterization of YqjM, an old yellow enzyme homolog from *Bacillus subtilis* involved in the oxidative stress response. *J. Biol. Chem.* **278**, 19891–19897.

22. Berkholz, D. S., Faber, H. R., Savvides, S. N. & Karplus, P. A. (2008). Catalytic cycle of human glutathione reductase near 1 Å resolution. *J. Mol. Biol.* **382**, 371–384.

23. Breinlinger, E. C., Keenan, C. J. & Rotello, V. M. (1998). Modulation of flavin recognition and redox properties through donor atom-π interactions. *J. Am. Chem. Soc.* **120**, 8606–8609.

24. Ghisla, S. & Massey, V. (1986). New flavins for old: artificial flavins as active site probes of flavoproteins. *Biochem. J.* **239**, 1–12.

25. Bruice, T. C. & Benkovic, S. J. (2000). Chemical basis for enzyme catalysis. *Biochemistry*, **39**, 6267–6274.

26. Bruice, T. C. & Pandit, U. K. (1960). Intramolecular models depicting the kinetic importance of "fit" in enzymatic catalysis. *Proc. Natl Acad. Sci. USA*, **46**, 402–404.

27. Jencks, W. P. (1963). Mechanism of enzyme action. *Annu. Rev. Biochem.* **32**, 639–676.

28. Fraaije, M. W. & Mattevi, A. (2000). Flavoenzymes: diverse catalysts with recurrent features. *Trends Biochem. Sci.* **25**, 126–132.

29. Wessjohann, L. A., Schneider, A., Abbas, M. & Brandt, W. (2007). Selenium in chemistry and biochemistry in comparison to sulfur. *Biol. Chem.* **388**, 997–1006.

30. Jimenez, J. I., Minambres, B., Garcia, J. L. & Diaz, E. (2002). Genomic analysis of the aromatic catabolic pathways from *Pseudomonas putida* KT2440. *Environ. Microbiol.* **4**, 824–841.

31. Sambrook, J. & Russel, D. (2001). *Molecular Cloning: A Laboratory Manual.* Cold Spring Harbor Laboratory Press Cold Spring Harbor, NY.

32. Aliverti, A., Curti, B. & Vanoni, M. A. (1999). Identifying and quantitating FAD and FMN in simple and in iron-sulfur-containing flavoproteins. *Methods Mol. Biol.* **131**, 9–23.

33. Massey, V., Stankovich, M. & Hemmerich, P. (1978). Light-mediated reduction of flavoproteins with flavins as catalysts. *Biochemistry*, **17**, 1–8.

34. Sucharitakul, J., Chaiyen, P., Entsch, B. & Ballou, D. P. (2005). The reductase of p-hydroxyphenylacetate 3-hydroxylase from *Acinetobacter baumannii* requires p-hydroxyphenylacetate for effective catalysis. *Biochemistry*, **44**, 10434–10442.

35. Loach, P. A. (1973). Oxidation-reduction potentials: absorbance bands and molar absorbance of compounds used in biochemical studies. In *Handbook of Biochemistry Selected Data for Molecular Biology* (Sorber, H. A., ed.), pp. J33–J40, CRC Press, Cleveland, OH.

36. Efimov, I. & McIntire, W. S. (2004). A study of the spectral and redox properties and covalent flavinylation of the flavoprotein component of p-cresol methylhydroxylase reconstituted with FAD analogues. *Biochemistry*, **43**, 10532–10546.

37. Strickland, S., Palmer, G. & Massey, V. (1975). Determination of dissociation constants and specific rate constants of enzyme-substrate (or protein-ligand) interactions from rapid reaction kinetic data. *J. Biol. Chem.* **250**, 4048–4052.

38. Essigke, T. (2008). *A continuum electrostatic approach for calculating the binding energetics of multiple ligans.* Dissertation, Universität Bayreuth.

39. Ullmann, G. M. & Knapp, E. W. (1999). Electrostatic models for computing protonation and redox equilibria in proteins. *Eur. Biophys. J.* **28**, 533–551.

40. Bashford, D. & Gerwert, K. (1992). Electrostatic calculations of the pK$_a$ values of ionizable groups in bacteriorhodopsin. *J. Mol. Biol.* **224**, 473–486.

41. MacKerell, A. D., Bashford, D., Bellott, M., Dunbrack, R. L., Jr, Evanseck, J. D., Field, M. J. *et al.* (1998). All-atom empirical potential for molecular modeling and dynamics studies of proteins. *J. Phys. Chem. B*, **102**, 3586–3616.

42. Bashford, D., Case, D. A., Dalvit, C., Tennant, L. & Wright, P. E. (1993). Electrostatic calculations of side-chain pKa values in myoglobin and comparison with NMR data for histidines. *Biochemistry*, **32**, 8045–8056.

43. TeVelde, G., Bickelhaupt, F. M., Baerends, E. J., Guerra, C. F., VanGisbergen, S. J. A., Snijders, J. G. & Ziegler, T. (2001). Chemistry with ADF. *J. Comput. Chem.* **22**, 931–967.

44. Klapper, I., Hagstrom, R., Fine, R., Sharp, K. & Honig, B. (1986). Focusing of electric fields in the active site of Cu-Zn superoxide dismutase: effects of ionic strength and amino-acid modification. *Proteins: Struct. Funct. Genet.* **1**, 47–59.

45. Kabsch, W. (1988). Automatic indexing of rotation diffraction patterns. *J. Appl. Crystalog.* **21**, 67–71.

46. Emsley, P. & Cowtan, K. (2004). Coot: model-building tools for molecular graphics. Acta Crystallogr. *D*, **60**, 2126–2132.

47. Adams, P. D., Grosse-Kunstleve, R. W., Hung, L. W., Ioerger, T. R., McCoy, A. J., Moriarty, N. W. *et al.* (2002). PHENIX: building new software for automated crystallographic structure determination. *Acta Crystallogr. D*, **58**, 1948–1954.

Supplementary Information

Figure 1: Spectral comparison of oxidized and coumarin bound XenA-wt, XenA-C25A and XenA-C25S. The spectra are scaled to give identical absorbance at 464 nm. (*A)* Shows the oxidized spectra of XenA-wt (solid line), XenA-C25A (dashed line) and XenA-C25S (dotted line) in the visible region around the absorption peaks for the flavin cofactor. The peaks of the flavin absorbance for wildtype enzyme are 376 nm and 464 nm, for XenA-C25A they are 378 nm and 456 nm and for XenA-C25S they are 376 nm and 460 nm. (*B)* Shows the same region in the visible spectra of XenA-wt (solid line), XenA-C25A (dashed line) and XenA-C25S (dotted line) in the coumarin bound state. Conditions: 50 mM Tris buffer, pH 8.0 at 20°C and saturating concentrations of coumarin. The peaks for the flavin absorbance are all blue shifted. The absorbance maximum for XenA-wt is 470 nm, for XenA-C25A it is 468 nm and for XenA-C25S it is 476 nm.
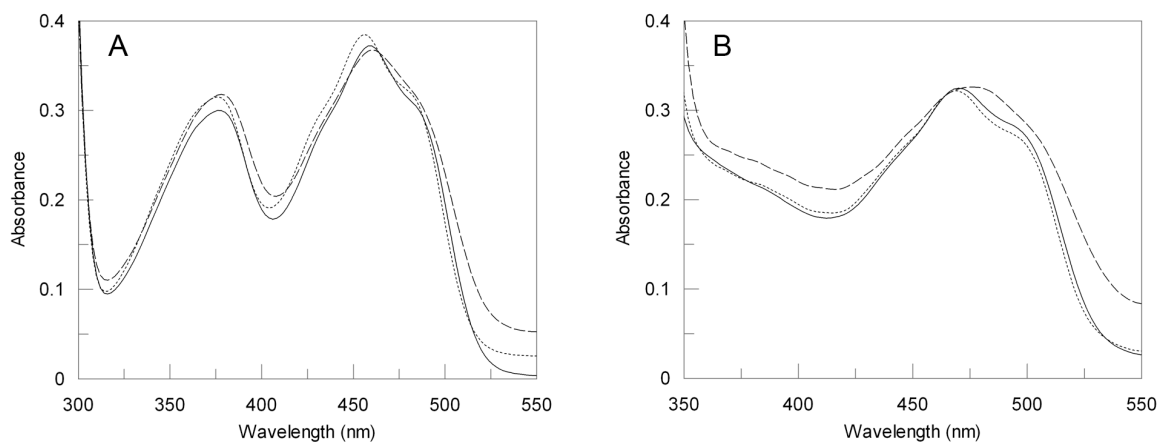
10 Publication C

Olivia Spiegelhauer, Sophia Mende, Stefan H. Knauer and Holger Dobbek: Determinants of substrate-binding and-protonation in the flavoenzyme xenobiotic reductase A. *Journal of Molecular Biology, in revision.*

Determinants of Substrate-Binding and -Protonation in the Flavoenzyme Xenobiotic Reductase A

Olivia Spiegelhauer[1], Sophia Mende[1], Stefan H. Knauer[1] and Holger Dobbek[1,2]

(1) Bioinorganic Chemistry, Universität Bayreuth, Universitätsstrasse 30, 95447 Bayreuth, Germany

(2) Present address: Institut für Biologie, Strukturbiologie/Biochemie, Humboldt-Universität zu Berlin, 10115 Berlin, Germany.

Correspondence should be addressed to: Holger Dobbek, Institut für Biologie, Strukturbiologie/Biochemie, Humboldt-Universität zu Berlin, (++49) 030-23016961, Holger.Dobbek@biology.hu-berlin.de.

ABSTRACT

Xenobiotic reductase A (XenA) from *Pseudomonas putida* 86 catalyzes the NAD(P)H-dependent reduction of various α,β-unsaturated carbonyl compounds, including 2-cyclohexenone and 8-hydroxycoumarin. XenA is a member of the old-yellow-enzyme (OYE) family of flavoproteins with which it shares parallels in the active site architecture. The reaction of XenA follows a ping-pong mechanism implying that its active site has to accommodate and correctly position the substrates to be oxidized (NADH/NADPH) and to be reduced (different α,β-unsaturated carbonyl compounds) to enable formal hydride transfers between the various compounds and the isoalloxazine ring.

The active site of XenA is lined by two tyrosine (Tyr27, Tyr183) and two tryptophan (Trp302, Trp358) residues, which were proposed to contribute to substrate binding. We analyzed the individual contributions of the four residues using site-directed mutagenesis, transient kinetics, redox potentiometry and crystal structure analysis. The Y183F exchange results in a substantially decreased affinity of XenA for NADPH and decreases the rate of the oxidative half-reaction by three orders of magnitude, the latter being in agreement with its function as a proton donor in the oxidative half-reaction. Trp302 swings into the active site of XenA upon reduction of the flavin and decreases the extent of the substrate-binding pocket. The W302A exchange results in multiphasic kinetics for both half-reactions. The C-terminal Trp358 is restricting the substrate binding pocket of the neighboring monomer and its replacement by alanine reduces the rate constant of the reductive half-reaction by two-orders of magnitude, while it only weakly affects the oxidative half-reaction. Trp358 is thus likely contributing to orient the nicotinamide ring of NAD(P)H by spatial exclusion.

Our analysis shows that while the principal catalytic mechanism of XenA, e.g. type of proton donor is analogous to that of other members of the old-yellow-enzyme family, its strategy to correctly position different substrates is unprecedented.

KEYWORDS Quinoline; *Pseudomonas putida*; old-yellow-enzyme; flavin; FMN

INTRODUCTION

Xenobiotic reductase A (XenA) is a versatile catalyst accepting a wide range of substrates. Its reaction cycle can be divided into a reductive half-reaction, in which a hydride ion is transferred from the reduced nicotinamide ring to the flavin, and an oxidative half-reaction, in which the equivalent of one hydride ion is transferred from the flavin to a substrate. In the reductive half-reaction NADH and NADPH serve as substrates, with NADPH reacting approximately 30 times faster with XenA than NADH [1]. In the oxidative half-reaction a variety of different α,β-unsaturated carbonyl compounds have been shown to react with reduced XenA[1-3]. One of the physiological roles of XenA is to catalyze the reduction of 8-hydroxycoumarin within the degradation pathway of quinoline by *Pseudomonas putida* 86 [4,5]. However, most likely XenA also participates in other reactions as it is also encoded in the genome of *P. putida* strains unable to degrade quinoline[6].

XenA shares with other members of the old-yellow-enzyme family the task to correctly orient and position very different substrates in one active site. The problem of accommodating two different substrates in the active site of flavoenzymes not employing ternary complexes, like *para*-hydroxybenzoate hydroxylase[7], has been overcome by different strategies. For example 2,4-dienoyl-CoA reductase has two flavin containing active sites, one in which NADPH is bound and the reductive half-reaction takes places, and one which is specific for binding dienoyl-CoA to catalyze the oxidative half-reaction[8]. A [4Fe-4S] cluster is connecting the two active sites and allows for a coupling of the reductive and oxidative half-reactions by electron transfer between the two sites[8]. Another approach of using two active sites to overcome the problem of reduced substrate specificity can be found in two-component flavin containing monooxygenases like styrene monooxygenase[9]. Styrene monooxygenase from *Pseudomonas putida* S12 is composed of a NADH-specific flavin reductase, which catalyzes the reduction of flavin with high turnover numbers and an FAD-specific styrene epoxidase, which binds the reduced FAD, dioxygen and styrene in a coupled process [10]. In enzymes of the old-yellow-enzyme (OYE) family the substrates of the oxidative and reductive half-reactions are binding to the same preconfigured active site, posing the problem of how productive substrate orientation is secured.

Our recent structural[4] and kinetic[1,11] studies of XenA did not reveal how the individual residues in the active site contribute to the proper binding and orientation of different substrates. We recently described the reactivity of XenA variants in which Cys25 was exchanged against serine and alanine[11]. These exchanges did not drastically alter the reactivity of XenA, but showed that Cys25 modulates the redox potential of FMN and thereby

the rate of the two half-reactions of XenA. Here we describe an investigation of the function of four residues in the active site of XenA, which contribute to different catalytic tasks like proton donation in the oxidative half-reaction and are important for a correct positioning of the substrates in the active site. We show that redox-dependent conformational changes of a tryptophan residue can be used to create two differently shaped substrate-binding pockets for the reductive and oxidative half-reaction.

RESULTS AND DISCUSSION

Mutagenesis and protein production

The QuickChange mutagenesis protocol from Stratagene was used to generate four different variants of XenA. Gene sequencing of the expression plasmids confirmed the single site mutations. Expression levels for all variants were as high as for the wildtype protein and all variants had an FMN content of 70 to 80%. The W302A-XenA variant lost most of the cofactor and had to be reconstituted after purification. The absorbance spectra (oxidized and reduced) of the four XenA variants are displayed in Figure S1.

Specific activities and reduction potentials of the four XenA variants

To analyze whether the amino acid exchanges had an effect on the overall reaction all four XenA variants were checked for their specific activity in a first screen. As detailed in table 1 the examined enzyme variants had only 1 – 20% of the specific activity of wt-XenA[1] (Table 1). We recently determined the specific activity of an enzyme variant (C25S-XenA) in which the reduction potential of the FMN/FMNH$^-$ couple is +82 mV more positive than in wt-XenA, which strongly influenced the rate constants of both half-reactions[11]. To assess whether a change in the relative stabilities of the oxidized and reduced states of the flavin cofactor were responsible for the loss of activity, we determined the reduction potentials of all four XenA variants (Table 1).

Table 1: Specific activities, reduction potentials and transient kinetic data of the XenA variants

Enzyme	Spec. Activity (U mg^{-1})	E^0_m (mV)	Reductive half-reaction		Oxidative half-reaction	
			K_d (μM)	k_{red} (s^{-1})	K_d (μM)	k_{red} (s^{-1})
wt-XenA[a]	6.7	-263	176 ± 14	35.7 ± 0.6	86 ± 2	13.1 ± 0.1
Y27F	0.54	-264	463 ± 54	3.6 ± 0.2	151 ± 11	23.0 ± 0.3
Y183F	0.06	-261	2770 ± 450	60 ± 7	83 ± 9	0.051 ± 0.001
W302A	1.27	-242	35 ± 6	4.29 ± 0.09	674 ± 200	24 ± 5
W358A	0.25	-265	509 ± 31	0.32 ± 0.01	192 ± 10	20.4 ± 0.3

[a] Data taken from reference[1].

None of the studied XenA variants shows a stabilization of one of the semiquinone states (Figure S1) and the determined reduction potentials are therefore reflecting the FMN/FMNH$^-$ couple. The reduction potential of the Y27F-, Y183F- and W358A-XenA variants are within the experimental errors identical to wt-XenA (wt-XenA: E°_m = -263 mV) (Table 1, Figure S2)[1]. The reduction potential of the W302A-XenA variant is +21 mV more positive than wt-XenA (Table 1).

Tyr183 – NAD(P)H binding and proton donor in the oxidative half-reaction

Tyr183 has a central position in the active site of wt-XenA, pointing with its phenolic hydroxyl group into the substrate-binding pocket (Figure 1).
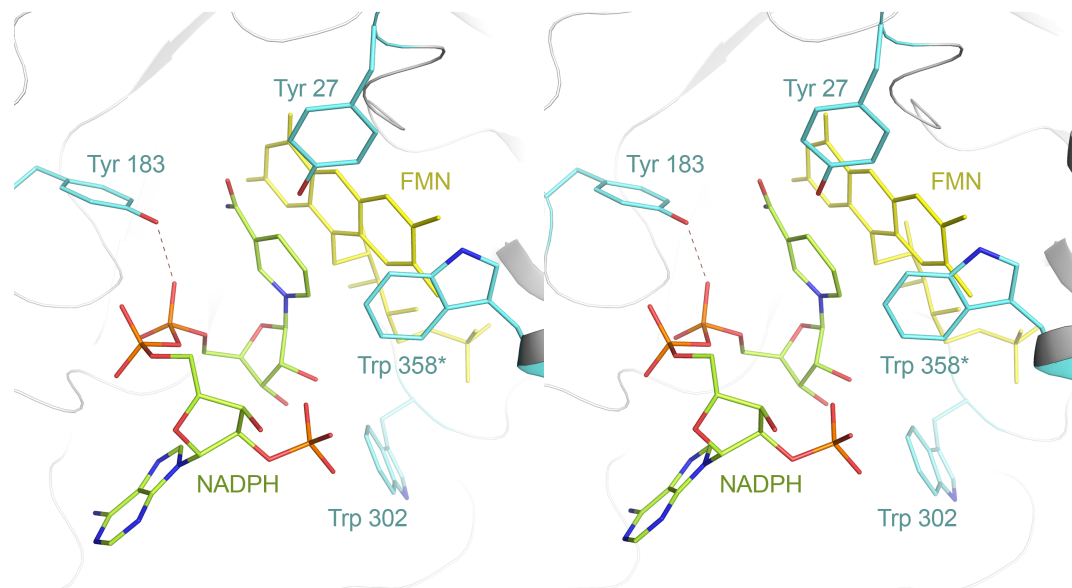
Figure 1: **XenA in complex with NADPH.** Stereoscopic view of the active site of XenA in complex with NADPH. The structure was derived by docking calculations[1]. All residues are displayed in stick representation. The FMN cofactor is shown in yellow. The carbon atoms of amino acid side chains are shown in light blue, carbon atoms of NADPH are shown in green, oxygen atoms in red, nitrogen atoms in blue and phosphorous atoms in orange. The broken lines (red) represent possible interactions between XenA and NADPH. All figures have been prepared using PyMol[38].

To determine whether the Y183F exchange has any effect on the local structure of the enzyme, we determined the crystal structure of Y183F-XenA at a resolution of 1.45 Å (Table 2). A superposition of the structures of Y183F- with wt-XenA shows that the only visible difference is the absence of the phenolic hydroxyl-group in the active site; all residues show the same conformation as in wt-XenA (Figure 2).

Table 2: Crystallographic data and refinement statistics

	XenA-wt reduced	*XenA-Y183F*	*XenA-W358A*
Data Collection			
Spacegroup	$P2_12_12$	$I222$	$I222$
cell constants			
a (Å)	83.78	58.32	59.88
b (Å)	158.03	83.41	83.27
c (Å)	57.85	156.41	156.29
Wavelength (Å)	0.9184	0.9184	0.9184
Total /	445,250 /	230,358 /	103,648 /
unique reflections	77,884	65,786	30,252
Resolution (Å)	1.75	1.44	1.9
	(1.75-1.80)	(1.44-1.48)	(2.0-1.9)
$R_s^{\,a}$ (%)	8.3 (51.6)	8.6 (48.5)	5.3 (9.2)
Completeness (%)	99.5 (96.5)	95.0 (90.6)	98.9 (98.1)
(I) / (σI)	15.0 (2.4)	12.1 (2.5)	18.0 (10.4)
Refinement			
R_{work} / R_{free}(%) [b]	20.3 / 25.6	15.8 / 19.6	18.7 / 23.4
R m. s. deviations			
Bonds (Å)	0.006	0.021	0.007
Angles (°)	1.04	1.8	1.13
No. molecules			
Atoms/ASU [c]	6,215	3,584	3,128
Ligand/ion	5	11	8
Water	575	553	367
Estimated coordinate errors [d]	0.25	0.15	0.15

[a] $R_s = \Sigma_h \Sigma_i \mid I_i(h) - <I(h)>\mid / \Sigma_h \Sigma_i I_i(h)$; where i are the independent observations of reflection h.
[b] The R_{free} factor was calculated from 5% of the data, which were removed at random before the refinement was carried out.
[c] Refined atoms in the asymmetric unit.
[d] Estimated coordinate error based on R value.
Values in parentheses are given for the highest resolution shell.

As the Y183F exchange reduced the specific activity approximately 100-fold, we studied each half-reaction individually using single-turnover kinetics to determine the origin of the activity loss (Figure S3 and S4). For the reductive half-reaction Y183F-XenA was mixed with NADPH and the limiting rate constant at high substrate concentrations and the dissociation constant (K_d) were determined using the rapid-equilibrium assumption, which was shown to be valid for wt-XenA[1]. While the rate constant was only slightly increased, the K_d value of

the Y183F-XenA * NADPH complex is about 11-fold larger compared to wt-XenA (Table 1). As the solubility of the stock solution of NADPH becomes limiting at this high concentrations, the K_d value is not well determinable and may be even larger (Figure S3). The high K_d value is in agreement with a model structure of the XenA-NADPH complex determined by computational docking and minimization techniques[1]. In this complex the phenolic hydroxyl group of Tyr183 forms a hydrogen bond with an oxygen atom of the β-phosphate of the ADP moiety of NADPH (Figure 1). An 11-fold increase of the dissociation constant is equivalent to a change in apparent binding energy ($\Delta G_{app} = RT \ln K_S / K'_S$) of 5.8 kJ/mol at room temperature, which would be in agreement with the loss of a hydrogen bond in the enzyme substrate complex.
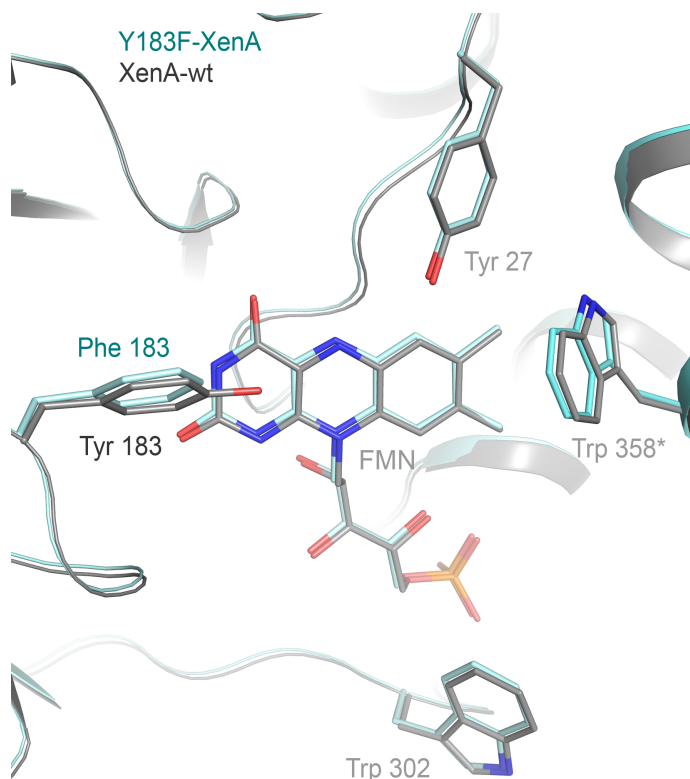
Figure 2: **Comparison of wt-XenA-wt and Y183F-XenA.** View on the superimposed active sites of XenA-wt (grey) and XenA-Y183F (light blue). All residues are shown in stick mode. Oxygen atoms are displayed in red, nitrogen atoms in blue and phosphorous atoms in orange.

The oxidative half-reaction was measured with 2-cyclohexenone as substrate. Reoxidation of the reduced FMN after mixing with substrate under anoxic conditions proceeded very slowly. However, at all concentrations the oxidation of FMN could be fit to a single exponential function and the resulting observed rate constants rise hyperbolicly with increasing substrate concentration and show saturating behavior. The limiting rate constant at high substrate

concentrations for the reoxidation of FMN by 2-cyclohexenone is 260-fold reduced compared to wt-XenA, while the K_d value of the enzyme substrate complex is not affected by the Y183F exchange (Table 1). Crystal structures of oxidized XenA in complex with the substrate coumarin show that the phenolic hydroxyl group of Tyr183 is 3.3 Å away from the α-carbon atom of the double bond to be reduced[4,11]. The oxidative half-reaction consists of a formal hydride transfer from the N5 atom of FMN to the β−carbon of the substrate carbonyl and an uptake of a proton by the carbon in α-position, two processes which can be coupled to varying degrees[12]. With Tyr183 as proton donor, the overall reaction can be described as a *trans*-addition with the reduced flavin delivering the hydride from one π-face of the olefinic double bond while Tyr183 provides the proton from the opposite side. It further indicates that either hydride and proton transfer in the reaction of reduced XenA with 2-cyclohexenone are coupled or that Tyr183 is necessary to stabilize the transition state during the hydride transfer, as it is the reoxidation of FMNH⁻ which is proceeding very slowly. Tyr196 of OYE is analogous to Tyr183 in XenA. The exchange of Tyr196 (OYE numbering) against phenylalanine results in a drastic decrease in the rates of the oxidative half-reaction with various substrates[12]. While with 2-cyclohexenone as substrate in the oxidative half-reaction Y196F-OYE reacts six orders of magnitude slower than wt-OYE, the reaction with 1-nitrocyclohexene is only marginally decreased by the Y196F exchange[12]. This has been explained by a coupled hydride/proton transfer with 2-cyclohexenone, due to the high energy of the enolate anion intermediate, in contrast to an uncoupled hydride/proton transfer with 1-nitrocyclohexene as the generated aci-nitro compound is thermodynamically more accessible[12]. In contrast to the behavior observed for OYE[12] and XenA (this work) the exchange of the corresponding tyrosine residue to phenylalanine (Y186F) in pentaerythritol tetranitrate reductase is not significantly impairing catalysis[13].

Tyr27 – Stabilizing the transition state in the reductive half-reaction
Like Tyr183 the phenolic hydroxyl group of Tyr27 is oriented towards the substrate-binding site and is approximately 5 Å above the N5 atom of FMN, ideally placed to interact with substrates in the active site (Figure 1). The exchange of Tyr27 against phenylalanine (Y27F-XenA) resulted in a tenfold lower specific activity (Table 1). We used single-turnover kinetics to determine the step most affected by the exchange. The time dependent changes in the reductive and oxidative half-reaction could be approximated by single-exponential functions and the concentration dependence of the observed rate constants showed clear saturation behavior. The limiting rate constant in the reductive half-reaction is 10-fold decreased in

Y27F-XenA and the K_d value of the Y27F-XenA * NADPH complex was slightly increased. The oxidative half-reaction with 2-cyclohexenone was only weakly affected by the loss of the hydroxyl-group and the limiting rate constant and the K_d value are both twofold increased compared to wt-XenA (Table 1). In the model complex of XenA with NADPH the hydroxyl group of Tyr27 is about 3.6 Å away from the hydride donating C4-atom of NADPH (Figure 1). The decreased rate constant of the reductive half-reaction may therefore likely be due to a weak interaction of the HO(Tyr27) with the transferred hydride ion, which can contribute to stabilize developing charges of the transition state.

Trp358 – Decreasing the activation energy in the reductive half-reaction

Trp358 is part of the C-terminal α-helix of XenA and is forming one wall of the substrate-binding site of the other monomer close to the dimethylbenzene ring of FMN (Figure 1). Trp358 is unique to XenA and in its closest structural homologues, YqjM from *Bacillus subtilis*[14] and the "ene" reductase from *Thermoanaerobacter pseudoethanolicus*[15], an arginine residue is found in its position.

Crystal structure analysis shows that the exchange of Trp358 against alanine (W358A-XenA) results in a small rearrangement within the C-terminal α-helix (Figure 3). The space formerly occupied by the indole ring of Trp358 is now partly filled by His357, whose side-chain rotated by approximately 80° towards the isoalloxazine ring of FMN. However, no further perturbations of the active site are recognizable in the structure (Figure 3).
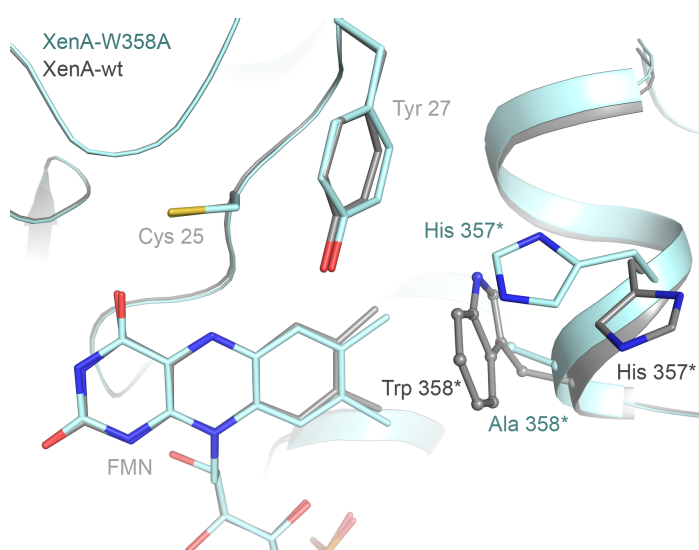
Figure 3: **Comparison of wt-XenA-wt and W358A-XenA.** View on the superimposed active sites of wt-XenA-wt (grey) and W358A-XenA (light blue). All residues are shown in stick mode. Oxygen atoms are displayed in red, nitrogen atoms in blue, phosphorous atoms in orange and sulfur atoms in yellow.

The specific activity of W358A-XenA is only 4% of that of wt-XenA, and consequently both half-reactions were studied individually (Table 1). The time dependent changes in the reductive and oxidative half-reaction were fitted by single-exponential functions and the concentration dependence of the observed rate constants showed clear saturation behavior. The limiting rate constant in the reductive half-reaction is 112-fold decreased in W358A, while the K_d value of the W358A-XenA * NADPH complex increased twofold. The slight increase of the K_d value is also observable in the oxidative half-reaction (W358A-XenA * 2-cyclohexenone complex), but in this half-reaction the limiting rate constant also increased slightly. Thus the reductive half-reaction is becoming rate limiting for the overall reaction of W358A-XenA and causes the low specific activity. Inspection of the modeled structure of the XenA*NADPH complex reveals that the indole moiety of Trp358 forms one wall of the substrate binding pocket and its absence could allow the placement of the nicotinamide ring in non-reactive positions above the dimethylbenzene ring of FMN. Additional interactions of NADPH may be possible with the re-oriented His357 and could further stabilize non-reactive conformers. The oxidative half-reaction is only weakly affected by the amino acid exchange, and shows a slightly increased K_d value and limiting rate constant. Structures of oxidized XenA with coumarin[4,11] showed that the substrate is mostly stabilized by two-hydrogen bonds with His178 and His181 acting as hydrogen-bond donors to the substrate carbonyl oxygen atom, which automatically restrains horizontal movements of the substrate. NAD(P)H in contrast is anchored mostly via the pyrophosphate moiety, allowing the nicotinamide ring to adopt different conformations. However, given the inherent context dependence of any energetic effect caused by site-directed mutagenesis,[16,17] we admit that more detailed studies are necessary to gain insight into the role(s) of Trp358 in the reductive half-reaction.

Trp302 - Redox dependent active site protection

Trp302 is located at the entrance of the substrate channel near the phosphate group of FMN (Figure 1). A structural peculiarity of Trp302 is the unusual conformation of its main chain, which places it in a Ramachandran disallowed region with $\phi=113°$ and $\psi=97°$.[4]

To gain further insight into conformational changes during the catalytic cycle we determined the crystal structure of XenA crystallized in the reduced state under an anoxic atmosphere. The crystals were colorless indicating that during the time of crystallization the enzyme remained in the reduced state. Despite practically identical conditions used for crystallization, except for the presence of NADH, crystals had a different space group than in the oxidized state ($P2_12_12$) and contained one homodimer per asymmetric unit. The structure of reduced

XenA has been refined to a resolution of 1.75 Å with an *R*-value of 20.5% and a free *R*-value of 25.0% (Table 2). As observed for several flavoenzymes[18] the isoalloxazine ring system is distinctly curved, and the N5 atom has a tetrahedral geometry and is positioned above the ring plane pointing towards the substrate-binding site (Figures 4 and 5). The most obvious difference between the structures of reduced and oxidized XenA is a large conformational change of residues 302-306, which changes the main chain torsion angles of Trp302 (ϕ=77° and ψ=39°) so that it is now in a Ramachandran allowed region. An even larger conformational change of the side chain of Trp302, which rotates approximately 90° around Cα-Cβ and 180° around Cβ-Cγ, folds the indole ring in the substrate-binding pocket ("in"-position) (Figure 4). The conformational changes also alter the hydrogen-bond network around the main chain atoms of Trp302 and Gly303. In the oxidized state of XenA Trp302 ("out"-position) does not interact with the terminal phosphate of FMN, but the amide nitrogen of Gly303 is hydrogen bonded to one of the phosphate oxygen atoms (Figure 4). The change in main chain conformation of Trp302 and Gly303 places the amide group of Trp302 as a hydrogen-bond donor to the phosphate ester oxygen, but destroys the hydrogen-bond interaction of Gly303 with FMN.
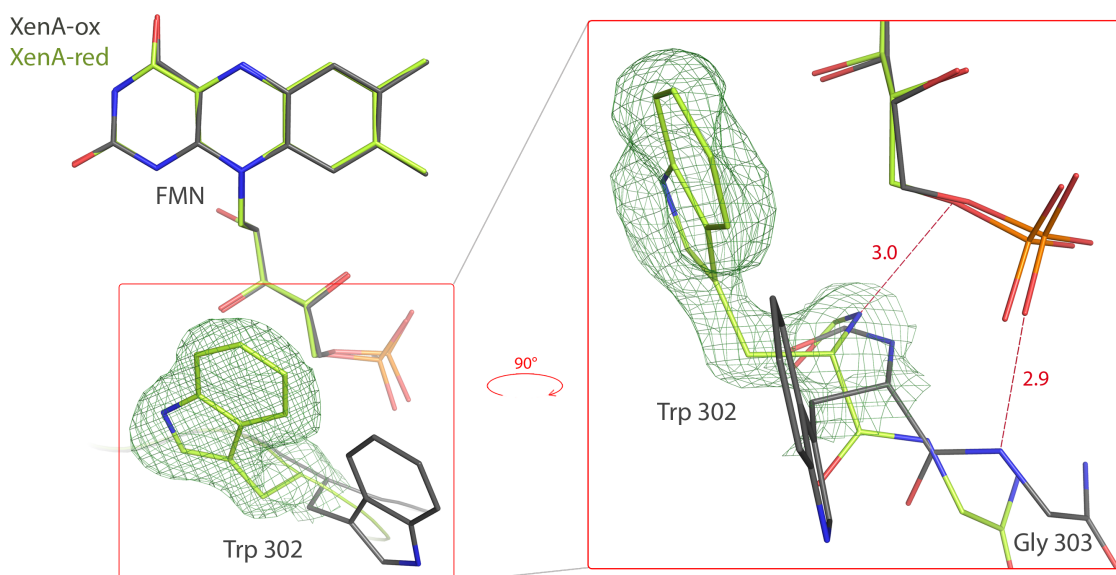
Figure 4: **Comparison of XenA in the oxidized and reduced state.** Active site view of XenA in the oxidized (grey) and reduced state (green). All residues are shown in stick mode. Oxygen atoms are shown in red, nitrogen atoms in blue and phosphorous in orange. The electron density map around Trp302 in the reduced state is shown as $2F_o$-F_c map contoured at 1.0σ in green mesh representation. Possible interactions between the terminal phosphate group of FMN and XenA in both redox states are displayed as broken lines in red. The distances are given in ångströms.

We can only speculate about the origin of the conformational change around Trp302, however as the main difference between the two structures is the oxidation state of FMN at otherwise identical crystallization conditions, we assume that the conformational changes originate from the small structural differences of the isoalloxazine ring caused by the reduction, which are transmitted through the ribityl group to the terminal phosphate of FMN. The phosphate is moved slightly towards the main chain atoms of Trp302, triggering the rearrangement of the hydrogen bond network between phosphate and main chain. Movement of the indole side chain from the "out"- to the "in"-position results in a narrowing of the substrate-binding pocket. A superposition of reduced XenA with the NADPH-XenA complex shows that when Trp302 is in the "in"-position the van-der-Waals radii of bound NADPH and the indole ring overlap with closest C-C and C-O distances of 1.9-2.1 Å between the two molecules (Figure 5).
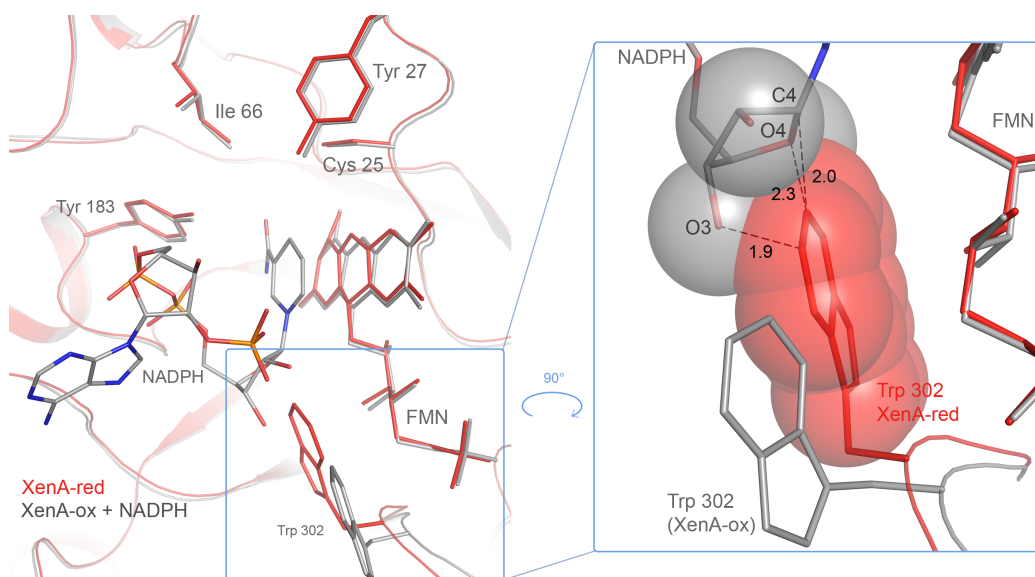
Figure 5: **Superimposition of the XenA-ox * NADPH complex with XenA-red.** The active site structure of oxidized XenA in complex with NADPH is shown in grey and reduced XenA in red. All residues are displayed in stick mode. Oxygen atoms are shown in red, nitrogen atoms in blue and phosphorous atoms in orange. Distances between NADPH and Trp302 of the reduced XenA are given in ångströms and are shown as broken lines in black. Van-der-Waals surfaces are shown in corresponding colors.

As the overlap occurs with the C1, O3 and O4-atoms of the ribose, the clash cannot be avoided by different conformations of NADPH, but would need a translation of the nicotinamide ring. This movement of the nicotinamide would only be possible after larger rearrangements, e.g. of the side chains of Cys25, Tyr27, Tyr183 and Ile66 forming the

opposite side of the substrate binding pocket. The functional consequence of the "out"- to "in"-movement of Trp302 would be a disfavored binding of NAD(P)H/NAD(P)$^+$ in the reduced state. This is in agreement with the absence of charge-transfer complexes between NAD(P)$^+$ and reduced XenA, the sufficiency of stoichiometric amounts of NAD(P)H to reduce XenA and no indications for a reaction between NAD(P)$^+$ and reduced XenA.[1]

Several crystal structures for reduced states of enzymes of the OYE family have been reported (OYE[19], PETN reductase[20], YqjM[14]), and none showed conformational changes similar to the ones described above. However, all reduced structures reported to date have been produced by reducing crystals of the oxidized flavoenzymes by soaking, where conformational changes may have been prevented by contacts within the crystal lattice. In contrast, we reduced XenA in solution before crystallization under anoxic conditions allowing conformational changes to occur in solution before a crystal lattice is formed.

The exchange of Trp302 against alanine (W302A-XenA) resulted in a fourfold lower specific activity and a change in the reduction potential of the FMN/FMNH$^-$ couple ($\Delta E^{\circ}_{m} = +21$ mV) (Table 1). Single turnover kinetics revealed multiple phases for the reductive and oxidative half-reactions. Whereas wt-XenA and all XenA variants studied so far react with kinetic transients, which can be fit to single exponential functions, two terms are necessary to describe the reductive half-reaction of W302A-XenA with NADPH and three terms are necessary to describe the oxidative half-reaction with 2-cyclohexenone (Figure S5), indicating either substantial heterogeneity of the protein preparation or multiple reactive configurations, as observed for morphinone reductase after the exchange of Asn189 to alanine.[21] Only the fastest rate constants derived for the oxidative half-reaction show a clear dependence on substrate concentrations and based on the relative amplitudes about half of the protein reacts one to two orders of magnitude slower. The enzyme population connected to the larger rate constants shows small changes in the reactivity due to the amino acid exchange (Table 1). The loss of the indole side chain reduces the limiting rate constant of the reductive half-reaction ninefold, while it increases the limiting rate constants of the oxidative half-reaction twofold. Both changes are contrary to what we expected based on the increased reduction potential of the FMN/FMNH$^-$ couple by 21 mV (Table 1). The dissociations constants of the W302A-XenA * substrate complexes changed by similar scales. While the dissociation constant of the W302A-XenA * NADPH complex increased fivefold, the dissociation constants of the W302A-XenA * 2-cyclohexenone complex decreased eightfold (Table 1). The W302A exchange eliminates the "out"- to "in"-change and enlarges the active site pocket. The more complex kinetics of W302A disfavors the measurement of the individual

on- and off-rate constants of NADPH binding to the enzyme, as determined for wt-XenA,[1] and we can not say whether the binding or the dissociation process is more affected by the exchange. Narrowing of the substrate-binding site by change from the "out"- to the "in"-position of Trp302 is likely an essential part of its contribution to bind and position 2-cyclohexenone in the oxidative half reaction and its lack is probably also responsible for the lower stability of the W302A-XenA * 2-cyclohexenone complex compared the wt-XenA (Table 1).

CONCLUSIONS

Crystal structures of various members of the old-yellow-enzyme family have been determined and allow to analyze the similarities and differences in the architectures of the active sites.[4,14,15,19,20,22,23,24] A distinct advantage of most members of this enzyme family is their broad substrate specificity and catalytic promiscuity,[25] allowing researchers to measure and compare the kinetics of enzymes with high and low sequence identities using the same substrates. While in the reductive half-reaction the reduced nicotinamides are the favored reducing agents, for the oxidative half-reaction 2-cyclohexenone has become the prototypical substrate. Figure 6 presents an overview on the different contributions of the active site residues studied in this and a preceding work.[11] We focused in our analysis on four residues, of which only Tyr183 was highly conserved. The other four residues, namely Cys25, Tyr27, Trp302 and Trp358, are not conserved: structural counterparts to Cys25 and Tyr27 only exist in the "ene" reductase[15] and YqjM,[14] while Trp302 and Trp358 have no counterparts in any of the other structures. However, the lack of conservation of these residues does not render them unimportant for catalysis and indeed the exchange of all three compromises the reactivity of XenA to different degrees. They certainly have different contributions to the catalytic mechanism, however all appear to indirectly shape the substrate-binding site, helping to overcome the problem of having one active site to bind and convert the various substrates of a ping-pong reaction. Trp302 is most remarkable in this respect as its redox dependent conformations, "in"-conformation in the reduced state and "out"-conformation in the oxidized state of the flavine, changes the shape of the substrate-binding pocket. A wider substrate-binding site exists in the oxidized state of XenA allowing to accommodate NAD(P)H, whereas a smaller substrate-binding site in the reduced state is sufficient to allow the binding of substrates with mono- and bicyclic rings like 2-cyclohexenone and coumarin.

In contrast to the four residues mentioned Tyr183 has counterparts in most members of the OYE family, morphinone reductase being a notable exception,[22] and has the same position and orientation in the crystal structures of OYE, PETN reductase and XenA. The effect of an exchange of Tyr183 and counterparts against phenylalanine has been studied in the three enzymes all of which are affected differently by the exchange. In XenA Tyr183 is involved in NADPH binding and the Y183F-exchange drastically reduced the rate of the oxidative half-reaction where it likely acts as a proton donor. The corresponding residue in OYE (Tyr196) acts also as a proton donor in the oxidative half-reaction but is not important for NAD(P)H binding, as the K_d of the NADPH*OYE complex is practically identical for wt-OYE and Y196F-OYE.[12] For Tyr186, the corresponding residue in PETN reductase, both functions are

not conserved. The K_d value of the NADPH*Y186F-PETN reductase complex has not been explicitly determined, but the observed rate constants of the reductive half-reaction were reported to be concentration independent for NADPH concentrations of 200 – 1300 μM NADPH, demonstrating that the K_d value can not be much larger than in wt-PETN reductase, where it is 33.4 μM.[13; 26] A function of Tyr186 as proton-donor in the oxidative half-reaction with 2-cyclohexenone in PETN reductase is unlikely, as the Y186F-exchange reduced the reactivity only weakly.[13] Thus, the example of Tyr183 (XenA numbering) in the OYE family demonstrates that sequence and structural conservation does not necessarily lead to the frequently assumed functional conservation, rendering functional assignments of active site residues solely based on conserved sequences/structures prone to misinterpretations.
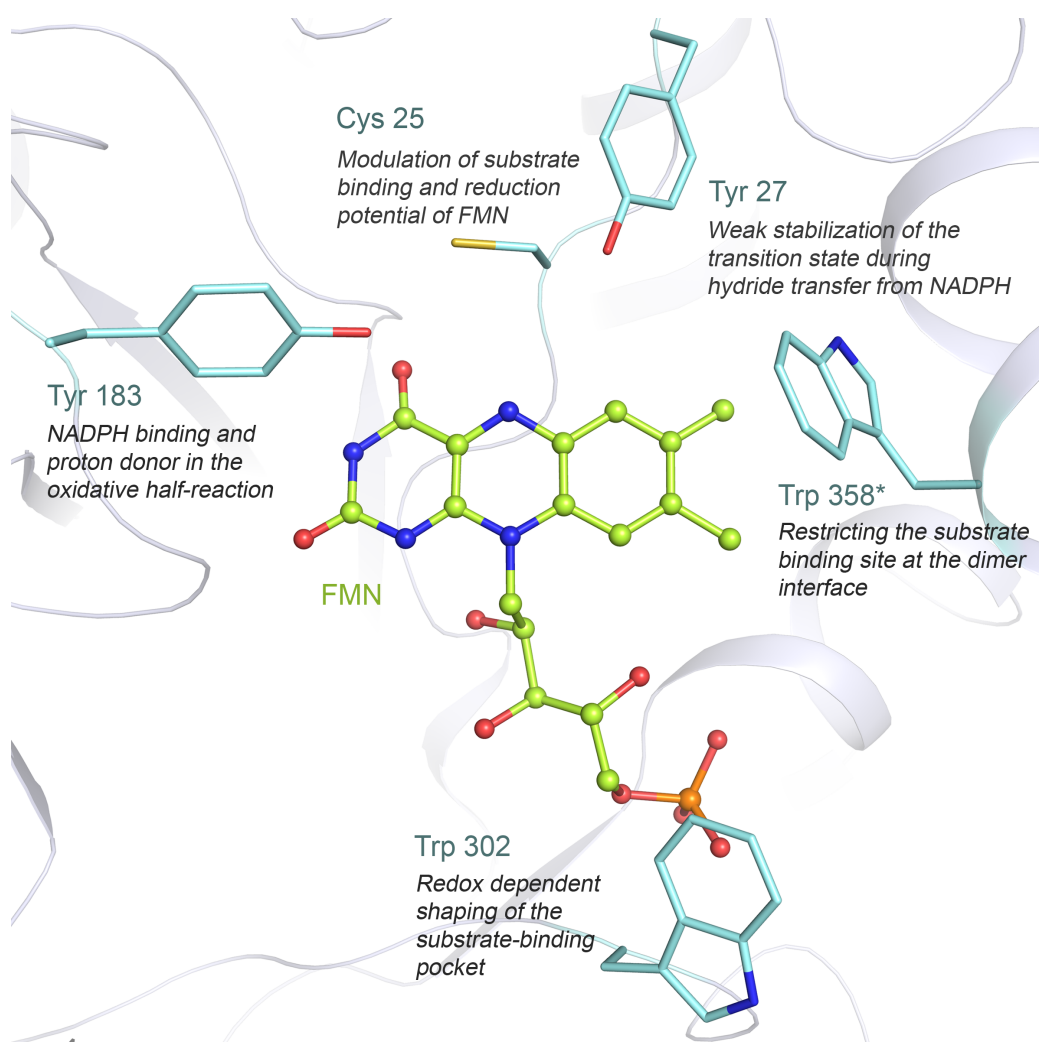
Figure 6: **Overall view of the active site of wt-XenA** Active site view of wt-XenA. All active site amino acid residues are displayed in stick mode. The FMN is shown in ball-and-stick representation. The carbon atoms of the amino acids are shown in light blue, the carbon atoms of FMN are shown in green. Oxygen atoms are shown in red, nitrogen atoms in blue, sulfur atoms in yellow and phosphorous atoms in orange.

MATERIALS AND METHODS

Chemicals and Enzymes

All materials were purchased from Fluka, AppliChem, Roth and Otto Nordwald. Microbial media were prepared as described in Sambrook *et al.*[27]. 5-deaza-10-methyl-3-sulfopropyl-isoalloxazine was a gift from Peter M.H. Kroneck (University of Konstanz, Germany).

Mutagenesis, protein expression and purification

The exchanges of Tyr27, Tyr183, Trp302 and Trp358 were performed using the QuickChange mutagenesis protocol from Stratagene. PCR primers described below:

For Y27F 5'-CCGCCGATGTGCCAA<u>TTC</u>ATGGCCGAAGACGGC-3' and

5'-GCCGTCTTCGGCCAT<u>GAA</u>TTGGCACATCGGCGG-3'

for Y183F 5'-CTGCACTTTGCCCATGGC<u>TTC</u>CTGGGTCAGAGCTTC-3' and

5'-GAAGCTCTGACCCAG<u>GAA</u>GCCATGGGCAAAGTGCAG-3'

for W302A 5'-TGACGTCGGCG<u>GCG</u>GGCTTTGGTAC-3' and

5'-GTACCAAAGCC<u>CGC</u>CGCCGACGTCA-3'

for W358A 5'-GGCACCGTATGCGCAC<u>GCG</u>CTCGAGCGTTATCG-3' and

5'-CGATAACGCTCGAG<u>CGC</u>GTGCGCATACGGTGCC-3'.

The plasmid pET_XenA[4] was used as template. The double stranded wild type DNA was removed by digestion with the restriction enzyme *Dpn*I. DNA sequencing of the mutated genes, carried out by Eurofins MWG Operon, was used to confirm the successful mutations. The mutated plasmids were transformed into the expression strain *E. coli* Rosetta(DE3)pLysS and the genes were expressed as the wild type gene *xenA* described previously[1,4]. All enzyme variants were purified as described for XenA-wt[1,4]. Activity was assayed in 50 mM Tris buffer (pH 8.0) containing 150 μM NADPH and 300 μM 2-cyclohexenone at 25°C. To remove dioxygen from the solution the reaction mixture was flushed with dinitrogen gas in a quartz cuvette sealed by a screw cap with rubber septum. Reactions were initiated by the addition of 5 μL of the XenA variants (2 mg mL^{-1}) with a Hamilton syringe to 995 μL reaction buffer. The time-dependent change of absorption at a wavelength of 340 nm was followed over 2 min. One unit (1 U) is defined as the oxidation of 1 μmol NADPH per minute. Flavin contents were determined as described by Aliverti *et al.*[28] as detailed recently[1].

Photoreduction and determination of reduction potentials

Photoreduction of the XenA variants were carried out in a glass tonometer with a cuvette side arm using the protocol of Massey *et al.*[29]. The potassium salt of 5-deaza-10-methyl-3-

sulfopropyl-isoalloxazine in catalytic amounts was used as photoreductant. The reaction mixture was made anoxic by repeated evacuation and flushing with dinitrogen gas and contained concentrations of 15 mM EDTA, 30 µM enzyme and 1 µM phenosafranine as electron mediator in 100 mM Tris buffer (pH 8.0). Solutions of the deazaflavin derivative and EDTA were stored in the side arm cuvette during this process and mixed with the enzyme directly before the light irradiation steps were performed with a 100 W lamp from a slide projector (Agfa, Opticus 100). Absorption spectra were recorded directly and three minutes after each illumination step. The reduction potentials were determined according to the protocol published by Sucharitakul and co-workers[30]. Phenosafranine served as reference dye for all variants ($E^0_{m,D}$ = -252 mV[31]). Concentrations of oxidized enzyme (E_{ox}) and oxidized dye (D_{ox}) were calculated from equations 1 and 2.

$$A_{456} = \varepsilon^{Eox}_{456}\, c^{Eox} + \varepsilon^{Dox}_{456}\, c^{Dox} + \varepsilon^{Ered}_{456}\, (c^{Etot} - c^{Eox}) + \varepsilon^{Dred}_{456}\, (c^{Dtot} - c^{Dtot}) \quad (1)$$

$$A_{521} = \varepsilon^{Eox}_{521}\, c^{Eox} + \varepsilon^{Dox}_{521}\, c^{Dox} + \varepsilon^{Ered}_{521}\, (c^{Etot} - c^{Eox}) + \varepsilon^{Dred}_{521}\, (c^{Dtot} - c^{Dtot}) \quad (2)$$

The reduction potentials ($E^0_{m,E}$) of the XenA variants were determined from the difference (ΔE^0) in the reduction potentials of enzyme and dye using equation 3.

$$E^0_{m,E} = E^0_{m,D} + \Delta E^0 \qquad (3)$$

Stopped-flow spectrophotometry

The reductive half-reactions of the enzymes variants with NADPH were measured in 50 mM Tris buffer (pH 8.0) under anaerobic conditions at 20°C as described previously[1]. Solutions containing 10 µM XenA were mixed with NADPH concentrations varying from 50 – 5000 µM. 2-cyclohexenone was used as oxidative substrate with concentrations varying from 50 – 1800 µM. To achieve complete reduction the enzymes were reduced by titration with appropriate amounts of NADH in a glass tonometer with cuvette side arm. The reactions were monitored at the absorbance maximum of FMN of the individual XenA variants using an Applied Photophysics SX-20MV spectrophotometer with a 1-cm observation path length cuvette. The measurements were repeated at least five times for each substrate concentration. The observed kinetic transients were approximated by single (Y27F-, Y183F-, W358A-XenA) or double/triple (W302-XenA) exponential equations using the Pro-Data software (Applied Photophysics, UK). The observed rate constants (k_{obs}) were plotted against the

respective substrate concentrations. The reductive half-reaction was modeled as shown in the general equation 4

$$A + B \xrightleftharpoons{K_d} C \xrightarrow{k_{red}} D \quad (4)$$

where A = the enzyme in the oxidized state, B = reductive substrate – NADPH, C = enzyme$_{ox}$-substrate charge-transfer complex and D = enzyme containing the two-electron reduced state of FMN and bound NADP$^+$. The oxidative half-reaction was modeled as shown in the general equation 5

$$E + F \xrightleftharpoons{K_d} G \xrightarrow{k_{ox}} H \quad (5)$$

where E = the enzyme in the reduced state, F = oxidative substrate – 2-cyclohexenone, coumarin, G = enzyme$_{red}$ -substrate charge-transfer complex and H = oxidized enzyme with bound 2-cyclohexanon.

The hyperbolic plots were fitted to equation 6 using the program GraFit-5 (Version 5.0, Erithacus Software Limited, UK) to obtain the limit of the reaction rate $k_{red/ox}$ at high substrate concentrations [S] and the dissociation constant K_d[32].

$$k_{obs} = k_X [S] / (K_d + [S]) \quad (6)$$

To relate the determined limiting rate constants to the steady-state catalytic constants equation 7 was used.

$$k_{cat} = \frac{k_{red} k_{ox}}{(k_{red} + k_{ox})} \quad (7)$$

Data collection and structure refinement

Crystals were grown as described earlier for wt-XenA[4]. Crystals of reduced XenA were grown using the same crystallization condition, which contained additionally 4 mM NADH in the crystallization drop and 4 mM sodium dithionite in the reservoir solution under anoxic conditions in an anaerobic glove box (Model B, Coy Laboratory Products, Michigan). The crystals were cross-linked for 1 hour in a harvesting solution containing 100 mM HEPES buffer (pH 7.5), 2.1 M ammonium sulfate, 4 mM NADH and 0.002% glutaraldehyde. Crystals were shock frozen in harvesting solution containing 20% (v/v) 2*R*,3*R*-butandiol and stored in

liquid nitrogen. The crystals belonged to two different space groups with cell dimensions listed in Table 2. X-ray diffraction data were collected at the beam line BL14.2 (BESSY, Berlin, Germany). The diffraction data were processed and scaled using the XDS package[34]. The structures of the XenA variants were solved using difference Fourier techniques using the isomorphous structure of $XenA_{ox}$ for phase calculations (PDB-Id: 2H8X[4]), the structure of reduced XenA was solved using Patterson search techniques with $XenA_{ox}$ (PDB-Id: 2H8X[4]) as homologous search model. Subsequent rounds of model building and refinement were performed using the programs COOT[35] and PHENIX[36] and Refmac5[37].

Accession numbers

The coordinates and structure factor amplitudes are deposited in the RCSB Protein Data Bank with ID codes: 3N14 (XenA-W358A), 3N16 (XenA-Y183F), and 3N19 (XenA-wt, reduced).

ACKNOWLEDGEMENTS

REFERENCES

11. Spiegelhauer, O., Dickert, F., Mende, S., Niks, D., Hille, R., Ullmann, M. & Dobbek, H. (2009). Kinetic characterization of xenobiotic reductase A from *Pseudomonas putida* 86. *Biochemistry* 48, 11412-20.

2. Blehert, D. S., Knoke, K. L., Fox, B. G. & Chambliss, G. H. (1997). Regioselectivity of nitroglycerin denitration by flavoprotein nitroester reductases purified from two *Pseudomonas* species. *J Bacteriol* 179, 6912-20.

3. Blehert, D. S., Fox, B. G. & Chambliss, G. H. (1999). Cloning and sequence analysis of two *Pseudomonas* flavoprotein xenobiotic reductases. *J Bacteriol* 181, 6254-63.

4. Griese, J. J., R, P. J., Schwarzinger, S. & Dobbek, H. (2006). Xenobiotic reductase A in the degradation of quinoline by *Pseudomonas putida* 86: physiological function, structure and mechanism of 8-hydroxycoumarin reduction. *J Mol Biol* 361, 140-52.

5. Fetzner, S., Tshisuaka, B., Lingens, F., Kappl, R. & Huttermann, J. (1998). Bacterial degradation of quinoline and derivatives - Pathways and their biocatalysts. *Angewandte Chemie-International Edition* 37, 577-597.

6. Jimenez, J. I., Minambres, B., Garcia, J. L. & Diaz, E. (2002). Genomic analysis of the aromatic catabolic pathways from *Pseudomonas putida* KT2440. *Environ Microbiol* 4, 824-41.

7. Entsch, B. & van Berkel, W. J. (1995). Structure and mechanism of para-hydroxybenzoate hydroxylase. *FASEB J* 9, 476-83.

8. Hubbard, P. A., Liang, X., Schulz, H. & Kim, J. J. (2003). The crystal structure and reaction mechanism of *Escherichia coli* 2,4-dienoyl-CoA reductase. *J Biol Chem* 278, 37553-60.

9. Kantz, A., Chin, F., Nallamothu, N., Nguyen, T. & Gassner, G. T. (2005). Mechanism of flavin transfer and oxygen activation by the two-component flavoenzyme styrene monooxygenase. *Arch Biochem Biophys* 442, 102-16.

10. Ukaegbu, U. E., Kantz, A., Beaton, M., Gassner, G. T. & Rosenzweig, A. C. Structure and ligand binding properties of the epoxidase component of styrene monooxygenase. *Biochemistry*.

11. Spiegelhauer, O., Mende, S., Dickert, F., Knauer, S. H., Ullmann, G. M. & Dobbek, H. (2010). Cysteine as a modulator residue in the active site of xenobiotic reductase A: A structural, thermodynamic and kinetic study. *J Mol Biol* 398, 66-82.

12. Kohli, R. M. & Massey, V. (1998). The oxidative half-reaction of Old Yellow Enzyme. The role of tyrosine 196. *J Biol Chem* 273, 32763-70.

13. Khan, H., Barna, T., Bruce, N. C., Munro, A. W., Leys, D. & Scrutton, N. S. (2005). Proton transfer in the oxidative half-reaction of pentaerythritol tetranitrate reductase. Structure of the reduced enzyme-progesterone complex and the roles of residues Tyr186, His181, His184. *Febs J* 272, 4660-71.

14. Kitzing, K., Fitzpatrick, T. B., Wilken, C., Sawa, J., Bourenkov, G. P., Macheroux, P. & Clausen, T. (2005). The 1.3 A crystal structure of the flavoprotein YqjM reveals a novel class of Old Yellow Enzymes. *J Biol Chem* 280, 27904-13.

15. Adalbjornsson, B. V., Toogood, H. S., Fryszkowska, A., Pudney, C. R., Jowitt, T. A., Leys, D. & Scrutton, N. S. Biocatalysis with thermostable enzymes: structure and properties of a thermophilic 'ene'-reductase related to old yellow enzyme. *Chembiochem* 11, 197-207.

16. Admiraal, S. J., Meyer, P., Schneider, B., Deville-Bonne, D., Janin, J. & Herschlag, D. (2001). Chemical rescue of phosphoryl transfer in a cavity mutant: a cautionary tale for site-directed mutagenesis. *Biochemistry* 40, 403-13.

17. Kraut, D. A., Carroll, K. S. & Herschlag, D. (2003). Challenges in enzyme mechanism and energetics. *Annu Rev Biochem* 72, 517-71.

18. Fraaije, M. W. & Mattevi, A. (2000). Flavoenzymes: diverse catalysts with recurrent features. *Trends Biochem Sci* 25, 126-32.

19. Fox, K. M. & Karplus, P. A. (1994). Old yellow enzyme at 2 Å resolution: overall structure, ligand binding, and comparison with related flavoproteins. *Structure* 2, 1089-105.

20. Barna, T. M., Khan, H., Bruce, N. C., Barsukov, I., Scrutton, N. S. & Moody, P. C. (2001). Crystal structure of pentaerythritol tetranitrate reductase: "flipped" binding geometries for steroid substrates in different redox states of the enzyme. *J Mol Biol* 310, 433-47.

21. Pudney, C. R., Hay, S., Pang, J., Costello, C., Leys, D., Sutcliffe, M. J. & Scrutton, N. S. (2007). Mutagenesis of morphinone reductase induces multiple reactive configurations and identifies potential ambiguity in kinetic analysis of enzyme tunneling mechanisms. *J Am Chem Soc* 129, 13949-56.

22. Barna, T., Messiha, H. L., Petosa, C., Bruce, N. C., Scrutton, N. S. & Moody, P. C. (2002). Crystal structure of bacterial morphinone reductase and properties of the C191A mutant enzyme. *J Biol Chem* 277, 30976-83.

23. Breithaupt, C., Strassner, J., Breitinger, U., Huber, R., Macheroux, P., Schaller, A. & Clausen, T. (2001). X-ray structure of 12-oxophytodienoate reductase 1 provides structural insight into substrate binding and specificity within the family of OYE. *Structure* 9, 419-29.

24. Breithaupt, C., Kurzbauer, R., Lilie, H., Schaller, A., Strassner, J., Huber, R., Macheroux, P. & Clausen, T. (2006). Crystal structure of 12-oxophytodienoate reductase 3 from tomato: self-inhibition by dimerization. *Proc Natl Acad Sci U S A* 103, 14337-42.

25. O'Brien, P. J. & Herschlag, D. (1999). Catalytic promiscuity and the evolution of new enzymatic activities. *Chem Biol* 6, R91-R105.

26. Khan, H., Harris, R. J., Barna, T., Craig, D. H., Bruce, N. C., Munro, A. W., Moody, P. C. & Scrutton, N. S. (2002). Kinetic and structural basis of reactivity of pentaerythritol tetranitrate reductase with NADPH, 2-cyclohexenone, nitroesters, and nitroaromatic explosives. *J Biol Chem* 277, 21906-12.

27. Sambrook, J. & Russel, D. (2001). *Molecular Cloning: A Laboratory Manual*, 1, Cold Spring Harbor Laboratory Press.

28. Aliverti, A., Curti, B. & Vanoni, M. A. (1999). Identifying and quantitating FAD and FMN in simple and in iron-sulfur-containing flavoproteins. *Methods Mol Biol* 131, 9-23.

29. Massey, V., Stankovich, M. & Hemmerich, P. (1978). Light-mediated reduction of flavoproteins with flavins as catalysts. *Biochemistry* 17, 1-8.

30. Sucharitakul, J., Chaiyen, P., Entsch, B. & Ballou, D. P. (2005). The reductase of p-hydroxyphenylacetate 3-hydroxylase from *Acinetobacter baumannii* requires p-hydroxyphenylacetate for effective catalysis. *Biochemistry* 44, 10434-42.

31. Loach, P. A. (1973). Oxidation-reduction potentials: Absorbance bands and molar absorbance of compounds used in biochemical studies. In *Handbook of Biochemistry Selected Data for Molecular Biology* (Sorber, H. A., ed.), pp. J33-J40. CRC Press, Cleveland, Ohio.

32. Strickland, S., Palmer, G. & Massey, V. (1975). Determination of dissociation constants and specific rate constants of enzyme-substrate (or protein-ligand) interactions from rapid reaction kinetic data. *J Biol Chem* 250, 4048-52.

33. Kabsch, W. (1988). Automatic indexing of rotation diffraction patterns. *J. Appl. Cryst.* 21, 67-71.

34. Emsley, P. & Cowtan, K. (2004). Coot: model-building tools for molecular graphics. *Acta Crystallogr D Biol Crystallogr* 60, 2126-32.

35. Adams, P. D., Grosse-Kunstleve, R. W., Hung, L. W., Ioerger, T. R., McCoy, A. J., Moriarty, N. W., Read, R. J., Sacchettini, J. C., Sauter, N. K. & Terwilliger, T. C. (2002). PHENIX: building new software for automated crystallographic structure determination. *Acta Crystallogr D Biol Crystallogr* 58, 1948-54.

36. Murshudov, G. N., Vagin, A. A. & Dodson, E. J. (1997). Refinement of macromolecular structures by the maximum-likelihood method. *Acta Crystallogr D Biol Crystallogr* 53, 240-55.

37. DeLano, W. L. (2002). The PyMol Molecular Graphics System. DeLano Scientific, San Carlos, CA, USA.

SUPPLEMENTARY INFORMATION
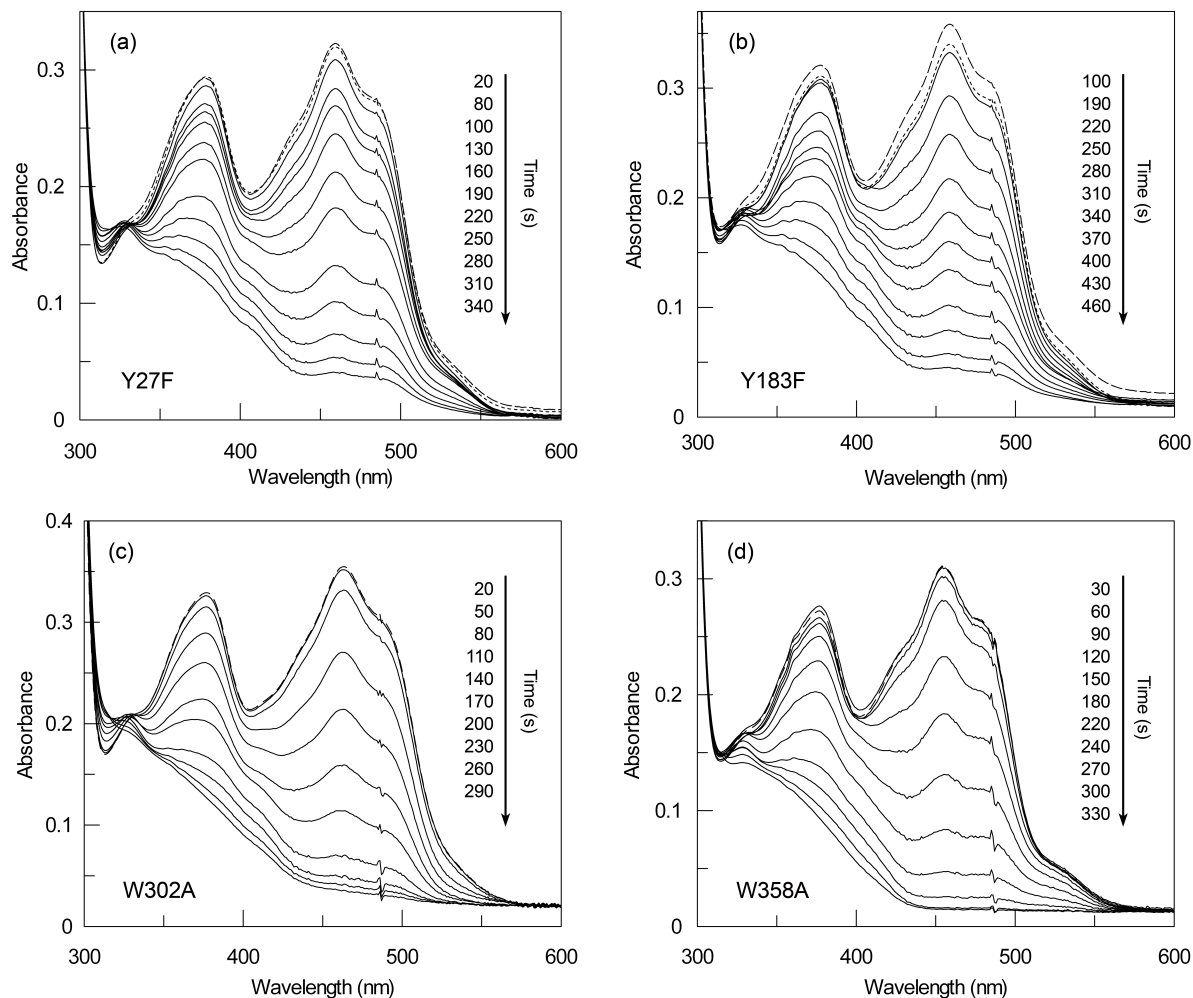
Figure S1:   Photoreduction of (a) Y27F-XenA, (b) Y183F-XenA, (c) W302A-XenA and (d) W358A-XenA. Conditions: 30 μM enzyme, 15 mM EDTA, 1 μM phenosafranine, 100 mM Tris buffer (pH 8.0) with traces of 5-deaza-10-methyl-3-sulfopropyl-isoalloxazine as catalyst. The spectra are displayed before the illumination (dashed line) and after the illumination steps (continuous lines). The dotted lines in panel (a) and (b) show spectra of the reoxidized enzyme.
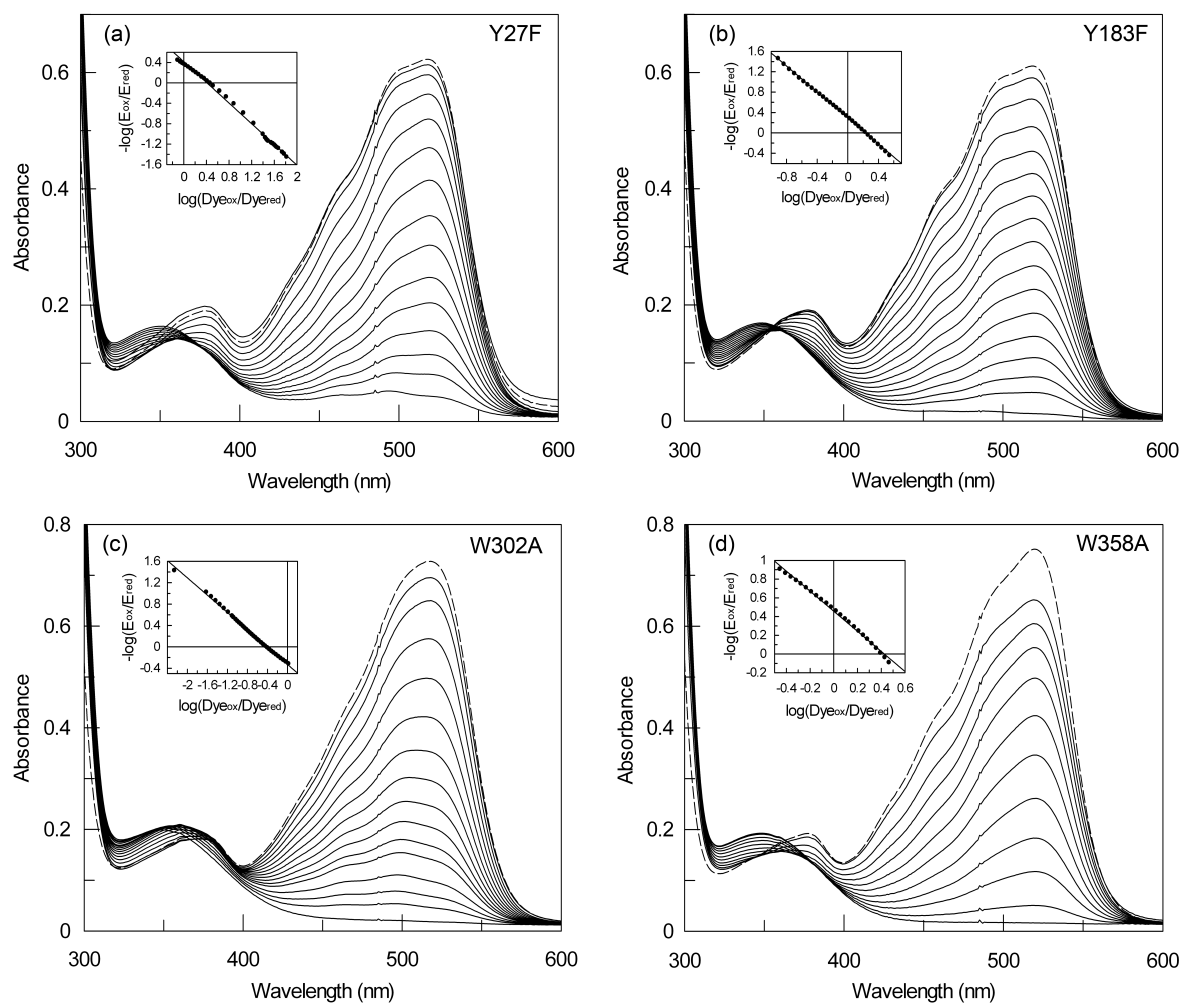
Figure S2: Determination of the reduction potential of the FMN/FMNH⁻ couple in (a) Y27F-XenA, (b) Y183F-XenA, (c) W302A-XenA and (d) W358A-XenA. Conditions: 15 μM enzyme, 15 μM phenosafranine, 2 μM methylviologen, 0.05 unit of xanthine oxidase and 50 mM Tris buffer (pH 8.0). The dotted lines show the reaction mixtures before the addition of xanthine. Reduction of enzyme and dye was followed over a time range of 1.5 h (continuous lines). Absorbance values at the maximum of FMN absorption of each XenA variant and values at 521 nm were used to calculate the concentrations of oxidized enzyme and dye, respectively. The insets show the plots of $\log(E_{\text{ox}}/E_{\text{red}})$ against $\log(Dye_{\text{ox}}/Dye_{\text{red}})$. The continuous lines display the linear fits with a slope of -1. Reduction potentials determined were: Y27F-XenA (-264 mV), Y183F-XenA (-261 mV), W302A-XenA (-242 mV) and W358A-XenA (-265 mV).
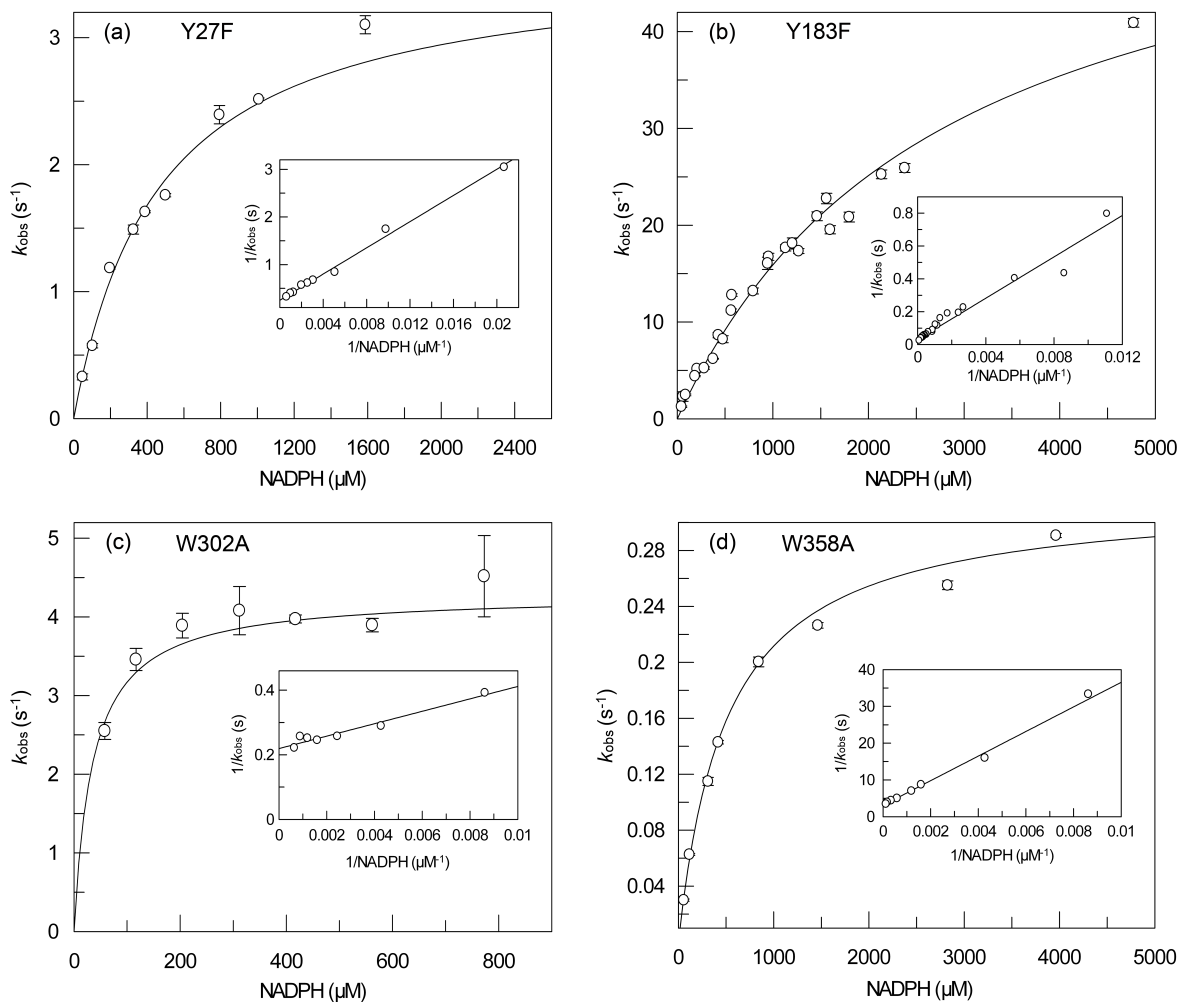
Figure S3: Reductive half-reactions of (a) Y27F-XenA, (b) Y183F-XenA, (c) W302A-XenA and (d) W358A-XenA with different concentrations of NADPH. The concentration dependences of the observed rate constants of the reaction of 5 μM XenA variant with NADPH are shown, with reciprocal plots in the insets. All experiments were conducted under anoxic conditions in 50 mM Tris buffer (pH 8.0) at 20°C.
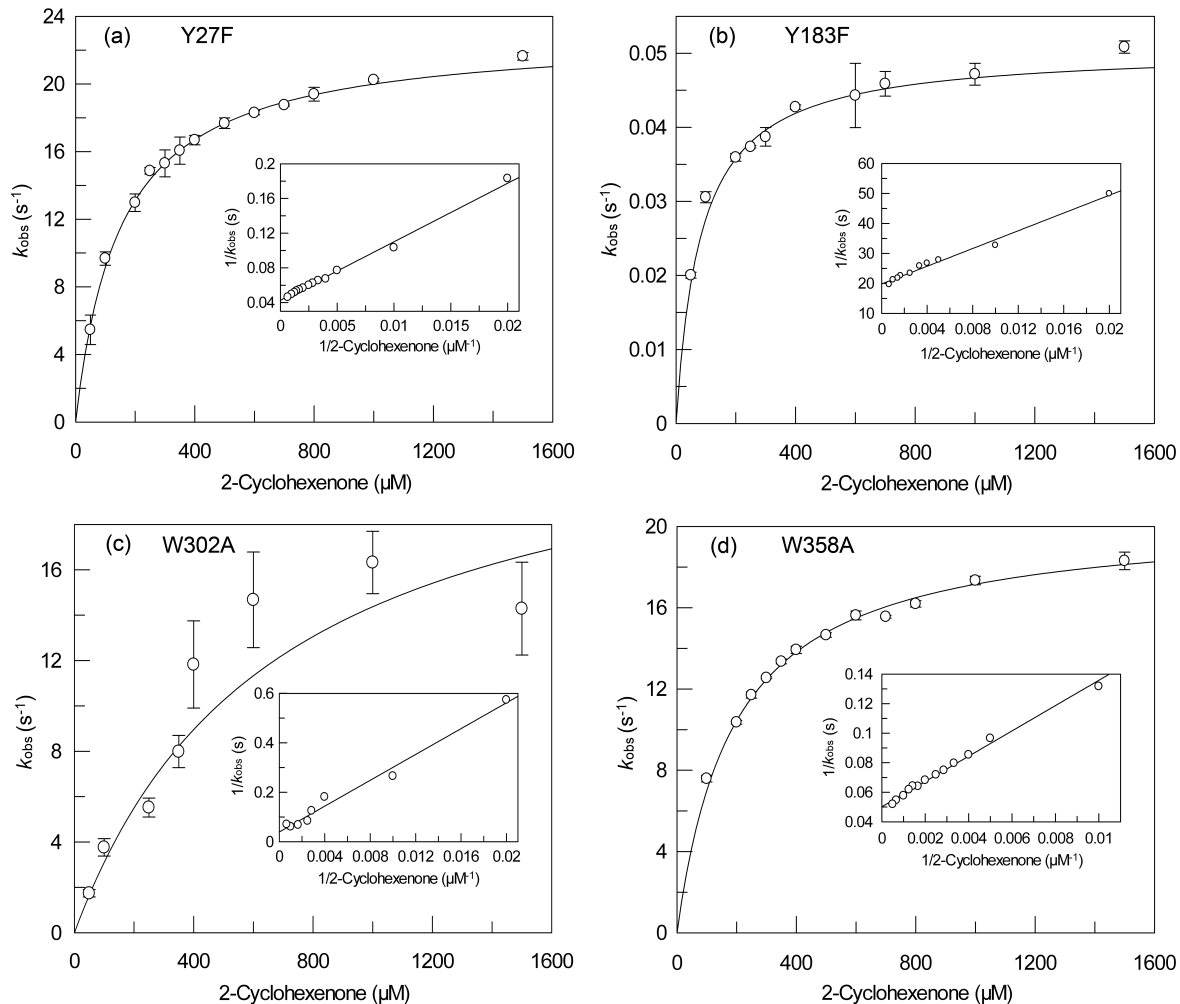
Figure S4: Oxidative half-reactions of (a) Y27F-XenA, (b) Y183F-XenA, (c) W302A-XenA and (d) W358A-XenA with different concentrations of NADPH. The concentration dependences of the observed rate constants for the reaction of 5 μM enzyme with 2-cyclohexenone are shown, with reciprocal plots in the insets. All experiments were conducted under anoxic conditions in 50 mM Tris buffer (pH 8.0) at 20°C.
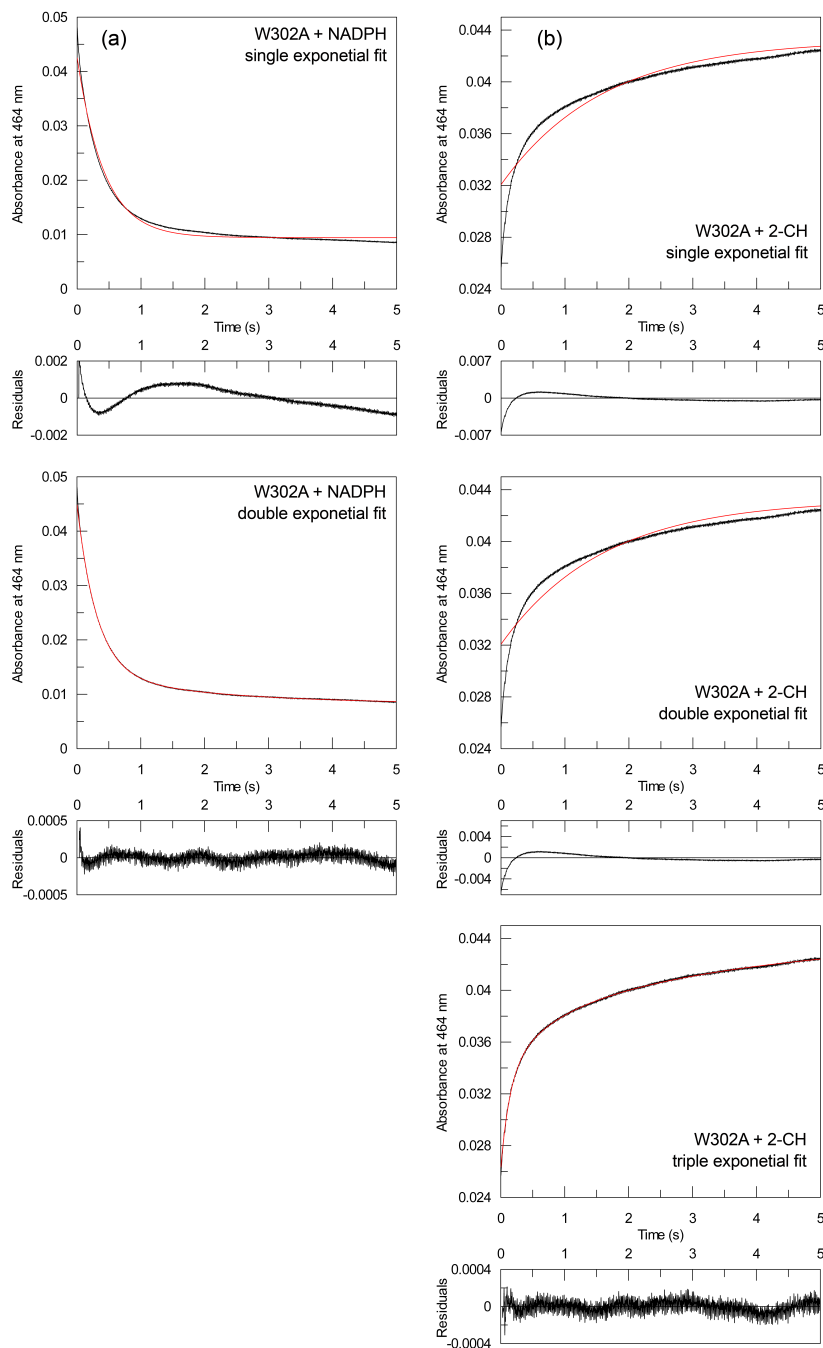
Figure S5: Time dependent absorbance changes at 464 nm for the (a) reductive and (b) oxidative half-reaction of W302A-XenA. Conditions: (a) 5 µM enzyme and 200 µM NADPH, (b) 5 µM enzyme and 400 µM 2-cyclohexenone. Both reactions were carried out in 50 mM Tris buffer (pH 8.0) at 20°C. Continuous lines represent the stopped-flow traces and red lines the single-, double- and triple exponential fits to the stopped-flow traces. Residual plots are displayed below each fit.

11 Publication D

Olivia Spiegelhauer and Holger Dobbek: Structures of Michaelis complexes provide evidence for redox dependent substrate binding in the flavoenzyme xenobiotic reductase A. *in preparation*

Classification: Biological Sciences, Biochemistry

Structures of Michaelis complexes provide evidence for redox dependent substrate binding in the flavoenzyme xenobiotic reductase A

Olivia Spiegelhauer and Holger Dobbek[*]

(1) Bioinorganic Chemistry, Universität Bayreuth, Universitätsstrasse 30, 95447 Bayreuth, Germany

(2) Present address: Institut für Biologie, Strukturbiologie/Biochemie, Humboldt-Universität zu Berlin, 10115 Berlin, Germany.

* To whom correspondence should be addressed: Holger Dobbek, Institut für Biologie, Strukturbiologie/Biochemie, Humboldt-Universität zu Berlin, phone: (++49) 030-23016961, Holger.Dobbek@biologie.hu-berlin.de.

Author contributions: O.S. and H.D. designed research, analyzed data and wrote the paper. O.S. performed research.

ABSTRACT

Crystal structures of enzyme substrate complexes are usually determined for non-reactive states, as the time needed for substrates to penetrate the crystal lattice is usually longer than the time needed for a single turnover. For redox-enzymes, like reductases, dehydrogenases and oxygenases, the structure of substrate complexes are typically derived for the non-reactive oxidation state. The underlying assumption in these structures is that the way the substrate binds to the enzyme is independent of the oxidation state of the cofactor relevant for the reaction. Here we provide evidence that this assumption is incorrect for enzyme-substrate complexes in the flavoenzyme xenobiotic reductase A (XenA).

XenA from *Pseudomonas putida* 86 catalyzes the NAD(P)H-dependent reduction of various substrates, including 2-cyclohexenone and 8-hydroxycoumarin. Using a XenA variant in which the proton donor of the oxidative half-reaction, Tyr183, has been exchanged against a phenylalanine allowed us to freeze-trap the Michaelis complexes of reduced XenA with three different substrates bound in the active site. These structures provide evidence for a redox-dependent binding of some substrates, as complexes of oxidized XenA with the same substrates result in non-productive binding modes. We argue that the oxidation state dependent electronic structure of the isoalloxazine ring influences bound substrates, e.g. by changing the pK_a value of the substrate associated hydroxyl groups, resulting in productive binding modes in the active and non-productive binding modes in the inactive oxidation state of the enzyme with phenolic substrates.

INTRODUCTION

To derive the chemical mechanism of an enzyme became a task strongly influenced by structural biology. Crystal structure analysis allows for a detailed spatial description of enzymes and enzyme-substrate complexes; the relative orientation of potential catalytic residues in the active site, the position and conformation of cofactors, as well as the position and orientation of the substrate(s) can be used to derive new mechanistic insights. A caveat of most crystallographic approaches is that it takes longer to prepare the reactive state, e.g. by soaking the enzyme crystal in substrate containing solutions, than the reaction needs to take place (1). A simple way to overcome this problem is to use either a substitute for the substrate, e.g. a slowly converted substrate or a competitive inhibitor, or to prepare the enzyme in an inactive state (2). The latter can be straightforward with enzymes carrying out redox reactions, which typically exist in different oxidation states of which only one is able to react with the substrate. Most redox enzymes depend on cofactors and it is the oxidation state of the cofactor, which determines the reactivity. With flavoenzymes catalyzing the reduction of substrates, stable enzyme-substrate complexes can be prepared in the oxidized state of the enzyme, which is inactive, as it does not carry the electrons necessary for the reduction. The underlying assumption is that the redox state does not influence the binding geometry of the substrate and that the structure reflects a physiological, ideally productive, state. However, the observation of so prepared enzyme substrate complexes in which the substrate is bound in a non-productive way indicates already that the assumption of equal binding in different redox states may be incorrect for some enzymes (3,4).

Xenobiotic reductase A (XenA) from the soil bacterium *Pseudomonas putida* 86 catalyzes the NAD(P)H dependent reduction of the olefinic bond of different α,β-unsaturated carbonyl compounds including ketones and esters. XenA belongs to the Old Yellow Enzyme (OYE) family, a wide spread enzyme family found in pro- and eukaryotic organisms. XenA was recently shown to be involved in the degradation of quinoline (5) along the 8-hydroxycoumarin pathway due to its ability to reduce the C3-C4 double bond of 8-hydroxycoumarin (4). Crystal structures of XenA have been determined for the oxidized enzyme alone and in complex with two different substrates bound to the active site (4,6). A structure of oxidized XenA in complex with the likely physiological substrate 8-hydroxycoumarin revealed a non-productive binding mode in which the distance between the hydride donor (N5 atom of flavin) and the hydride acceptor (C4 of 8-hydroxycoumarin) is with 4.7 Å far larger than typically observed (7). This observation motivated us to search for conditions to stabilize the reactive complex between reduced XenA and 8-hydroxycoumarin.

By investigating the individual contribution of several active site residues to substrate binding and catalysis in the two half-reactions of XenA, we identified Tyr 183 as the likely proton donor in the oxidative half-reaction (8). A variant of XenA in which Tyr 183 has been replaced by phenylalanine (Y183F-XenA) reacts with 2-cyclohexenone about 260-fold slower than wt-XenA, while its affinity in terms of the K_d of the Y183-XenA: 2-cyclohexenone complex is basically unaltered (8). Here we report the crystals structures of reduced Y183F-XenA in complex with different substrates. We exploited the reduced activity of Y183F-XenA with unaltered substrate binding to demonstrate that the binding affinity and binding mode of several molecules to the active site XenA is dependent on the redox chemistry of the flavin cofactor.

RESULTS AND DISCUSSION

Structures of oxidized and reduced XenA in complex with the substrate 8-hydroxycoumarin

The crystal structure of oxidized XenA in complex with the substrate 8-hydroxycoumarin has recently been determined (4). To determine the crystal structure of reduced Y183F-XenA in complex with 8-hydroxycoumarin and the other substrates reported here, Y183F-XenA was reduced using NADH and crystallized in the reduced state under anoxic conditions in a glovebox to suppress reoxidation of XenA by its oxidase activity. Reduced Y183F-XenA crystals were soaked for 5-10 s with the oxidizing substrates and were flash frozen in liquid nitrogen. Like in the structure of reduced wt-XenA all reduced Y183F-XenA structures display the "in"-conformation for Trp-302 and have a distinctly non-planar isoalloxazine ring with N5 lying above the ring plane with a tetrahedral geometry (8).

A crystal soaked with 8-hydroxycoumarin diffracted to a resolution of 2.3 Å at the synchrotron (Table 1). The difference electron density reveals a large, flat molecule bound above the isoalloxazine ring. Attempts to place 8-hydroxycoumarin as found in the crystal structure of oxidized XenA into the electron density resulted in a clear misfit and it was necessary to reverse the orientation and binding mode of the substrate to satisfy the difference density (Figure 1a). Whereas the phenolic hydroxyl group of 8-hydroxycoumarin forms the main interactions through hydrogen-bonds with His-178 and His-181 in the complex of oxidized XenA, the two histidine side chains are in hydrogen-bonding distance to the carbonyl oxygen of 8-hydroxycoumarin in the reduced enzyme complex (Figure 1a). This is equivalent to a 180° flip and a rotation of about 30° of 8-hydroxycoumarin when comparing the two substrate orientations (Figure 2a). In the oxidized complex the distance between C4 of 8-hydroxycoumarin and N5 of FMN are with 4.7 Å too far apart to allow hydride transfer (4). In the reduced complex both atoms are substantially closer and refined to a distance of 3.7 Å. While the oxidized enzyme-substrate complex could not explain how 8-hydroxycoumarin could be efficiently reduced by XenA, the structure of reduced XenA shows the typical separation found for hydride donors and acceptors in flavoenzymes and is thus in agreement with the formation of a productive enzyme-substrate complex (7).

For complexes of oxidized OYE with phenolic compounds it was shown that charge-transfer (CT) complexes with long-wavelength absorption are developed (9). The clear dependence of CT complex formation of different phenols on the pH suggests that phenolate anions (9) are formed as the pK_a values of the phenols are shifted by about three to four units as compared to the free phenols in water.

TABLE 1: Data collection and refinement statistics

	Y183F_2CH	Y183F_C	Y183F_7HC	Y183F_8HC
Data collection				
Space group	$P2_12_12$	$P2_12_12$	$P2_12_12$	$P2_12_12$
Cell dimensions				
a, b, c (Å)	83.87, 158.12, 57.38	84.09, 158.10, 57.21	83.96, 158.34, 57.31	84.03, 159.07, 58.04
α, β, γ (°)	90, 90, 90	90, 90, 90	90, 90, 90	90, 90, 90
Resolution (Å)	30 – 2.1	30 – 2.0	30 – 2.3	30 – 2.3
R_{sym}	4.1 (12.0)	13.9 (42.4)	2.9 (6.9)	5.1 (8.6)
$I / \sigma I$	23.54 (10.92)	8.56 (3.32)	34.31 (16.86)	19.76 (13.18)
Completeness (%)	97.6 (97.4)	97.4 (93.8)	98.5 (96.7)	98.5 (97.4)
Redundancy	3.7 (3.7)	4.4 (4.2)	3.6 (3.5)	3.5 (3.5)
Refinement				
Resolution (Å)	20 – 2.1	29 – 2.2	28 – 2.3	29 – 2.3
No. reflections	44356	38543	34257	34886
R_{work} / R_{free}	0.158 / 0.213	0.912 / 0.277	0.156 / 0.228	0.202 / 0.297
No. atoms				
Protein	5562	5554	5555	5555
Ligand/ion	76 / 45	90 / 25	98 / 35	74 / 25
Water	451	575	433	413
B-factors				
Protein	18.509	15.787	18.243	18.202
Ligand/ion	34.356	28.463	26.598	30.618
Water	27.835	23.735	25.469	30.211
R.m.s. deviations				
Bond lengths (Å)	0.007	0.008	0.007	0.007
Bond angles (°)	1.043	1.079	1.057	1.188

*Values in parentheses are for highest-resolution shell.

Formation of the anionic state is most likely stabilized by the positive electrostatic potential of the electron deficient oxidized isoalloxazine ring (10). Very similar long-wavelength CT complexes are observed upon addition of 8-hydroxycoumarin to oxidized XenA, which are not observable with the related coumarin and are most likely characteristic for the interaction of the phenolate anion with the oxidized flavin (4). The phenolate oxygen atom is a strong hydrogen-bond acceptor and is in hydrogen-bonding distance to His-178 and His-181 in the crystal structure of oxidized XenA (4). Reduced flavin is electron-rich and under physiological conditions mostly anionic ($FMNH^-$) and thus destabilizes the binding and

formation of anions in its direct environment. As phenolic substrates will bind in the neutral, protonated state to the reduced flavin hydrogen-bond interaction with the protein can be different than for the phenolate states of the substrate.
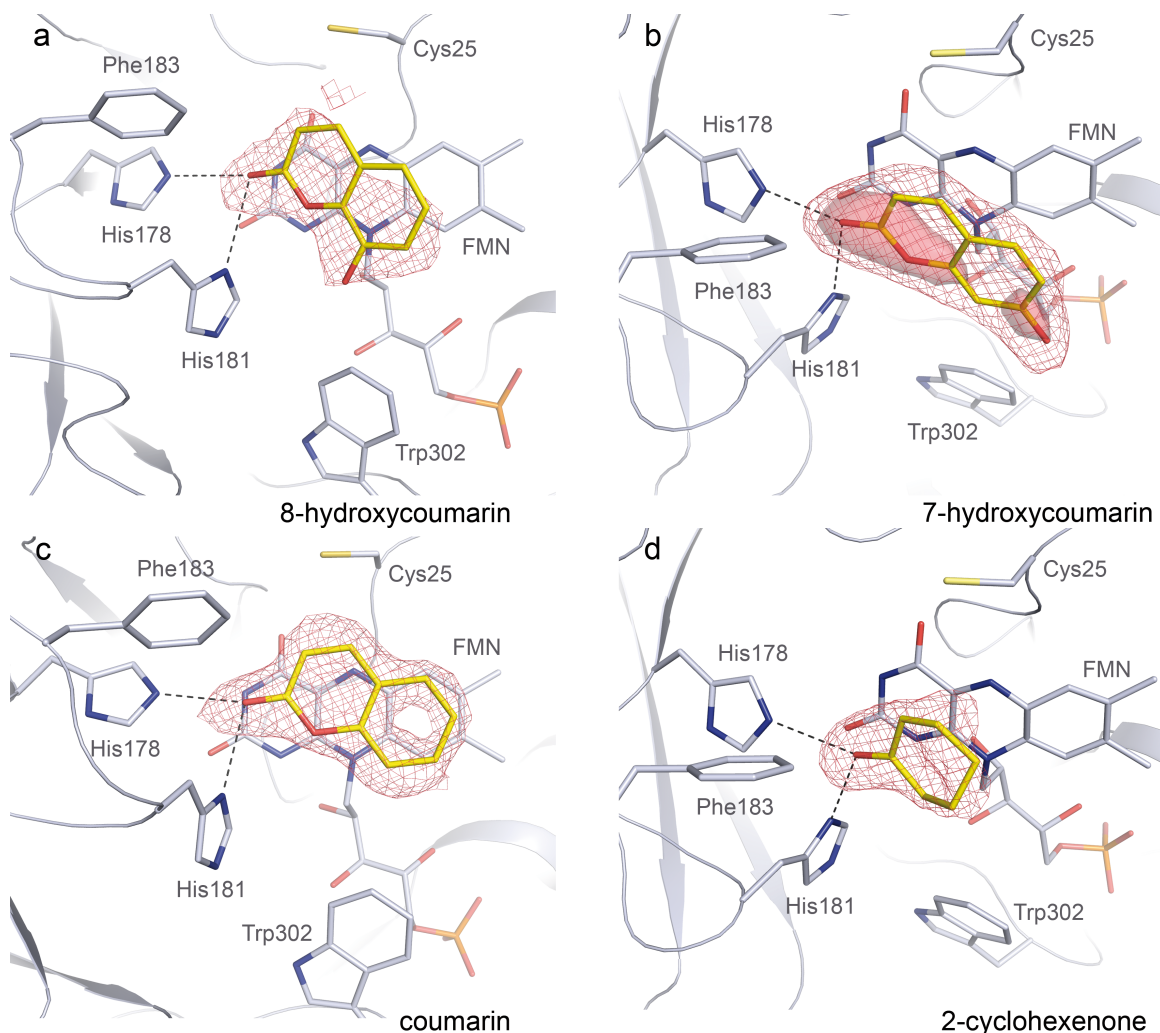

Figure 1: **Structures of Michaelis complexes of reduced XenA-Y183F and different substrates.** (a) View of the active site of reduced XenA-Y183F in complex with 8-hydroxycoumarin (yellow). The F_o-F_c map of 8-hydroxycoumarin is contoured at 2.5σ and is shown in red mesh representation. (b) View of the active site of reduced XenA-Y183F in complex with 7-hydroxycoumarin (yellow). The F_o-F_c map of 7-hydroxycoumarin is contoured at 3.0σ (red mesh representation) and at 6.0σ (red surface representation). (c) View of the active site of reduced XenA-Y183F in complex with coumarin (yellow). The F_o-F_c map of coumarin is contoured at 2.5σ and is shown in red mesh representation. (d) View of the active site of reduced XenA-Y183F in complex with 2-cyclohexenone (yellow). The F_o-F_c map of 2-cyclohexenone is contoured at 3.0σ and is shown in red mesh representation. The FMN and the amino acid side chain residues are displayed in stick mode. Carbon atoms shown in grey, nitrogen atoms are shown in blue, sulfur atoms are shown in light yellow and phosphorous atoms are shown in orange. Hydrogen bonding interactions between the enzyme and the substrates are displayed in dashed lines in grey.

For the interaction of 8-hydroxycoumarin with XenA hydrogen-bond formation between His-178 and His-181 and the carbonyl oxygen of the substrate appears to be favored compared to the alternative hydrogen bonds with the phenolic hydroxyl-group, most likely because both histidines act preferentially as hydrogen-bond donors. Thus the redox-dependent deprotonation of substrates in the active site of flavoenzymes can cause different binding modes in different oxidation states.
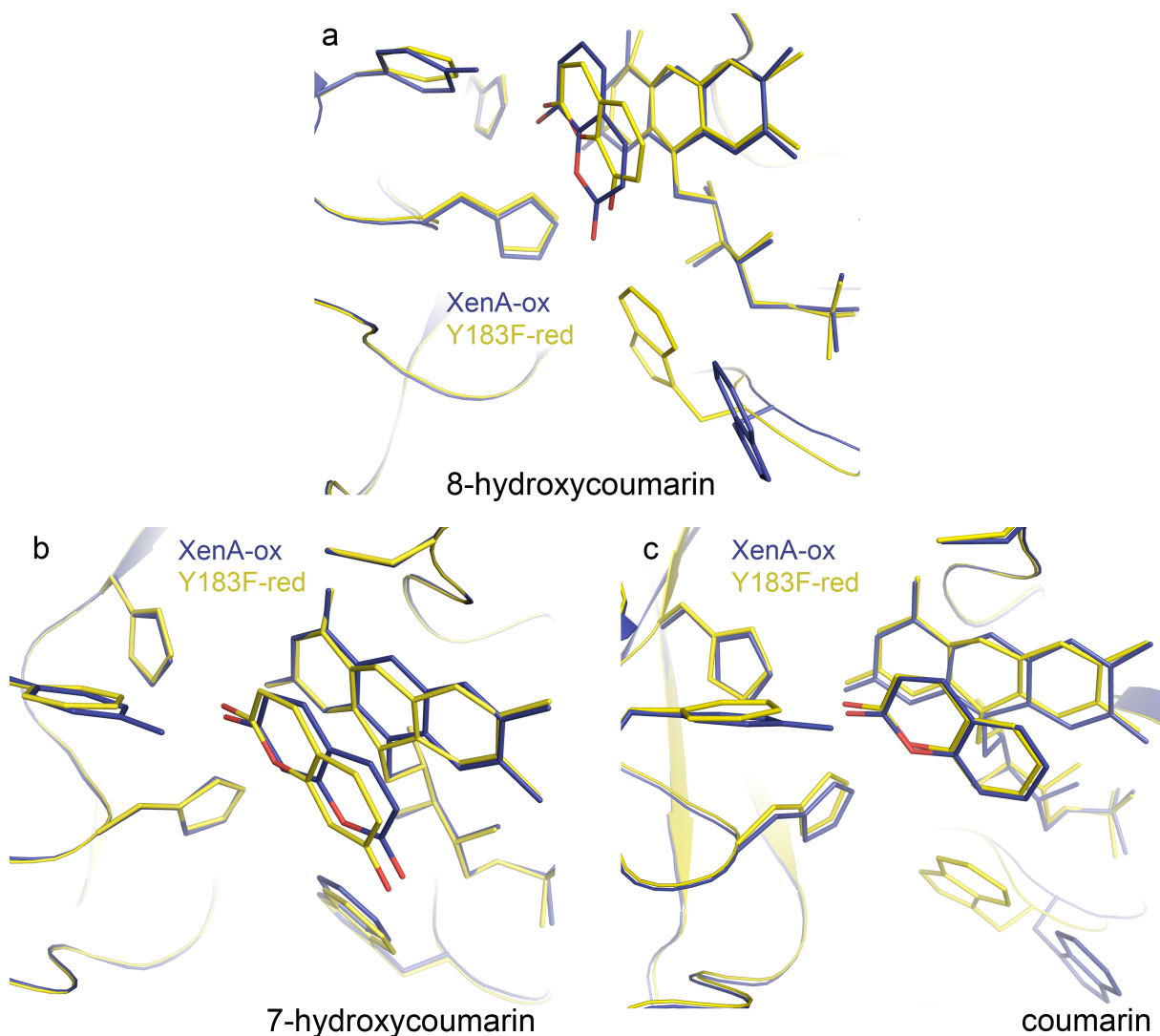
Figure 2: **Comparison of oxidized XenA-wt and reduced XenA-Y183F in complex with different substrates.** (a) View of the active site of both enzyme forms in complex with 8-hydroxycoumarin. (b) View of the active site of both enzyme forms in complex with 7-hydroxycoumarin. (c) View of the active site of both enzyme forms in complex with coumarin. Amino acid side chain residues, FMN and the substrates are displayed in stick mode. Oxygen atoms of the substrates are shown in red. XenA-wt (oxidized) is displayed in blue and XenA-Y183F (reduced) is displayed in yellow.

Structures of oxidized and reduced XenA in complex with the substrates coumarin and 7-hydroxycoumarin

To further test the hypothesis whether it is the presence of the phenolic hydroxyl group, which causes the redox-dependent binding modes of 8-hydroxycoumarin, the interaction of two other substrates, namely coumarin and 7-hydroxycoumarin, have been investigated with oxidized and reduced XenA. Coumarin and 7-hydroxycoumarin are reduced by XenA with similar observed rate constants (Figure 5). The crystal structure of oxidized XenA in complex with 7-hydroxycoumarin reveals an unusual binding geometry for the ligand in which the phenolic oxygen is in hydrogen-bonding distance to His-178 and His-181 and the carbonyl and lactone ring oxygens are close to Trp-302 (Figure 3), in a distance suitable to form a O…H-C hydrogen bond frequently found for tryptophan side chains (11).
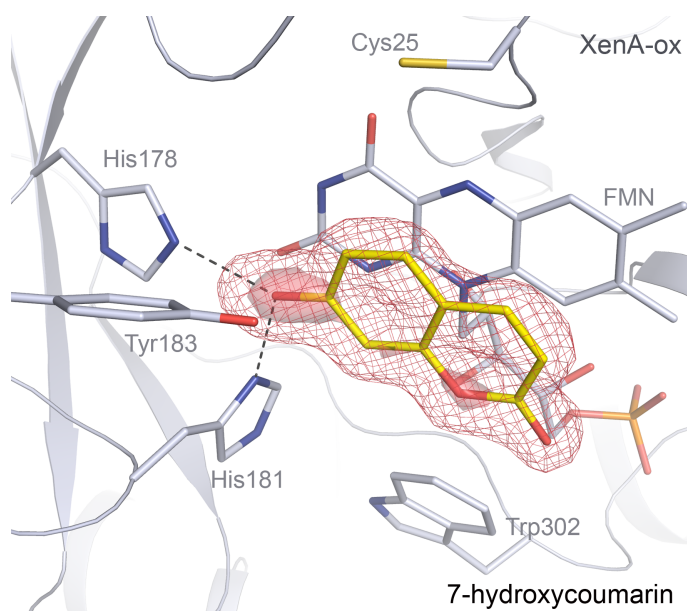
Figure 3: **Crystal structure of 7-hydroxycoumarin bound in the active site of oxidized XenA.** View of the active site of oxidized wt-XenA in complex with 7-hydroxycoumarin (yellow). The F_o-F_c map of 7-hydroxycoumarin is contoured at 4.0σ (red mesh representation) and at 11.0σ (red surface representation). The FMN and the amino acid side chain residues are displayed in stick mode. Carbon atoms shown in grey, nitrogen atoms are shown in blue, sulfur atoms are shown in light yellow and phosphorous atoms are shown in orange. Hydrogen bonding interactions between the enzyme and the substrates are displayed in dashed lines in grey.

A similar conformation for Trp-302, termed "in" conformation, was detected so far only in reduced states of XenA (8). We suggest that this conformation is formed in 7-hydroxycoumarin bound oxidized XenA, because of the favorable interaction between Trp-302 and the substrate and not because of a reduction of the flavin. On a first glance the

structure of reduced Y183F-XenA in complex with 7-hydroxycoumarin is very similar to the oxidized complex (Figure 1b and 2b). However, the distribution of the electron density for the two rings suggests that in the reduced state the carbonyl oxygen of the lactone function is in hydrogen-bonding distance to the histidine couple and not the hydroxyl-group as in the oxidized state. Thus the principal binding mode of binding of 7-hydroxycoumarin is similar to 8-hydroxycoumarin.

If different orientations can also be observed in substrate binding when there is no phenolic hydroxyl group present in the substrate has been investigated for coumarin complexes of XenA. The crystal structure of oxidized XenA in complex with coumarin has been reported before (4,6) and in contrast to the 8-hydroxycoumarin complex no long-wavelength CT interactions have been observed in solution (4). The coumarin – XenA complexes are practically identical in the oxidized and reduced state (Figure 1c and 2c), except for the conformational change of Trp-302 and the increased bending of the isoalloxazine ring found in the reduced state. The main ligand protein interactions are formed in both states by the carbonyl oxygen of the coumarin and the histidine couple, which are in hydrogen bonding distance. In both structures suitable distances between hydride donor and acceptor are found which are with 2.9 Å in the reduced structure and 3.05 Å in the oxidized enzyme very close together.

Structure of reduced XenA with 2-cyclohexenone

2-Cyclohexenone is used as the prototypical substrate in most kinetic studies of enzymes of the OYE family. Despite its common use and the large number of co-crystal structures determined for members of the OYE family it has not been described how 2-cyclohexenone binds to any flavoprotein. This is most likely due to the low affinity of 2-cyclohexenone for the oxidized enzymes. Attempts to determine the co-crystal structure of oxidized XenA with 2-cyclohexenone failed despite soaking concentrations of 50 – 100 mM 2-cyclohexenone for several minutes to hours, conditions under which saturation of the substrate-binding site with coumarin, 7- and 8-hydroxycoumarin can easily be achieved. On the other hand a kinetic K_d of 86 μM and 83 μM have been determined for the complex between 2-cyclohexenone and reduced wt-XenA (12), respectively between 2-cyclohexenone and reduced Y183-XenA (8), indicating that reduced XenA has a sufficient affinity to become saturated even at low concentrations of 2-cyclohexenone. The co-crystal structure of reduced Y183F-XenA soaked for 5 s with approximately 5 mM 2-cyclohexenone has been solved at 2.1 Å resolution. Its electron density reveals a clear binding site for 2-cyclohexenone above the isoalloxazine ring

(Figure 1d and Figure 4). The electron density is of sufficient quality to define the stereochemistry of 2-cyclohexenone, which is in *endo*-conformation with the double bond positioned such that the hydride acceptor βC is 3.6 Å above N5, again confirming a productive enzyme-substrate arrangement for this complex. The main ligand protein interactions are between the carbonyl oxygen of 2-cyclohexenone and the histidine couple in hydrogen-bonding distance.
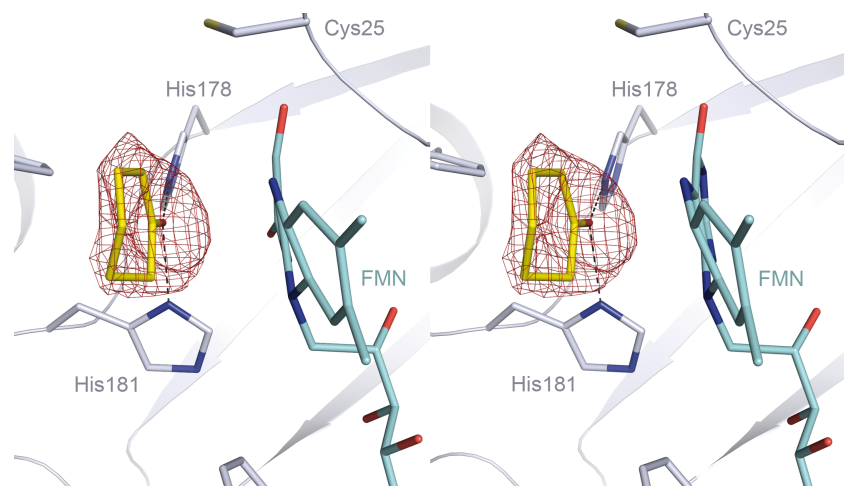

Figure 4: **View on the active site of reduced XenA-Y183F in complex with 2-cyclohexenone.** Stereoscopic view on the active site of reduced XenA-Y183F in complex with 2-cyclohexenone. Amino acid side chain residues and the FMN are displayed in stick mode. Carbon atoms of the FMN are shown in light blue, carbon atoms of the side chains are shown in grey, nitrogen atoms are shown in blue and sulfur atoms are shown in light yellow. The F_o-F_c map of 2-cyclohexenone is contoured at 3.0σ and is shown in red mesh representation.

Hydrogen-bonding, aromatic stacking and cation-π interactions are three fundamental forces found in molecular recognition (10). It is not directly obvious how these possible interactions have been altered by the reduction of the flavin. Nevertheless, donor atom π-bonding to the electron poor flavin allows for the binding of anions, e.g. sulfate and chloride, which are typically observed in the substrate-binding pocket of oxidized OYE proteins. These anions may act as competitively binding ligands in the oxidized state, which, as they have no affinity for the reduced flavin, are not competing with 2-cyclohexenone for the substrate-binding site above reduced flavin.
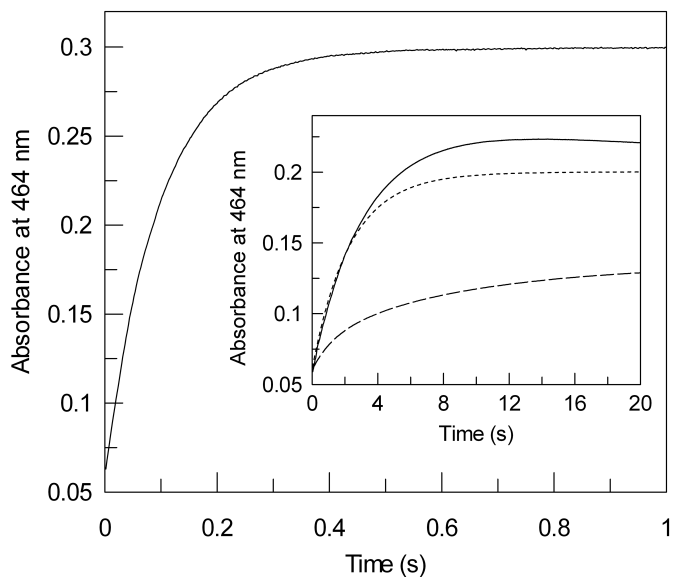
Figure 5: **Oxidative half-reactions of reduced wt-XenA.** Time-dependent absorbance changes of the reaction of 70 µM reduced wt-XenA with 1600 µM of different oxidative substrates. The figure shows the time trace for the reaction with 2-cyclohexenone. The inset shows the time traces of the reactions with coumarin (solid line), 8-hydroxycoumarin (dotted line) and 7-hydroxycoumarin (dashed line). Measurements were performed under anaerobic conditions in 50 mM Tris buffer (pH 8.0) at 20°C. The observed rate constants are 10.5 s^{-1} (with 2-cyclohexenone), 0.34 s^{-1} (with coumarin), 0.19 s^{-1} (with 7-hydroxycoumarin) and 0.43 s^{-1} (with 8-hydroxycoumarin).

CONCLUSIONS

The presented Michaelis-complexes provide direct evidence for redox-dependent modes of substrate binding in flavoenzymes. Redox-dependent substrate binding has been proposed for other flavoenzymes, based on the observation of non-productive binding modes in the inactive redox state of the enzyme (3,13), however direct insight into the reactive states were missing. Our results demonstrate that substrate recognition and productive orientation are directly linked to the redox chemistry of the flavin. However one can easily imagine that the modulated substrate affinity also facilitates product egress after the oxidation state change and open new ways to distinguish between the "right" and "wrong" substrates.

MATERIALS AND METHODS

Protein expression and purification

The proteins have been expressed and purified as described in (12). Mutagenesis to derive the Y183F variant of XenA has been described in (8).

Pre-steady state kinetic experiments

The oxidative half-reactions of reduced wt-XenA with 2-cyclohexenone, coumarin, 7-hydroxycoumarin and 8-hydroxycoumarin were measured in 50 mM Tris buffer (pH 8.0) under anaerobic conditions at 20°C as described previously (8). 70 μM of enzyme was mixed with 1600 μM of the oxidative substrate. To achieve complete reduction the enzyme it was reduced by titration with appropriate amounts of NADH in a glass tonometer with cuvette side arm. The reactions were monitored at the absorbance maximum of the FMN at 464 nm with using an Applied Photophysics SX-20MV spectrophotometer with a 1-cm observation path length cuvette. The measurements were repeated at least five times for each substrate concentration.

Crystallization and structure determination

Reduced crystals of XenA-Y183F were grown as described for the reduced wild type XenA under anoxic conditions in a glovebox (Coy type B) (8). The crystals were cross-linked for 1 hour in a harvesting solution containing 100 mM HEPES buffer (pH 7.5), 2.1 M ammonium sulfate, 4 mM NADH and 0.002% glutaraldehyde. To soak crystals with substrate, they were further incubated for 10 sec in harvesting buffer containing approximately 5 mM of the oxidative substrate. Crystals were shock frozen in harvesting buffer containing 20% (v/v) 2*R*,3*R*-butandiol and stored in liquid nitrogen.

X-ray diffraction data were collected at the beam line BL14.2 (BESSY, Berlin, Germany), at a wavelength of 0.91841 Å and 100 K. The diffraction data were processed and scaled using the XDS package (14). The structures of the XenA-Y183F variants were solved using Patterson search techniques using PHASER (15) with XenA$_{ox}$ (PDB-Id: 2H8X (4)) as homologous search model. Subsequent rounds of model building and refinement were performed using the programs COOT (16), PHENIX (17) and Refmac5 (18).

ACKNOWLEDGEMENTS

REFERENCES

1. Geremia S, Campagnolo M, Demitri N, Johnson LN (2006) Simulation of diffusion time of small molecules in protein crystals. Structure 14: 393-400.

2. Hassell AM*, et al.* (2007) Crystallization of protein-ligand complexes. Acta Crystallogr D Biol Crystallogr 63: 72-79.

3. Race PR*, et al.* (2005) Structural and mechanistic studies of *Escherichia coli* nitroreductase with the antibiotic nitrofurazone. Reversed binding orientations in different redox states of the enzyme. J Biol Chem 280: 13256-13264.

4. Griese JJ, R PJ, Schwarzinger S, Dobbek H (2006) Xenobiotic reductase A in the degradation of quinoline by *Pseudomonas putida* 86: physiological function, structure and mechanism of 8-hydroxycoumarin reduction. J Mol Biol 361: 140-152.

5. Fetzner S*, et al.* (1998) Bacterial degradation of quinoline and derivatives - Pathways and their biocatalysts. Angew Chem Int Edit 37: 577-597.

6. Spiegelhauer O*, et al.* (2010) Cysteine as a modulator residue in the active site of xenobiotic reductase A: A structural, thermodynamic and kinetic study. J Mol Biol 398: 66-82.

7. Fraaije MWMattevi A (2000) Flavoenzymes: diverse catalysts with recurrent features. Trends Biochem Sci 25: 126-132.

8. Spiegelhauer O, Mende S, Knauer SH, Dobbek H (submitted) Determinants of Substrate-Binding and -Protonation in the Flavoenzyme Xenobiotic Reductase A.

9. Abramovitz ASMassey V (1976) Interaction of phenols with old yellow enzyme. Physical evidence for charge-transfer complexes. J Biol Chem 251: 5327-5336.

10. Breinlinger EC, Kennan CJ, Rotello VM (1998) Modulation of Flavin Recognition and Redox Properties through Donor Atom-pi Interactions. J Am Chem Soc 120: 8606-8609.

11. Petrella RJKarplus M (2004) The role of carbon-donor hydrogen bonds in stabilizing tryptophan conformations. Proteins 54: 716-726.

12. Spiegelhauer O*, et al.* (2009) Kinetic characterization of xenobiotic reductase A from *Pseudomonas putida* 86. Biochemistry 48: 11412-11420.

13. Barna TM*, et al.* (2001) Crystal structure of pentaerythritol tetranitrate reductase: "flipped" binding geometries for steroid substrates in different redox states of the enzyme. J Mol Biol 310: 433-447.

14. Kabsch W (1988) Automatic indexing of rotation diffraction patterns. J. Appl. Cryst. 21: 67-71.

15. McCoy AJ (2007) Solving structures of protein complexes by molecular replacement with Phaser. Acta Crystallogr D Biol Crystallogr 63: 32-41.

16. Emsley P, Cowtan K (2004) Coot: model-building tools for molecular graphics. Acta Crystallogr D Biol Crystallogr 60: 2126-2132.

17. Adams PD, *et al.* (2002) PHENIX: building new software for automated crystallographic structure determination. Acta Crystallogr D Biol Crystallogr 58: 1948-1954.

18. Murshudov GN, Vagin AA, Dodson EJ (1997) Refinement of macromolecular structures by the maximum-likelihood method. Acta Crystallogr D Biol Crystallogr 53: 240-255.

12 Acknowledgement

13 Erklärung

Hiermit erkläre ich, dass ich diese Arbeit selbstständig verfasst und keine anderen als die von mir angegebenen Quellen und Hilfsmittel benutzt habe.

Ferner erkläre ich, dass ich anderweitig mit oder ohne Erfolg nicht versucht habe, diese Dissertation einzureichen. Ich habe keine gleichartige Doktorprüfung an einer anderen Hochschule endgültig nicht bestanden.

Bayreuth, den 16. August 2010